Rapid sea-level rise and climate change: lessons from the early Holocene

Graham Phillip Rush

Doctor of Philosophy

University of York

Environment and Geography

December 2020

"Another mode of explanation presented itself in supposing the sea to have been the agent. Sink the country to the level of the highest line, and we should have a sea-margin corresponding to it; and then as the land gradually emerged, successive coast-lines might be traced corresponding to all those we find."

Thomas Jamieson, Ellon, 1863

Abstract

The '8.2 ka climate event' is believed to have been driven by meltwater pulses draining into the North Atlantic, emanating from the Laurentide Ice Sheet. It is important to quantify the precise timing and magnitude of meltwater that was released; this is critical information for climate models that simulate the impact of freshwater forcing on the Atlantic Meridional Overturning Circulation in a well-established interglacial climate state.

Relative sea-level (RSL) reconstructions enable quantification of the timing and magnitude of the meltwater pulses and identification of their origin. This research presents RSL reconstructions for a North Atlantic (Ythan Estuary, UK) and a South Atlantic (Swan Inlet, Falkland Islands) site to test three hypotheses related to the meltwater pulses prior to the 8.2 ka climate event.

A new inter-tidal foraminifera training set and transfer function for the North Sea basin is presented. Based on this and a high-resolution chronology, a probabilistic RSL reconstruction is produced for the Ythan Estuary 8800–8100 cal yr BP. Two meltwater pulses are quantified that demonstrate that drainage of Lake Agassiz-Ojibway (LAO) was not the major contributor of freshwater, but that the Hudson Bay Ice Saddle (HBIS) collapse was the likely major component.

Twenty new sea-level index points are presented for Swan Inlet based on litho-, chrono- and bio-stratigraphical analyses from c. 8500 cal yr BP to present. While there is some evidence for rapid sea-level rise coincident with the timing of the meltwater pulses, it was not possible to quantify the magnitude. The results do have important implications for understanding global ice melt history and the processes of isostatic adjustment on continental shelves.

The research suggests that the HBIS was the major contributor of freshwater prior to the 8.2 ka climate event and that further work following similar lines of enquiry can help test this hypothesis.

Contents

3   Development of an intertidal foraminifera training set for the North Sea and an assessment of its application for Holocene sea-level reconstructions   60

4   Relative sea-level reconstruction for the Ythan Estuary, eastern Scotland, and implications for the cause of the 8.2 ka climate event   101

List of Tables

List of Figures

Acknowledgments

I would like to thank everyone who has been part of my journey during this PhD and thesis. They are too numerous to mention all by name but they are, without exception, wonderful people.

I would like to thank my supervisor Roland Gehrels for at first believing in me and then for his unwavering support, patience and friendship no matter what the circumstance. I would also like to thank my co-supervisors Mark Bateman and Grant Bigg who have always been there for me when I have needed them. Latterly, Ed Garrett has provided immeasurable support and this thesis would not exist without him so I thank him too.

As a thesis by papers the contributions and advice of my co-authors has been greatly appreciated. Thanks are therefore due to Patrick McDarby, Robin Edwards, Yvonne Milker, Fiona Hibbert, David Smith, Tom Newton, Sarah Bradley, Matthew Brain, Mike Bentley, Anthony Long, Emma Brooks, Tom Hill and Tim Daley for their contributions.

The sea-level group at York, now in full flower, have provided much needed support and smiles. I am particularly grateful to Geoff Richards who helped plant the seed and to Sophie Williams who has tended the tree for their support and friendship. Thanks to the many who helped with my fieldwork, particularly Patrick McDarby, Chris Lucas and Matt Clint and also to Richard Payne who is sadly no longer with us but continues to inspire.

Finally, my friends and family who know who they are have been rocks throughout my PhD and I thank them all for that and everything they have done for me along my wandering journey. Claire Duck has never doubted me and been there during this thesis when I have needed her despite having so many challenges of her own and so I thank her and will be eternally grateful.

2020 has been a challenging yet important year. The Black Lives Matter movement has gained much traction and has led to important conversations and actions. It became clear to me that the geologist Louis Agassiz, whom the palaeo lake Agassiz is named after, was

a deeply racist individual and it is with some discomfort that I refer to his name. In that light I use the term lake Agassiz-Ojibway and better still the abbreviation LAO whenever possible and in an ideal world I would like to see the palaeo lake renamed. I thank all those who have been undervalued by some sections of society.

Declaration

I declare that this thesis is a presentation of original work and I am the sole author. This work has not previously been presented for an award at this, or any other, University. All sources are acknowledged as References. Chapters 3–5 have been written as journal articles and have been reproduced as the original manuscripts. Co-authors have contributed to all three chapters. The contributions are given at the end of the Acknowledgements section of the chapters using the relevant CRediT roles. I performed all data collection, analysis and writing with the following notable exceptions: Patrick McDarby performed the sample preparation and counting of the modern foraminifera under my supervision as part of his BSc dissertation (Chapter 3); Tom Newton collected cores and radiocarbon samples in 2012; Mike Bentley and Anthony Long collected cores and radiocarbon samples in 2012; Tom Hill counted the diatom slides (Chapter 5); Matt Brain performed the geotechnical tests and modelling for the post-depositional lowering (Chapter 5); Mark Bateman calculated the OSL ages following my laboratory work (Chapter 5); Sarah Bradley performed the GIA modelling (Chapter 5).

Abbreviations

AMOC	Atlantic meridional overturning circulation
AMS	Accelerator mass spectrometry
boot	Bootstrapping
AIS	Antarctic Ice Sheet
cal yr BP	Calibrated years before present (where present = 1950)
DCA	Detrended correspondence analysis
DCCA	Detrended canonical correspondence analysis
DGPS	Differential global positioning system
FIS	Fennoscandian Ice Sheet
GIA	Glacial-isostatic adjustment
GMSL	Global mean sea-level
GRD	Earth gravity, Earth rotation and viscoelastic solid-Earth deformation
GrIS	Greenland Ice Sheet
HAT	Highest astronomical tide
HBIS	Hudson Bay Ice Saddle
HoF	Highest occurrence of foraminifera
ka	Thousand years before present (where present = 1950)
LAO	Lake Agassiz-Ojibway
LIS	Laurentide Ice Sheet
LOSO	Leave-one-site-out
MAT	Modern analogue technique
MHHW	Mean higher high water
MHWST	Mean high water spring tide
MinDC	Minimum dissimilarity coefficient
MTL	Mean tide level
OD	Ordnance Datum
OSL	Optically stimulated luminescence
PAM	Partitioning around medoids
RMSEP	Root mean squared error of prediction
RSL	Relative sea level
SD	Stanley chart Datum
sd	Standard deviations
SLE	Sea-level event
SLIP	Sea-level index points
SWLI	Standardised water level index
WA	Weighted averaging
WA-PLS	Weighted averaging with partial least square regression
^{14}C	Radiocarbon

Chapter 1

Introduction

1.1 Background and rationale

Rising greenhouse gas concentrations and global mean temperature is accelerating Greenland Ice Sheet (GrIS) melting and retreat (Trusel *et al.*, 2018). The resultant freshwater input into the North Atlantic is in turn driving a reduction in the Atlantic meridional overturning circulation (AMOC) that is set to continue; however, predictions of the quantity of melting and its impact on the AMOC are highly uncertain (Bakker *et al.*, 2016).

The AMOC is an ocean current system that in part transports heat northward through a warm, near-surface flow from equatorial regions. Evaporation then transfers heat from the warmer waters to the atmosphere, contributing to the moderate climate of northwest Europe relative to other regions at a similar latitude. Following evaporation, the then cooler, more saline waters sink and return southward at deeper depths before upwelling occurs in the Southern Atlantic (Buckley and Marshall, 2016). The increased freshwater inputs have interrupted the AMOC, in turn affecting reducing the northward heat transport (Drijfhout, 2015) and affecting the Earth's heat transport system (Thornalley *et al.*, 2018, Spooner *et al.*, 2020).

Global climate model simulations (e.g. Weaver *et al.*, 2012) differ from the current observations of the AMOC, limiting the reliability of future predictions. The predictive ability of climate models is limited because of uncertainties around climate sensitivity to greenhouse-gas concentration changes and AMOC changes, ice-sheet sensitivity to climate and dynamical deglacial processes, and AMOC sensitivity to climate changes and meltwater forcing (Bakker *et al.*, 2016). Studying causes and consequences of past AMOC changes can provide the nec-

essary input parameters to improve accuracy of the simulations and better understand their underlying causes.

Holocene sea-level reconstructions demonstrate that Northern Hemisphere ice sheets have undergone previous periods of melting and retreat that have been linked to AMOC reductions or possibly even a complete shut down (e.g. Ellison *et al.*, 2006). During the early Holocene, increased insolation caused the Earth's temperature to warm and the Northern Hemisphere ice sheets to retreat resulting in a global mean sea-level rise of ~ 60 m between 11,650–7,000 cal yr BP (Fig. 1.1) (Lambeck *et al.*, 2014). In the final phase of the Laurentide Ice Sheet (LIS) deglaciation between 8,200 and 7,000 BP the initially high rates of rise slowed, before progressively decreasing through the mid Holocene. Driven by anthropogenic warming, in the last century accelerated ice-sheet melting and retreat (Mouginot *et al.*, 2019, Rignot *et al.*, 2019) has increased and rates of sea-level rise have increased again (Kopp *et al.*, 2016). Fig. 1.1 highlights the general trend of ice-equivalent sea-level rise, but ice-sheet response to climate forcing was non-linear and resulted in large meltwater pulses into the oceans and thus variable rates of global sea-level rise over time that are not fully captured in the figure (Clarke *et al.*, 2004).
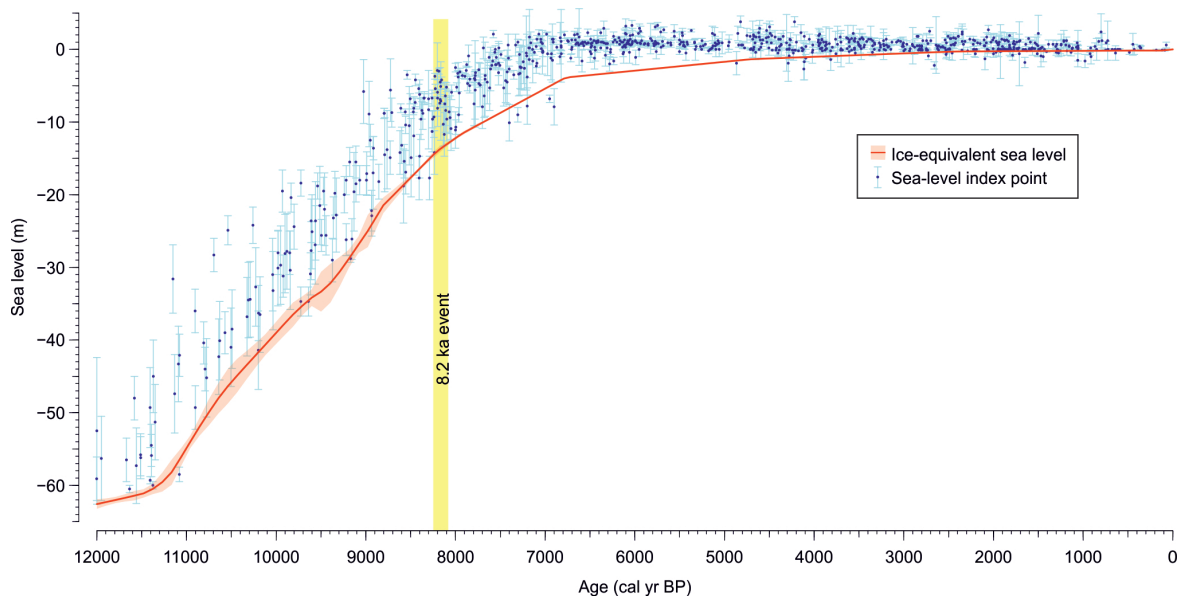
Figure 1.1: Far-field sea-level index points produced from corals and sedimentary deposits shown in blue with 2σ uncertainty given for sea level (data from Lambeck *et al.* (2014) and references provided therein). The red curve shows the simulations of ice-equivalent, or barystatic, sea-level change following glacio-isostatic modelling by Lambeck *et al.* (2014) with the 2σ accuracy estimate.

One such example of non-linear ice-sheet response occurred around 8,500 years ago during the LIS deglaciation and produced an increase in meltwater drainage into the North Atlantic that resulted in weakening, or complete shutdown, of the AMOC (Barber *et al.*, 1999). The largest AMOC change of the Holocene caused a reduction in the poleward heat transport and a climate shift known as the '8.2 ka climate event' (Daley *et al.*, 2011). The 8.2 ka climate event is a well-established climate anomaly identified in numerous palaeo reconstructions, particularly characterised by cooler temperatures around the North Atlantic region, that is believed to have been driven by meltwater pulses (e.g. Morrill *et al.*, 2013). The 8.2 ka climate event therefore provides an almost unique opportunity to study a past event in order to: 1) better understand the consequences of large-scale freshwater inputs in to the North Atlantic; 2) test the skill of climate models to produce accurate simulations of the effect on the AMOC and climate from different scenarios of freshwater input. Relative sea-level (RSL) reconstructions provide the opportunity to quantify the magnitude and timing of meltwater pulses which can then be replicated as the inputs for 'hosing experiments' in climate models. If the models produce simulations similar to the climate signal, then greater confidence can be taken in their ability to produce accurate future predictions of the effect on the AMOC and climate from different scenarios of GIS melt. The results of the study have implications for what the effect of Greenland Ice Sheet (GrIS) melt and retreat may have on the AMOC and future climate change.

Importantly, the record of the anomalously cold climate during the 8.2 ka climate event is reasonably well recognised (Morrill *et al.*, 2013). Ice-core records show a period of ~ 160 years with a $\sim 5°$ cooling (Thomas *et al.*, 2007) in Greenland. Anomalous cooling is also seen in regions from the Gulf of Mexico (Ellwood and Gose, 2006), across much of Europe (see Morrill *et al.*, 2013, for references therein) to east Asia (Park *et al.*, 2018). Proxy reconstructions also demonstrate a reorganisation of precipitation patterns in both the North Atlantic region and further afield, particularly in monsoonal regions (Cheng *et al.*, 2009). Although the climate signal is well recognised and the cause is believed to be known, uncertainties around the timing, magnitude and location of the meltwater forcing persist. Resolving these uncertainties would increase understanding of internal processes in the climate system and aid the applicability of the 8.2 ka climate event to test models that simulate these processes.

The cause of the 8.2 ka climate event was first attributed to drainage of the coalesced pro-glacial lakes Agassiz-Ojibway (LAO) through Hudson Bay into the North Atlantic by

Alley *et al.* (1997) and supported with field data by Barber *et al.* (1999). Evidence from marine sediment cores (Ellison *et al.*, 2006, Hillaire-Marcel *et al.*, 2007, Kleiven *et al.*, 2008) and relative sea-level (RSL) records (Hijma and Cohen, 2010, Li *et al.*, 2012) suggested the lake drained twice. Ice-sheet modelling also demonstrated that LAO drainage events were likely supplemented by a more sustained freshwater contribution from the collapse of the Hudson Bay Ice Saddle (HBIS) (Gregoire *et al.*, 2012, Matero *et al.*, 2020). Based on marine, terrestrial and RSL records it has been suggested that the combination of the HBIS and LAO may even have produced a three-phase drainage model (Jennings *et al.*, 2015, Lawrence *et al.*, 2016, Lochte *et al.*, 2019, Gauthier *et al.*, 2020). However, uncertainties remain about possible contributions from the Greenland and Antarctic ice sheets.

Evidence for the meltwater pulse(s) has not only come from marine cores and RSL records, but also from terrestrial geomorphology and ice-sheet modelling. RSL reconstructions are important and stand out, as they can be used to quantify the magnitude of the meltwater pulse and, in combination with numerical modelling (e.g. Kendall *et al.*, 2008), the origin of the freshwater. Meltwater pulses generate changes in Earth gravity, Earth rotation and viscoelastic solid-Earth deformation (GRD), resulting in the ice-ocean mass flux being redistributed from the mean in a predictable geographic pattern of sea-level rise, or a barystatic-GRD 'fingerprint', which can be numerically modelled (Mitrovica *et al.*, 2001). Based on this, a RSL rise from a specific point can be appropriately scaled to quantify the global mean. Furthermore, comparisons of various modelled barystatic-GRD fingerprints allow hypotheses pertaining to the meltwater source to be tested. The barystatic-GRD fingerprint produced following drainage of LAO at 8,400 cal yr BP through Hudson Bay has been modelled by Kendall *et al.* (2008) and enables the meltwater magnitude to be quantified from RSL reconstructions at suitable locations (Fig. 1.2).

To date, well-resolved RSL reconstructions from the USA (Li *et al.*, 2012), the Netherlands (Hijma and Cohen, 2010, 2019) and Scotland (Lawrence *et al.*, 2016) have produced quantifications of the magnitude and timing of the meltwater pulse(s) but they remain unresolved because of different inherent uncertainties within the records, inconsistent methodologies, and lack of far-field data. The latter is particularly important, because the RSL rise in the Southern Hemisphere will be much larger than in the North Atlantic if the drainage emanated from the LIS (see Fig. 1.2). On the other hand, if Antarctica provided a significant contemporaneous meltwater contribution then the difference would be reduced or even

reversed.
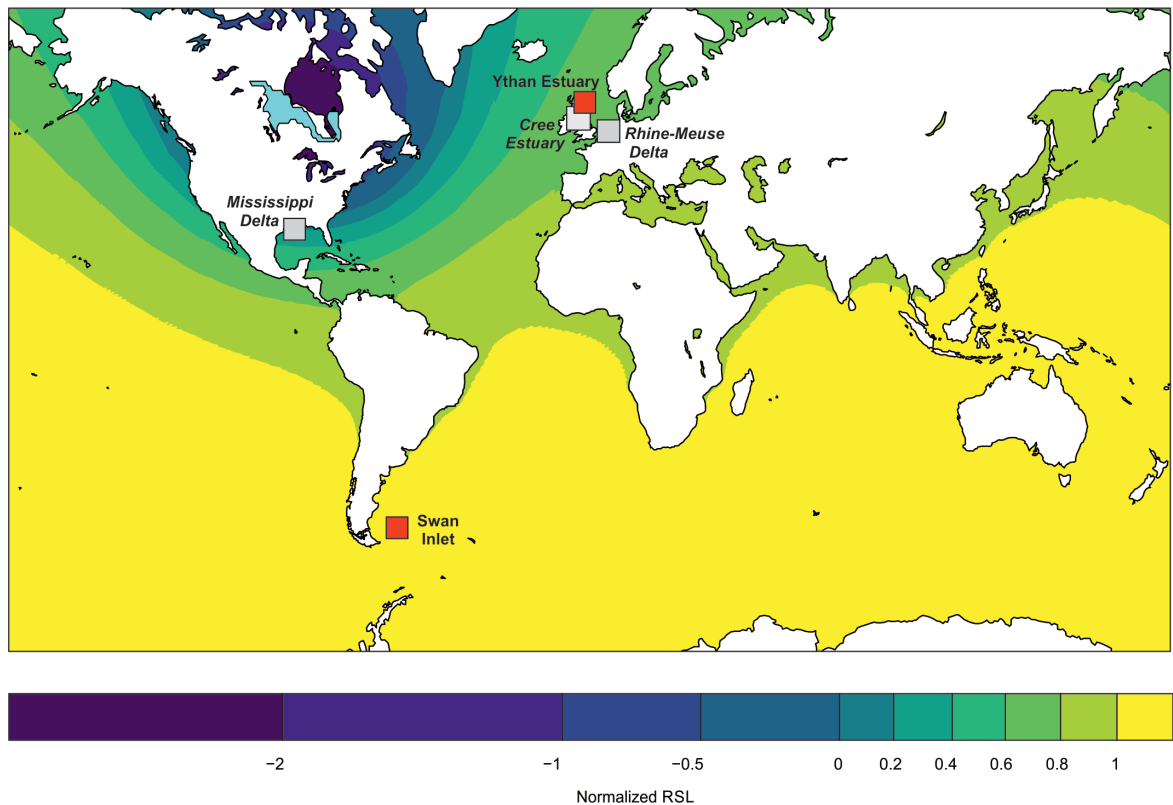
Figure 1.2: Numerically predicted Barystatic-GRD fingerprint following the drainage of LAO at 8400 cal yr BP, normalized by the global mean sea-level rise (0.4 m) by Kendall et al. (2008). The blue contours show the zone of predicted sea-level fall; the remaining contours are regions of progressively higher sea-level rise. The grey boxes represent sites of previous sea-level reconstructions referred to in the text and the red boxes are the study sites in this research. (Adapted from: Kendall et al. (2008))

To address the uncertainties in the timing, magnitude and location of the meltwater pulses this study will, for the first time, compare the early-Holocene RSL histories of a North and South Atlantic site, using a consistent methodology. Inter-tidal sediments and microfossils from the Ythan Estuary in eastern Scotland and Swan Inlet in the Falkland Islands are used to reconstruct RSL in order to constrain the drivers of the 8.2 ka climate event.

The Ythan Estuary was selected as a near-field site based on previous work by Smith *et al.* (1983, 1999, 2013), described in Chapter 2.4, that appears to show a RSL rise of at least 2 m between c. 8,500 and 8,200 cal yr BP. Swan Inlet was similarly selected based on previous work and described in Chapter 2.4 as a far-field site. Based on stratigraphical interpretations and range finder ^{14}C dates, Newton (2016) demonstrated that a widespread

drowning event occurred c. 8,400 cal yr BP, with an estimated magnitude of around 1 m based on sediment thickness alone. The ^{14}C dates and stratigraphy from previous work at both sites suggests that the same sea-level event is registered but higher resolution chronologies and reconstruction of RSL change is required to constrain the events within them.

1.2   Aims and objectives

The overall aim of this study is to test hypotheses pertaining to the source of the meltwater that drove the 8.2 ka climate event, namely:

1. That there was only one meltwater pulse in the centuries leading up to the 8.2 ka climate event.

2. That LAO was the source of the meltwater pulse(s) without contributions from the HBIS.

3. That the origin of the meltwater pulse(s) was the (LIS).

In order to test these hypotheses the following objectives are addressed in the listed chapters:

- Review the current understanding of the 8.2 ka climate event and its drivers (Chapter 2).

- Develop a dataset of modern microfossils and a sea-level transfer function for the Ythan Estuary in eastern Scotland (Chapter 3).

- Reconstruct RSL change for the Ythan Estuary in eastern Scotland at a high resolution for the period of interest prior to the 8.2 climate event (Chapter 4).

- Reconstruct Holocene RSL change for Swan Inlet in the Falkland Islands and quantify the local and global magnitude of meltwater pulses for the first time from a Southern Hemisphere site (Chapter 5).

- Compare the results from the Ythan Estuary and Swan Inlet to ultimately test the three hypotheses (Chapter 6).

1.3 Thesis structure

The three main Chapters (chapters 3–5) are journal manuscripts, two of which were under review at the time of submission of this thesis and the third is to be submitted once co-authors have had the chance to respond and contribute to a final draft. Here I outline the content of each chapter.

Chapter 2: "Literature review" reviews the scientific literature to present the current understanding of areas that are important to the thesis, namely: the early-Holocene sea-level rise; the 8.2 ka climate event and its drivers; and the two study sites.

Chapter 3: "Development of an inter-tidal foraminifera training set for the North Sea and an assessment of its application for Holocene sea-level reconstructions" was submitted to Marine Micropaleontology in September 2020. The main objective of the chapter in the context of this thesis is to develop a foraminifera transfer function that could be used in Chapter 4. A modern training set is developed for the Ythan Estuary and integrated with others from around the North Sea to develop a regional training set. It goes on to demonstrate the most effective transfer function and develops a method that can be applied in other settings using a range of quantitative and qualitative approaches to make the decision as to which transfer function model is most suitable.

Chapter 4: "Relative sea-level reconstruction for the Ythan Estuary, eastern Scotland, and implications for the cause of the 8.2 ka climate event" was submitted to Quaternary Science Reviews in November 2020. The chapter presents a RSL reconstruction for the Ythan Estuary for the period 8,770–8,130 cal yr BP. Periods of elevated rates of sea-level rise are identified that enable the magnitude of meltwater pulses to be quantified. From this record, combined with wider evidence the chapter addresses the first and third hypotheses of the thesis.

Chapter 5: "Holocene relative sea-level reconstruction for the Falkland Islands (Islas Malvinas)" is intended for submission to The Holocene. The chapter presents a dataset of sea-level index points for the Falkland Islands from 8,500 cal yr BP to present day. A RSL reconstruction provides evidence of long-term changes that are compared to GIA predictions and other regional RSL reconstructions. A palaeogeographic reconstruction aids the study of possible sea-level events prior to the 8.2 ka climate event.

Chapter 6: "Conclusions" synthesises the work presented in the previous chapters and links the research back to the three hypotheses. Suggestions are made for directions of future

work following this study.

References

Alley, R. B., Mayewski, P. A., Sowers, T., Stuiver, M., Taylor, K. C. and Clark, P. U. (1997), 'Holocene climatic instability: A prominent, widespread event 8200 yr ago', *Geology* **25**(6), 483–486.

Bakker, P., Schmittner, A., Lenaerts, J., Abe-Ouchi, A., Bi, D., van den Broeke, M., Chan, W.-L., Hu, A., Beadling, R., Marsland, S. *et al.* (2016), 'Fate of the atlantic meridional overturning circulation: Strong decline under continued warming and greenland melting', *Geophysical Research Letters* **43**(23), 12–252.

Barber, D. C., Dyke, A., Hillaire-Marcel, C., Jennings, A. E., Andrews, J. T., Kerwin, M. W., Bilodeau, G., McNeely, R., Southon, J., Morehead, M. D. and Gagnon, J. M. (1999), 'Forcing of the cold event of 8,200 years ago by catastrophic drainage of Laurentide lakes', *Nature* **400**(6742), 344–348.

Buckley, M. W. and Marshall, J. (2016), 'Observations, inferences, and mechanisms of the atlantic meridional overturning circulation: A review', *Reviews of Geophysics* **54**(1), 5–63.

Cheng, H., Fleitmann, D., Edwards, R. L., Wang, X., Cruz, F. W., Auler, A. S., Mangini, A., Wang, Y., Kong, X., Burns, S. J. and Matter, A. (2009), 'Timing and structure of the 8.2. kyr B.P. event inferred from δ 18O records of stalagmites from China, Oman, and Brazil', *Geology* **37**(11), 1007–1010.

Clarke, G. K. C., Leverington, D. W., Teller, J. T. and Dyke, A. S. (2004), 'Paleohydraulics of the last outburst flood from glacial Lake Agassiz and the 8200 BP cold event', *Quaternary Science Reviews* **23**(3-4), 389–407.

Daley, T. J., Thomas, E. R., Holmes, J. A., Street-Perrott, F. A., Chapman, M. R., Tindall, J. C., Valdes, P. J., Loader, N. J., Marshall, J. D., Wolff, E. W., Hopley, P. J., Atkinson, T., Barber, K. E., Fisher, E. H., Robertson, I., Hughes, P. D. and Roberts, C. N. (2011), 'The 8200yr BP cold event in stable isotope records from the North Atlantic region', *Global and Planetary Change* **79**(3-4), 288–302.

Drijfhout, S. (2015), 'Competition between global warming and an abrupt collapse of the amoc in earth's energy imbalance', *Scientific reports* **5**(1), 1–12.

Ellison, C. R. W., Chapman, M. R. and Hall, I. R. (2006), 'Surface and deep ocean interactions during the cold climate event 8200 years ago', *Science* **312**(5782), 1929–1932.

Ellwood, B. B. and Gose, W. A. (2006), 'Heinrich H1 and 8200 yr B.P. climate events recorded in Hall's Cave, Texas', *Geology* **34**(9), 753–756.

Gauthier, M. S., Kelley, S. E. and Hodder, T. J. (2020), 'Lake Agassiz drainage bracketed Holocene Hudson Bay Ice Saddle collapse', *Earth and Planetary Science Letters* **544**, 116372.

Gregoire, L. J., Payne, A. J. and Valdes, P. J. (2012), 'Deglacial rapid sea level rises caused by ice-sheet saddle collapses', *Nature* **487**(7406), 219–222.

Hijma, M. P. and Cohen, K. M. (2010), 'Timing and magnitude of the sea-level jump preluding the 8200 yr event', *Geology* **38**(3), 275–278.

Hijma, M. P. and Cohen, K. M. (2019), 'Holocene sea-level database for the Rhine-Meuse Delta, The Netherlands: Implications for the pre-8.2 ka sea-level jump', *Quaternary Science Reviews* **214**, 68–86.

Hillaire-Marcel, C., de Vernal, A. and Piper, D. J. W. (2007), 'Lake Agassiz final drainage event in the northwest North Atlantic', *Geophysical Research Letters* **34**(15).

Jennings, A., Andrews, J., Pearce, C., Wilson, L. and Olfasdotttir, S. (2015), 'Detrital carbonate peaks on the Labrador shelf, a 13-7 ka template for freshwater forcing from the Hudson Strait outlet of the Laurentide Ice Sheet into the subpolar gyre', *Quaternary Science Reviews* **107**, 62–80.

Kendall, R. A., Mitrovica, J. X., Milne, G. A., Tornqvist, T. E. and Li, Y. X. (2008), 'The sea-level fingerprint of the 8.2 ka climate event', *Geology* **36**(5), 423–426.

Kleiven, H. F., Kissel, C., Laj, C., Ninnemann, U. S., Richter, T. O. and Cortijo, E. (2008), 'Reduced North Atlantic Deep Water coeval with the glacial Lake Agassiz freshwater outburst', *Science* **319**(5859), 60–64.

Kopp, R. E., Kemp, A. C., Bittermann, K., Horton, B. P., Donnelly, J. P., Gehrels, W. R., Hay, C. C., Mitrovica, J. X., Morrow, E. D. and Rahmstorf, S. (2016), 'Temperature-driven global sea-level variability in the Common Era', *Proceedings of the National Academy of Sciences of the United States of America* **113**(11), E1434–E1441.

Lambeck, K., Rouby, H., Purcell, A., Sun, Y. Y. and Sambridge, M. (2014), 'Sea level and global ice volumes from the Last Glacial Maximum to the Holocene', *Proceedings of the National Academy of Sciences of the United States of America* **111**(43), 15296–15303.

Lawrence, T., Long, A. J., Gehrels, W. R., Jackson, L. P. and Smith, D. E. (2016), 'Relative sea-level data from southwest Scotland constrain meltwater-driven sea-level jumps prior to the 8.2 kyr BP event', *Quaternary Science Reviews* **151**, 292–308.

Li, Y. X., Törnqvist, T. E., Nevitt, J. M. and Kohl, B. (2012), 'Synchronizing a sea-level jump, final Lake Agassiz drainage, and abrupt cooling 8200 years ago', *Earth and Planetary Science Letters* **315**, 41–50.

Lochte, A. A., Repschlaeger, J., Kienast, M., Garbe-Schoenberg, D., Andersen, N., Hamann, C. and Schneider, R. (2019), 'Labrador Sea freshening at 8.5 ka BP caused by Hudson Bay Ice Saddle collapse', *Nature Communications* **10**(1), 1–9.

Matero, I. S. O., Gregoire, L. J. and Ivanovic, R. F. (2020), 'Simulating the Early Holocene demise of the Laurentide Ice Sheet with BISICLES', *Geoscientific Model Development* **13**(9), 4555–4577.

Mitrovica, J. X., Tamisiea, M. E., Davis, J. L. and Milne, G. A. (2001), 'Recent mass balance of polar ice sheets inferred from patterns of global sea-level change', *Nature* **409**(6823), 1026–1029.

Morrill, C., Anderson, D. M., Bauer, B. A., Buckner, R., Gille, E. P., Gross, W. S., Hartman, M. and Shah, A. (2013), 'Proxy benchmarks for intercomparison of 8.2 ka simulations', *Climate of the Past* **9**(1), 423–432.

Mouginot, E., Rignot, E., Bjørk, A. A., van den Broeke, M., Millan, R., Morlighem, M., Nö el, B., Scheuchl, B. and Wood, M. (2019), 'Forty-six years of Greenland Ice Sheet mass balance from 1972 to 2018', *Proceedings of the National Academy of Sciences* **116**(19), 9239–9244.

Newton, T. (2016), Holocene and Common Era sea-level changes in the Falkland Islands, PhD thesis, Plymouth University.

Park, J., Park, J., Yi, S., Kim, J. C., Lee, E. and Jin, Q. (2018), 'The 8.2 ka cooling event in coastal East Asia: High-resolution pollen evidence from southwestern Korea', *Scientific reports* **8**(1), 1–9.

Rignot, E., Erémieer´erémie Mouginot, J. , Scheuchl, B., van den Broeke, M., Van Wessem, M. J., Morlighem, M., Forster, R. R., Stearns, L. A., Mouginot, J., Scheuchl, B., van den Broeke, M., Van Wessem, M. J. and Morlighem, M. (2019), 'Four decades of Antarctic Ice Sheet mass balance from 1979–2017', *Proceedings of the National Academy of Sciences* **116**(4), 1095–1103.

Smith, D. E., Cullingford, R. A. and Brooks, C. L. (1983), 'Flandrian relative sea-level changes in the Ythan Valley, northeast Scotland', *Earth Surface Processes and Landforms* **8**(5), 423–438.

Smith, D. E., Firth, C. R., Brooks, C. L., Robinson, M. and Collins, P. E. F. (1999), 'Relative sea-level rise during the Main Postglacial Transgression in NE Scotland, UK', *Transactions of the Royal Society of Edinburgh-Earth Sciences* **90**, 1–27.

Smith, D. E., Harrison, S. and Jordan, J. T. (2013), 'Sea level rise and submarine mass failures on open continental margins', *Quaternary Science Reviews* **82**, 93–103.

Spooner, P. T., Thornalley, D. J. R., Oppo, D. W., Fox, A. D., Radionovskaya, S., Rose, N. L., Mallett, R., Cooper, E. and Roberts, J. M. (2020), 'Exceptional 20th Century Ocean Circulation in the Northeast Atlantic', *Geophysical Research Letters* **47**(10).

Thomas, E. R., Wolff, E. W., Mulvaney, R., Steffensen, J. P., Johnsen, S. J., Arrowsmith, C., White, J. W. C., Vaughn, B. and Popp, T. (2007), 'The 8.2 ka event from Greenland ice cores', *Quaternary Science Reviews* **26**(1-2), 70–81.

Thornalley, D. J., Oppo, D. W., Ortega, P., Robson, J. I., Brierley, C. M., Davis, R., Hall, I. R., Moffa-Sanchez, P., Rose, N. L., Spooner, P. T., Yashayaev, I. and Keigwin, L. D. (2018), 'Anomalously weak Labrador Sea convection and Atlantic overturning during the past 150 years', *Nature* **556**(7700), 227–230.

Trusel, L. D., Das, S. B., Osman, M. B., Evans, M. J., Smith, B. E., Fettweis, X., McConnell, J. R., Noël, B. P. and van den Broeke, M. R. (2018), 'Nonlinear rise in Greenland runoff in response to post-industrial Arctic warming'.

Weaver, A. J., Sedláček, J., Eby, M., Alexander, K., Crespin, E., Fichefet, T., Philippon-Berthier, G., Joos, F., Kawamiy, M., Matsumoto, K., Steinacher, M., Tachiiri, K., Tokos,

K., Yoshimori, M. and Zickfeld, K. (2012), 'Stability of the Atlantic meridional overturning circulation: A model intercomparison', *Geophysical Research Letters* **39**(20).

Chapter 2

Literature review

2.1 Introduction

This chapter reviews the literature relevant to the aims of this thesis. The trend of global early-Holocene sea-level rise are assessed to provide context for the background rates of sea level and introduce some of the concepts related to Holocene relative sea-level (RSL) reconstructions. The climate changes that mark the 8.2 ka climate event are described, followed by a discussion of the hypothesised cause of the event. The existing evidence for drainage events originating from the Laurentide Ice Sheet are presented that will demonstrate the accumulated knowledge and also the uncertainty of the proposed drainage events. Finally, previous investigations in the Ythan Estuary and Swan Inlet are discussed providing background and rationale for their selection.

2.2 Early Holocene sea-level rise

Following the Younger Dryas at 11,600 cal yr BP, a stadial (Dansgaard *et al.*, 1989) which marks the start of the Holocene (Walker *et al.*, 2012), atmospheric temperatures rose driven by increased insolation. In Greenland a rapid 40 year climate transition is recorded (Steffensen *et al.*, 2008) that was followed by a longer period of warming, with data from ice cores suggesting a rise of c. 15 °C over 1,500 years (Taylor *et al.*, 1997). This rate of warming, ~ 1 °C every 100 years in contemporary terms, is similar to that of the last century (Marcott *et al.*, 2013). As a consequence of the warming, significant ice-sheet retreat occurred (Carlson and Clark, 2012), producing an apparent global mean sea-level (GMSL) rise of around 60 m

(Fairbanks, 1989) that was punctuated by periods of more rapid sea-level rise (Bird *et al.*, 2010). Marked deceleration in rates of GMSL rise corresponds to the ultimate decay of the Laurentide Ice Sheet (LIS) (Carlson *et al.*, 2008). The term early Holocene is used here to describe this period of GMSL rise from 11,640–7,000 cal yr BP (thousand years before present, where present is 1,950) following Smith *et al.* (2011) and Törnqvist *et al.* (2012).

The principal sources of early-Holocene GMSL rise were the Fennoscandian Ice Sheet (FIS), the Antarctic Ice Sheet (AIS) and the LIS; however, the relative contribution of each is not fully resolved (Carlson and Clark, 2012). Geological mapping of the FIS (Stroeven *et al.*, 2016) and the LIS (Dyke, 2004, Dalton *et al.*, 2020) along with ice-sheet modelling (e.g. Ullman *et al.*, 2016) agree with previous estimates (see Carlson and Clark, 2012, for a review) and suggest that the relative contributions of the FIS and LIS to GMSL were $\sim$ 3–5 m and 25–35 m respectively. There remains considerable debate over the contribution of the AIS and the processes behind it, but it appears unlikely to exceed 15 m (e.g. Anderson *et al.*, 2002, Whitehouse *et al.*, 2012, Argus *et al.*, 2014, Bentley *et al.*, 2014, Briggs *et al.*, 2014, Lambeck *et al.*, 2014, Pollard *et al.*, 2015, DeConto and Pollard, 2016, Edwards *et al.*, 2019, Gomez *et al.*, 2020). The disparity between the total relative contributions and the 60 m of GMSL rise (Fairbanks, 1989) may also be explained by inaccurate sea-level data as discussed below or steric components.

As the most recent period of broadly similar environmental conditions to present, such that driven by a warming climate rates of sea-level rise were similar to the last century, Abe-Ouchi *et al.* (2010) state that the early Holocene may be key to understanding future sea-level rise. Despite this, there is a shortage of empirically-based sea-level reconstructions for the full period, primarily due to two main difficulties: 1) coral reef based reconstructions (e.g. Fairbanks, 1989, Bard *et al.*, 1996) have difficulties associated with temporal resolution (Camoin and Webster, 2015) and limited resolution after 10,000–9,000 cal yr BP (Törnqvist *et al.*, 2012); 2) data density within sedimentary archives decreases dramatically before 8,000–6,000 cal yr BP associated with difficulties accessing older coastal sediments in suitable regions (Engelhart *et al.*, 2011).

Because of overlapping processes related to local and regional responses of the solid earth to the ice-ocean mass flux and the redistribution of water away from the global mean, GMSL rise cannot be measured directly at a single location; rather, the RSL, the height of the ocean surface relative to the land surface or ocean floor, is recorded. Following deglaciation, at near-

field sites, i.e. in regions close to the former ice-sheet centres, glacio-isostactic adjustment (GIA) dominates RSL either through uplift or forebulge collapse, such as in the UK (Shennan *et al.*, 2018). In the far field, i.e. away from ice-sheet centres, the barystatic sea-level change resulting from the ice-ocean flux becomes dominant and these regions are more appropriate for recording GMSL rise, although no location on Earth is truly stable in GIA terms. (Milne and Mitrovica, 2008). The barystatic sea-level rise (defined by Gregory *et al.* (2019) as "the part of global-mean sea-level rise which is due to the addition to the ocean of water mass that formerly resided within the land area or in the atmosphere"), is redistributed from the mean because of changes in Earth gravity and Earth rotation on top of the solid Earth deformation (GRD). This produces a distinctive and highly varied geographic pattern of sea-level change, or 'barystatic-GRD fingerprint' (Mitrovica *et al.*, 2001, Gregory *et al.*, 2019). Hydro-elastic deformation as a result of the flooding of continental shelves and loading from increased ocean mass also impact RSL change (e.g. ocean siphoning and continental levering (Lambeck and Nakada, 1990, Mitrovica and Milne, 2002)), although these effects became relatively more important in the mid and late Holocene.

Although GMSL rise cannot be directly measured, Lambeck *et al.* (2014) synthesise early-Holocene reconstructions from far-field locations and argue that a similar, near-uniform global rise between 11,600 and 8,200 cal yr BP of ~ 1.5 cm yr^{-1} is detected, followed by a reduced rate through to the end of the early Holocene. The oft reported early-Holocene sea level rise of 60 m (e.g. Smith *et al.*, 2011) is based on original work by in Barbados by Fairbanks (1989) and latterly supplemented by Peltier and Fairbanks (2006) and work in Tahiti (Bard *et al.*, 1996, 2010). The reconstructions are based on assumptions of coral accumulation and environmental conditions of formation, which Hibbert *et al.* (2016) show may not always be accurate. It is also assumed that the regions of Barbados and Tahiti respectively are free from isostatic uplift and approximations of tectonic related uplift are made that others suggest may not be correct (Milne and Mitrovica, 2008, Gehrels, 2010). Sedimentary archives from the South China Sea (Xiong *et al.*, 2018) and the Sunda Shelf (Hanebuth *et al.*, 2011) show that the sea-level change in these regions are in agreement with the Barbados and Tahiti curves providing support that the Barbados and Tahiti reconstructions provide reasonable evidence of a general trend of rates of GMSL change, although large uncertainties evidently exist. It may therefore be that the 60 m of sea-level rise is an over-estimation, which would reconcile the disparity between the data and the total estimated

ice-sheet contribution.

Sea-level reconstructions from regions where GIA is a major factor are still important as they enable the assessment of the contributions of individual ice-sheets (e.g. Engelhart *et al.*, 2011, Shennan *et al.*, 2018). Indeed many of these archives demonstrate that as well as spatial variability, temporal variability in the rates of GMSL rise was also a feature of the early Holocene (Lambeck *et al.*, 2014). As a consequence of non-linear ice-sheet retreat periods of rapid sea-level rise punctuated the early-Holocene sea-level rise (Smith *et al.*, 2011).

Periods of rapid sea-level rise have been identified at 11,300, 9,200, 8,400 and 7,600 cal yr BP (Harrison *et al.*, 2018) and have been termed 'meltwater pulses' (Fairbanks, 1989), 'catastrophic reef events' and 'sea-level jumps' (Hijma and Cohen, 2010). The first apparent early-Holocene rapid sea-level rise, observed by Fairbanks (1989), is centred at 11,300 cal yr BP (MWP-1B) and has been quantified by Abdul *et al.* (2016) as a 14 ± 2 m rise in Barbados at 11,450–11,100 cal yr BP, with rates approaching 40 mm yr^{-1}. The absence of MWP-1B in the Tahiti record led Bard *et al.* (2010) to question its occurrence in Barbados as an artefact of accelerated uplift rates of the two different cores. However, Abdul *et al.* (2016) argue that there is no evidence of an offshore fault line or episodic vertical movement and that even double the accepted uplift would still have a negligible impact; rather, that the absence of MWP-1B in Tahiti is a consequence of a lack of resolution for the relevant period and inappropriate coralgal assemblages. Further evidence is observed in a number of global records as synthesised by Dlabola *et al.* (2015), adding credence to the existence of MWP-1B, although its duration may have been centuries to millennia (Stanford *et al.*, 2011). The cause was attributed to retreating Northern Hemisphere ice sheets in a delayed response to the northward retreat of the polar front following the termination of the Younger Dryas (Abdul *et al.*, 2016). However, modelled rapid Antarctic ice-sheet retreat between 12,400 and 11,400 cal yr BP (Golledge *et al.*, 2014) and geological evidence of increased Antarctic iceberg rafted debris at 11,300 cal yr BP (Weber *et al.*, 2014) suggests that an Antarctic contribution to MWP-1B may well be significant.

A period of rapid sea-level rise around 9,300 cal yr BP was termed 'MWP-1C' by Liu *et al.* (2004) based on sedimentary evidence in China. An apparent climate anomaly at 9,200 cal yr BP has been linked to the MWP-1C (Fleitmann *et al.*, 2008, Zhang *et al.*, 2018) producing a similar, though notably smaller, effect as the 8.2 ka climate event discussed in

section 2.3. However, further studies from the region suggest that the higher rates of sea-level rise persisted for a longer period (e.g. Xiong *et al.*, 2018). Evidence is lacking from elsewhere and led Smith *et al.* (2011) to suggest that the occurrence of a specific event is questionable, while Stanford *et al.* (2011) argue that the rise is all encompassed by MWP-1B. It appears hard to define MWP-1C as a specific event, but the size of both the climate anomaly and the meltwater pulse make them hard to identify and may thus result in the above conclusions. It is also notable that in the literature 'MWP-1C' is occasionally confused with the later rapid rise c 8,400 cal yr BP prior to the 8.2 ka climate event (Cooper *et al.*, 2016, 2019).

The third period of rapid sea-level rise that has been termed a sea-level jump precedes the 8.2 ka climate event. Well-resolved reconstructions show evidence of rapid sea-level rise around the North Atlantic (Törnqvist *et al.*, 2004, Hijma and Cohen, 2010, 2019, Li *et al.*, 2012, Lawrence *et al.*, 2016) and is supplemented by less well-resolved records from further afield (e.g. De Lecea *et al.*, 2017, Wang *et al.*, 2013). The details of this are discussed in section 2.3.

Finally, a rapid sea-level rise at c. 7,600 cal yr BP, first identified by Blanchon and Shaw (1995) as reef drowning, has been quantified from isolation basin studies in the Baltic Sea as a local sea-level rise of ~ 4.5 m (Yu *et al.*, 2007). The timing coincides with a similar rise recorded in China by Liu *et al.* (2004) that they termed MWP-1D, and linked to a drop in sea-surface salinity in the Black Sea (Herrle *et al.*, 2018). The evidence for a rapid sea-level rise is compelling, although there is no evidence as to the source of a barystatic sea-level rise.

It is evident that the rate of early-Holocene sea-level rise was highly variable, but evidence of specific events or 'meltwater pulses' appears inconclusive, which may in part be due to challenges identifying them during a time of generally high rates (Harrison *et al.*, 2018). This also raises the question of how to define periods of rapid sea-level rise. The debate about the duration of MWP-1B, the occurrence and possible misuse of MWP-1C show that currently there appears to be no consensus. Furthermore the term 'sea-level jump' was coined to describe "an abrupt, annual to decadal-scale sea-level rise" (Törnqvist *et al.*, 2012), but seems to relate to a very specific type of stratigraphic evidence whereby sea level literally appears to jump from one elevation to the next with no record in between. Even when change is rapid, sea level does not simply jump from one point to another, and so this definition is unsatisfactory. I use the term 'sea-level event' (SLE) as described in chapter 4.1

to encompass a decadal to centennial-scale anomalous period of RSL rise relative to longer term rise which may be subsequently linked back to a meltwater pulse.

2.3 The 8.2 ka climate event

2.3.1 Records of the climate anomaly

The 8.2 ka climate event is recognised as a prominent climate anomaly (Alley *et al.*, 1997) that lasted 160.5 ± 5.5 yr, beginning c. 8,250 cal yr BP, with a 'central event' lasting 69 ± 2 yr, beginning c. 8,220 cal yr BP (Fig. 2.1a) (Kobashi *et al.*, 2007, Thomas *et al.*, 2007, Cheng *et al.*, 2009). First identified in Greenland ice-core records by Dansgaard (1987), the event has been further constrained by oxygen and nitrogen isotope analysis, such that an abrupt cooling of 3.3 ± 1.1 °C and an 8 % reduction in precipitation in Greenland is registered (Kobashi *et al.*, 2007, Thomas *et al.*, 2007). The cooling signal is contemporaneously observed in palaeoclimate proxies around the North Atlantic region, as well as both increasing and decreasing amounts of precipitation more locally to the region (see Morrill *et al.*, 2013, for references therein), establishing it as the largest climate anomaly of the Holocene in the region (Daley *et al.*, 2011).

The 8.2 ka climate event is often referred to in relation to North Atlantic climate (e.g. Daley *et al.*, 2011), but a geographically wider climate event does appear to be observed in other regions. Notably, an anomalous cooling is observed in east Asia (Park *et al.*, 2018) and changes in the position and strength of monsoons. Cheng *et al.* (2009) describe changes in the South American summer monsoon recorded in speleothems that are coeval with the event. In Asia, monsoon changes are expressed in speleothem records (Wu *et al.*, 2012, Liu and Hu, 2016) and sediment records from the Okinawa Trough (Yu *et al.*, 2008). Ljung *et al.* (2008) also observed a prominent increase in precipitation on Tristan de Cunha, in the South Atlantic, at 8,280–8,030 cal yr BP which they attribute to warmer sea surface temperatures owing to heat accumulation in the South Atlantic. A shift in the Intertropical Convergence Zone appears likely to have caused widespread precipitation changes.

Whether the climate event can be considered 'global' is ambiguous. For example, the suggested evidence of Antarctic environmental change, including temperature decreases, in the EPICA Dome C ice core (Stenni *et al.*, 2001, 2004, Röthlisberger *et al.*, 2002, Jouzel *et al.*, 2007) is in isolation compared to other Antarctic cores and should therefore be treated with

caution. Stenni *et al.* (2001) argue that an "increased southern latitudinal temperature gradient [between 9,000 and 8,000 cal yr BP] is in phase with the last abrupt decay of the Laurentide ice cap at 8,200 cal yr BP" this appears somewhat erroneous considering the beginning (c. 8,250 cal yr BP) and the duration (c. 160 yrs) of the event recorded in Greenland. Although the climate seems to not have changed globally, widespread and varied climate change does seem apparent and thus I use '8.2 ka climate event' throughout this thesis as opposed to the sometimes used '8.2 ka cold event' (e.g. Hede *et al.*, 2010, Bondevik *et al.*, 2012).

2.3.2   The driver of the climate event

The cause of the 8.2 ka climate event has been attributed to a weakening, or complete shutdown, of the Atlantic meridional overturning circulation (AMOC) reducing the poleward heat transport (Alley *et al.*, 1997) as a result of density-driven changes in circulation caused by increased freshwater drainage through the Hudson Strait (Barber *et al.*, 1999). Barber *et al.* (1999) provided evidence of a large freshwater input into the North Atlantic from the coalesced proglacial lake Agassiz-Ojibway (LAO) that they proposed forced the hypothesised AMOC weakening. The work dated the freshwater release at c. 8,470 cal yr BP due to an anomalous marine ^{14}C reservoir effect, furthering work by Andrews *et al.* (1999) that had identified a 'red bed' in Hudson Strait that shared a common source with red glacial deposits in the sediments from the former LAO basin. The proposed lake drainage appeared to be supported by evidence of a single rapid sea-level rise in the Mississippi Delta at 8,310–8,180 cal yr BP (Törnqvist *et al.*, 2004, Li *et al.*, 2012) (Fig. 2.1e) and a reduction in Lower North Atlantic Deep Water influence around 8,380–8,270 cal yr BP (Kleiven *et al.*, 2008). However, problems with this single drainage hypothesis were consistently identified by global climate models failing to simulate the magnitude and duration of the climate event from a single forcing event alone (LeGrande *et al.*, 2006, Wiersma *et al.*, 2006). Furthermore, more recent evidence suggests a more complex sequence of drainage events.
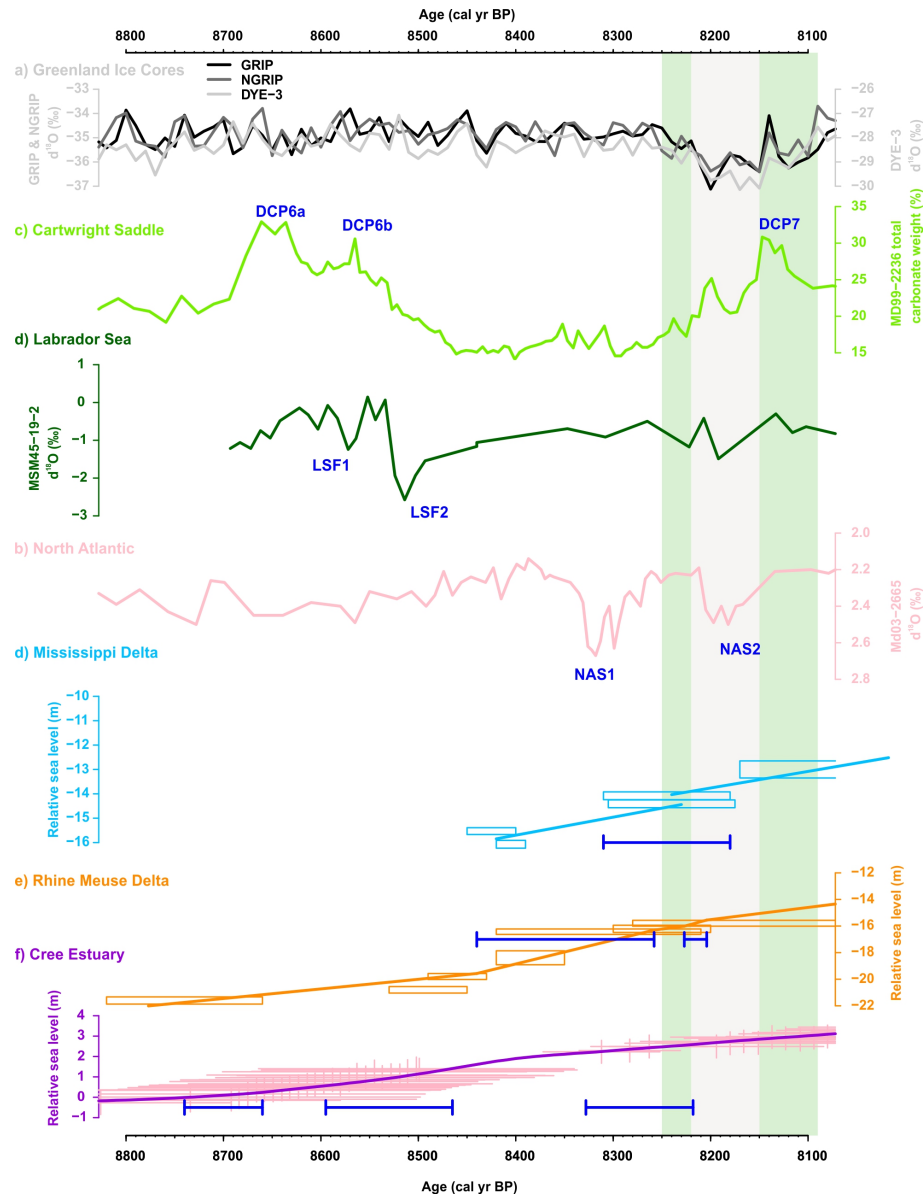
Figure 2.1: Proxy records of climate, oceanography and sea level related to the 8.2 ka climate event. a) Greenland ice cores which express the cooling anomaly with the 8.2 ka climate event highlighted by the green and grey box (Thomas et al., 2007). b) Sea-floor detrital carbonate, with peaks (DCP) representing freshwater discharge events (Jennings et al., 2015). c) Labrador Sea sea-floor sediments, with LSF representing surface freshening (Lochte et al., 2019). d) North Atlantic sediments, with NAS representing AMOC slowdown (Kleiven et al., 2008). e-g) Relative sea levels with inferred sea-level events represented by blue bars (Li et al., 2012, Hijma and Cohen 2019, Lawrence et al., 2016).

Observations of two stages of ocean freshening and cooling in sub-polar North Atlantic proxy records (Ellison *et al.*, 2006) and of two terrestrial sourced detrital carbonate peaks in the Cartwright Saddle (Hillaire-Marcel *et al.*, 2007) suggested that two LAO drainage events occurred. The Cartwright Saddle is a depression on the Labrador shelf that became a distal trap for sediments released from the eastern sector of the LIS during its early-Holocene retreat (Josenhans *et al.*, 1986, Andrews *et al.*, 1999) and as such provides evidence of Hudson Strait drainage events. Changes in ocean flow regimes reconstructed using silt size and foraminiferal isotope records as proxies in the Hudson Strait (Hoffman *et al.*, 2012) and in the northwest (Tegzes *et al.*, 2014) and northeast (Hoogakker *et al.*, 2011) Atlantic basins do however appear to provide more direct evidence of AMOC weakening. The two peaks in a relatively low temporal resolution Cartwright Saddle core were attributed to two LAO drainage events between 8,500–8,350 cal yr BP (Hillaire-Marcel *et al.*, 2007), again potentially showing evidence of the corresponding meltwater pulses.

A RSL record reconstructed from the Rhine-Meuse Delta, Netherlands, constrained and dated sea-level index points derived from basal peat, was recently updated and shows two 'sea-level jumps' between 8,440–8,180 cal yr BP (Hijma and Cohen, 2010) representative of meltwater pulses (Hijma and Cohen, 2010, 2019) (Fig. 2.1f). A later chronological reanalysis by Lawrence *et al.* (2016) of the North Atlantic deep water core originally published by Kleiven *et al.* (2008) suggests it too contains two stages of ocean freshening and cooling at 8,492–8,338 and 8,308–8,114 cal yr BP (Fig. 2.1d). Although caution is necessitated when referring to the Ellison *et al.* (2006) chronology owing to the critical period being constrained by only two ^{14}C dates, the inferred changes beginning at $\sim 8,490$ cal yr BP and $\sim 8,260$ cal yr BP do overlap with the Kleiven *et al.* (2008) record, suggesting that the same changes are being observed in both records. Neither Ellison *et al.* (2006) or Kleiven *et al.* (2008) provided direct evidence of AMOC weakening, but rather proxies of freshening and cooling, of both surface and deep water, which they infer to be AMOC weakening.

Evidence of a further third pulse has been recognised by Jennings *et al.* (2015) (Fig. 2.1b) and Lawrence *et al.* (2016), potentially increasing the complexity of the event further (Fig. 2.1g). Jennings *et al.* (2015) improved previous research of cores from the Cartwright Saddle (Andrews *et al.*, 1999, Barber *et al.*, 1999, Hillaire-Marcel *et al.*, 2007) by developing a more detailed chronology and utilising higher resolution data which provided evidence of three peaks in detrital carbonate. Jennings *et al.* (2015) argue that the first two, remarkably close

but largely separate, events (DCP6a at 8,694–8,609 cal yr BP and DCP6b at 8,609–8,489 cal yr BP) represent the opening of the Tyrrell Sea by calving and meltwater output during LIS retreat, and that it is DCP6b which is the 'red bed' as documented by Barber *et al.* (1999). The final documented pulse (DCP7 at 8219–7998 cal yr BP) which curiously post-dates the onset of the climate event recorded in Greenland (Thomas *et al.*, 2007) is attributed to LAO drainage. Lawrence *et al.* (2016) on the other hand, attribute LAO drainage to both the second and third observed pulses in their high-resolution RSL reconstruction using sedimentology and diatom analysis for the Cree Valley, Scotland. The dates of the observed sea-level jumps (8,760–8,640, 8,595–8,465, 8,323–8,218 cal yr BP) broadly agree with Jennings *et al.* (2015) with the final drainage pre-dating and overlapping the climate event. Lawrence *et al.* (2016) attribute the first event, with a GMSL rise of 0.35–0.65 m (assuming a 70 % fingerprint (Kendall *et al.*, 2008)), to the collapse of the Hudson Bay Ice Saddle (HBIS) between the Keewatin and Labrador domes.

The collapse of the HBIS was first proposed by Gregoire *et al.* (2012) following modelling of the LIS, producing an associated large meltwater pulse at c. 8,500 cal yr BP as a consequence of a positive feedback whereby negative mass balance caused lower ice elevations and higher temperatures, driving further ice loss. The LIS was recently modelled in greater detail by Matero *et al.* (2020). They used three different ice-sheet reconstructions and showed a similar collapse producing a large meltwater pulse equivalent to 1.57–3.39 m GMSL rise in the different runs. The model also included marine-ice interactions which produced a further positive feedback. Geological evidence has also demonstrated that the HBIS contributed meltwater at this time. Terrestrial evidence in the form of geomorphic mapping and dating for the HBIS collapse has been provided by Gauthier *et al.* (2020) and constrains the collapse to between $8,570 \pm 280$ and $8,101 \pm 190$ cal yr BP. Lochte *et al.* (2019) demonstrated that meltwater pulses were produced c. 8,500 cal yr BP directly from the ice-sheet as opposed to via the LAO because of a large age offset. Much older radiocarbon (^{14}C) ages observed in the record were interpreted to have been because much older carbon dioxide stored in the HBIS was introduced into the ocean, producing the age offset (Fig. 2.1c).

The probable relative contributions of LAO and the HBIS to GMSL have been estimated by geomorphic mapping. The volume of freshwater within LAO was suggested to be around 1.63×10^{14} m^3 by Teller *et al.* (2002) but has recently been shown to have been smaller by Godbout *et al.* (2020), although they do not provide an estimate. Therefore LAO drainage

would produce a barystatic sea-level rise of < 0.45 m. The HBIS on the other hand, although difficult to calculate, has been suggested to contain a freshwater volume of around 4.51 x 10^{14} m^3, equivalent to 1.25 m of barystatic sea-level rise (Ullman *et al.*, 2016).

Global climate model simulations have supported the hypothesis that an AMOC weakening following freshwater input reduces poleward heat transfer initiating the observed climatic changes (e.g. Renssen *et al.*, 2001, LeGrande *et al.*, 2006, Wiersma *et al.*, 2006, Morrill *et al.*, 2014). However, the models fail to reproduce the magnitude of observed climate change following freshwater hosing experiments based on LAO drainage. A recent modelling study using a simulated HBIS collapse and a magnitude based on RSL reconstructions produced a climate event very similar to that observed in the palaeo records (Matero *et al.*, 2017). It appears that HBIS collapse may have been important in forcing the weakening of the AMOC and that the models may perform well under such a scenario.

2.3.3   Relative sea-level rise as a proxy for meltwater pulses

As described in Chapter 1, relative sea-level reconstructions stand out from other sources of evidence as they are able to provide quantifications of the magnitudes of the meltwater pulses and the volume of freshwater released directly from the ice sheet and LAO (Wiersma *et al.*, 2006). Presently, RSL reconstructions from three sites exist for the period prior to and including the 8.2 ka climate event that show well-resolved SLEs (Fig. 2.1). All three reconstructions suggest a different number of meltwater pulses and variations in their timing and magnitudes (Fig. 2.2).

In the Mississippi Delta, USA, Törnqvist *et al.* (2004) first recognised a single SLE that was developed in later work by Li *et al.* (2012). They studied the stratigraphy and dated basal peats along an elevation gradient. The evidence for a SLE is based on the premise that salt-marsh peats, which normally form within the inter-tidal zone as RSL rises, are unable to form during rapidly rising sea levels. Therefore basal peats from below and above the elevation that peat is absent provide the timing of the SLE. The results suggest a SLE occurred around between 8,310–8,180 cal yr BP. After up-scaling the local magnitude of 0.20– 0.56 m to account for the barystatic-GRD fingerprint of an LAO drainage event (Kendall *et al.*, 2008), the global magnitude is 0.8–2.2 m. As a near-field location, the local magnitude is only around 25 % of the total barystatic sea-level rise and therefore arguably places an over-reliance on the Kendall *et al.* (2008) simulation. Older dates of basal peats found at
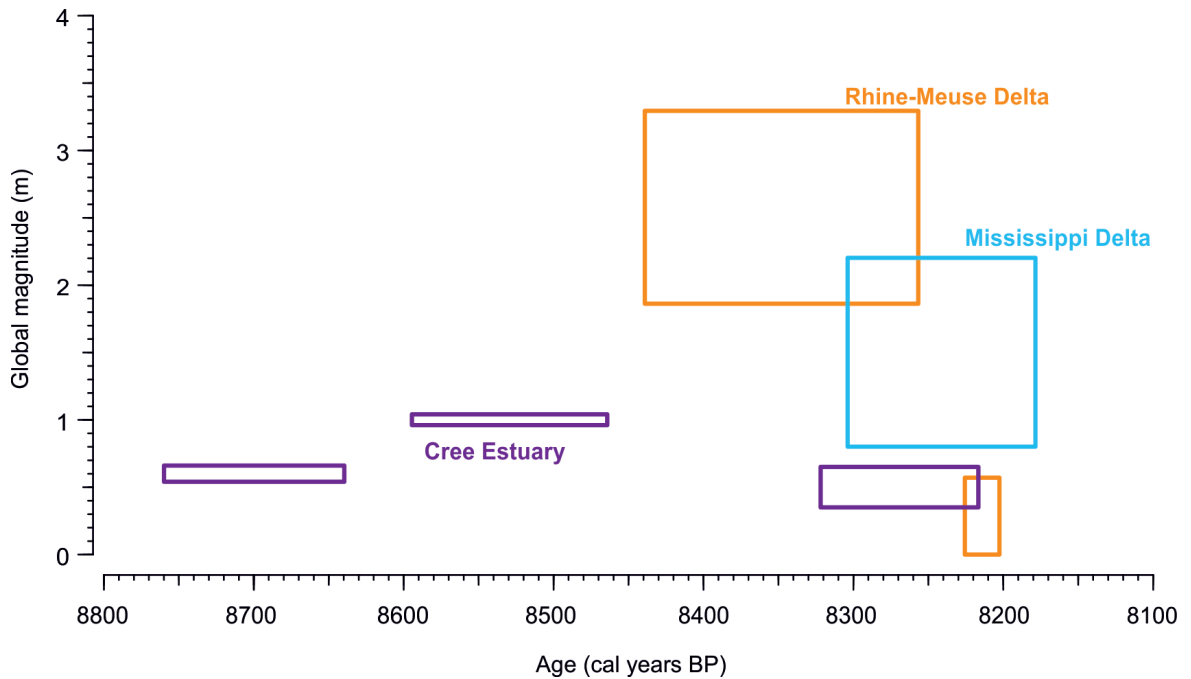
Figure 2.2: The timing and global magnitude of sea-level events from the reconstructions presented in Fig. 2.1e–g for the Mississippi Delta (Li et al., 2012), Rhine-Meuse Delta (Hijma and Cohen 2019) and Cree Estuary (Lawrence et al., 2016). The boxes represent the ranges for the timing and magnitude of each event after being scaled up to the global equivalent to account for the barystatic-GRD fingerprint.

lower elevations are also evident in the Mississippi Delta record but because of likely erosion the authors do not link these to SLEs. Milliken *et al.* (2008) do provide evidence of an earlier drowning event c. 8,600 cal yr BP from the Gulf of Mexico that suggests that a SLE may indeed be evident in the region.

Hijma and Cohen (2010) applied a similar approach as used in the Mississippi Delta to demonstrate the occurrence of a SLE in the Rhine-Meuse Delta, Netherlands, based on pairs of sea-level index points (SLIPs) $\sim$ 35 km apart. After the addition of further SLIPs, a second SLE was identified in the region (Hijma and Cohen, 2019). The start of the two SLEs are well constrained (8,440 $\pm$ 40 cal yr BP and 8,220 $\pm$ 30 cal yr BP) but the ends are less well constrained. The local magnitude of the two SLEs (1.1–2.3 m and 0–0.4 m) include a relatively large uncertainty, mainly because of the calculation of the background sea-level rise. Unlike Li *et al.* (2012), who assume no background GIA signal because of the relatively short time span, Hijma and Cohen (2019) use longer term SLIPs from the region to calculate the background rise which yields rates of 10 $\pm$ 1.5 mm yr^{-1}. The high background rates are mainly due to tectonic and glacial-isostatic related subsidence (Hijma and Cohen,

2010). After accounting for the site being 70 % of the barystatic sea-level rise, the global magnitude is 1.6–3.3 and 0–0.6 m respectively.

The third reconstruction is from the Cree Estuary, west Scotland, and is underpinned by a different approach (Lawrence *et al.*, 2016). A continuous RSL reconstruction is produced from a single core that shows evidence of three SLEs between 8,760 and 8,218 cal yr BP with global magnitudes of 0.35–0.65, 0.96–1.04 and 0.54–0.61 m having corrected for the site being 70 % of the barystatic sea-level rise. The approach uses microfossils as sea-level indicators. The chronological model relies on interpolation between ^{14}C dates over 2 m apart potentially leading an over reliance on the age-depth model. A statistical model is then used to produce a probabilistic reconstruction, although importantly the stratigraphy still helps to inform the interpretations.

RSL reconstructions from other regions have also shown evidence of periods of rapid RSL rise that have been linked to the 8.2 ka climate event. In the UK an apparent rapid sea-level rise has been observed in the Solway Firth at c. 8,600 cal yr BP (Lloyd *et al.*, 1999, Smith *et al.*, 2020), Skye at c. 8,400 cal yr BP (Selby and Smith, 2016), Morecambe Bay at c. 8,500 cal yr BP (Tooley, 1974, Zong and Tooley, 1996) and a previous reconstruction from the Ythan Estuary (Smith *et al.*, 1983, 1999) described in section 2.4. The resolution of these studies prevents either multiple meltwater pulses to be identified, or their magnitudes. In the Po Delta, Italy, a drowning event at c. 8,500 cal yr BP is evident (Amorosi *et al.*, 2017), and also, notably, in Maputo Bay, Mozambique at c. 8,600 cal yr BP (De Lecea *et al.*, 2017) based on palaeogeographic reconstructions. Maputo Bay is the only evidence thus far from the Southern Hemisphere, but the drowning is constrained by one ^{14}C age and no attempt is made at reconstructing RSL change.

Studies of a number of river deltas in southeast Asia appear to show periods of rapid sea-level rise that are linked to the 8.2 ka climate event. In the Mekong Delta (Tamura *et al.*, 2009, Nguyen *et al.*, 2010, Tjallingi *et al.*, 2014), Singapore (Bird *et al.*, 2007, 2010), Pearl Delta (Zong *et al.*, 2012), Yangtze Delta (Wang *et al.*, 2013) and Hangzou Bay (Xiong *et al.*, 2020) rapid rates of RSL rise (around 30 mm yr^{-1}) are observed between c. 8,600 cal yr BP and 8,300 cal yr BP. However, none of the studies attempt to quantify the background rates or the magnitude of possible SLEs.

2.3.4   Summary

It is apparent from the literature that a significant temperature cooling in the North Atlantic region occurred, along with monsoonal changes and possible additional climatic changes further afield during the 8.2 ka climate event. The event appears to have been driven by meltwater pulses originating from the retreating LIS, although this is yet to be tested. The number of meltwater pulses believed to have forced the weakening of the AMOC has changed with time from one to two or three, but there is still no clear consensus. Different methods have been applied to quantify the magnitude of the meltwater pulses from RSL reconstructions but again the timing and magnitude remains uncertain. Therefore, it is important that these uncertainties are resolved in order to better understand the driver(s) of the climate event.

2.4   Study sites

Two study sites have been identified that provide the opportunity to test the hypotheses presented in Chapter 1. Here I review previous studies at these sites.

2.4.1   Ythan Estuary, east Scotland

The Ythan Estuary is located on the east coast of Scotland, $\sim$ 20 km north of Aberdeen. The site was originally studied by Jamieson (1865), whose house overlooked the Estuary. The stratigraphy of the inter-tidal deposits in the estuary have been described in previous studies (Smith *et al.*, 1983, 1999). Estuarine silts and peats indicate a transgressive sequence between 9,000 and 6,500 cal yr BP (Fig. 2.3). Fossil diatoms indicate that a transition from salt marsh to tidal flat conditions occurred at the upper contact of a thin intercalated peat unit. The contact has been dated to 8,640–8,450 cal yr BP following re-calibration of the ^{14}C dates based on 2cm thick bulk peat samples (Smith *et al.*, 2002, 2013). Pollen analysis demonstrates that sediment deposition was continuous and thus that a rapid transition occurs that Smith *et al.* (2013) link to a meltwater pulse prior to the 8.2 ka climate event. Basal peat higher in the sequence, dated to 8,360–8,070 cal yr BP, indicate that RSL had risen by at least 2 m in a few centuries prior to the 8.2 ka climate event.

The apparent sea-level rise is further constrained by a sand unit overlying the estuarine silts that appears likely to have been deposited by the Storegga Tsunami (Smith *et al.*, 1999).

The Storegga Tsunami was caused by a large submarine slide that would have resulted in a large tsunami wave striking the Ythan Estuary (Hill *et al.*, 2014) and has been dated to 8,110 ± 100 cal yr BP (Dawson *et al.*, 2011, Bondevik *et al.*, 2012). Despite its size the wave does not appear to have significantly eroded the the underlying sediments. The age of the tsunami deposit, occurring towards the end of the 8.2 ka climate event, make it a useful chrono-horizon and should permit a continuous reconstruction of RSL from a single representative core.
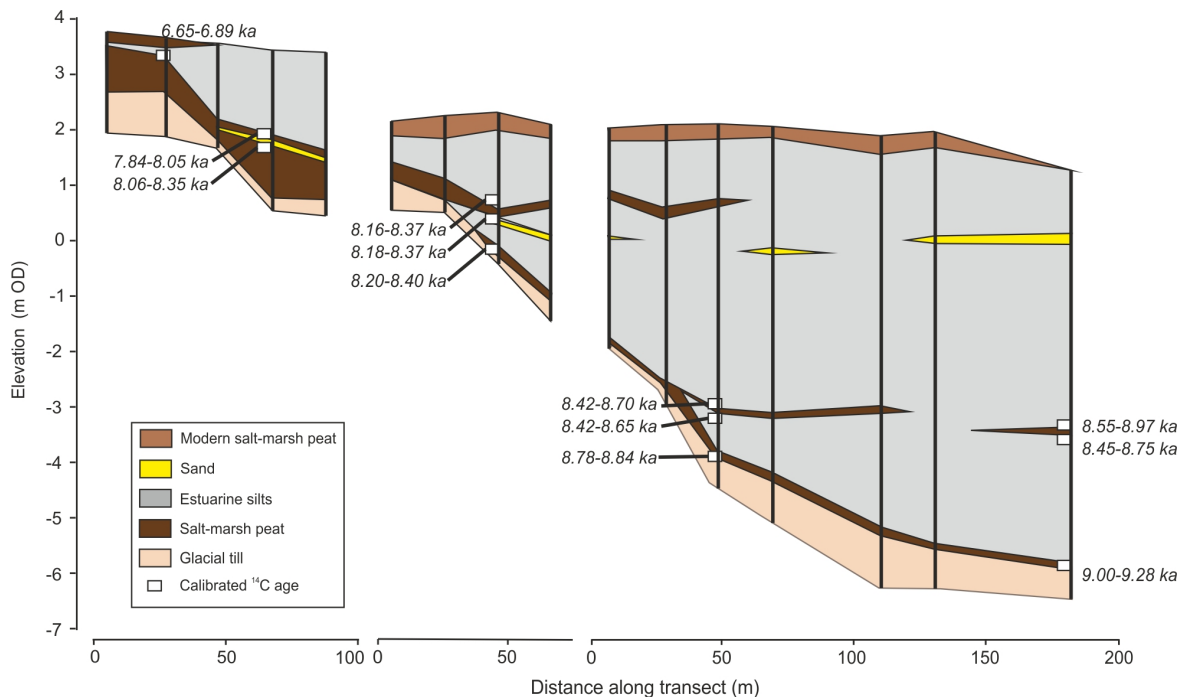
Figure 2.3: Stratigraphy of the Ythan Estuary adapted from Smith et al. (1999). The three drawn transects are taken from across the site. The ^{14}C ages (1σ range) have been calibrated using Intcal20 (Reimer *et al.*, 2020).

2.4.2 Swan Inlet, Falkland Islands

To date, there are no high-quality Holocene sea-level data for the Falkland Islands. The only data is a single age, taken from peat overlying a raised beach deposit, of 4,090–3,840 cal yr BP, which suggests RSL may have been several metres higher than present during the mid Holocene (Roberts, 1984). Swan Inlet is the largest and best developed salt marsh in the Falkland Islands and has been studied by Newton (2016) as part of a PhD thesis. The site was also studied by researchers from Durham University in 2005, but the work remains unpublished. Based on foraminiferal analysis the stratigraphy shows an organic clay of salt-

marsh origin overlying the bedrock that is in turn overlain by tidal-flat sediments (Fig. 2.4). A series of range-finder dates suggests that the marsh was drowned at c. 8,400 cal yr BP. Newton (2016) suggests that the stratigraphy provides evidence of a rapid sea-level rise with an estimated magnitude of 0.89 ± 0.22 m. The estimate is based on sediment thickness only and assumes the sand was deposited rapidly during a single event. The estimate does not account for changes in the height of sea-level relative to the palaeo marsh surface, that once quantified would likely increase the estimated magnitude, and the age reversals of the ^{14}C dates suggest that significant reworking may have occurred, further complicating matters.
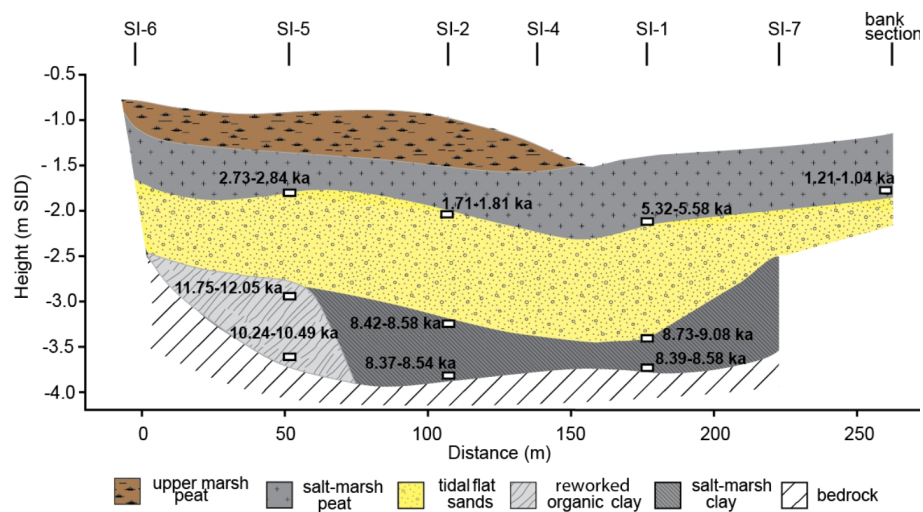
Figure 2.4: Stratigraphy of Swan Inlet from Newton (2016). Palaeoenvironmental interpretations of the sediments calibrated ^{14}C ages are shown.

In order to quantify the magnitude of a SLE or identify if there are multiple SLEs, more detailed stratigraphic mapping and analysis is required along with a better chronology. The relationship between modern microfossils and elevation relative to sea level has been studied and suggests that diatoms and testate amoebae are appropriate indicators of sea level, enabling transfer functions to be used to predict palaeo sea level (Newton *et al.*, 2021). Analysis of microfossils should therefore help produce a more precise quantification of the magnitude of the SLE. Reconstructing sea level from the Falkland Islands would also allow the origin of the meltwater pulses to be better constrained. As a far-field location with respect to the LIS, (Kendall *et al.*, 2008) shows that the Falkland Islands should record the full magnitude of a SLE following LAO drainage, allowing hypotheses 2 and 3 to be tested.

As well as evidence of a major drowning event, the work by Newton (2016) also suggested

a subsequent sea-level highstand between c. 7,000 and 5,400 cal yr BP based on dating of the the regressive contact above the sand deposit. A sea-level highstand has been observed from the Argentinian coast but is poorly constrained (Porter *et al.*, 1984, Gordillo *et al.*, 1992, Codignotto *et al.*, 1992, Borromei and Quattrocchio, 2007, Zanchetta *et al.*, 2014, Prieto *et al.*, 2017, Bini *et al.*, 2018, Pappalardo *et al.*, 2019). Importantly the Falkland Islands are tectonically stable and unaffected by local ice-loading unlike the South America continent (Milne *et al.*, 2005). Relative sea-level was therefore controlled by ice-ocean mass flux and GIA, making it well placed for Holocene sea-level reconstructions (Milne and Mitrovica, 2008). Constraining the highstand on the Falkland Islands can therefore be used to constrain the melt histories of the large ice sheets using GIA models.

References

Abdul, N. A., Mortlock, R. A., Wright, J. D. and Fairbanks, R. G. (2016), 'Younger Dryas sea level and meltwater pulse 1B recorded in Barbados reef crest coral Acropora palmata', *Paleoceanography* **31**(2), 330–344.

Abe-Ouchi, A., Andersen, M., Antonioli, F., Bamber, J., Bard, E., Clark, J., Clark, P., Deschamps, P., Dutton, A., Elliot, M., Gallup, C., Gomez, N., Gregory, J., Huybers, P., Kawamura, K., Kelly, M., Lambeck, K., Lowell, T., Mitrovica, J., Otto-Bliesner, B., Richards, D., Siddall, M., Stanford, J., Stirling, C., Stocker, T., Thomas, A., Thompson, B., Törnqvist, T., Riveiros, N. V., Waelbroeck, C., Yokoyama, Y., Yu, S. Y., Abe-Ouchi, A., Andersen, M., Antonioli, F., Bamber, J., Bard, E., Clark, J., Clark, P., Deschamps, P., Dutton, A., Elliot, M., Gallup, C., Gomez, N., Gregory, J., Huybers, P., Kawarnura, K., Kelly, M., Lambeck, K., Lowell, T., Milrovica, J., Otto-Bliesner, B., Richards, D., Stanford, J., Stirling, C., Stocker, T., Thomas, A., Thompson, B., Tornqvist, T., Vazquez Riveiros, N., Waelbroeck, C., Yokoyama, Y., Yu, S. Y. and Grp, P. L. W. (2010), 'The sea-level conundrum: case studies from palaeo-archives', *Journal of Quaternary Science* **25**(1), 19–25.

Alley, R. B., Mayewski, P. A., Sowers, T., Stuiver, M., Taylor, K. C. and Clark, P. U. (1997), 'Holocene climatic instability: A prominent, widespread event 8200 yr ago', *Geology* **25**(6), 483–486.

Amorosi, A., Bruno, L., Campo, B., Morelli, A., Rossi, V., Scarponi, D., Hong, W., Bohacs, K. M. and Drexler, T. M. (2017), 'Global sea-level control on local parasequence architecture from the Holocene record of the Po Plain, Italy', *Marine and Petroleum Geology* **87**, 99–111.

Anderson, J. B., Shipp, S. S., Lowe, A. L., Wellner, J. S. and Mosola, A. B. (2002), 'The Antarctic Ice Sheet during the Last Glacial Maximum and its subsequent retreat history: a review', *Quaternary Science Reviews* **21**(1-3), 49–70.

Andrews, J. T., Keigwin, L., Hall, F. and Jennings, A. E. (1999), 'Abrupt deglaciation events and holocene palaeoceanography from high-resolution cores, Cartwright Saddle, Labrador Shelf, Canada', *Journal of Quaternary Science* **14**(5), 383–397.

Argus, D. F., Peltier, W. R., Drummond, R. and Moore, A. W. (2014), 'The Antarctica component of postglacial rebound model ICE-6G_C (VM5a) based on GPS positioning, exposure age dating of ice thicknesses, and relative sea level histories', *Geophysical Journal International* **198**(1), 537–563.

Barber, D. C., Dyke, A., Hillaire-Marcel, C., Jennings, A. E., Andrews, J. T., Kerwin, M. W., Bilodeau, G., McNeely, R., Southon, J., Morehead, M. D. and Gagnon, J. M. (1999), 'Forcing of the cold event of 8,200 years ago by catastrophic drainage of Laurentide lakes', *Nature* **400**(6742), 344–348.

Bard, E., Hamelin, B., Arnold, M., Montaggioni, L., Cabioch, G., Faure, G. and Rougerie, F. (1996), 'Deglacial sea-level record from Tahiti corals and the timing of global meltwater discharge', *Nature* **382**(6588), 241–244.

Bard, E., Hamelin, B. and Delanghe-Sabatier, D. (2010), 'Deglacial Meltwater Pulse 1B and Younger Dryas Sea Levels Revisited with Boreholes at Tahiti', *Science* **327**(5970), 1235–1237.

Bentley, M. J., Ocofaigh, C., Anderson, J. B., Conway, H., Davies, B., Graham, A. G. C., Hillenbrand, C. D., Hodgson, D. A., Jamieson, S. S. R., Larter, R. D., Mackintosh, A., Smith, J. A., Verleyen, E., Ackert, R. P., Bart, P. J., Berg, S., Brunstein, D., Canals, M., Colhoun, E. A., Crosta, X., Dickens, W. A., Domack, E., Dowdeswell, J. A., Dunbar, R., Ehrmann, W., Evans, J., Favier, V., Fink, D., Fogwill, C. J., Glasser, N. F., Gohl, K., Golledge, N. R., Goodwin, I., Gore, D. B., Greenwood, S. L., Hall, B. L., Hall, K., Hedding, D. W., Hein, A. S., Hocking, E. P., Jakobsson, M., Johnson, J. S., Jomelli, V., Jones, R. S., Klages, J. P., Kristoffersen, Y., Kuhn, G., Leventer, A., Licht, K., Lilly, K., Lindow, J., Livingstone, S. J., Massé, G., McGlone, M. S., McKay, R. M., Melles, M., Miura, H., Mulvaney, R., Nel, W., Nitsche, F. O., O'Brien, P. E., Post, A. L., Roberts, S. J., Saunders, K. M., Selkirk, P. M., Simms, A. R., Spiegel, C., Stolldorf, T. D., Sugden, D. E., van der Putten, N., van Ommen, T., Verfaillie, D., Vyverman, W., Wagner, B., White, D. A., Witus, A. E. and Zwartz, D. (2014), 'A community-based geological reconstruction of Antarctic Ice Sheet deglaciation since the Last Glacial Maximum', *Quaternary Science Reviews* **100**, 1–9.

Bini, M., Isola, I., Zanchetta, G., Pappalardo, M., Ribolini, A., Ragaini, L., Baroni, C.,

Boretto, G., Fuck, E., Morigi, C., Cristina Salvatore, M., Bassi, D., Marzaioli, F. and Terrasi, F. (2018), 'Mid-Holocene relative sea-level changes along Atlantic Patagonia: New data from Camarones, Chubut, Argentina', *The Holocene* **28**(1), 56–64.

Bird, M. I., Austin, W. E. N., Wurster, C. M., Fifield, L. K., Mojtahid, M. and Sargeant, C. (2010), 'Punctuated eustatic sea-level rise in the early mid-Holocene', *Geology* **38**(9), 803–806.

Bird, M. I., Fifield, L. K., Teh, T. S., Chang, C. H., Shirlaw, N. and Lambeck, K. (2007), 'An inflection in the rate of early mid-Holocene eustatic sea-level rise: A new sea-level curve from Singapore', *Estuarine, Coastal and Shelf Science* **71**(3–4), 523–536.

Blanchon, P. and Shaw, J. (1995), 'Reef drowning during the last deglaciation: Evidence for catastrophic sea-level rise and ice-sheet collapse', *Geology* **23**(1), 4.

Bondevik, S., Stormo, S. K. and Skjerdal, G. (2012), 'Green mosses date the Storegga tsunami to the chilliest decades of the 8.2 ka cold event', *Quaternary Science Reviews* **45**, 1–6.

Borromei, A. M. and Quattrocchio, M. (2007), 'Holocene sea-level change inferred from palynological data in the Beagle Channel, southern Tierra del Fuego, Argentina', *Ameghiniana* **44**(1), 161–171.

Briggs, R. D., Pollard, D. and Tarasov, L. (2014), 'A data-constrained large ensemble analysis of Antarctic evolution since the Eemian', *Quaternary Science Reviews* **103**, 91–115.

Camoin, G. F. and Webster, J. M. (2015), 'Coral reef response to Quaternary sea-level and environmental changes: State of the science', *Sedimentology* **62**(2), 401–428.

Carlson, A. E. and Clark, P. U. (2012), 'Ice sheet sources of sea level rise and freshwater discharge during the last deglaciation', *Reviews of Geophysics* **50**.

Carlson, A. E., Legrande, A. N., Oppo, D. W., Came, R. E., Schmidt, G. A., Anslow, F. S., Licciardi, J. M. and Obbink, E. A. (2008), 'Rapid early Holocene deglaciation of the Laurentide ice sheet', *Nature Geoscience* **1**(9), 620–624.

Cheng, H., Fleitmann, D., Edwards, R. L., Wang, X., Cruz, F. W., Auler, A. S., Mangini, A., Wang, Y., Kong, X., Burns, S. J. and Matter, A. (2009), 'Timing and structure of

the 8.2. kyr B.P. event inferred from δ 18O records of stalagmites from China, Oman, and Brazil', *Geology* **37**(11), 1007–1010.

Codignotto, J. O., Kokot, R. R. and Marcomini, S. C. (1992), 'Neotectonism and Sea-Level Changes in the Coastal Zone of Argentina', *Source: Journal of Coastal Research* **8**(1), 125–133.

Cooper, J. A., Green, A. N., Meireles, R., Klein, A. H., de Abreu, J. G. and Toldo, E. E. (2019), 'Tidal strait to embayment: Seismic stratigraphy and evolution of a rock-bounded embayment in the context of Holocene sea level change', *Marine Geology* **415**, 105972.

Cooper, J. A., Green, A. N., Meireles, R. P., Klein, A. H., Souza, J. and Toldo, E. E. (2016), 'Sandy barrier overstepping and preservation linked to rapid sea level rise and geological setting', *Marine Geology* **382**, 80–91.

Daley, T. J., Thomas, E. R., Holmes, J. A., Street-Perrott, F. A., Chapman, M. R., Tindall, J. C., Valdes, P. J., Loader, N. J., Marshall, J. D., Wolff, E. W., Hopley, P. J., Atkinson, T., Barber, K. E., Fisher, E. H., Robertson, I., Hughes, P. D. and Roberts, C. N. (2011), 'The 8200yr BP cold event in stable isotope records from the North Atlantic region', *Global and Planetary Change* **79**(3-4), 288–302.

Dalton, A. S., Margold, M., Stokes, C. R., Tarasov, L., Dyke, A. S., Adams, R. S., Allard, S., Arends, H. E., Atkinson, N., Attig, J. W., Barnett, P. J., Barnett, R. L., Batterson, M., Bernatchez, P., Borns, H. W., Breckenridge, A., Briner, J. P., Brouard, E., Campbell, J. E., Carlson, A. E., Clague, J. J., Curry, B. B., Daigneault, R. A., Dubé-Loubert, H., Easterbrook, D. J., Franzi, D. A., Friedrich, H. G., Funder, S., Gauthier, M. S., Gowan, A. S., Harris, K. L., Hétu, B., Hooyer, T. S., Jennings, C. E., Johnson, M. D., Kehew, A. E., Kelley, S. E., Kerr, D., King, E. L., Kjeldsen, K. K., Knaeble, A. R., Lajeunesse, P., Lakeman, T. R., Lamothe, M., Larson, P., Lavoie, M., Loope, H. M., Lowell, T. V., Lusardi, B. A., Manz, L., McMartin, I., Nixon, F. C., Occhietti, S., Parkhill, M. A., Piper, D. J., Pronk, A. G., Richard, P. J., Ridge, J. C., Ross, M., Roy, M., Seaman, A., Shaw, J., Stea, R. R., Teller, J. T., Thompson, W. B., Thorleifson, L. H., Utting, D. J., Veillette, J. J., Ward, B. C., Weddle, T. K. and Wright, H. E. (2020), 'An updated radiocarbon-based ice margin chronology for the last deglaciation of the North American Ice Sheet Complex', *Quaternary Science Reviews* **234**, 106223.

Dansgaard, W. (1987), Ice core evidence of abrupt climatic changes, *in* W. J. Begre and L. Labeyrie, eds, 'Abrupt climatic change', Springer, pp. 223–233.

Dansgaard, W., White, J. W. C. and Johnsen, S. J. (1989), 'The abrupt termination of the Younger Dryas climate event', *Nature* **339**(6225), 532–534.

Dawson, A., Bondevik, S. and Teller, J. T. (2011), 'Relative timing of the Storegga submarine slide, methane release, and climate change during the 8.2 ka cold event', *Holocene* **21**(7), 1167–1171.

De Lecea, A. M., Green, A. N., Strachan, K. L., Cooper, J. A. G. and Wiles, E. A. (2017), 'Stepped Holocene sea-level rise and its influence on sedimentation in a large marine embayment: Maputo Bay, Mozambique', *Estuarine Coastal and Shelf Science* **193**, 25–36.

DeConto, R. M. and Pollard, D. (2016), 'Contribution of Antarctica to past and future sea-level rise', *Nature* **531**(7596), 591–597.

Dlabola, E. K., Wilson, G. S., Gorman, A. R., Riesselman, C. R. and Moy, C. M. (2015), 'A post-glacial relative sea-level curve from Fiordland, New Zealand', *Global and Planetary Change* **131**, 104–114.

Dyke, A. S. (2004), An outline of North American deglaciation with emphasis on central and northern Canada, *in* J. Ehlers and P. L. Gibbard, eds, 'Quaternary Glaciations-extent and Chronology, Part II', Elsevier Science and Technology Books, Amsterdam.

Edwards, T. L., Brandon, M. A., Durand, G., Edwards, N. R., Golledge, N. R., Holden, P. B., Nias, I. J., Payne, A. J., Ritz, C. and Wernecke, A. (2019), 'Revisiting antarctic ice loss due to marine ice-cliff instability', *Nature* **566**(7742), 58–64.

Ellison, C. R. W., Chapman, M. R. and Hall, I. R. (2006), 'Surface and deep ocean interactions during the cold climate event 8200 years ago', *Science* **312**(5782), 1929–1932.

Engelhart, S. E., Peltier, W. R. and Horton, B. P. (2011), 'Holocene relative sea-level changes and glacial isostatic adjustment of the US Atlantic coast', *Geology* **39**(8), 751–754.

Fairbanks, R. G. (1989), 'A 17,000-Year Glacio-Eustatic Sea-Level Record - Influence of Glacial Melting Rates on the Younger Dryas Event and Deep-Ocean Circulation', *Nature* **342**(6250), 637–642.

Fleitmann, D., Mudelsee, M., Burns, S. J., Bradley, R. S., Kramers, J. and Matter, A. (2008), 'Evidence for a widespread climatic anomaly at around 9.2 ka before present', *Paleoceanography* **23**(1).

Gauthier, M. S., Kelley, S. E. and Hodder, T. J. (2020), 'Lake Agassiz drainage bracketed Holocene Hudson Bay Ice Saddle collapse', *Earth and Planetary Science Letters* **544**, 116372.

Gehrels, R. (2010), 'Sea-level changes since the Last Glacial Maximum: an appraisal of the IPCC Fourth Assessment Report', *Journal of Quaternary Science* **25**(1), 26–38.

Godbout, P. M., Roy, M. and Veillette, J. J. (2020), 'A detailed lake-level reconstruction shows evidence for two abrupt lake drawdowns in the late-stage history of the eastern Lake Agassiz-Ojibway basin', *Quaternary Science Reviews* **238**, 106327.

Golledge, N. R., Menviel, L., Carter, L., Fogwill, C. J., England, M. H., Cortese, G. and Levy, R. H. (2014), 'Antarctic contribution to meltwater pulse 1A from reduced Southern Ocean overturning', *Nature Communications* **5**.

Gomez, N., Weber, M. E., Clark, P. U., Mitrovica, J. X. and Han, H. K. (2020), 'Antarctic ice dynamics amplified by northern hemisphere sea-level forcing', *Nature* **587**(7835), 600–604.

Gordillo, S., Bujalesky, G. G., Pirazzoli, P. A., Rabassa, J. O. and Saliège, J. F. (1992), 'Holocene raised beaches along the northern coast of the Beagle Channel, Tierra del Fuego, Argentina', *Palaeogeography, Palaeoclimatology, Palaeoecology* **99**(1-2), 41–54.

Gregoire, L. J., Payne, A. J. and Valdes, P. J. (2012), 'Deglacial rapid sea level rises caused by ice-sheet saddle collapses', *Nature* **487**(7406), 219–222.

Gregory, J. M., Griffies, S. M., Hughes, C. W., Lowe, J. A., Church, J. A., Fukimori, I., Gomez, N., Kopp, R. E., Landerer, F., Cozannet, G. L., Ponte, R. M., Stammer, D., Tamisiea, M. E. and van de Wal, R. S. (2019), 'Concepts and Terminology for Sea Level: Mean, Variability and Change, Both Local and Global', *Surveys in Geophysics* **40**(6), 1251–1289.

Hanebuth, T. J. J., Voris, H. K., Yokoyama, Y., Saito, Y. and Okuno, J. (2011), 'Formation and fate of sedimentary depocentres on Southeast Asia's Sunda Shelf over the past sea-level cycle and biogeographic implications', *Earth-Science Reviews* **104**(1-3), 92–110.

Harrison, S., Smith, D. E. and Glasser, N. F. (2018), 'Late Quaternary meltwater pulses and sea level change', *Journal of Quaternary Science* **34**, 1–15.

Hede, M. U., Rasmussen, P., Noe-Nygaard, N., Clarke, A. L., Vinebrooke, R. D. and Olsen, J. (2010), 'Multiproxy evidence for terrestrial and aquatic ecosystem responses during the 8.2 ka cold event as recorded at højby sø, denmark', *Quaternary Research* **73**(3), 485–496.

Herrle, J. O., Bollmann, J., Gebühr, C., Schulz, H., Sheward, R. M. and Giesenberg, A. (2018), 'Black Sea outflow response to Holocene meltwater events', *Scientific reports* **8**(1), 1–6.

Hibbert, F. D., Rohling, E. J., Dutton, A., Williams, F. H., Chutcharavan, P. M., Zhao, C. and Tamisiea, M. E. (2016), 'Coral indicators of past sea-level change: A global repository of U-series dated benchmarks', *Quaternary Science Reviews* **145**, 1–56.

Hijma, M. P. and Cohen, K. M. (2010), 'Timing and magnitude of the sea-level jump preluding the 8200 yr event', *Geology* **38**(3), 275–278.

Hijma, M. P. and Cohen, K. M. (2019), 'Holocene sea-level database for the Rhine-Meuse Delta, The Netherlands: Implications for the pre-8.2 ka sea-level jump', *Quaternary Science Reviews* **214**, 68–86.

Hill, J., Collins, G. S., Avdis, A., Kramer, S. C. and Piggott, M. D. (2014), 'How does multiscale modelling and inclusion of realistic palaeobathymetry affect numerical simulation of the Storegga Slide tsunami?', *Ocean Modelling* **83**, 11–25.

Hillaire-Marcel, C., de Vernal, A. and Piper, D. J. W. (2007), 'Lake Agassiz final drainage event in the northwest North Atlantic', *Geophysical Research Letters* **34**(15).

Hoffman, J. S., Carlson, A. E., Winsor, K., Klinkhammer, G. P., LeGrande, A. N., Andrews, J. T. and Strasser, J. C. (2012), 'Linking the 8.2 ka event and its freshwater forcing in the Labrador Sea', *Geophysical Research Letters* **39**(17), 2005–2009.

Hoogakker, B. A. A., Chapman, M. R., McCave, I. N., Hillaire-Marcel, C., Ellison, C. R. W., Hall, I. R. and Telford, R. J. (2011), 'Dynamics of North Atlantic Deep Water masses during the Holocene', *Paleoceanography* **26**(4).

Jamieson, T. F. (1865), 'On the history of the last geological changes in Scotland', *Quarterly Journal of the Geological Society of London* **21**(1-2), 161–204.

Jennings, A., Andrews, J., Pearce, C., Wilson, L. and Olfasdotttir, S. (2015), 'Detrital carbonate peaks on the Labrador shelf, a 13-7 ka template for freshwater forcing from the Hudson Strait outlet of the Laurentide Ice Sheet into the subpolar gyre', *Quaternary Science Reviews* **107**, 62–80.

Josenhans, H. W., Zevenhuizen, J. and Klassen, R. A. (1986), 'The Quaternary geology of the Labrador Shelf.', *Canadian Journal of Earth Sciences* **23**(8), 1190–1213.

Jouzel, J., Stievenard, M., Johnsen, S. J., Landais, A., Masson-Delmotte, V., Sveinbjorns-dottir, A., Vimeux, F., Von Grafenstein, U. and White, J. W. (2007), 'The grip deuterium-excess record', *Quaternary Science Reviews* **26**(1-2), 1–17.

Kendall, R. A., Mitrovica, J. X., Milne, G. A., Tornqvist, T. E. and Li, Y. X. (2008), 'The sea-level fingerprint of the 8.2 ka climate event', *Geology* **36**(5), 423–426.

Kleiven, H. F., Kissel, C., Laj, C., Ninnemann, U. S., Richter, T. O. and Cortijo, E. (2008), 'Reduced North Atlantic Deep Water coeval with the glacial Lake Agassiz freshwater outburst', *Science* **319**(5859), 60–64.

Kobashi, T., Severinghaus, J. P., Brook, E. J., Barnola, J. M. and Grachev, A. M. (2007), 'Precise timing and characterization of abrupt climate change 8200 years ago from air trapped in polar ice', *Quaternary Science Reviews* **26**(9-10), 1212–1222.

Lambeck, K. and Nakada, M. (1990), 'Late Pleistocene and Holocene sea-level change along the Australian coast', *Palaeogeography, Palaeoclimatology, Palaeoecology* **89**(1-2), 143–176.

Lambeck, K., Rouby, H., Purcell, A., Sun, Y. Y. and Sambridge, M. (2014), 'Sea level and global ice volumes from the Last Glacial Maximum to the Holocene', *Proceedings of the National Academy of Sciences of the United States of America* **111**(43), 15296–15303.

Lawrence, T., Long, A. J., Gehrels, W. R., Jackson, L. P. and Smith, D. E. (2016), 'Relative sea-level data from southwest Scotland constrain meltwater-driven sea-level jumps prior to the 8.2 kyr BP event', *Quaternary Science Reviews* **151**, 292–308.

LeGrande, A. N., Schmidt, G. A., Shindell, D. T., Field, C. V., Miller, R. L., Koch, D. M., Faluvegi, G. and Hoffmann, G. (2006), 'Consistent simulations of multiple proxy responses to an abrupt climate change event', *Proceedings of the National Academy of Sciences of the United States of America* **103**(4), 837–842.

Li, Y. X., Törnqvist, T. E., Nevitt, J. M. and Kohl, B. (2012), 'Synchronizing a sea-level jump, final Lake Agassiz drainage, and abrupt cooling 8200 years ago', *Earth and Planetary Science Letters* **315**, 41–50.

Liu, J. P., Milliman, J. D., Gao, S. and Cheng, P. (2004), 'Holocene development of the Yellow River subaqueous delta, North Yellow Sea', *Marine Geology* **209**(1-4), 45–67.

Liu, Y. and Hu, C. (2016), 'Quantification of southwest China rainfall during the 8.2kaBP event with response to North Atlantic cooling', *Climate of the Past* **12**(7), 1583–1590.

Ljung, K., Bjorck, S., Renssen, H. and Hammarlund, D. (2008), 'South Atlantic island record reveals a South Atlantic response to the 8.2 kyr event', *Climate of the Past* **4**(1), 35–45.

Lloyd, M. J., Shennan, I., Kirby, J. R. and Rutherford, M. M. (1999), 'Holocene relative sea-level changes in the inner Solway Firth', *Quaternary International* **60**(1), 83–105.

Lochte, A. A., Repschlaeger, J., Kienast, M., Garbe-Schoenberg, D., Andersen, N., Hamann, C. and Schneider, R. (2019), 'Labrador Sea freshening at 8.5 ka BP caused by Hudson Bay Ice Saddle collapse', *Nature Communications* **10**(1), 1–9.

Marcott, S. A., Shakun, J. D., Clark, P. U. and Mix, A. C. (2013), 'A Reconstruction of Regional and Global Temperature for the Past 11,300 Years', *Science* **339**(6124), 1198–1201.

Matero, I. S. O., Gregoire, L. J. and Ivanovic, R. F. (2020), 'Simulating the Early Holocene demise of the Laurentide Ice Sheet with BISICLES', *Geoscientific Model Development* **13**(9), 4555–4577.

Matero, I. S. O., Gregoire, L. J., Ivanovic, R. F., Tindall, J. C. and Haywood, A. M. (2017), 'The 8.2 ka cooling event caused by Laurentide ice saddle collapse', *Earth and Planetary Science Letters* **473**, 205–214.

Milliken, K. T., Anderson, J. B. and Rodriguez, A. B. (2008), 'A new composite Holocene sea-level curve for the northern Gulf of Mexico', *Geological Society of America Special Papers* **443**, 1–11.

Milne, G. A., Long, A. J. and Bassett, S. E. (2005), 'Modelling Holocene relative sea-level observations from the Caribbean and South America', *Quaternary Science Reviews* **24**(10-11), 1183–1202.

Milne, G. A. and Mitrovica, J. X. (2008), 'Searching for eustasy in deglacial sea-level histo-
ries', *Quaternary Science Reviews* **27**(25-26), 2292–2302.

Mitrovica, J. X. and Milne, G. A. (2002), 'On the origin of late Holocene sea-level highstands
within equatorial ocean basins', *Quaternary Science Reviews* **21**(20-22), 2179–2190.

Mitrovica, J. X., Tamisiea, M. E., Davis, J. L. and Milne, G. A. (2001), 'Recent mass
balance of polar ice sheets inferred from patterns of global sea-level change', *Nature*
409(6823), 1026–1029.

Morrill, C., Ward, E. M., Wagner, A. J., Otto-Bliesner, B. L. and Rosenbloom, N. (2014),
'Large sensitivity to freshwater forcing location in 8.2ka simulations', *Paleoceanography*
29(10), 930–945.

Newton, T. (2016), Holocene and Common Era sea-level changes in the Falkland Islands,
PhD thesis, Plymouth University.

Newton, T. L., Gehrels, W. R., Fyfe, R. M. and Daley, T. J. (2021), 'Reconstructing sea-level
change in the Falkland Islands (Islas Malvinas) using salt-marsh foraminifera , diatoms
and testate amoebae', *Marine Micropaleontology* **162**, 101923.

Nguyen, V. L., Ta, T. K. O. and Saito, Y. (2010), 'Early Holocene initiation of the Mekong
River delta, Vietnam, and the response to Holocene sea-level changes detected from DT1
core analyses', *Sedimentary Geology* **230**(3-4), 146–155.

Pappalardo, M., Baroni, C., Bini, M., Isola, I., Ribolini, A., Salvatore, M. C. and Zanchetta,
G. (2019), 'Challenges in relative sea-level change assessment highlighted through a case
study: The central coast of atlantic patagonia', *Global and Planetary Change* **182**, 103008.

Park, J., Park, J., Yi, S., Kim, J. C., Lee, E. and Jin, Q. (2018), 'The 8.2 ka cooling event
in coastal East Asia: High-resolution pollen evidence from southwestern Korea', *Scientific
reports* **8**(1), 1–9.

Peltier, W. R. and Fairbanks, R. G. (2006), 'Global glacial ice volume and Last Glacial
Maximum duration from an extended Barbados sea level record', *Quaternary Science
Reviews* **25**(23-24), 3322–3337.

Pollard, D., Chang, W., Haran, M., Applegate, P. and DeConto, R. (2015), 'Large ensemble modeling of last deglacial retreat of the west antarctic ice sheet: Comparison of simple and advanced statistical techniques', *GMDD* **8**(11), 9925–9963.

Porter, S. C., Stuiver, M. and Heusser, C. J. (1984), 'Holocene sea-level changes along the Strait of Magellan and Beagle Channel, southernmost South America', *Quaternary Research* **22**(1), 59–67.

Prieto, A. R., Mourelle, D., Peltier, W. R., Drummond, R., Vilanova, I. and Ricci, L. (2017), 'Relative sea-level changes during the Holocene in the Río de la Plata, Argentina and Uruguay: A review', *Quaternary International* **442**, 35–49.

Reimer, P. J., Austin, W. E., Bard, E., Bayliss, A., Blackwell, P. G., Ramsey, C. B., Butzin, M., Cheng, H., Edwards, R. L., Friedrich, M., , Grootes, P. M., Guilderson, T. P., Hajdas, I., Heaton, T. J., Hogg, A. G., Hughen, K. A., Kromer, B., Manning, S. W., Muscheler, R., Palmer, J. G., Pearson, C., van der Plicht, J., Reimer, R. W., Richards, D. A., Scott, E. M., Southon, J. R., Turney, C. S. M., Wacker, L., Adolphi, F., Büntgen, U., Capano, M., Fahrni, S. M., Fogtmann-Schulz, A., Friedrich, R., Köhler, P., Kudsk, S., Miyake, F., Olsen, J., Reinig, F., Sakamoto, M., Sookdeo, A. and Talamo, S. (2020), 'The intcal20 northern hemisphere radiocarbon age calibration curve (0–55 cal kbp)', *Radiocarbon* **62**(4), 725–757.

Renssen, H., Goosse, H., Fichefet, T. and Campin, J. M. (2001), 'The 8.2 kyr BP event simulated by a global atmosphere-sea-ice-ocean model', *Geophysical Research Letters* **28**(8), 1567–1570.

Roberts, D. E. (1984), Quaternary history of the Falklands, PhD thesis, University of Aberdeen.

Röthlisberger, R., Mulvaney, R., Wolff, E. W., Hutterli, M. A., Bigler, M., Sommer, S. and Jouzel, J. (2002), 'Dust and sea salt variability in central east antarctica (dome c) over the last 45 kyrs and its implications for southern high-latitude climate', *Geophysical Research Letters* **29**(20), 24–1.

Selby, K. A. and Smith, D. E. (2016), 'Holocene Relative Sea-Level Change on the Isle of Skye, Inner Hebrides, Scotland', *Scottish Geographical Journal* **132**(1), 42–65.

Shennan, I., Bradley, S. L. and Edwards, R. (2018), 'Relative sea-level changes and crustal movements in Britain and Ireland since the Last Glacial Maximum', *Quaternary Science Reviews* **188**, 143–159.

Smith, D. E., Cullingford, R. A. and Brooks, C. L. (1983), 'Flandrian relative sea-level changes in the Ythan Valley, northeast Scotland', *Earth Surface Processes and Landforms* **8**(5), 423–438.

Smith, D. E., Firth, C. R., Brooks, C. L., Robinson, M. and Collins, P. E. F. (1999), 'Relative sea-level rise during the Main Postglacial Transgression in NE Scotland, UK', *Transactions of the Royal Society of Edinburgh-Earth Sciences* **90**, 1–27.

Smith, D. E., Firth, C. R. and Cullingford, R. A. (2002), 'Relative sea-level trends during the early-middle Holocene along the eastern coast of mainland Scotland, UK', *Boreas* **31**(2), 185–202.

Smith, D. E., Harrison, S., Firth, C. R. and Jordan, J. T. (2011), 'The early Holocene sea level rise', *Quaternary Science Reviews* **30**(15-16), 1846–1860.

Smith, D. E., Harrison, S. and Jordan, J. T. (2013), 'Sea level rise and submarine mass failures on open continental margins', *Quaternary Science Reviews* **82**, 93–103.

Smith, D. E., Tipping, R. M., Jordan, J. T. and Blackett, M. (2020), 'Holocene coastal change at Luce Bay, South West Scotland', *Journal of Quaternary Science* **35**(6), 743–759.

Stanford, J. D., Hemingway, R., Rohling, E. J., Challenor, P. G., Medina-Elizalde, M. and Lester, A. J. (2011), 'Sea-level probability for the last deglaciation: A statistical analysis of far-field records', *Global and Planetary Change* **79**(3-4), 193–203.

Steffensen, J. P., Andersen, K. K., Bigler, M., Clausen, H. B., Dahl-Jensen, D., Fischer, H., Goto-Azuma, K., Hansson, M., Johnsen, S. J., Jouzel, J., Masson-Delmotte, V., Popp, T., Rasmussen, S. O., Rothlisberger, R., Ruth, U., Stauffer, B., Siggaard-Andersen, M. L., Sveinbjornsdottir, A. E., Svensson, A. and White, J. W. C. (2008), 'High-resolution Greenland Ice Core data show abrupt climate change happens in few years', *Science* **321**(5889), 680–684.

Stenni, B., Jouzel, J., Masson-Delmotte, V., Röthlisberger, R., Castellano, E., Cattani, O., Falourd, S., Johnsen, S., Longinelli, A., Sachs, J. *et al.* (2004), 'A late-glacial high-

resolution site and source temperature record derived from the epica dome c isotope records (east antarctica)', *Earth and Planetary Science Letters* **217**(1-2), 183–195.

Stenni, B., Masson-Delmotte, V., Johnsen, S., Jouzel, J., Longinelli, A., Monnin, E., Röthlisberger, R. and Selmo, E. (2001), 'An oceanic cold reversal during the last deglaciation', *Science* **293**(5537), 2074–2077.

Stroeven, A. P., Hattestrand, C., Kleman, J., Heyman, J., Fabel, D., Fredin, O., Goodfellow, B. W., Harbor, J. M., Jansen, J. D., Olsen, L., Caffee, M. W., Fink, D., Lundqvist, J., Rosqvist, G. C., Stromberg, B. and Jansson, K. N. (2016), 'Deglaciation of Fennoscandia', *Quaternary Science Reviews* **147**, 91–121.

Tamura, T., Saito, Y., Sieng, S., Ben, B., Kong, M., Sim, I., Choup, S. and Akiba, F. (2009), 'Initiation of the Mekong River delta at 8 ka: evidence from the sedimentary succession in the Cambodian lowland', *Quaternary Science Reviews* **28**(3–4), 327–344.

Taylor, K. C., Mayewski, P. A., Alley, R. B., Brook, E. J., Gow, A. J., Grootes, P. M., Meese, D. A., Saltzman, E. S., Severinghaus, J. P., Twickler, M. S., White, J. W. C., Whitlow, S. and Zielinski, G. A. (1997), 'The Holocene Younger Dryas transition recorded at Summit, Greenland', *Science* **278**(5339), 825–827.

Tegzes, A. D., Jansen, E. and Telford, R. J. (2014), 'The role of the northward-directed (sub)surface limb of the Atlantic Meridional Overturning Circulation during the 8.2 ka event', *Climate of the Past* **10**(5), 1887–1904.

Teller, J. T., Leverington, D. W. and Mann, J. D. (2002), 'Freshwater outbursts to the oceans from glacial Lake Agassiz and their role in climate change during the last deglaciation', *Quaternary Science Reviews* **21**(8-9), 879–887.

Thomas, E. R., Wolff, E. W., Mulvaney, R., Steffensen, J. P., Johnsen, S. J., Arrowsmith, C., White, J. W. C., Vaughn, B. and Popp, T. (2007), 'The 8.2 ka event from Greenland ice cores', *Quaternary Science Reviews* **26**(1-2), 70–81.

Tjallingi, R., Stattegger, K., Stocchi, P., Saito, Y. and Wetzel, A. (2014), 'Rapid flooding of the southern Vietnam shelf during the early to mid-Holocene', *Journal of Quaternary Science* **29**(6), 581–588.

Törnqvist, T. E., Bick, S. J., Gonzalez, J. L., van der Borg, K. and de Jong, A. F. M. (2004), 'Tracking the sea-level signature of the 8.2 ka cooling event: New constraints from the Mississippi Delta', *Geophysical Research Letters* **31**(23).

Törnqvist, T. E., Hijma, M. P., Trnqvist, T. E. and Hijma, M. P. (2012), 'Links between early Holocene ice-sheet decay, sea-level rise and abrupt climate change', *Nature Geoscience* **5**(9), 601–606.

Ullman, D. J., Carlson, A. E., Hostetler, S. W., Clark, P. U., Cuzzone, J., Milne, G. A., Winsor, K. and Caffee, M. (2016), 'Final Laurentide ice-sheet deglaciation and Holocene climate-sea level change', *Quaternary Science Reviews* **152**, 49–59.

Walker, M., Berkelhammer, M., Björck, S., Cwynar, L., Fisher, D., Long, A., Lowe, J., Newnham, R., Rassmussen, S. and Weiss, H. (2012), 'Formal subdivision of the holocene series/epoch: a discussion paper by a working group of intimate and the subcommission on quaternary stratigraphy', *Journal of Quaternary Science* **27**, 649–659.

Wang, Z. H., Zhan, Q., Long, H. Y., Saito, Y., Gao, X. Q., Wu, X. X., Li, L. and Zhao, Y. A. (2013), 'Early to mid-Holocene rapid sea-level rise and coastal response on the southern Yangtze delta plain, China', *Journal of Quaternary Science* **28**(7), 659–672.

Weber, M. E., Clark, P. U., Kuhn, G., Timmermann, A., Sprenk, D., Gladstone, R., Zhang, X., Lohmann, G., Menviel, L., Chikamoto, M. O., Friedrich, T. and Ohlwein, C. (2014), 'Millennial-scale variability in Antarctic ice-sheet discharge during the last deglaciation', *Nature* **510**(7503), 134–138.

Whitehouse, P. L., Bentley, M. J. and Le Brocq, A. M. (2012), 'A deglacial model for Antarctica: Geological constraints and glaciological modelling as a basis for a new model of Antarctic glacial isostatic adjustment', *Quaternary Science Reviews* **32**, 1–24.

Wiersma, A. P., Renssen, H., Goosse, H. and Fichefet, T. (2006), 'Evaluation of different freshwater forcing scenarios for the 8.2 ka BP event in a coupled climate model', *Climate Dynamics* **27**(7-8), 831–849.

Wu, J. Y., Wang, Y. J., Cheng, H., Kong, X. G. and Liu, D. B. (2012), 'Stable isotope and trace element investigation of two contemporaneous annually-laminated stalagmites from northeastern China surrounding the "8.2 ka event"', *Climate of the Past* **8**(5), 1497–1507.

Xiong, H., Zong, Y., Li, T., Long, T., Huang, G. and Fu, S. (2020), 'Coastal GIA processes revealed by the early to middle Holocene sea- level history of east China', *Quaternary Science Reviews* **233**, 106249.

Xiong, H., Zong, Y., Qian, P., Huang, G. and Fu, S. (2018), 'Holocene sea-level history of the northern coast of South China Sea', *Quaternary Science Reviews* **194**, 12–26.

Yu, H., Xiong, Y. Q., Liu, Z. X., Berne, S., Huang, C. Y. and Jia, G. D. (2008), 'Evidence for the 8,200 a BP cooling event in the middle Okinawa Trough', *Geo-Marine Letters* **28**(3), 131–136.

Yu, S. Y., Berglund, B. E., Sandgren, P. and Lambeck, K. (2007), 'Evidence for a rapid sea-level rise 7600 yr ago', *Geology* **35**(10), 891–894.

Zanchetta, G., Bini, M., Isola, I., Pappalardo, M., Ribolini, A., Consoloni, I., Boretto, G., Fucks, E., Ragaini, L. and Terrasi, F. (2014), 'Middle- to late-Holocene relative sea-level changes at Puerto Deseado (Patagonia, Argentina)', *The Holocene* **24**(3), 307–317.

Zhang, W., Yan, H., Dodson, J., Cheng, P., Liu, C., Li, J., Lu, F., Zhou, W. and An, Z. (2018), 'The 9.2 ka event in Asian summer monsoon area: the strongest millennial scale collapse of the monsoon during the Holocene', *Climate Dynamics* **50**(7-8), 2767–2782.

Zong, Y. Q., Huang, K. Y., Yu, F. L., Zheng, Z., Switzer, A., Huang, G. Q., Wang, N. and Tang, M. (2012), 'The role of sea-level rise, monsoonal discharge and the palaeo-landscape in the early Holocene evolution of the Pearl River delta, southern China', *Quaternary Science Reviews* **54**, 77–88.

Chapter 3

Development of an intertidal foraminifera training set for the North Sea and an assessment of its application for Holocene sea-level reconstructions

Graham Rush [1], Patrick McDarby[1], Robin Edwards[2], Yvonne Milker[3], Ed Garrett[1], Roland Gehrels[1]

[1] *Department of Environment and Geography, University of York,York, UK*

[2] *School of Natural Sciences, Trinity College Dublin, Ireland*

[3] *Center for Earth System Research and Sustainability, Institute for Geology, University of Hamburg, Germany*

Abstract

Regional datasets of the vertical distribution of intertidal foraminifera are useful to reconstruct Holocene sea-level changes from fossil foraminifera in estuaries and salt marshes. In this paper, we present a new foraminiferal dataset from the Ythan Estuary (Scotland) and combine it with data from eight other coastal sites from England, Denmark and Germany to produce a regional modern training set for the North Sea. We recognise a correlation between foraminifera and tidal elevation which makes the foraminifera suitable as sea-level indicators. We subdivide the data into subregional training sets and develop WA and WA-PLS transfer functions. Applying a variety of statistical methods, including detrended canonical analysis, cross-validation by bootstrapping and leave-one-site-out, and the modern analogue technique, we establish the most appropriate transfer function from which to reconstruct early Holocene sea-level changes in a sediment core from the western North Sea coast. Results show that the subregional England/Scotland training set provides the most appropriate sea-level reconstructions, with decimetre-scale uncertainties. The techniques we use in this study, that consider both the modern and fossil assemblages to determine the best training set and transfer function, are suggested as a template for the development of regional transfer functions based on foraminifera and other intertidal microfossils.

Highlights

- New foraminifera modern training set for the Ythan Estuary, east Scotland.

- Synthesis of North Sea foraminifera data for sea-level reconstructions.

- Template for determining the most effective regional transfer function.

keyword

Sea level; Transfer function; Foraminifera; Salt marsh

3.1   Introduction

Foraminifera have long been recognised as accurate and precise sea-level indicators in Holocene intertidal deposits (Scott and Medioli, 1978). This is because foraminiferal assemblages form in narrow vertical zones across the intertidal zone as a result of variations in tidal submergence. The correlation with elevation relative to the tidal frame provides a tool to reconstruct sea-level changes from fossil intertidal foraminifera preserved in sediment cores (Gehrels, 2000). When the relationship between foraminifera and elevation in the modern environment is quantified, regression methods can be applied to develop predictive transfer functions that are capable of reconstructing sea-level changes from fossil foraminiferal assemblages in subsurface intertidal deposits. Relative sea-level reconstructions based on foraminifera in salt-marsh deposits have been established in many temperate coastal regions with high vertical precision, often quoted as sub-decimetre (e.g. Gehrels *et al.*, 2004, Horton *et al.*, 2009, Hawkes *et al.*, 2010, Engelhart *et al.*, 2011, Wright *et al.*, 2011, Barnett *et al.*, 2016), leading salt marshes to be labelled 'geological tide gauges' (Barlow *et al.*, 2013). Although it is not possible to assess the accuracy of palaeo reconstructions prior to pre-instrumental records, instead consistency is used as an informal indicator and the assumption of uniformitarianism is applied.

Many studies use foraminiferal assemblages in modern samples from a proximal site, collectively known as a training set, to develop local transfer functions that are then applied to reconstruct sea level based on fossil assemblages from a core (e.g. Gehrels *et al.*, 2004, 2005). This method relies on the assumption that the assemblages in the modern environment are an accurate analogue for the past environment and fossil foraminifera preserved in the core. In the absence of appropriate analogues in local training sets, and therefore a likely non-conformity of environmental conditions, a regional training set developed from multiple sites may be more appropriate (Watcham *et al.*, 2013, Barlow *et al.*, 2013). A regional dataset is a collection of training sets from multiple sites along a stretch of coastline, although the size of the region is not defined (Barlow *et al.*, 2013). Regional foraminifera training sets have been developed for regions such as the UK (Horton *et al.*, 1999*a*), southwest Europe (Leorri *et al.*, 2011), Oregon, western USA (Hawkes *et al.*, 2010) and the eastern coast of the USA (Wright *et al.*, 2011, Kemp *et al.*, 2013). The method has been used to produce continuous sea-level records for the late Holocene (e.g. Hawkes *et al.*, 2010, Engelhart *et al.*, 2011) and the early Holocene using foraminifera (Horton *et al.*, 1999*b*) and diatoms (Lawrence *et al.*,

2016). Barlow *et al.* (2013) discuss the relative benefit of local and regional approaches, but in general a regional training set that comprises sites where microfossils are responding to tidal inundation in a similar manner increases natural variability and therefore the potential of providing an analogous environment.

For early and middle Holocene sea-level reconstructions developed from intertidal microfossils, the likelihood that environmental conditions and/or the realised niches of taxa at a single site have remained constant may be small. For example, Edwards and Horton (2000) found that of 26 fossil assemblages from cored intertidal sediments in the south of England, 10 were unlike any other modern surface assemblage. A lack of modern analogues requires the inclusion of additional sites in to a larger training set. Assemblages from multiple sites are more likely to capture a wider range of environmental conditions with a greater chance of providing a suitable modern analogue (Legendre and Fortin, 1989, Juggins and Birks, 2012), with the caveat that the precision of the prediction may be reduced. For example, Lawrence *et al.* (2016) applied a regional diatom transfer function to generate an early Holocene sealevel reconstruction in southwest Scotland based on samples from nine sites on the west coast of Scotland. Yet a key taxon found in the fossil record had become extinct in the area and a further site from the English North Sea coast was therefore included to provide the missing analogue. This reduced the mean precision of the sea-level reconstruction, which was calculated at $\pm$ 56 cm (Lawrence *et al.*, 2016). These examples highlight that whilst generally reducing precision, regional transfer functions are generally required to ensure reconstructions of early Holocene sea-level changes based on microfossils are more likely to be accurate. We deem a reconstruction to be accurate if it is consistent with others using different training sets and models where foraminifera show a similar inter-site relationship with tidal inundation.

In this paper we compile a new regional training set of intertidal foraminifera for the North Sea basin. The training set includes nine sites from the eastern (England and Scotland) and western (Denmark and Germany) coasts of the North Sea. Data from eight sites have been previously published and we add to this by presenting a new local dataset for a site on the east coast of Scotland, the Ythan Estuary. The aims of this paper are:

1. to study the relationship with elevation relative to sea level of the modern foraminifera in the Ythan Estuary and the regional composite training set, known forthwith as the *North Sea* training set, and hence its suitability for reconstructing sea-level changes.

2. to assess the best choice of transfer function between regional, sub-regional and local training sets, to reconstruct relative sea-level change from an early Holocene sediment core and provide a template for decision making in similar studies.

3.2 Materials and Methods

3.2.1 Ythan Estuary training set development

The Ythan Estuary consists of mudflats, salt marshes and freshwater marshes (Fig. 3.1). The River Ythan is tidal up to 11 km from the mouth of the estuary (Stapleton and Pethick, 1996) and the intertidal area is approximately 1.85 km^2, of which 0.13 km^2 is intact salt marsh. The mean tidal range at the mouth of the estuary is 2.48 m as calculated by taking a weighted average of two nearby tidal gauge stations at Aberdeen (57°8.64' N, 2°4.82' W) and Peterhead (57°29.84' N, -2°13.69' W), 18 km and 15 km away respectively (UK Hydrographic Office, 2016). To the north and west, the estuary is mostly bounded by arable farmland. However, in the 'Sleek of Tarty' area adjacent to the mouth of the Tarty Burn tributary (see Fig. 3.1) the salt marsh extends into a freshwater marsh and woodland. In this area the salt marsh is characteristically undulating with many well defined ponds and creeks. The lower salt marsh generally terminates at a small tidally cut cliff, although occasionally grades into the mudflat.

We established a local benchmark using a Trimble R6 model 3 DGPS with a vertical uncertainty of 0.006 m. The benchmark was tied to two local Ordnance Survey benchmarks to provide elevation measurements relative to the UK national vertical geodetic ordnance datum (OD). Transects were designed to capture the elevation gradient from the highest occurrence of foraminifera (HoF) to mean tide level (MTL) and included a freshwater reed bed, high, middle and low salt marsh zones and mudflat. Sampling was timed to coincide with a large spring tide to maintain standardisation with other studies and to allow sampling at lower elevations (e.g. Avnaim-Katav *et al.*, 2017). Sampling sites were established at c. 5 cm elevation intervals along two transects using a Trimble M1 DR2 total station. Standardised surface samples of 10 cm^2 by 1 cm deep were collected (e.g. Gehrels, 2000). After collection samples were stored at 4 °C before processing.

Preparations of foraminifera samples followed standard laboratory procedures (Gehrels, 2002). The 63 – 500 µm fraction of a 5 cc subsample was wet sieved and stored in a Rose
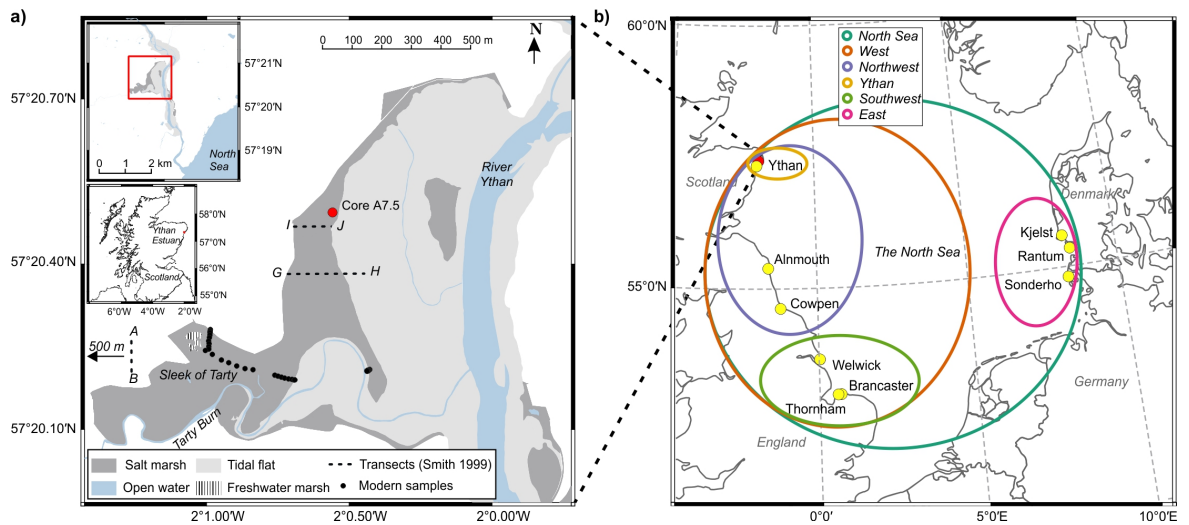
Figure 3.1: Map of the Ythan Estuary and North Sea sites. a) The Ythan Etsuary showing the transects of modern samples, the transects from Smith *et al.* (1999) shown in Fig. b) Map of modern foraminifera sites (yellow markers) that make up the training sets. Red marker indicates the site of the core used in the reconstruction. Coloured ellipses indicate groupings of sites for regional and subregional datasets. The names for each region or subregion correspond to the main text.

Bengal and ethanol solution within seven days of collection to enable identification of living and dead foraminifera (Murray and Bowser, 2000). Tests containing stained protoplasm within the last few chambers were assumed to be living and only the dead foraminiferal taxa were investigated to avoid seasonal bias (Culver and Horton, 2005) and provide the most representative analogue for material found in fossil records (Horton *et al.*, 1999*b*, Horton and Edwards, 2006, Berkeley *et al.*, 2007, Kemp *et al.*, 2009). Samples were split using a wet splitter (Scott and Hermelin, 1993) and picked and counted until a target of at least 200 individuals was met in even 1/8 splits. If this number was not achieved the full sample was counted. Individuals were identified with reference to the taxonomy of de Rijk (1995), Wright *et al.* (2011), Edwards and Wright (2015), Müller-Navarra *et al.* (2017), Hayward *et al.* (2020). A total of 37 samples were counted and individual taxa expressed as their percentage relative abundance of the sample.

3.2.2   Regional training set compilation

Existing modern salt-marsh foraminifera training sets, collected from around the North Sea, include Alnmouth, Brancaster, Cowpen, Thornham and Welwick (Horton and Edwards, 2006), Brancaster (Gehrels *et al.*, 2001), Kjelst (Gehrels and Newman, 2004), Rantum,

So(Müller-Navarra *et al.*, 2017) and Tümlau (Müller-Navarra *et al.*, 2016) (see Fig. 3.1). All of the data was included except Tümlau, because of human interference that makes it unsuitable for sea-level reconstructions (Müller-Navarra *et al.*, 2016), and two Alnmouth transects because of our doubts over the accuracy of the elevation measurements. The data was screened such that samples were retained if total counts were 75 in order to be able to reconstruct sea-level change at a decimetre- and decadal-scale (Kemp *et al.*, 2020). The nine sites provided a total of 265 samples of foraminifera assemblages from 52 different taxa. The screening of the raw data of each training set resulted in between 17 and 35 % (*Northwest and Ythan* respectively) of samples being removed. The large variation in samples being removed is largely due to zero counts being included in some sites. Tidal datums were taken from the original publications and the tidal range was modelled for each site using the TPXO8-ATLAS global model of ocean tides (Egbert and Erofeeva, 2010). The data are summarised in Table 3.1 and throughout the text. The *North Sea* training set was sub-divided in order to test the effect on model performance of training set size and tidal range, that naturally coincides with geographic regions (Fig. 3.1b) owing to the North Sea tidal set up.

Table 3.1: Summary of intertidal sites included in the regional training sets. Geomorphic classifications are based on Allen (2000). The number of taxa and samples are given for the raw data and after screening.

Site	Classification	No. of samples Raw / Screened	No. of taxa	Tidal range (m)	References
Alnmouth	Estuarine back-barrier	20 / 20	29	3.13	Horton and Edwards (2006)
Brancaster	Open coast back-barrier	59 / 49	24	3.89	Gehrels *et al.* (2001), Horton and Edwards (2006)
Cowpen	Estuarine back-barrier	31 / 30	24	3.21	Horton and Edwards (2006)
Kjelst	Open embayment	27 / 12	12	1.04	Gehrels and Newman (2004)
Rantum	Open coast back-barrier	33 / 28	14	1.75	Müller-Navarra *et al.* (2017)
Sønderho	Open embayment	14 / 12	12	1.66	Müller-Navarra *et al.* (2017)
Thornham	Open coast back-barrier	24 / 23	23	3.62	Horton and Edwards (2006)
Welwick	Estuarine back-barrier	20 / 20	20	3.92	Horton and Edwards (2006)
Ythan	Estuarine back-barrier	37 / 24	15	2.48	This study

In order for the local training sets to be incorporated into a regional model, taxonomy was standardised using the World Register of Marine Species (Hayward *et al.*, 2020) (Table A.1) and the sample elevation was standardised using a standardised water level index (SWLI) which accounts for differences in tidal range between the sites (Zong and Horton, 1999, Gehrels, 2000). The lowest common phylogenic level was applied which resulted in some taxa being grouped at genus level. The only common environmental variable across all sites was elevation relative to a local datum. While inundation frequency is a more direct ecological parameter (Gehrels, 2000, Gehrels *et al.*, 2001, Müller-Navarra *et al.*, 2017), elevation is a linear approximation that is widely used and is applied here in the absence of inundation

information across all sites. Generally MTL and mean high water spring tide (MHWS) or mean higher high water (MHHW) have been used for standardisation between sites with different tidal ranges in sea-level studies; however, transfer functions are sensitive to the choice of tidal datum (Woodroffe and Long, 2010, Wright *et al.*, 2011). Woodroffe and Long (2010) demonstrate that highest astronomical tide (HAT) causes less distortion in the upper tidal range, a key locale in foraminifera reconstructions (Gehrels *et al.*, 2004). Wright *et al.* (2011) investigated this cross site standardisation further and concluded that the well-established ecological relationship between HoF and the upper limit of marine influence is more effective yet. However, sampling up to the elevation of HoF is only definitively reached at two of the sites (Brancaster and Ythan) and we therefore use the highest common datum, HAT, in the standard SWLI equation (Eq. 3.1) (Horton *et al.*, 1999*b*)

$$SWLI_n = \frac{100(h_n - MTL_s)}{HAT_s - MTL_s} + 100 \tag{3.1}$$

such that where $SWLI_n$ is the standardised water level index of the sample (n), h_n is the height of the sample in the local datum, MTL_s and HAT_s are the mean tide level and highest astronomical tide of the site (s) in the local datum.

3.2.3   Transfer functions and data analysis

Detrended canonical correspondence analysis (DCCA) (Hill and Gauch, 1980) was applied using the software CANOCO version 5.1 (ter Braak and Smilauer, 2012) to test whether the taxa response is linear or unimodal along the elevation gradient. All datasets had a DCCA axis gradient length greater than two standard deviations, generally accepted as being the threshold, such that unimodal statistical models are appropriate for exploration of the training sets (Birks, 1995). We therefore developed unimodal transfer functions for the six training sets using two different techniques: weighted averaging with classical deshrinking (WA) (Ter Braak and Barendregt, 1986) and weighted averaging with partial least square regression (WA-PLS) (ter Braak and Juggins, 1993).

WA based transfer functions take the average of all the optima of all the taxa weighted such that those with greater abundances are given more prominence. This causes the vertical range to be compressed and thus a 'deshrinking' correction is necessary. Inverse deshrinking, equivalent to WA-PLS component 1, is more suitable for reconstructions close to the middle

of the environmental gradient, whilst classical deshrinking is more suitable for reconstructions close to the limits of the gradient (Juggins and Birks, 2012, Kemp and Telford, 2015). We aim to capture the maximum environmental gradient and we therefore favour the use of the classical method for the WA transfer functions.

WA-PLS based transfer functions (components 2 and higher) exploit correlations that remain in the residuals after fitting SWLIs that are not taken into account in WA by adjusting taxa optima (Juggins and Birks, 2012, Kemp and Telford, 2015). Each extra component can be seen as adding extra, hypothetical, environmental variables. WA-PLS generally outperforms WA because; 1) 'edge effects' that affect WA (where optima are overestimated at the low end and underestimated at the high end (Mohler, 1983)) can be reduced or eliminated by WA-PLS; and/or 2) because in reality the composition of taxa assemblages is influenced by additional factors other than elevation, and WA-PLS can exploit the resultant structured pattern in the residuals after WA; and/or 3) the fit of outliers may be improved (Birks, 1995, Juggins and Birks, 2012). WA-PLS is thus favoured in many sea-level studies (Barlow et al., 2013). We chose the best performing model with the fewest numbers of components, limited to three, following the rule of parsimony (Birks, 2012), only selecting successive components if a significant performance increase, based on the root mean squared error of prediction (RMSEP) and R^2 values (Birks, 1998), of > 5 % is observed. These are from here on known as the WA-PLS transfer functions with the number of components given as c (e.g *WAPLS-c1*).

To assess the best choice of transfer function for a sea-level reconstruction, we collected a core (A7.5) from the Ythan Estuary using a 50 mm Russian corer at 57°20.49' N, 2°0.54' W. The site was selected based on the published stratigraphy by Smith *et al.* (1999) who dated the peat at the base of a core at 5.19 m core depth to c. 8,500 ka cal BP. This basal peat is overlain by salt-marsh and mudflat deposits, and topped by a sand deposit that is attributed to the Storegga tsunami of c. 8,150 ka cal BP (Dawson *et al.*, 2011, Bondevik *et al.*, 2012). We took 1-cm-thick subsamples from the core at appropriate depths with respect to lithological and biological changes in an iterative manner between the basal peat at 5.17 m and the base of the sand deposit at 2.28 m core depth. Thus the core spans a period in the early Holocene that is of interest as it potentially includes the sea-level rise associated with the drainage of glacial lakes Agassiz and Ojibway at c. 8,400 ka cal BP (Barber *et al.*, 1999, Li *et al.*, 2012, Hijma and Cohen, 2010, 2019, Lawrence *et al.*, 2016).

A total of 24 samples were prepared and foraminifera counted as described above.

The resultant WA and WA-PLS transfer functions were used to predict SWLIs from the core fossil foraminifera. This was converted to an indicative meaning in metres by reversing Eq. 5.1 using the following equation:

$$I_f = \frac{(SWLI_f - 100)(HAT_b - MTL_b)}{100} + MTL_b \qquad (3.2)$$

where I_f is the indicative meaning of the fossil sample ($_f$) in the local datum, $SWLI_f$ is the predicted SWLI of the fossil sample ($_f$), HAT_b and MTL_b are the highest astronomical tide and mean tide level of the site (b) in the local datum. The transfer functions also produce prediction sample specific errors (SSE) for the fossil samples that is converted in the same manner and used as the range of the reconstructions (range = $I_f \pm SSE$).

To assess training set and transfer function performance and decide on the most suitable to use for our core reconstruction, we conducted qualitative and quantitative analyses in a step-wise manner. All analyses were carried out in R version 3.6.1 using the packages rioja (Juggins, 2017), vegan (Oksanen *et al.*, 2013) and fpc (Hennig, 2010). We used the following methods:

1. Detrended correspondence analysis (DCA) with fossil samples passively projected to assess the samples and taxa groupings and relationships (Edwards and Wright, 2015).

2. Cluster analysis using partitioning around medoids (PAM) with Euclidean distances (Kaufmann and Rousseeuw, 1990, Rousseeuw, 1987) to recognise clusters of modern and fossil foraminiferal assemblages. The highest average silhouette width was used to determine the appropriate number of partitions (Kemp *et al.*, 2013) .

3. Modern analogue technique (MAT) using the minimum dissimilarity coefficient (MinDC) to measure the dissimilarity between fossil samples and the closest modern analogue using the commonly applied Chord-squared distance metric (Kemp and Telford, 2015). We applied the conservative method of defining 'good' and 'close' modern analogues for fossil samples as having a MinDC lower than the 5th and 20th percentiles respectively and samples with a larger MinDC defined as 'poor' (Watcham *et al.*, 2013, Barlow *et al.*, 2013).

4. Transfer function performance statistics using bootstrapping (boot) and leave-one-

site-out (LOSO) cross-validation to assess the quality of the transfer functions and the independence of samples (Telford and Birks, 2005, Payne *et al.*, 2012, Kemp *et al.*, 2013).

5. If using WA-PLS with > 2 components, the pattern of taxa optima updates were analysed to assess the effect of introducing more statistical complexity that may distort reconstructions (Wright *et al.*, 2011) .

6. Ranges of the different core reconstructions were compared to evaluate the likely accuracy of each regional, subregional and local transfer function.

7. The statistical significance of the reconstructions was measured by comparing the reconstructions from the training sets against a set of 999 randomly generated data using redundancy analysis ordination (Telford and Birks, 2011).

3.3   Results and Discussion

3.3.1   Training set development

3.3.1.1   Ythan Estuary data

Foraminifera occur in the Ythan Estuary from the lowest sampled point of just above MTL across the elevation gradient of the tidal zone to just above HAT. Both dead and living individuals were found up to an elevation of 2.45 m OD (SWLI = 202). A total of 15 taxa were found although four had a maximum abundance < 10 %. The majority of taxa show some relationship with elevation (see Fig. 3.2). Taxa elevation optima (the abundance weighted average of SWLI in all samples in which they occur (Ter Braak and Barendregt, 1986)) and tolerances (the abundance weighted standard deviation (Birks *et al.*, 1990)) following WA show that the different taxa occupy a gradient of different elevations (Fig. 3.2c). The highest marsh samples, above MHWS at 1.96 m OD where tidal inundation is infrequent, are low in total foraminifera counts and hence only one was retained following screening. In these samples *Balticammina pseudomacrescens* appears in relatively high abundance much like in the eastern North Sea marshes (Gehrels and Newman, 2004, Müller-Navarra *et al.*, 2017). The salt-marsh samples are almost entirely composed of agglutinated taxa. *Entzia macrescens*, also commonly referred to as *Jadammina macrescens*, is the most common salt-marsh taxon and is found in similar abundances across the marsh. *Miliammina fusca* is

found in greatest abundances in the lower marsh like in many marshes globally (see Berkeley *et al.*, 2007).

Cluster analysis (Fig. 3.2a) shows that the salt-marsh samples can be subdivided into three clusters that are also somewhat evident in the DCA plot (Fig. 3.2b). A low marsh cluster is formed with high abundance of *Miliammina fusca*, a mid-high marsh cluster with a mixture of agglutinated taxa and a final cluster with *Haplophragmoides* spp. found in unusually high abundances (> 75 %) compared to other UK salt marshes (Horton *et al.*, 1999*b*). There is a clear shift to assemblages dominated by calcareous species at 1.22 m OD just below the transition from salt marsh to mudflat, along with occasional *Trochammina ochracea* and *Haplophragmoides* spp.. PAM clustering displays two distinct clusters of these mudflat samples, one with *Haynesina germanica* most abundant and featuring high abundances of *Buliminella elegantissima* and *Brizalina variabilis*, and a second with few *Buliminella elegantissima* and *Brizalina variabilis* and dominated by *Elphidium williamsoni*, *Trochammina ochracea* and *Haplophragmoides* spp.. Though usually found in the vegetated zone (Berkeley *et al.*, 2007) *Haplophragmoides* spp. are also found on mudflats in the east of the North Sea (Müller-Navarra *et al.*, 2017). The modern foraminifera surface distributions of the sampled tidal zone in the Ythan Estuary display a well-established relationship with elevation and are therefore suitable sea-level indicators.

3.3.1.2 Compiled North Sea data

The foraminifera of the eight previously published sites and the Ythan Estuary (see Table 3.1) combined in the regional *North Sea* data occur at elevations from 273 SWLI, well above HAT, to 70, below MTL (Fig. 3.4). The highest 14 samples (> 210 SWLI), well above HAT, are all from the sites in Denmark and Germany. This could be due to the wind-induced setup that occurs in these areas (Bartholdy *et al.*, 2004, Pedersen *et al.*, 2009), where tides > 3 m above HAT in Esbjerg have been recorded (Bartholdy *et al.*, 2010). These samples are generally restricted to *Balticammina pseudomacrescens* and *Entzia macrescens* which are species able to survive despite infrequent flooding (Berkeley *et al.*, 2007). Although micro tidal sites are generally desired because they provide higher precision reconstructions (Callard *et al.*, 2011, Barlow *et al.*, 2013, Edwards and Wright, 2015), they will be more influenced by this effect and hence the micro tidal range of the eastern sites (all < 1 m) may be causing the extremely high SWLI values seen in these sites a phenomenon also

(a)

(b)

(c)
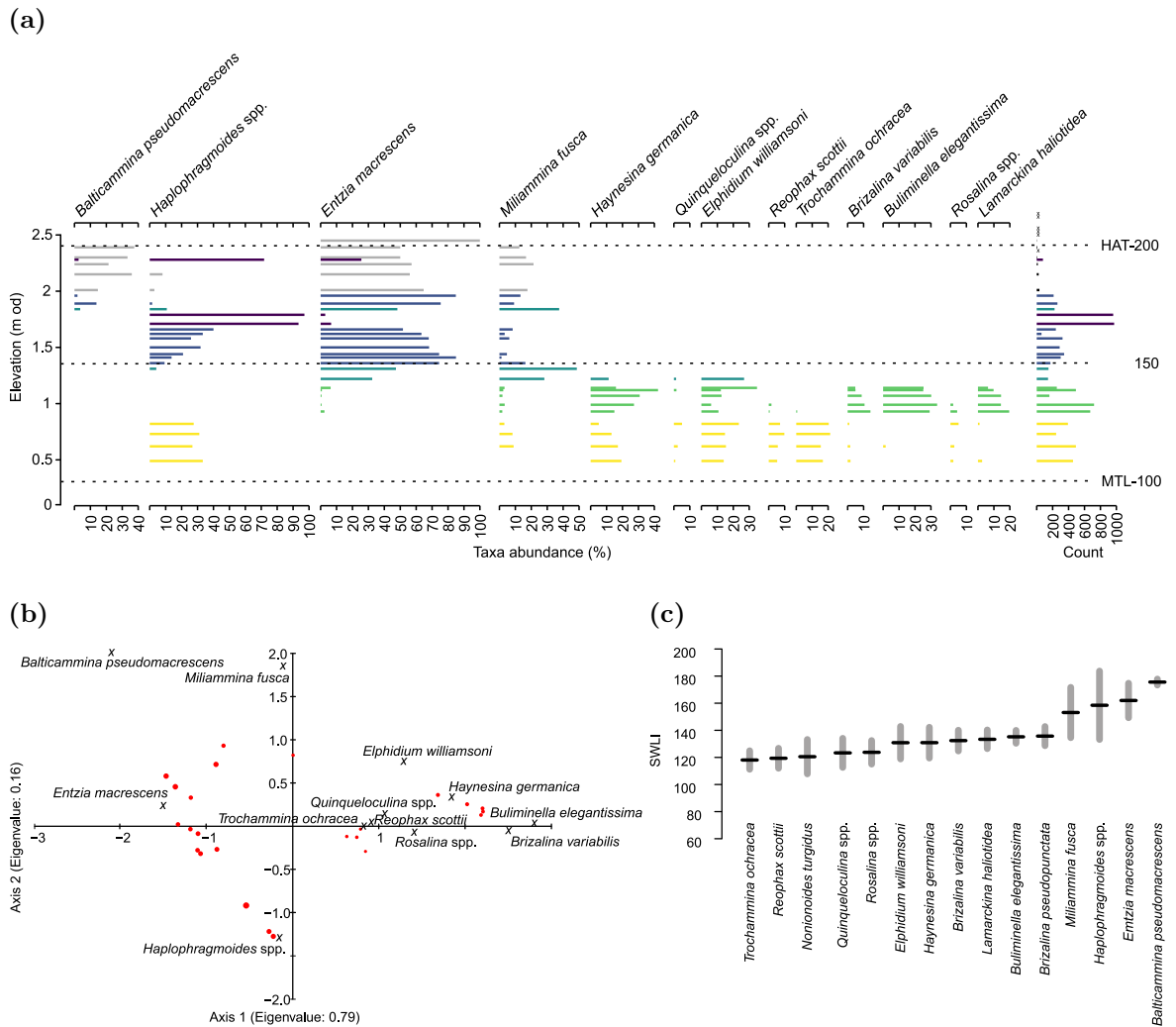
Figure 3.2: Summary diagrams of the modern foraminifera assemblages for the Ythan: a) Foraminifera abundances as percentages of the count of total dead specimens (given in the final column) against elevation. Only taxa with > 5 % maximum abundance are shown. Grey bars denote samples that were excluded following screening and Xs mark where no foraminifera were found. The bars are coloured according to PAM clustering of the dataset (average sillhoutte width = 0.53). Dashed lines indicate tidal datums and SWLI values. b) Detrended correspondence analysis (DCA) of surface foraminifera assemblages showing samples in circles, sized according to SWLI, and taxa. c) Taxa tolerances (grey bar) and optima (black lines) of the Ythan Estuary foraminifera taxa following WA with classical deshrinking.

seen in some sites in the US (Wright *et al.*, 2011). The assemblages of the remaining salt-marsh samples are dominated by agglutinated foraminifera. *Entzia macrescens* is abundant across the marsh, as is *Miliammina fusca* although in lower abundances. *Trochammina inflata* appears mainly restricted to the higher marsh, while *Haplophragmoides* spp. become

more prevalent in the middle-lower marsh mainly at Rantum, Sand Ythan. Calcareous taxa become more abundant in the lower marsh, although are found much higher particularly in eastern marshes which may be due to the wind-induced setup and/or high pH promoting better preservation (Müller-Navarra *et al.*, 2016). Relatively high abundances of *Ammonia* spp. are found at Brancaster and Thornham compared to the other sites, while *Haynesina germanica* is notably abundant at Welwick. Foraminifera were not sampled below 140 SWLI, approximately at the transition between the salt marsh and the mudflat, at Brancaster, Kjelst and Thornham. However, the assemblages from the sites that were sampled show a clear dominance of calcareous taxa. The taxa abundances appear to show a relationship with elevation across the training set, although it may be reduced at the eastern sites due to local conditions.

The relationship between taxa and elevation is confirmed by the cluster analysis (Fig. 3.4) and DCA (Fig. 3.3). PAM clustering produces the highest average silhouette width when samples are split into three clusters, shown in Fig. 3.4 and Fig. A.1. Cluster 1 mainly comprises the mudflat samples (defined as SWLI approximately < 140) dominated by calcareous taxa from a mixture of sites. Cluster 2 mainly comprise samples where *Haplophragmoides* spp. is abundant as described above. While *Haplophragmoides* spp. are not rare taxa and are found at varying elevations relative to tidal inundation in other marshes (e.g. Berkeley *et al.*, 2007, for a review), they are marked out in these samples by their high abundance that cause high intra-cluster similarity and low dissimilarity with other samples. Finally, samples in cluster 3 contain the majority of salt-marsh samples. The majority of samples are dominated by *Entzia macrescens* and encompass the full elevation range of the salt marsh. A cluster of samples that are almost entirely found above 170 SWLI and comprise *Entzia macrescens*, *Miliammina fusca* and *Trochammina inflata* is identified from within cluster 3 if we add extra clusters.

A feature of the data appears to be a small degree of clustering by sites. This could be due to a lack of independence of samples because of spatial auto-correlation that may cause transfer function performance statistics to be overly optimistic (Telford and Birks, 2005, Payne *et al.*, 2012), or that each site has unique controls that could make a regional transfer function either problematic or arguably more robust (Legendre and Fortin, 1989). To investigate this further, LOSO cross-validation was applied and is discussed in Section 3.3.2.3.

The DCA plots summarise the unconstrained relationship between samples, taxa and SWLI (Fig. 3.3). The plot shows that the samples tend to align towards axis 1 and appear somewhat correlated with SWLI with general clustering of higher and lower SWLI samples. A number of samples diverge from axis 1 and may therefore be influenced by secondary variables. These samples are those described above, where *Haplophragmoides* spp. is found at higher elevations. The taxa-sample relationships shown in Fig. 3.3b confirm the effect of *Haplophragmoides* spp. and also notably how *Balticammina pseudomacrescens* drives the samples with the highest elevations. Collections of taxa are evident along axis 1, where agglutinated and calcareous taxa show a general partition. Some modern Ythan samples appear to be consistently distal from other sites and/or axis 1, suggesting they are providing assemblages with somewhat differing response to elevation. However, similarities with other samples from across the North Sea suggest comparable conditions may be occurring at a wide range of sites.

PAM and DCA analysis suggests that the foraminifera assemblages that make up the *North Sea* training set are appropriate as sea-level indicators. The agglutinated taxa appear particularly well suited, as observed by others, although may lack more definitive zonation (e.g. Horton *et al.*, 1999*b*, Gehrels, 2000, Gehrels *et al.*, 2005, Horton and Edwards, 2006, Kemp *et al.*, 2013, Barnett *et al.*, 2016). Calcareous taxa are useful indicators of tidal flats in the data and hence useful for transfer functions where a wide environmental range may be sought. However, the lowest occurrence of some taxa is not sampled meaning the full range is not captured, which could be problematic for predicting the lowest range of some fossil samples and so these should be treated with an element of caution (Woodroffe, 2009). Calcareous taxa also occur across a wide elevation range in the region, which may impact the predictive ability of the transfer functions. This wide range may be due to in-wash resulting in allochthonous foraminifera (Murray, 2003, Horton and Murray, 2006). Some studies attempt to avoid this effect by either not sampling the tidal flat (e.g. Gehrels, 2000, Kemp *et al.*, 2013) and/or removing these so termed 'exotic' taxa (e.g. Horton and Edwards, 2006, Kemp *et al.*, 2009, Leorri *et al.*, 2011, Mills *et al.*, 2013) resulting in better predictability in some cases. However, Mills *et al.* (2013), observe that performance does not improve in their Mersey training set and that this method does not preclude the mixing of lower marsh agglutinated foraminifera. We include all samples, as our core includes a fossil mudflat environment and thus the lower samples are critical as well as providing a lower limit

to some of the agglutinated marsh taxa (Wright *et al.*, 2011). However, other cores that are limited to salt marsh environments may warrant investigation of the effect of removing lower elevation samples or taxa.
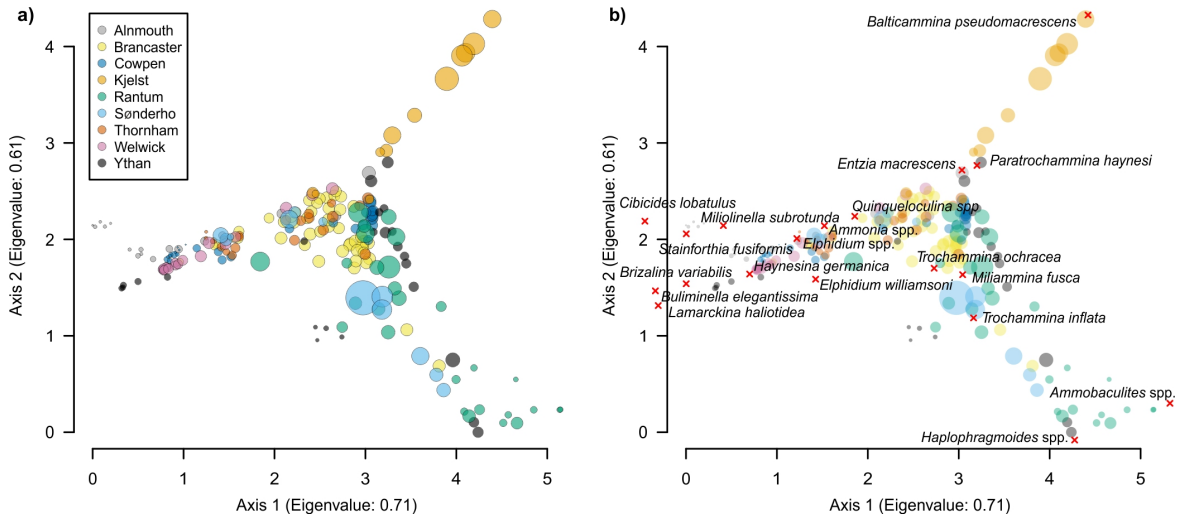
Figure 3.3: Detrended canonical analysis (DCA) of the North Sea training set. (a) Samples are plotted against elevation and coloured according to site and sized according to SWLI value. (b) Species are added and labelled if the maximum abundance > 10 %.
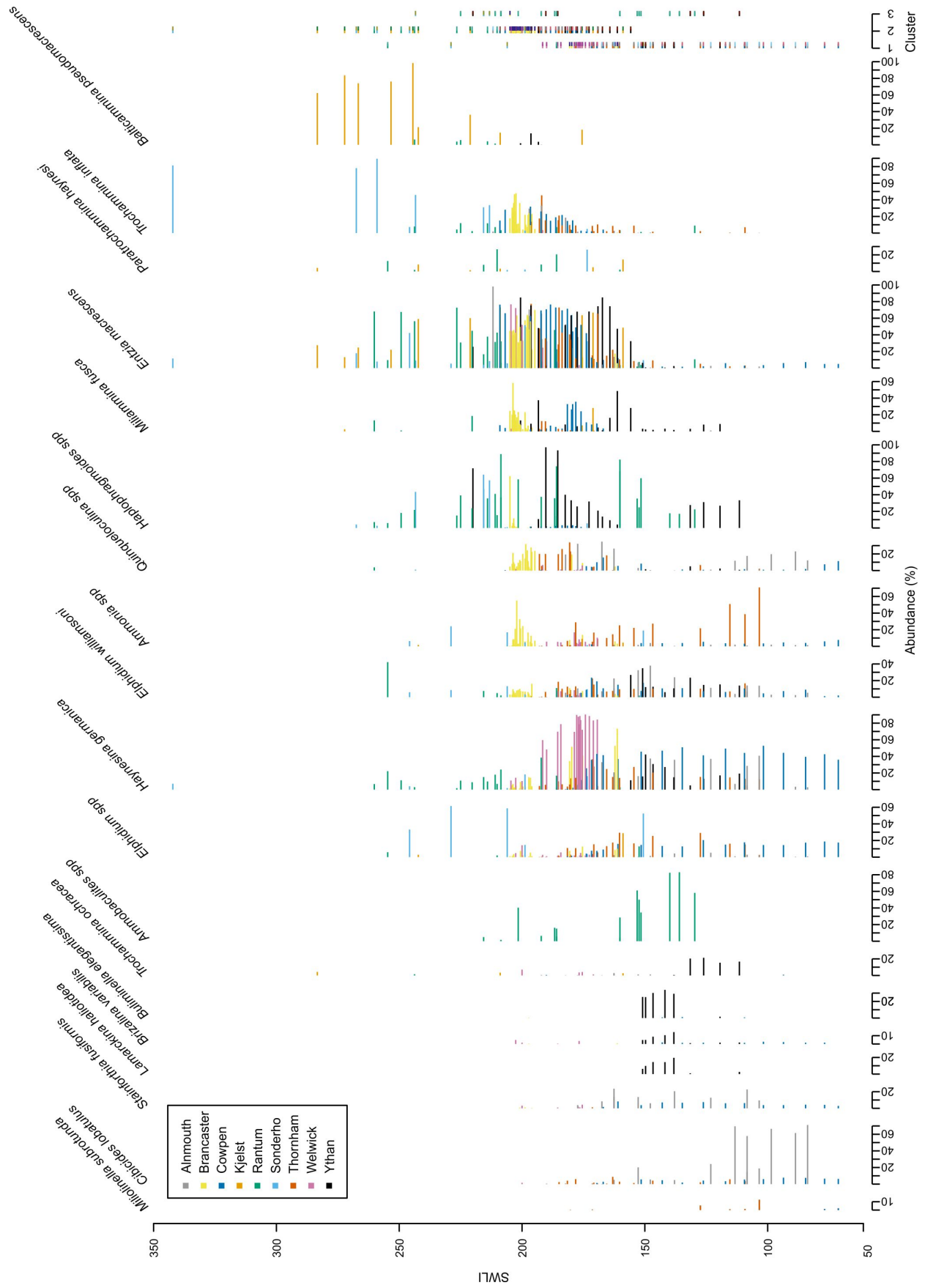
Figure 3.4: The combined North Sea foraminifera data of 218 samples from 9 sites ordered by SWLI value as shown in the first column. Taxa are included that have a maximum abundance > 10 % and occur in more than 10 % of the samples. The bar colour denotes the site corresponding to the legend. The final column shows the groups according to PAM clustering and marked by clusters 1-3.

3.3.2   Comparison of training sets and transfer functions

3.3.2.1   Correspondence and cluster analysis

In order to assess which of the regional, subregional and local training sets is most appropriate for reconstructing sea-level from the core samples shown in Fig. 3.5, we began by plotting DCA, with the core samples passively projected, and PAM, with modern and fossil samples combined. The core lithology and fossil foraminifera assemblages are summarised in Fig. 3.5 and show salt marsh clays that are dominated by *Entzia macrescens* and *Milliammina fusca* abruptly transitioning to estuarine silts comprising mainly calcareous taxa. DCA results for all of the training sets shown in Fig. 3.6 demonstrate an alignment of modern samples with axis 1 and a correlation with elevation. The samples are broadly clustered according to elevation, with a separation between salt-marsh and mudflat samples. There is also a clear distinction between core samples from within the apparent salt-marsh and mudflat zones in all of the plots. The fossil samples appear to show a wider dispersal and closer similarity to modern samples with increasing training set size, whereby the *North Sea* and *West* appear to perform well. Although DCA shows that many Ythan samples are occasionally distal from other sites and/or axis 1 in the regional training sets, it is important to observe that they appear to provide closer matches to many fossil samples. This is perhaps not surprising as they come from the same site and that conditions and taxa response show similarities between modern and 8,000 years ago. There are clearly still exceptions that may be due to different taxa niches, and emphasise the importance of developing regional training sets. The DCA analysis is supported by plotting of the PAM results (Fig. A.2) where clusters of modern samples become more clearly grouped by elevation as the training sets reduce in size, although there are overlaps in SWLI values in all. The fossil samples are dispersed between all clusters of each training set. However, the fossil samples become more closely bunched to each other, a measure of the similarity between samples, in the *Northwest* and *Ythan* versions and appear most widespread in the *West*. The correspondence and cluster analysis suggest that the *North Sea* and *West* training sets are best suited for reconstructing sea level based on the fossil foraminifera in the Ythan core.

(a)

(b)
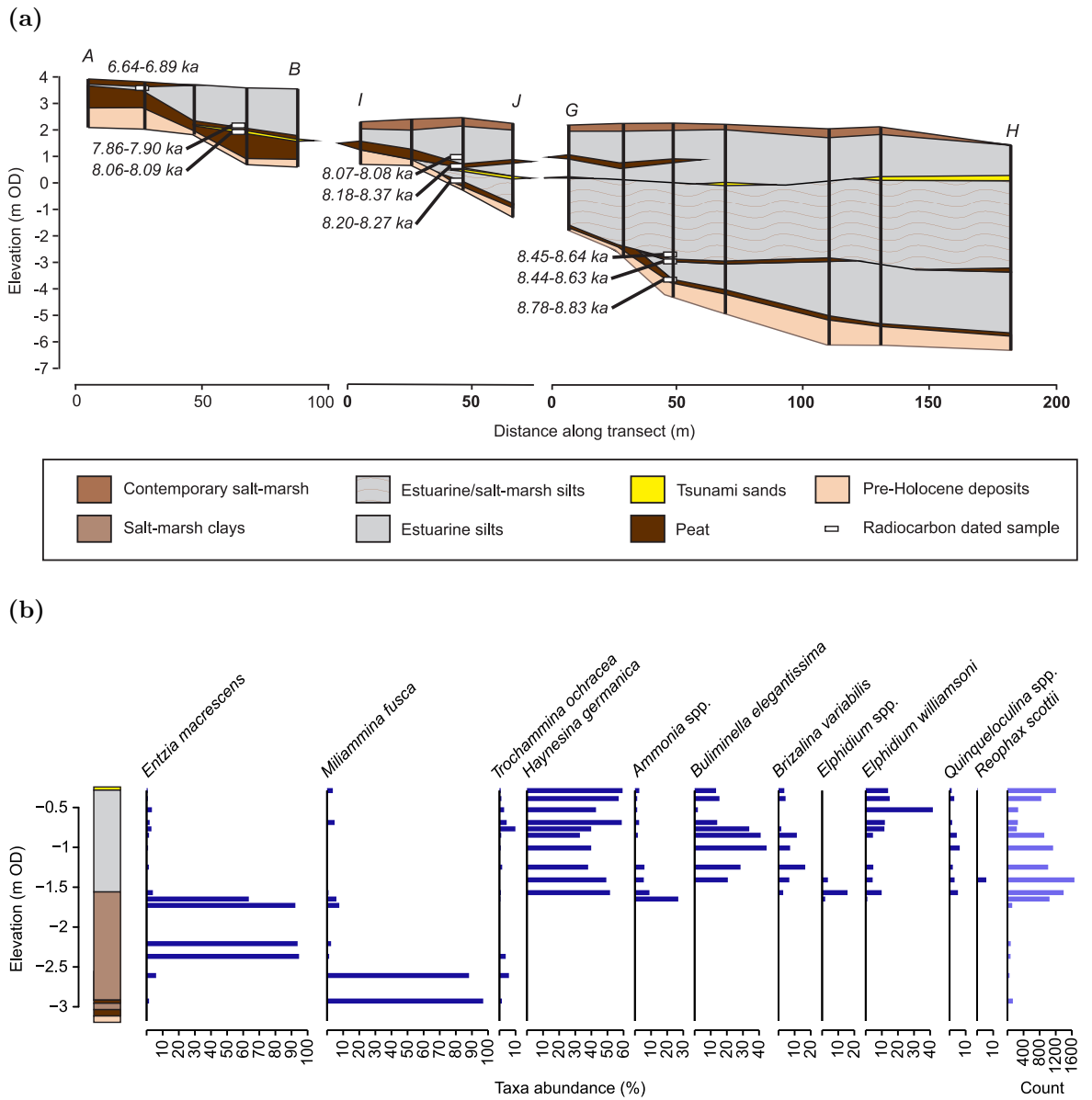
Figure 3.5: Summary of Ythan palaeo data: a) The lithology and calibrated radiocarbon ages of the transects sampled in the work by Smith *et al.* (1999) that correspond to Fig. 3.1. b) Lithology and fossil foraminifera assemblages of core A7.5 from the Ythan Estuary. Foraminifera abundances are given for taxa that have a maximum abundance > 5 %.
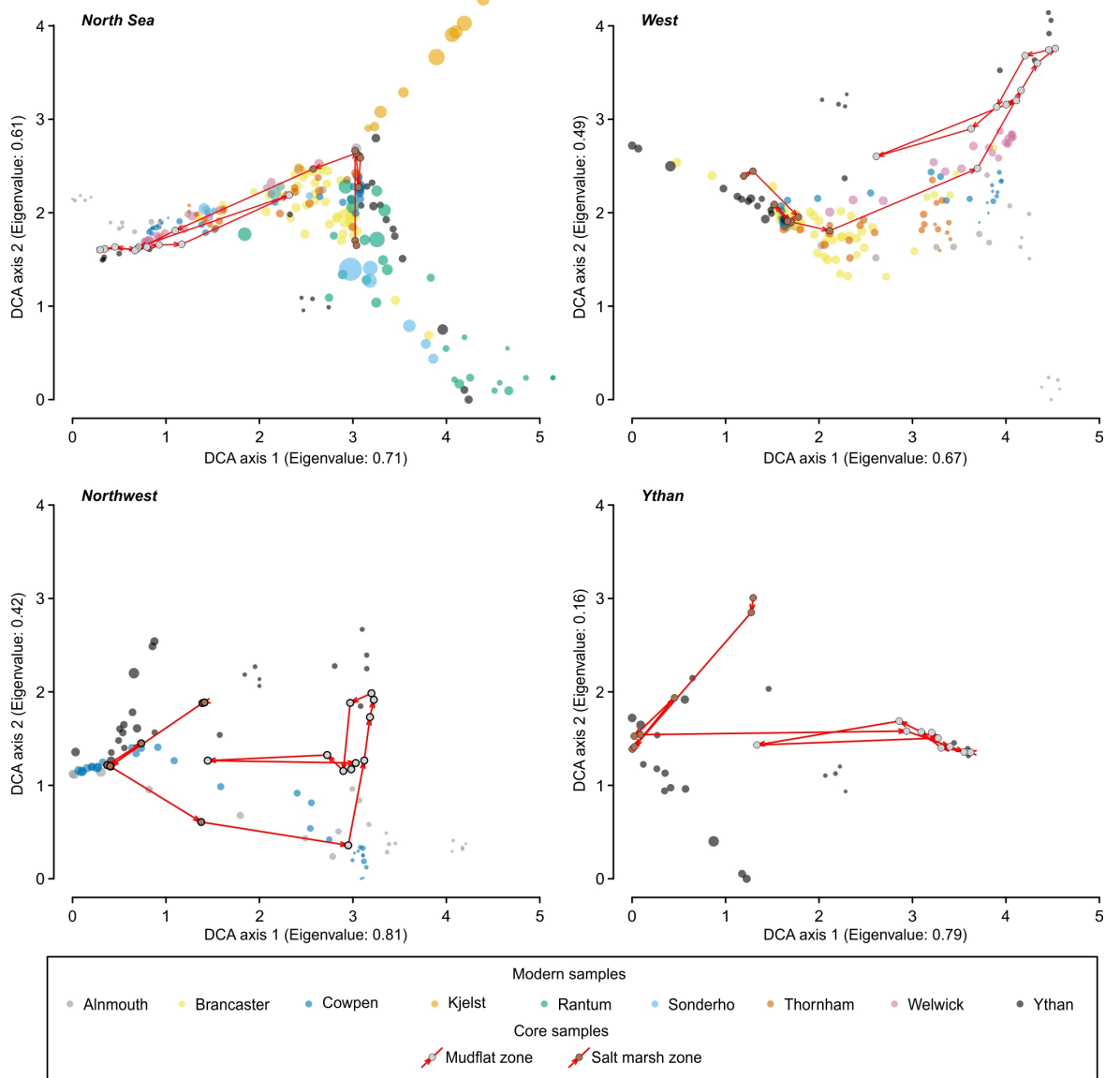
Figure 3.6: Correspondence analysis of training sets and fossil data showing the four sub-regional training sets and Ythan core samples using detrended correspondence analysis (DCA). The modern samples are coloured by site and the size is scaled by SWLI. The core samples are coloured by the lithology of the core and reflect the stratigraphic succession shown by the red lines with arrows indicating the stratigraphic order.

3.3.2.2   Modern Analogue Technique

An assessment of the five closest modern analogues identified by MAT shows that almost all of the closest analogues for every core sample are from sites on the west of the North Sea (Table A.2). Only Kjelst from the east provides any of the five closest analogues. The Ythan provides 51 % of the analogues showing that inclusion of the local data is imperative, particularly for the fossil mudflat samples. All sites from the west, with the exception of Thornham, contribute analogues within the closest two, suggesting that in agreement with DCA and cluster analysis, inclusion of the sites in the *West* training set is required as a minimum to provide acceptable modern analogues to reconstruct sea level from core A7.5.

3.3.2.3   Transfer Function performance

We applied transfer functions using WA with classical deshrinking or WA-PLS using the different training sets. Generally performance statistics, shown in Table 3.2, improve when transfer functions use more localised training sets, in common with other sea-level studies (Horton and Edwards, 2006, Woodroffe and Long, 2010, Barlow *et al.*, 2013). The exceptions are the *East* transfer functions that perform particularly poorly, and the *Northwest* that performs worse than the *West*. The taxa optima and tolerance plots (Fig. 3.7) demonstrate that the taxa optima within the eastern sites are highly variable and hence the poor performance of the *East*, which in turn negatively impacts the performance of the *North Sea* transfer functions. Whilst this provides a wider range of environmental response, it comes at the expense of less precision. All of the WA transfer functions have a higher RMSEP and average bias than the corresponding WA-PLS models, although they do tend to have a lower maximum bias, and variable R^2 values. This suggests that classical deshrinking performs better at the extreme ends of the gradient, while inverse deshrinking (used in WA-PLS models) provides higher accuracy for those in the middle, as indicated by Birks (1995) and Juggins and Birks (2012). Comparison of the predicted SWLI against observed SWLI (Fig. 3.8) shows that although better fitting for the most extreme sample may be better in WA transfer functions, WA-PLS appears to be perform better across the full elevation gradient.

To assess the independence of samples, either because of training set samples being clustered by sites or the possibility of spatial auto-correlation, we compared cross-validation using LOSO with bootstrapping. Spatial auto-correlation, whereby nearby samples tend to resemble one another more than randomly selected locations, can occur when samples
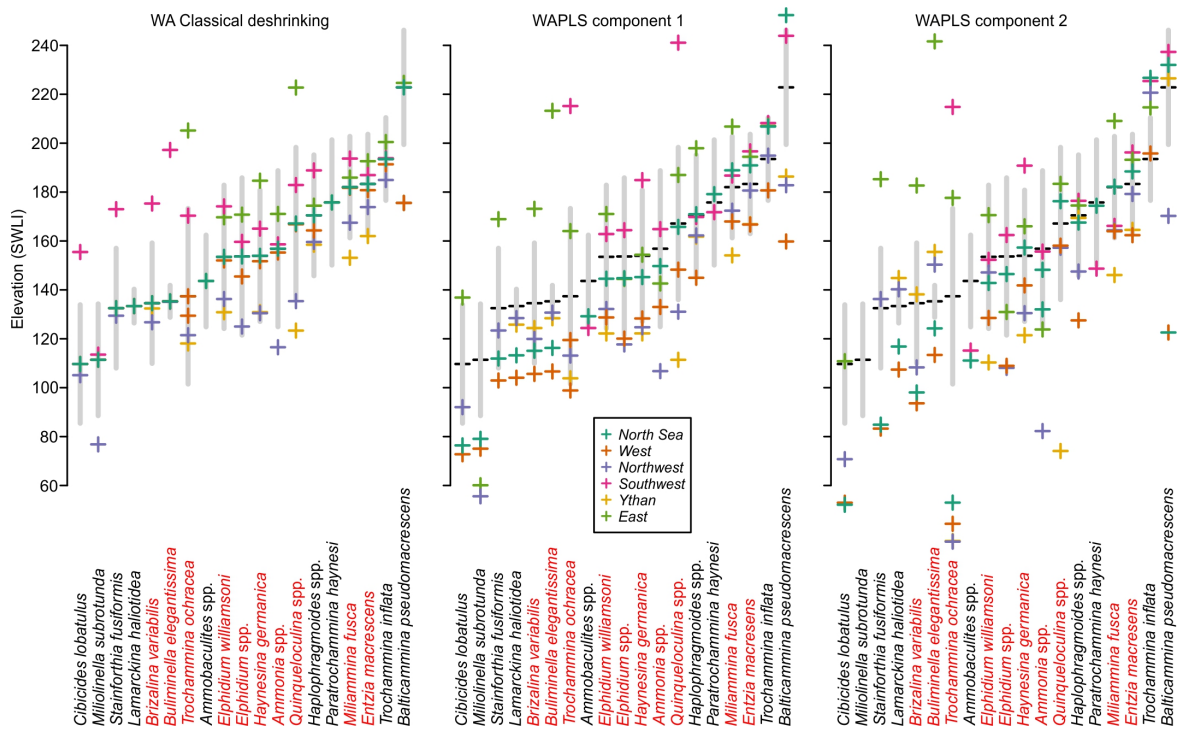
Figure 3.7: Comparison of the progressive taxa optima updates for the different training sets from WA with classical and inverse (equivalent to WAPLS component 1) to more complex WA-PLS transfer functions with multiple components. Taxa tolerances are shown for WA by the grey bar. Taxa are included that have a maximum abundance > 10 % and occur in more than 10 % of the samples. Taxa labels coloured red are taxa that are also found in the Ythan Estuary core (A7.5)

are collected along transects (as is common procedure in sea-level research) as opposed to the more ecologically sound methods such as random sampling (Telford and Birks, 2005). If spatial auto-correlation is present it can result in overly-optimistic RMSEP values and hence misguided model choice (Payne *et al.*, 2012, Kemp and Telford, 2015). LOSO cross-validation removes all samples from one site and predicts the SWLI for them using the remaining sites, and repeats the process for each site (Payne *et al.*, 2012). In all regions RMSEP$_{loso}$ was greater than RMSEP$_{boot}$ (see Table 3.2). However, the differences are relatively small, suggesting only a limited degree of possible spatial auto-correlation may be present, or alternatively the clustering of samples between sites reflects variable local environmental conditions. The inclusion of many sites also minimises the effect of spatial auto-correlation (Legendre and Fortin, 1989, Telford and Birks, 2005) whilst simultaneously making the larger regional transfer functions more robust against environmental changes occurring at a particular site (Barnett *et al.*, 2016). Fig. 3.9 shows that the sites perform
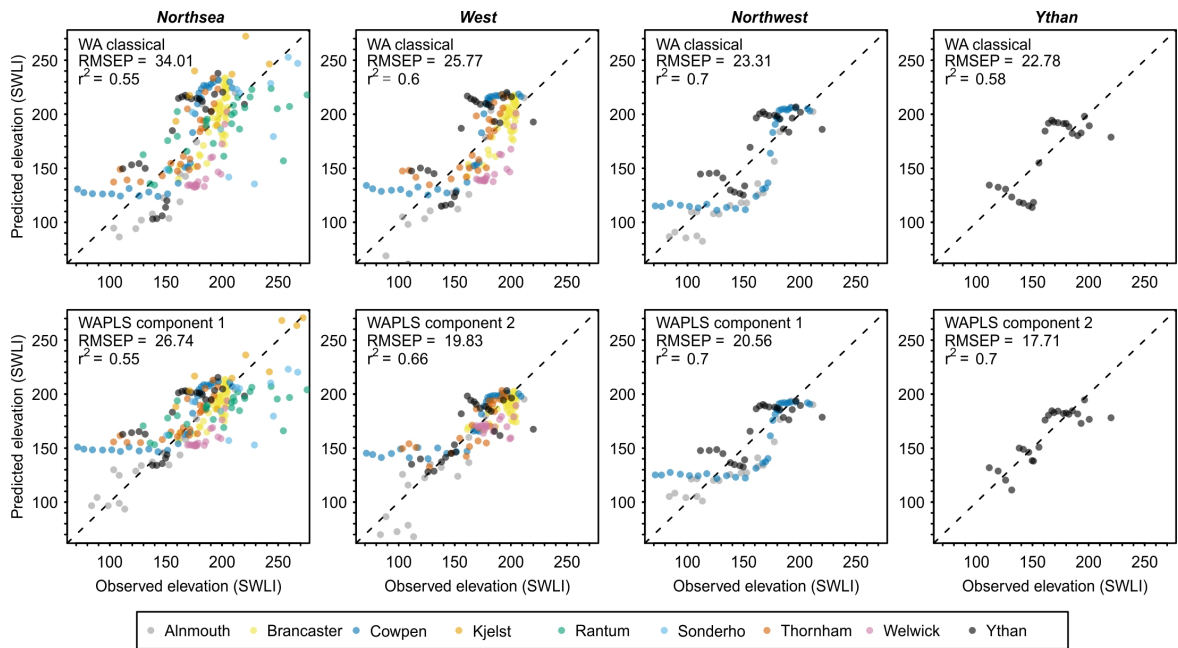
Figure 3.8: Scatter plots of the observed SWLI against the predicted SWLI for WA classical deshrinking and WA-PLS components 1 or 2 depending on which was selected (see text). The samples are coloured according to site as shown in the legend.

relatively consistently, suggesting that one particular site is not being unduly effected and that all sites likely display some environmental variability.

To further assess transfer function performance and understand the effect of deshrinking methods and adding extra complexity in WA-PLS with components > 2, we compared scatterplots of observed versus predicted SWLI and the updated taxa optima (Wright *et al.*, 2011). Fig. 3.8 shows that when inverse deshrinking (WA-PLS component 1) as opposed to classical is applied, low elevation taxa are under predicted and high salt-marsh taxa are over predicted, although this is less apparent in Fig. 3.8 where WA-PLS consistently provides more accurate predictions. This is likely because the most abundant taxa tend to have optima towards the centre of the elevation gradient in the training set and are therefore more suitable for inverse deshrinking. Although there is noticeable variability between training sets in Fig. 3.7, the *North Sea* and *West* taxa optima are very similar and both appear relatively stable to the effect of adding extra components in WA-PLS transfer functions. Adding a second component to the *West* WA-PLS transfer function can be seen to produce accurate sample predictions shown in Fig. 3.8 by updating many of the taxa optima (Fig. 3.7). However, of the taxa that receive major updates, only *Trochammina ochracea* is found in the core and in low abundances and therefore the reconstructions will not be distorted.
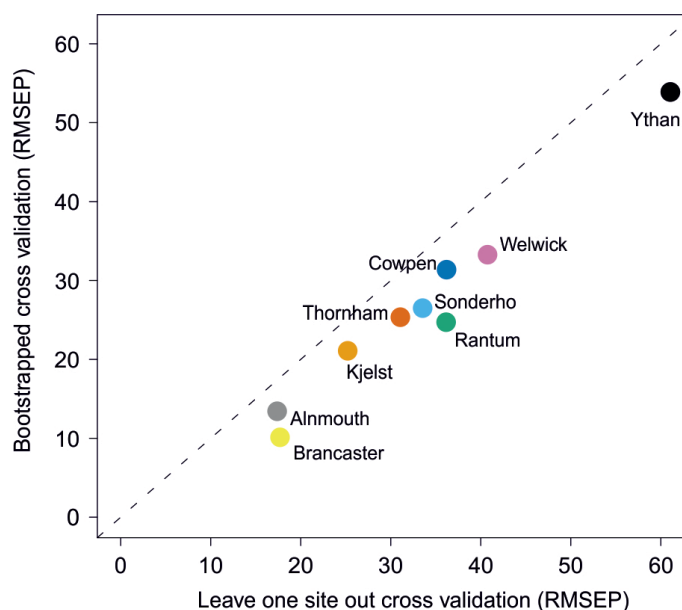
Figure 3.9: Comparison of root-mean-square error prediction (RMSEP) under bootstrapping (boot) and leave-one-site-out (LOSO) cross-validation using a WA-PLS component 1 model. The points represent the value when an individual site is excluded. RSMEP values for the full data are bootstrapping = 20.84 and leave-one-site-out = 32.57.

Despite the good performance, structure remains in the dataset (see Fig. 3.8) such that some of the samples found across the elevation gradient of the mudflat (particularly those of Cowpen) have very similar predictions because the samples have very similar taxa abundances. This demonstrates the difficulty in the application of mudflat samples. One option would be to remove these samples but they represent the full environmental gradient of the samples and so we favour retaining all samples but treating predictions with SWLI values < 140 with extra caution.

Based on transfer function performance statistics alone, the inclination would be to choose the more localised training sets for sea-level reconstructions for core A7.5. However, incorporating more sites provides more robustness against the possible effects of clustered samples and add additional variability in taxa-elevation relationship that is likely important for providing analogues for early Holocene foraminifera. Taxa optima are also more stable with a greater number of sites and suggest these may also be valid.

3.3.2.4   Relative sea-level reconstructions

We applied the preferred WA and WA-PLS transfer functions to reconstruct the palaeo marsh elevation relative to MTL at the Ythan Estuary using the fossil assemblages found

Table 3.2: Performance statistics for the final transfer functions from each training set. The values given are the cross-validated statistics using leave-one-site-out (LOSO) or bootstrapping (boot). The bootstrapped statistics are converted to metres based on the Ythan tidal regime for core A7.5. Significance is based on 999 trials and the * denotes significant results ($p = < 0.05$).

	SWLI$_{loso}$	SWLI$_{boot}$				Ythan A7.5 (m)$_{boot}$		Significance
Model	RMSEP	RMSEP	R^2	Av. Bias	Max. Bias	RMSEP	Max. bias	p
NorthSea-WA	0.36	32.86	0.56	0.09	109.05	0.54	1.80	0.07
Northsea-WAPLS-c1	0.30	23.43	0.58	0.37	111.40	0.39	1.84	0.07
West-WA	0.37	24.71	0.60	0.14	32.92	0.41	0.54	0.11
West-WAPLS-c2	0.30	17.30	0.66	0.41	45.67	0.29	0.75	0.02*
Northwest-WA	0.61	21.88	0.70	-0.10	29.66	0.36	0.49	0.11
Northwest-WAPLS-c1	0.52	15.19	0.76	0.39	34.17	0.25	0.56	0.14
Ythan-WA	NA	18.66	0.58	1.52	40.99	0.31	0.68	0.15
Ythan-WAPLS-c2	NA	11.65	0.69	0.87	42.44	0.19	0.70	0.08
Southwest-WA	0.41	16.04	0.55	-0.25	40.75	0.26	0.67	NA
Southwest-WAPLS-c2	0.36	10.55	0.67	-0.15	36.40	0.17	0.60	NA
East-WA	45.94	32.00	0.55	1.67	71.43	0.53	1.18	NA
East-WAPLS-c1	44.54	24.68	0.53	0.90	68.49	0.41	1.13	NA

in core A7.5 (see Fig. 3.5). All of the reconstructions show a similar pattern of indicative meaning change, with periods of rapid decreases (i.e. relative sea-level rise) at core depths of around -3 m and -1.6 m set against a trend of more gradual decrease (Fig. 3.10). The reconstructions produced notable differences depending on the training set and whether WA or WA-PLS transfer functions were used. The reconstructions using the *North Sea* and *West* training sets display very similar patterns to each other, although the precision, as quantified by the sample specific error, increases from *North Sea* to *West*. The *West* model occasionally predicts slightly lower SWLI which is due to the exclusion of the eastern sites that generally have higher taxa optima. The ranges of the *Northwest* and *Ythan* reconstructions show divergence from the *North Sea* and *West* at differing periods and magnitudes across WA and WA-PLS transfer functions. The number of good and close modern analogues as assessed by the MinDC become greater with increased number of sites in the training sets, for example increasing from nine for the *Ythan* to 24 for the *West* and *North Sea* (Fig. 3.10). The extra samples in the *North Sea* and *West* training sets evidently provide better analogues that also drive differing SWLI predictions from the others and hence suggest the *Northwest* and *Ythan* produce inaccurate reconstructions.

The ranges of the WA and WA-PLS reconstructions show overlap in all cases, although there is a probable difference in the magnitude of both the first and second decrease in indicative meaning. The WA based reconstructions tend to predict lower surface elevations for mudflat samples and higher surface elevations for salt-marsh samples than the WA-PLS

models. This results in the first period of change being apparently larger in the WA-PLS reconstructions compared to the WA, whilst the second is greater in the WA reconstructions. The fossil samples that bound the periods of rapid change appear indicative of mudflats and middle-upper salt marsh with taxa, from towards the gradient ends; predictions of assemblages in these zones are therefore important. Fig. 3.7 shows that WA-PLS appears better at removing the edge-effects than WA, even when one component is used (Mohler, 1983), and should thus provide more accurate reconstructions of the fossil mudflat samples. Small changes in species abundances towards the ends of the gradient can substantially alter predictions (Gehrels, 2000). At the upper end this is generally beneficial because of the high precision of high salt-marsh species (Scott and Medioli, 1978, Gehrels, 2000), but can be problematic at lower ends where taxa tolerance can be less precise due to wide apparent niches and taxa sometimes being found at sub-tidal elevations (Berkeley *et al.*, 2007). Lower elevation samples are sometimes removed because of the uncertainty in taxa response to elevation on the mudflats (Edwards and Wright, 2015), especially those that show nonlinearity with elevation (Hamilton and Shennan, 2005). However, despite the difficulties of trying to reconstruct mudflat environments, including the lower elevation samples is required to provide appropriate modern analogues and are therefore justified here. WA-PLS transfer functions are consequently likely to provide better predictions of both the higher and lower elevation samples.
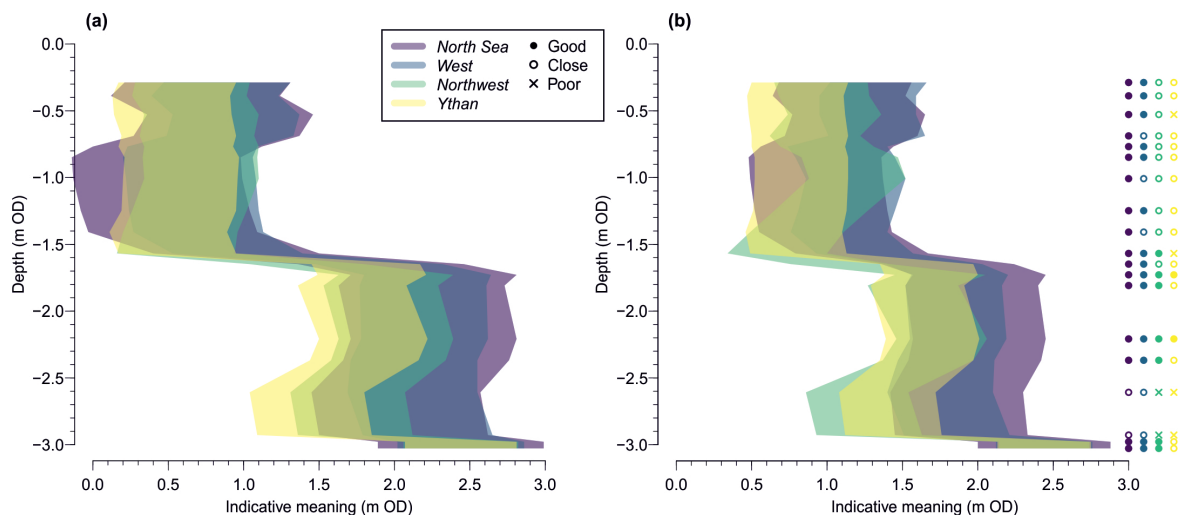

Figure 3.10: Reconstructed indicative meaning of core A7.5 samples from the different training sets using a) WA and b) WA-PLS based transfer functions. 'Good', 'Close' and 'Poor' are measures of the closeness of modern analogues and are taken from the modern analogue technique (MAT) with MinDC values of < 5, $5 - 20$ and > 20th percentiles respectively.

3.3.2.5   Statistical significance of reconstructions

We tested whether the reconstructions trained on the different training sets explained more variance in the core samples than the majority of reconstructions trained on randomly derived sets of data (n = 999) as proposed by Telford and Birks (2011). The results show that only the *West-WAPLS-c2* produced a statistically significant reconstruction ($p < 0.05$) (Table 3.2). The *West-WA* and *North Sea-WA* and *North Sea-WAPLS-c1* reconstructions perform relatively well and the similarity of reconstructions suggests they these are still valid. Telford and Birks (2011) argue that palaeoclimatology should not be exempt from interpreting common constraints of insignificant results which can be equally applied to sea-level studies, although Kemp *et al.* (2013) show that some salt-marsh cores do not provide sufficient downcore variability to outperform random data. In this case the fossil assemblages do provide notable variety and thus the significant result is []somewhat relevant and provides support for the *West-WAPLS-c2* transfer function.

3.3.3   Training set and transfer function selection

The challenge of which combination of training set and transfer function model to apply is not a straightforward decision and may lead to different outcomes, as described above in the core reconstruction (seen in Fig. 3.10) and by Barlow *et al.* (2013). Including all samples from a wider geographic region and a longer elevation gradient captures wider taxa tolerances and provides more modern analogues. One could therefore argue for including as wide a range as possible. However, the challenge is minimising the range of the reconstructed indicative meanings as much as possible by keeping variability of taxa tolerances to a minimum, whilst still providing an analogue for the past environment that can produce suitably precise and accurate quantitative reconstructions. We have built on suggested methods for developing transfer functions (Wright *et al.*, 2011, Watcham *et al.*, 2011, Barlow *et al.*, 2013, Kemp and Telford, 2015) with particular consideration for early Holocene sea-level reconstructions to assess this.

Assessment of transfer function performance statistics alone could lead to the more localised models being preferred due to the lower RMSEP and maximum bias. However, MAT, DCA and PAM silhouette plots show that fossil samples often lack appropriate analogues and similarity with the modern environment in the *Ythan* and *Northwest* training sets. The lack of analogues and poor clustering of the Ythan and fossil samples suggest that the likelihood

of the foraminifera-elevation relationship at a single site remaining unchanged over a period of thousands of years is unlikely. Even relatively local regional microfossil training sets such as the *Northwest* here and the West coast of Scotland diatom set (Lawrence *et al.*, 2016) do not necessarily provide suitable modern microfossil analogues and therefore including sites that encompass different environmental conditions in a larger training set appears necessary. A shift in the reconstructed ranges of the reconstructions when moving to the more localised training sets from the *West* and *North Sea* training sets is evident, further suggesting the reconstructions from the more localised training may lose accuracy. On the basis of missing analogues and lack of similarity we rule out using the *Ythan* and *Northwest* training sets for reconstructing the Ythan core.

DCA and cluster analysis suggests that the *North Sea* and *West* models both perform well and indeed both have no 'poor' analogues according to MAT. The *North Sea* training set has more spread in the modern foraminifera tolerances due to the eastern sites. This may simply be adding unnecessary noise, or on the other hand be providing additional analogues and thus better accuracy. However, the foraminifera in the eastern sites appear to be overly affected by the wind-driven water levels that reduces their utility for reconstructing sea level reflected in their higher optima. Using tide loggers as opposed to relying on modelled tidal data may help overcome this issue that will be particularly important at micro-tidal sites. Both *West* and *North Sea* training sets do still produce very similar reconstructions for either WA and WA-PLS transfer functions suggesting that the small increase in precision in the reconstructions and better predictive ability from the *West* training set does not come with a loss of consistency. It therefore appears that the modern environment captured by the sites in the *West* training set provides a suitable analogue for the conditions found at the Ythan Estuary around 8 ka without the noise introduced by eastern sites. We therefore select the *West* training set for our transfer functions.

The WA and WA-PLS transfer functions result in similar reconstructions, with overlapping ranges. The main difference is the prediction of mudflat samples which cause periods of smaller magnitude changes in the WA-PLS-derived indicative meanings. WA-PLS arguably provides better accuracy for this zone by removing edge effects (Mohler, 1983, Juggins and Birks, 2012) and indeed towards the centre. Furthermore, the *West-WAPLS-c2* is the only transfer function to produce a statistically significant reconstruction. Analysis of the taxa optima updates (Fig. 3.7) when an extra component is added in the *West-WAPLS-c2* transfer

function show a number of calcareous taxa from some sites are shifted to well above HAT, so these more complex transfer functions should be treated with caution (Wright *et al.*, 2011). However, the taxa found in the fossil assemblages are not shifted so dramatically and therefore, in this instance, we accept the updates as appropriate for reconstructing the core. Whilst WA and WA-PLS both produce similar reconstructions and the decision between the two does not therefore produce significantly different results, we prefer the *West-WAPLS-c2* transfer function owing to the better fitting of predicted SWLI, the reduction in edge-effects compared to WA, the reconstruction being statistically significant and without producing dramatic taxa optima updates of the important foraminifera. The *West-WAPLS-c2* transfer function produces a mean sample specific error of 38 cm for the Ythan fossil samples which can be considered good, particularly in light of the approximately 50 cm precision obtained in the Lawrence *et al.* (2016) sea-level reconstruction.

3.4   Conclusions

We have produced a North Sea training set of modern foraminifera based on eight previously published sites and one new site (Ythan Estuary, Scotland). The foraminifera cover an elevation gradient from the highest elevation at which foraminifera occur to mean tide level. The foraminifera display a relationship with elevation relative to sea level. Foraminifera in marshes in the east (Denmark and Germany) were shown to be very variable, often displaying exceptionally broad elevation ranges that may be due to additional environmental factors such as wind build up that is enhanced by the relatively small tidal range.

We assessed the effectiveness of a modern regional training set for reconstructing early Holocene sea level at a coastal site in the western North Sea (Ythan Estuary, Scotland) by dividing the data into different sub-regional training sets and by comparing the results of parallel analyses. We applied a step-wise approach that considered understanding the core lithology and the fossil samples and understanding of the core alongside the modern samples in each of the training sets. In summary we used the following approach, which we also recommend for choosing the most effective transfer function and training set in similar studies:

1. We qualitatively assessed how appropriate for reconstructing sea level each training set was by applying detrended correspondence analysis (DCA) and partitioning around

medoids (PAM) clustering. The results highlighted that clustering of modern samples is apparent and is occasionally driven by certain taxa, however these are generally rare or absent in the fossil record and therefore of lesser importance in this example. The modern samples from smaller, more localised, training sets show a more clearly defined relationship with elevation but often lack similarity with fossil samples. Other methods of correspondence and cluster analysis are available but some form should be included alongside fossil samples to enable a truer understanding of the suitability of different training sets in each context.

2. The modern analogue technique (MAT) was used as a statistical measure of the similarity between fossil and modern samples. More localised training sets produced fewer 'good' or 'close' modern analogues, while larger training sets produce no 'poor' analogues. This step is almost certainly necessary to validate that the training set is providing a modern environment analogous to that found at the reconstructed site for the period of interest []and should be assessed in conjunction with more qualitative approaches such as in steps 1 and 4.

3. We ran transfer functions using WA with classical deshrinking and WA-PLS components 1 or 2 with cross-validation by bootstrapping and by leave-one-site-out (LOSO) to reconstruct palaeo marsh surface elevation changes from the Ythan core. Precision improved in more localised regional models although at a loss of predictive ability. LOSO cross-validation showed that the precision of reconstructions are not unduly over-optimistic and that inter-site variability is present and likely capture different conditions.

4. We analysed the taxa updates when extra components were added in the WA-PLS transfer functions. The taxa are occasionally altered beyond the extent of the sampled elevation range and caution is therefore necessary in choosing these more complex transfer functions. However, comparison with fossil samples showed that the relevant taxa are not fundamentally altered in our example. The updates complement MAT in showing the suitability of analogues. This test is a necessary step and should be carried out along with knowledge of fossil samples.

5. We compared all of the reconstructions to assess the accuracy. All reconstructions showed a similar pattern of surface elevation change, although differences were evident

in the uncertainty between WA and WA-PLS and when trained on different training sites. As opposed to reconstructions from the more localised training sets, the *West* models consistently plotted inside the range of the *North Sea* predictions suggesting that the *West* models retain the accuracy alongside an improvement in model performance. This procedure provides a good understanding of the consistency and hence the likelihood of producing accurate reconstructions.

6. We tested the significance of the reconstructions. Our results showed that only the *West-WAPLS-c2* model significantly outperformed transfer functions run on randomly generated data. This test should be ideally included in studies at this stage, although bearing in mind that many cores used in sea-level studies may not have enough variability to outperform random data it may not always be relevant.

Combining data from multiple sites will almost always be necessary to produce early Holocene sea-level reconstructions that are most likely to be accurate. Thus an approach that utilises qualitative and quantitative techniques to assess which training set and transfer function is most suitable is also necessary. We have shown how our approach can provide an evidence-based decision that should help ensure a model is chosen that has good performance and produces predictions that are plausibly accurate. We chose the *West* WA-PLS transfer function as the best performing across the full suite of analysis for reconstructing relative sea levels in the Ythan core. However, the decision may well be different for different cores and regions so we recommend that a similar procedure to ours should be followed even when using the same training set. Although we focus on foraminifera here, the techniques are equally applicable to other microfossils such as diatoms and testate amoebae. We advocate that similar step-wise approaches to ours are adopted when assessing model choice and that accuracy be prioritised over precision.

Acknowledgements

CRediT roles

References

Avnaim-Katav, S., Gehrels, W. R., Brown, L. N., Fard, E. and MacDonald, G. M. (2017), 'Distributions of salt-marsh foraminifera along the coast of SW California, USA: Implications for sea-level reconstructions', *Marine Micropaleontology* **131**, 25–43.

Barber, D. C., Dyke, A., Hillaire-Marcel, C., Jennings, A. E., Andrews, J. T., Kerwin, M. W., Bilodeau, G., McNeely, R., Southon, J., Morehead, M. D. and Gagnon, J. M. (1999), 'Forcing of the cold event of 8,200 years ago by catastrophic drainage of Laurentide lakes', *Nature* **400**(6742), 344–348.

Barlow, N. L., Shennan, I., Long, A. J., Gehrels, W. R., Saher, M. H., Woodroffe, S. A. and Hillier, C. (2013), 'Salt marshes as late Holocene tide gauges', *Global and Planetary Change* **106**, 90–110.

Barnett, R. L., Garneau, M. and Bernatchez, P. (2016), 'Salt-marsh sea-level indicators and transfer function development for the Magdalen Islands in the Gulf of St. Lawrence, Canada', *Marine Micropaleontology* **122**, 13–26.

Bartholdy, A. T., Bartholdy, J. and Kroon, A. (2010), 'Salt marsh stability and patterns of sedimentation across a backbarrier platform', *Marine Geology* **278**(1-4), 31–42.

Bartholdy, J., Christiansen, C. and Kunzendorf, H. (2004), 'Long term variations in backbarrier salt marsh deposition on the Skallingen peninsula - The Danish Wadden Sea', *Marine Geology* **203**(1-2), 1–21.

Berkeley, A., Perry, C. T., Smithers, S. G., Horton, B. P. and Taylor, K. G. (2007), 'A review of the ecological and taphonomic controls on foraminiferal assemblage development in intertidal environments', *Earth-Science Reviews* **83**(3-4), 205–230.

Birks, H. J. (1995), Quantitative palaeoenvironmental reconstructions, *in* D. Maddy and J. Brew, eds, 'Statistical Modelling of Quaternary Science Data', Quaternary Research Association, Cambridge, chapter 6, p. 271.

Birks, H. J. (1998), 'Numerical tools in palaeolimnology - Progress, potentialities, and problems', *Journal of Paleolimnology* **20**(4), 307–332.

Birks, H. J. B. (2012), Overview of numerical methods in palaeolimnology, *in* H. John B. Birks, André F. Lotter, Steve Juggins and John P. Smol, eds, 'Tracking environmental change using lake sediments', Springer, pp. 19–92.

Birks, H. J., Line, J. M., Juggins, S., Stevenson, A. C. and Ter Braak, C. J. (1990), 'Diatoms and pH reconstruction', *Philosophical Transactions - Royal Society of London, B* **327**(1240), 263–278.

Bondevik, S., Stormo, S. K. and Skjerdal, G. (2012), 'Green mosses date the Storegga tsunami to the chilliest decades of the 8.2 ka cold event', *Quaternary Science Reviews* **45**, 1–6.

Callard, S. L., Gehrels, W. R., Morrison, B. V. and Grenfell, H. R. (2011), 'Suitability of salt-marsh foraminifera as proxy indicators of sea level in Tasmania', *Marine Micropaleontology* **79**(3-4), 121–131.

Culver, S. J. and Horton, B. P. (2005), 'Infaunal marsh foraminifera from the outer banks , North Carolina, U.S.A.', *The Journal of Foraminiferal Research* **35**(2), 148–170.

Dawson, A., Bondevik, S. and Teller, J. T. (2011), 'Relative timing of the Storegga submarine slide, methane release, and climate change during the 8.2 ka cold event', *Holocene* **21**(7), 1167–1171.

de Rijk, S. (1995), *Agglutinated Foraminifera as Indicators of Salt Marsh Development in Relation to Late Holocene Sea Level Rise:(Great Marshes at Barnstable, Massachusetts)*, Utrecht.

Edwards, R. J. and Horton, B. P. (2000), 'Reconstructing relative sea-level change using UK salt-marsh foraminifera', *Marine Geology* **169**(1–2), 41–56.

Edwards, R. J. and Wright, A. (2015), Foraminifera, *in* B. P. Shennan, I., Long, A. J., Horton, ed., 'Handbook of Sea-level Research', 1 edn, John Wiley & Sons, Ltd, chapter 13, pp. 191–217.

Egbert, G. and Erofeeva, L. (2010), 'The OSU TOPEX/Poseidon Global Inverse Solution TPXO 8 Atlas v. 1 Africa'.

Engelhart, S. E., Peltier, W. R. and Horton, B. P. (2011), 'Holocene relative sea-level changes and glacial isostatic adjustment of the US Atlantic coast', *Geology* **39**(8), 751–754.

Gehrels, W. R. (2000), 'Using foraminiferal transfer functions to produce high-resolution sea-level records from salt-marsh deposits, Maine, USA', *Holocene* **10**(3), 367–376.

Gehrels, W. R. (2002), Intertidal foraminifera as palaeoenvironmental indicators, *in* 'Quaternary environmental micropalaeontology', Arnold Publishers, pp. 91–114.

Gehrels, W. R., Kirby, J. R., Prokoph, A., Newnham, R. M., Achterberg, E. P., Evans, H., Black, S. and Scott, D. B. (2005), 'Onset of recent rapid sea-level rise in the western Atlantic Ocean', *Quaternary Science Reviews* **24**(18-19), 2083–2100.

Gehrels, W. R., Milne, G. A., Kirby, J. R., Patterson, R. T. and Belknap, D. F. (2004), 'Late Holocene sea-level changes and isostatic crustal movements in Atlantic Canada', *Quaternary International* **120**(1), 79–89.

Gehrels, W. R. and Newman, S. W. G. (2004), 'Salt-marsh foraminifera in Ho Bugt, western Denmark, and their use as sea-level indicators', *Geografisk Tidsskrift-Danish Journal of Geography* **104**(1), 97–106.

Gehrels, W. R., Roe, H. M. and Charman, D. J. (2001), 'Foraminifera, testate amoebae and diatoms as sea-level indicators in UK saltmarshes: A quantitative multiproxy approach', *Journal of Quaternary Science* **16**(3), 201–220.

Hamilton, S. and Shennan, I. (2005), 'Late Holocene relative sea-level changes and the earthquake deformation cycle around upper Cook Inlet, Alaska', *Quaternary Science Reviews* **24**(12-13), 1479–1498.

Hawkes, A. D., Horton, B. P., Nelson, A. R. and Hill, D. F. (2010), 'No Title', *Quaternary International* **221**(1-2), 116–140.

Hayward, B. W., Le Coze, F., Varchard, D., Gross, O. and Gross, O. (2020), 'World modern foraminifera database'.

Hennig, C. (2010), 'fpc: Flexible procedures for clustering', *R package version* **2**(2), 0–3.

Hijma, M. P. and Cohen, K. M. (2010), 'Timing and magnitude of the sea-level jump preluding the 8200 yr event', *Geology* **38**(3), 275–278.

Hijma, M. P. and Cohen, K. M. (2019), 'Holocene sea-level database for the Rhine-Meuse Delta, The Netherlands: Implications for the pre-8.2 ka sea-level jump', *Quaternary Science Reviews* **214**, 68–86.

Hill, M. O. and Gauch, H. G. (1980), Detrended Correspondence Analysis: An Improved Ordination Technique, *in* 'Classification and Ordination', Springer Netherlands, pp. 47–58.

Horton, B. P. and Edwards, R. J. (2006), 'Quantifying holocene sea-level change using intertidal foraminifera: lessons from the British Isles', *Cushman Foundation Special Publication* **40**, 1–97.

Horton, B. P., Edwards, R. J. and Lloyd, J. M. (1999*a*), 'A foraminiferal-based transfer function: Implications for sea-level studies', *Journal of Foraminiferal Research* **29**(2), 117–129.

Horton, B. P., Edwards, R. J. and Lloyd, J. M. (1999*b*), 'Reconstruction of former sea levels using a foraminiferal-based transfer function', *Journal of Foraminiferal Research* **29**(2), 117–129.

Horton, B. P. and Murray, J. W. (2006), 'Patterns in cumulative increase in live and dead species from foraminiferal time series of Cowpen Marsh, Tees Estuary, UK: Implications for sea-level studies', *Marine Micropaleontology* **58**(4), 287–315.

Horton, B. P., Peltier, W. R., Culver, S. J., Drummond, R., Engelhart, S. E., Kemp, A. C., Mallinson, D., Thieler, E. R., Riggs, S. R., Ames, D. V. and Thomson, K. H. (2009), 'Holocene sea-level changes along the North Carolina Coastline and their implications for glacial isostatic adjustment models', *Quaternary Science Reviews* **28**(17-18), 1725–1736.

Juggins, S. (2017), 'rioja: Analysis of Quaternary Science Data'.

Juggins, S. and Birks, H. J. B. (2012), Quantitative environmental reconstructions from biological data, *in* H. John B. Birks, André F. Lotter, Steve Juggins and John P. Smol, eds, 'Tracking Environmental Change Using Lake Sediments. Volume 5: Handling and Numerical Techniques', Springer, pp. 431–494.

Kaufmann, L. and Rousseeuw, P. J. (1990), *Finding groups in data: an introduction to cluster analysis*, John Wiley, New York.

Kemp, A. C., Horton, B. P. and Culver, S. J. (2009), 'Distribution of modern salt-marsh foraminifera in the Albemarle-Pamlico estuarine system of North Carolina, USA: Implications for sea-level research', *Marine Micropaleontology* **72**(3-4), 222–238.

Kemp, A. C. and Telford, R. J. (2015), Transfer functions, *in* B. P. Shennan, I., Long, A. J., & Horton, ed., 'Handbook of Sea-level Research', 1 edn, John Wiley & Sons, Ltd, pp. 470–499.

Kemp, A. C., Telford, R. J., Horton, B. P., Anisfeld, S. C. and Sommerfield, C. K. (2013), 'Reconstructing Holocene sea level using salt-marsh foraminifera and transfer functions: Lessons from New Jersey, USA', *Journal of Quaternary Science* **28**(6), 617–629.

Kemp, A. C., Wright, A. J. and Cahill, N. (2020), 'Enough is Enough, or More is More? Testing the Influence of Foraminiferal Count Size on Reconstructions of Paleo-Marsh Elevation', *Journal of Foraminiferal Research* **50**(3), 266–278.

Lawrence, T., Long, A. J., Gehrels, W. R., Jackson, L. P. and Smith, D. E. (2016), 'Relative sea-level data from southwest Scotland constrain meltwater-driven sea-level jumps prior to the 8.2 kyr BP event', *Quaternary Science Reviews* **151**, 292–308.

Legendre, P. and Fortin, M. J. (1989), 'Spatial pattern and ecological analysis', *Vegetatio* **80**(2), 107–138.

Leorri, E., Fatela, F., Cearreta, A., Moreno, J., Antunes, C. and Drago, T. (2011), 'Assessing the performance of a foraminifera-based transfer function to estimate sea-level changes in northern Portugal', *Quaternary Research* **75**(1), 278–287.

Li, Y. X., Törnqvist, T. E., Nevitt, J. M. and Kohl, B. (2012), 'Synchronizing a sea-level jump, final Lake Agassiz drainage, and abrupt cooling 8200 years ago', *Earth and Planetary Science Letters* **315**, 41–50.

Mills, H., Kirby, J., Holgate, S. and Plater, A. (2013), 'The distribution of contemporary saltmarsh foraminifera in A macrotidal estuary: An assessment of their viability for sea-level studies', *Journal of Ecosystem & Ecography* **3**, 1–16.

Mohler, C. L. (1983), 'Effect of sampling pattern on estimation of species distributions along gradients', *Vegetatio* (54), 97–102.

Müller-Navarra, K., Milker, Y. and Schmiedl, G. (2016), 'Natural and anthropogenic influence on the distribution of salt marsh foraminifera in the Bay of Tümlau, German North Sea', *The Journal of Foraminiferal Research* **46**(1), 61–74.

Müller-Navarra, K., Milker, Y. and Schmiedl, G. (2017), 'Applicability of transfer functions for relative sea-level reconstructions in the southern North Sea coastal region based on salt-marsh foraminifera', *Marine Micropaleontology* **135**, 15–31.

Murray, J. W. (2003), 'Patterns in the cumulative increase in species from foraminiferal time-series', *Marine Micropaleontology* **48**(1-2), 1–21.

Murray, J. W. and Bowser, S. S. (2000), 'Mortality, protoplasm decay rate, and reliability of staining techniques to recognize 'living' foraminifera: a review', *The Journal of Foraminiferal Research* **30**(1), 66–70.

Oksanen, J., Blanchet, F. G., Kindt, R., Legendre, P., Minchin, P. R., O'hara, R. B., Simpson, G. L., Solymos, P., Stevens, M. H. H. and Wagner, H. (2013), 'Package 'vegan'', *Community ecology package, version* **2**(9), 1–295.

Payne, R. J., Telford, R. J., Blackford, J. J., Blundell, A., Booth, R. K., Charman, D. J., Lamentowicz, Ł., Lamentowicz, M., Mitchell, E. A. D., Potts, G., Swindles, G. T., Warner, B. G. and Woodland, W. (2012), 'Testing peatland testate amoeba transfer functions: Appropriate methods for clustered training-sets', *Holocene* **22**(7), 819–825.

Pedersen, J. B. T., Svinth, S. and Bartholdy, J. (2009), 'Holocene evolution of a drowned melt-water valley in the Danish Wadden Sea', *Quaternary Research* **72**(1), 68–79.

Rousseeuw, P. J. (1987), 'Silhouettes: a graphical aid to the interpretation and validation of cluster analysis', *Journal of Computational and Applied Mathematics* **20**, 53–65.

Scott, D. B. and Hermelin, J. O. R. (1993), 'A device for precision splitting of micropaleontological samples in liquid suspension', *Journal of Paleontology* **67**(1), 151–154.

Scott, D. S. and Medioli, F. S. (1978), 'Vertical zonations of marsh foraminifera as accurate indicators of former sea-levels', *Nature* **272**(5653), 528–531.

Smith, D. E., Firth, C. R., Brooks, C. L., Robinson, M. and Collins, P. E. F. (1999), 'Relative sea-level rise during the Main Postglacial Transgression in NE Scotland, UK', *Transactions of the Royal Society of Edinburgh-Earth Sciences* **90**, 1–27.

Stapleton, C. and Pethick, J. (1996), Coastal processes and management of Scottish estuaries-III: The Dee, Don and Ythan Estuaries, Technical report.

Telford, R. J. and Birks, H. J. (2005), 'The secret assumption of transfer functions: Problems with spatial autocorrelation in evaluating model performance', *Quaternary Science Reviews* **24**(20-21), 2173–2179.

Telford, R. J. and Birks, H. J. (2011), 'A novel method for assessing the statistical significance of quantitative reconstructions inferred from biotic assemblages', *Quaternary Science Reviews* **30**(9-10), 1272–1278.

Ter Braak, C. J. F. and Barendregt, L. G. (1986), 'Weighted averaging of species indicator values: Its efficiency in environmental calibration', *Mathematical Biosciences* **78**(1), 57–72.

ter Braak, C. J. F. and Juggins, S. (1993), Weighted averaging partial least squares regression (WA-PLS): an improved method for reconstructing environmental variables from species assemblages, *in* 'Twelfth international diatom symposium', Springer, pp. 485–502.

ter Braak, C. J. F. and Smilauer, P. (2012), 'Canoco reference manual and user's guide: software for ordination, version 5.0'.

UK Hydrographic Office (2016), *Admiralty Tide Tables, 2016, Volume 1, United Kingdom and Ireland (Including European channel ports).*, United Kingdom Hydrographic Office.

Watcham, E. P., Bentley, M. J., Hodgson, D. A., Roberts, S. J., Fretwell, P. T., Lloyd, J. M., Larter, R. D., Whitehouse, P. L., Leng, M. J., Monien, P. and Moreton, S. G. (2011), 'A new Holocene relative sea level curve for the South Shetland Islands, Antarctica', *Quaternary Science Reviews* **30**(21-22), 3152–3170.

Watcham, E. P., Shennan, I. and Barlow, N. L. M. (2013), 'Scale considerations in using diatoms as indicators of sea-level change: lessons from Alaska', *Journal of Quaternary Science* **28**(2), 165–179.

Woodroffe, S. A. (2009), 'Recognising subtidal foraminiferal assemblages: implications for quantitative sea-level reconstructions using a foraminifera-based transfer function', *Journal of Quaternary Science* **24**(3), 215–223.

Woodroffe, S. A. and Long, A. J. (2010), 'Reconstructing recent relative sea-level changes in West Greenland: Local diatom-based transfer functions are superior to regional models', *Quaternary International* **221**(1-2), 91–103.

Wright, A. J., Edwards, R. J. and van de Plassche, O. (2011), 'Reassessing transfer-function performance in sea-level reconstruction based on benthic salt-marsh foraminifera from the Atlantic coast of NE North America', *Marine Micropaleontology* **81**(1-2), 43–62.

Zong, Y. and Horton, B. P. (1999), 'Diatom-based tidal-level transfer functions as an aid in reconstructing Quaternary history of sea-level movements in the UK', *Journal of Quaternary Science* **14**(2), 153–167.

Summary

In this chapter I have demonstrated that the modern Foraminifera in Swan Inlet provide suitable sea-level indicators. By combining the training set with others from around the North Sea basin I have shown that the resultant transfer functions provide accurate predictions of indicative meaning from fossil samples. Although I don't explicit say so in the manuscript, the fossil foraminifera that I use in the study are those that I also use in Chapter 4 to help reconstruct palaeo relative sea level for the Ythan Estuary. Without this work the subsequent research and determination of sea-level events would not be possible. The chapter stands alone in that it helps to refine methods in choosing suitable training sets and transfer functions, particularly for early-Holocene reconstructions where it is unlikely that accurate predictions can be guaranteed when from local training sets alone.

Chapter 4

Relative sea-level reconstruction for the Ythan Estuary, eastern Scotland, and implications for the cause of the 8.2 ka climate event

Graham Rush[1], Ed Garrett[1], Mark Bateman[2], Grant Bigg[2], Fiona Hibbert[1], David Smith[3], Roland Gehrels[1]

[1]Department of Environment and Geography, University of York, Wentworth Way, York, YO10 5NG, UK

[2]Geography Department, University of Sheffield, Winter Street, Sheffield, S10 2TN UK

[3]School of Geography, University of Oxford, South Parks Road, Oxford, OX1 3QY, UK

Abstract

Freshwater pulses from the melting Laurentide Ice Sheet (LIS) draining into the North Atlantic Ocean are commonly thought to have driven the 8.2 ka climate event, the most significant North Atlantic cooling event during the Holocene, by perturbing the Atlantic meridional overturning circulation (AMOC).

The timing, magnitude and number of freshwater pulses, however, remain uncertain. This is problematic because it prevents testing of coupled ocean–atmosphere climate models against an otherwise excellent test case of the effect on the climate of meltwater inputs in to the North Atlantic that is relevant for present and future scenarios. To address this knowledge gap we present a high-resolution relative sea-level record from the Ythan Estuary, Scotland, for the centuries leading up to the 8.2 ka climate event. The results show that two 'sea-level events' (SLE) occurred between c. 8,615 and 8,180 cal yr BP, whereby rates of sea-level rise departed from the background rates. The first SLE contains two distinct stages, with rates of around 10 and 15 mm/yr respectively. The local magnitudes of the sea-level rises were 0.64–1.35 and 1.15–1.96 m (2σ), which equate to barystatic magnitudes of 0.91–1.92 and 1.64–2.81 (2σ) respectively after considering the geographic location relative to the source. The second SLE had rates of around 4 mm/yr with a local and barystatic magnitude of -0.18–0.34 and -0.25–0.48 m (2σ) respectively.

For the first time, we demonstrate that Lake Agassiz-Ojibway (LAO) drainage alone is insufficient to explain the large volumes of North Atlantic freshwater input based on quantification of the magnitudes of the meltwater pulses, and that the collapse of the Hudson Bay Ice Saddle (HBIS) therefore appears to have been the main source of meltwater into the North Atlantic. By comparing the Ythan sea-level record with multiple sources of evidence we hypothesise that the sea-level events were the result of a series of related meltwater sourced freshwater pulses. An initial thinning of the LIS set up subglacial drainage of LAO and a subsequent collapse of the HBIS that was the primary source of freshwater. This was followed by the terminal drainage of LAO completing a sequence of events that likely forced the shift in the AMOC and hence the 8.2 ka climate event.

Highlights

- We present a well-resolved continuous sea-level reconstruction for the Ythan Estuary, east Scotland

- Three meltwater pulses occurred prior to the 8.2 ka climate event

- Collapse of the Hudson Bay Ice Saddle, not drainage of Lake Agassiz-Ojibay, was the main source of freshwater

Keywords:

Holocene, Sea-Level changes, North Atlantic, Micropaleontology, Foraminifera, 8.2 ka climate event, Laurentide Ice Sheet, Atlantic Meridional Overturning Circulation (AMOC)

4.1   Introduction

The '8.2 ka climate event' is considered to be the largest climate anomaly of the Holocene in the North Atlantic region (Daley *et al.*, 2011) and is increasingly recognized in palaeo-climate records from other regions of the Earth (Morrill *et al.*, 2013). Greenland ice-core records indicate a mean cooling of 3.3 ± 1.1 °C and a mean ∼ 8% reduction in precipitation between c. 8,250 and 8,090 cal yr BP (years before 1950), with a central cooling event lasting c. 70 years within it beginning c. 8,220 BP (Thomas *et al.*, 2007). The climate event has been attributed to a major perturbation of the Atlantic meridional overturning circulation (AMOC) caused by meltwater events during the deglaciation of the Laurentide Ice Sheet (LIS) (Alley *et al.*, 1997, Barber *et al.*, 1999).

The AMOC plays a crucial role in the Earth's climate by redistributing heat. Freshwater inputs are hypothesised to have caused an observed weakening in the strength of the AMOC during the most recent century relative to the last 10,000 years (Srokosz and Bryden, 2015, Thornalley *et al.*, 2018, Spooner *et al.*, 2020). Recent observations differ somewhat from climate model simulations for the most recent century (Weaver *et al.*, 2012), suggesting that the models may not accurately simulate the interactive responses of climate and the AMOC. Knowledge of past events can provide necessary understanding of these processes and, importantly, how they may be impacted by future melting of the Greenland Ice Sheet. The 8.2 ka climate event was described by Schmidt and LeGrande (2005) as a 'Goldilocks abrupt climate-change event' for testing coupled ocean–atmosphere climate models because of the following factors: 1) the climate signal is reasonably well constrained (e.g. Morrill *et al.*, 2013); 2) the background environment is not dissimilar to present; 3) the duration and magnitude are of a size to be recognised in proxy records and relevant to future climate change; and 4) the drainage of the ice-dammed proglacial lake Agassiz-Ojibay (LAO) as the driver was believed to be well understood (e.g. Barber *et al.*, 1999). While the first three points remain valid, more recent evidence and understanding have led to somewhat competing hypotheses for the source(s) of the meltwater forcing, meaning that the driver(s) to force climate models still needs resolving.

The drainage of LAO as the source of the meltwater event was originally proposed by Alley *et al.* (1997), Barber *et al.* (1999) and subsequently supported by geological evidence (Dyke, 2004, Godbout *et al.*, 2019, 2020), oceanic reconstructions from the Labrador Sea (Barber *et al.*, 1999, Hoffman *et al.*, 2012) and North Atlantic (Ellison *et al.*, 2006, Kleiven

et al., 2008, Thornalley *et al.*, 2009), and sea-level reconstructions (Törnqvist *et al.*, 2004, Hijma and Cohen, 2010, Li *et al.*, 2012), and is still commonly referred to as the driver (e.g. Crump *et al.*, 2020, Fisher, 2020). The records also introduced a debate that LAO may have even drained at least twice (Ellison *et al.*, 2006, Kleiven *et al.*, 2008, Hijma and Cohen, 2010). More recently as a result of ice-sheet modelling, a collapse of the Hudson Bay Ice Saddle (HBIS) has been hypothesised as a significant additional source of meltwater release (Gregoire *et al.*, 2012). The HBIS was initially considered as a minor contribution alongside lake drainage in oceanic (Jennings *et al.*, 2015) and sea-level reconstructions (Lawrence *et al.*, 2016, Hijma and Cohen, 2019), but has gained support recently as the major contributor based on new geological evidence (Gauthier *et al.*, 2020) oceanic reconstructions (Lochte *et al.*, 2019) and climate (Matero *et al.*, 2017) and ice-sheet modelling (Matero *et al.*, 2020). Identifying the driver(s) of the 8.2 ka climate event is therefore crucial for testing climate models and understanding the ocean-climate responses to meltwater fluxes.

In this paper we aim to test two hypotheses: *i*) that there was only one meltwater pulse in the centuries prior to and including the 8.2 ka climate event, i.e. 8,800–8,100 cal yr BP, and *ii*) that the meltwater pulse(s) was/were primarily the result of LAO drainage without a significant contribution from the HBIS.

Geological evidence and ocean proxies of meltwater events are able to provide a clue as to the source, but the magnitude of the event cannot be directly quantified because persistent chronological uncertainties in palaeoreconstructions make inferring a precise timing difficult. On the other hand, relative sea-level (RSL) reconstructions provide a method with which to quantify the magnitude of a meltwater event. This is because a barystatic change (i.e change in ocean mass due to freshwater input) is redistributed from the mean by changes in Earth gravity, Earth rotation and viscoelastic solid-Earth deformation (GRD) producing a distinctive and highly varied geographic pattern of sea-level change, or 'barystatic-GRD fingerprint' (Mitrovica *et al.*, 2001, Gregory *et al.*, 2019). The barystatic-GRD fingerprint resulting from the drainage of LAO has been computed by Kendall *et al.* (2008); consequently, by reconstructing RSL at a particular location, the local magnitude can then be appropriately scaled to quantify the source magnitude. The volume of freshwater is believed to have been $< 1.63 \times 10^{14}$ m^3 in LAO (Teller *et al.*, 2002, Godbout *et al.*, 2020) and approximately 4.51×10^{14} m^3 (Ullman *et al.*, 2016) in the HBIS, equivalent to ~ 0.45 m and 1.25 m barystatic sea-level rise. Therefore by reconstructing and scaling the magnitude of RSL rise

to the barystatic rise it should be possible to differentiate between the two likely sources of meltwater.

Presently, three well resolved RSL reconstructions exist for the period prior to and including the 8.2 ka climate event that show a notable sea-level event (Li *et al.*, 2012, Lawrence *et al.*, 2016, Hijma and Cohen, 2019). We use the term 'sea-level event' (SLE) to describe a RSL rise that is an abrupt, decadal to centennial-scale departure from and subsequent return to background rates. This is opposed to a 'sea-level jump' that was defined by Törnqvist *et al.* (2012) as 'an abrupt, annual to decadal-scale sea-level rise'. We prefer the term SLE because: 1) the longer timescales compared to a sea-level jump, and 2) a sea-level jump infers a jump from one point to another from lithological evidence (whereby sea-level rise outpaces peat formation and hence peat formation 'jumps' from one location and elevation). In the Mississippi Delta, USA, a SLE is observed at 8,310–8,180 cal yr BP of 0.8–2.2 m (Törnqvist *et al.*, 2004, Li *et al.*, 2012) and in the Rhine-Meuse Delta, The Netherlands, two events between 8,440 and 8,180 cal yr BP are registered of 1.6–2.4 m and 0–0.3 m respectively when converted to the barystatic rise. The third well resolved reconstruction, based on a continuous stratigraphy from the Cree Estuary, Scotland, is argued to show evidence of three SLEs of smaller magnitude (0.5, 1 and 0.4 m) between 8,760 and 8,218 cal yr BP (Lawrence *et al.*, 2016). The two former reconstructions rely on a large number of sea-level index points (SLIPs) derived from basal peat over a wide geographical area, while the latter, although stratigraphically continuous, is based on a single-core chronology that relies on interpolating between ages up to 2.2 m apart in the core. Less well-resolved evidence of SLEs is also observed in RSL reconstructions from various field locations: the Solway Firth at c. 8,600 cal yr BP (Lloyd *et al.*, 1999, Smith *et al.*, 2020), Skye at c. 8,400 cal yr BP (Selby and Smith, 2016), Morecambe Bay at c. 8,500 cal yr BP (Tooley, 1974, Zong and Tooley, 1996) and a previous reconstruction from our study site in the Ythan Estuary (Smith *et al.*, 1983, 1999) all in northern Britain; the Po Delta, Italy, c. 8,500 cal yr BP (Amorosi *et al.*, 2017); Maputo Bay, Mozambique (De Lecea *et al.*, 2017) c. 8,600 cal yr BP; as well as a number of far-field sites in southeast Asia (Zong *et al.*, 2012, Wang *et al.*, 2013, Tamura *et al.*, 2009, Nguyen *et al.*, 2010, Tjallingi *et al.*, 2014, Xiong *et al.*, 2020). For many of these studies methodological related uncertainties, limited resolution and variance in the observed timing and magnitudes of the SLEs persist and hence the magnitude, timing and origin (i.e. HBIS or LAO) of the meltwater pulses remain unresolved.

In order to test our two hypotheses we build on the work of Smith *et al.* (1983, 1999) and establish a new high-resolution RSL reconstruction for the Ythan Estuary, Scotland. We base our analysis on inter-tidal sediment and a probabilistic assessment that utilises the full uncertainties in age and elevation.

4.2   Materials and Methods

4.2.1   Field work

The Ythan Estuary (N 57°20', W 2°00') is located at the confluence of the rivers Ythan and Tarty Burn on the east coast of Scotland. The site is around 2 km from the mouth of the River Ythan, which remains tidal a further 9 km inland (Fig. 4.1). The present day inter-tidal area is approximately 1.85 km^2 of which 0.13 km^2 is pristine salt marsh. The mean tidal range at the mouth of the estuary is 2.5 m calculated using the TPXO8-ATLAS global model of ocean tides (Egbert and Erofeeva, 2010) . The site was originally studied by Jamieson (1865) and latterly by Smith *et al.* (1983, 1999) to determine Holocene relative sea-level change. A sequence of minerogenic sediments overlying basal and thin intercalated peats dated to c. 8,500 cal yr BP is overlain by a widespread sand horizon that is interpreted as having been deposited by the Storegga tsunami (Smith *et al.*, 1999) of c. 8,150 cal yr BP (Dawson *et al.*, 2011, Bondevik *et al.*, 2012). Smith *et al.* (2013) calculate a a local relative sea-level rise of between 2.6 and 4.8 m between 8,545 ± 95 and 8,275 ± 95 cal yr BP.

To complement previous work and further map the stratigraphy, 23 hand-driven cores were collected along two transects across the modern day salt marsh (Fig. 4.1). The sediments were described following Troels-Smith (1955) and two cores (A7.5 and B7.5) that were deemed representative of the site stratigraphy were collected with a Russian peat corer. We collected two further cores (A2.4, A10) for radiocarbon dating at important stratigraphic contacts. The surface elevations of cores were established using a Trimble R4 RTK differential global positioning system (DGPS). The base station was tied to two local Ordnance Survey benchmarks to provide elevation measurements relative to the UK national vertical geodetic datum (Ordnance datum - OD) with a vertical uncertainty of ± 0.006 m.
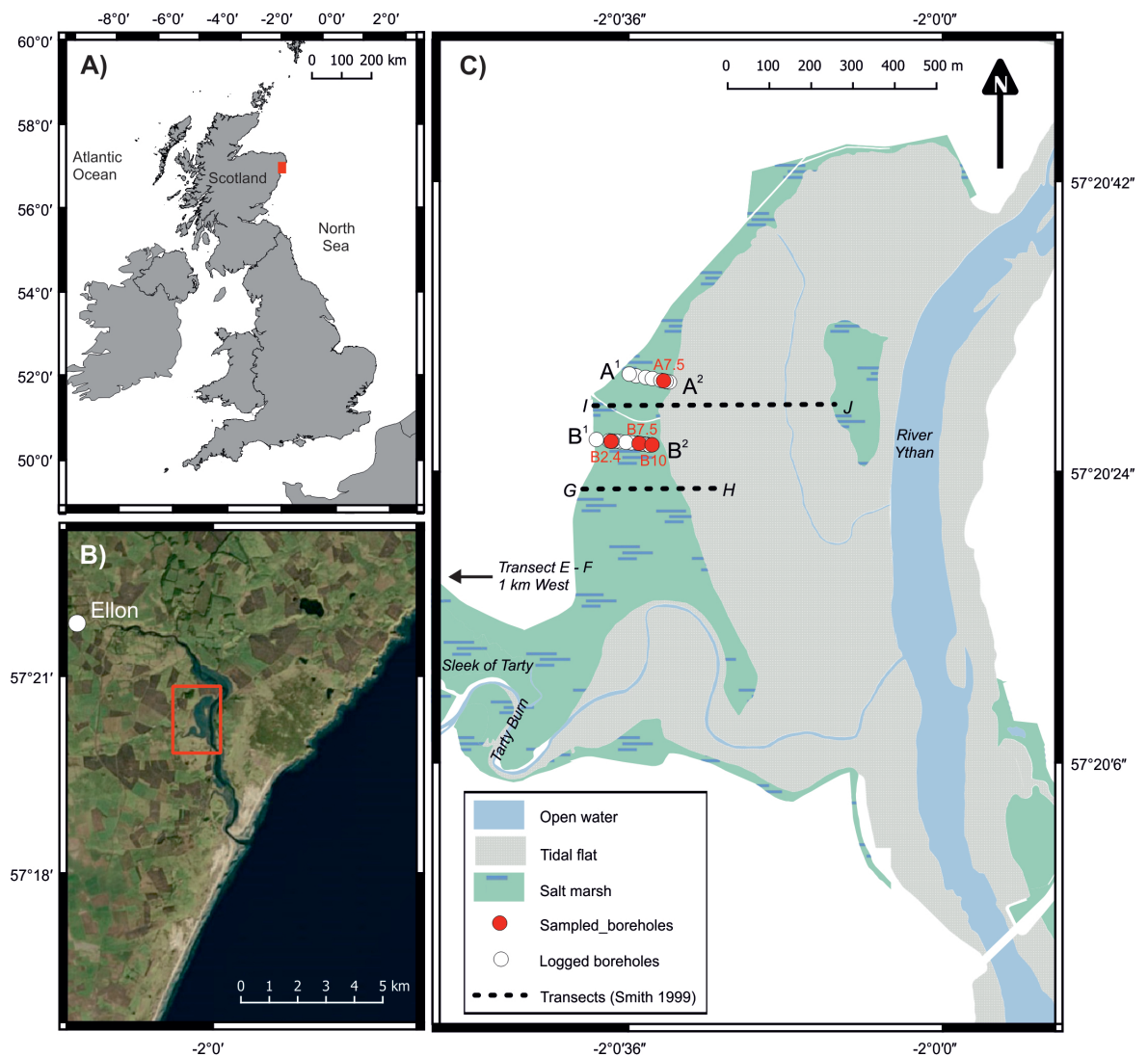
Figure 4.1: Location maps of the field site in the Ythan Estuary. A) An overview of the UK, showing the location of B) A satellite image from Bing maps of the Ythan Estuary, west coast of Scotland. C) Map of the the field site showing the location of the new transects and boreholes taken in this study and the existing transects from Smith *et al.* (1999) drawn in Fig. 4.2.

4.2.2   Sea-level reconstruction

In order to reconstruct relative sea-level changes with appropriate precision for the period prior to the 8.2 ka climate event we exploit the relationship between inter-tidal foraminifera and elevation relative to the tidal frame (Scott and Medioli, 1978) alongside high-resolution radiocarbon dating. This produces SLIPs with an x (age) and y (palaeo sea level) component

which were then modelled to produce a continuous record.

4.2.2.1 Chronology

To produce the age component of our sea-level reconstruction we targeted horizontally bedded plant fragments for accelerator mass spectrometry (AMS) radiocarbon (^{14}C) dating throughout the two cores in the section of interest. Core B7.5 was largely lacking suitable material so A7.5 provides the best-resolved chronology. Nine plant and two marine shell samples were collected for dating from A7.5 and three plant samples from B7.5. The Storegga tsunami sand deposit was identified by Smith *et al.* (1999, 2013) and we confirmed its age by dating peat directly below the layer and shells in the layer itself in cores B2.4 and A7.5 respectively. Sample preparation and dating was carried out at the Scottish Universities Environmental Research Centre (SUERC), NERC Radiocarbon Facility, East Kilbride, UK following standard procedure (Stuiver and Polach, 1977).

The ^{14}C ages were calibrated in Oxcal v4.4 using a Bayesian model, specifically Markov Chain Monte Carlo sampling (Bronk Ramsey, 2009). ^{14}C ages of plant macrofossil were calibrated using the IntCal20 calibration curve (Reimer *et al.*, 2020) and marine shells with the Marine20 curve (Heaton *et al.*, 2020) and are reported as 2σ, ranges in calendar years before present (cal yr BP). The ^{14}C ages of the marine shells require an additional local correction due to the marine reservoir effect. This is because of lower ^{14}C activity that could be due to the input of older carbon from hinterland carbonates, or 'ageing' of carbon in deep water masses when separated from the atmosphere and how that water may then interact with freshwater in the estuary (Stuiver and Polach, 1977).

To establish a suitable local reservoir correction (ΔR) applicable to our marine shell samples, we worked on the basis that sample yt-11, the marine shells located within the sand, is of the known age of the Storegga tsunami. We first verified that the sand horizon was indeed deposited by the Storegga as previously suggested (Smith *et al.*, 1999). To do so we compared our AMS ^{14}C ages from directly below the sand horizon (yt-12) and the bulk sediment ^{14}C ages from below and above the horizon of Smith *et al.* (1999) (SRR-47171 and SRR-4718 with an additional 100 year 'bulk error' (Hijma *et al.*, 2015)), with ages from samples in equivalent positions from the well-dated Storegga deposits of the 'Green Moss' sequence, northern Norway (Bondevik *et al.*, 2012). We grouped related samples, i.e. before, during or after the tsunami, as a *Phase* using the OxCal *Sequence* model. The model

compares the *unmodelled* or 'prior' probability distributions with the *modelled* or 'posterior' densities and gives an agreement index as a measure of the agreement between them. The related samples were modelled with a high posterior agreement (agreement index > 100%) and the sand was thus confirmed to be consistent with deposition by the Storegga tsunami. We then updated the calibrated age of the Storegga tsunami by re-modelling the Green Moss ^{14}C ages using the more recent IntCal20 calibration curve with the original *Sequence* function from Bondevik *et al.* (2012). The re-calibrated model for the Green Moss sequence shows the Storegga tsunami occurred at 8,180–8,080 cal yr BP (8,173–8,125 1σ), a slight improvement in precision from the original age of 8,180–8,030 (8,175–8,120 1σ) (Bondevik *et al.*, 2012). Following the methods of Reimer and Reimer (2017) for paired samples we reverse-calibrated the discrete points (n = 10,000) of the re-modelled probability density function (PDF) of the Green Moss sequence with the Marine20 calibration curve. The resulting PDF of the modelled marine ^{14}C age was then approximated as a normal distribution and the offset with the measured ^{14}C age of sample yt-11 was calculated to give a ΔR of -136 years. The 1σ error of $\pm$ 44 years for the ΔR was calculated by propagating the 1σ errors of the modelled and measured marine ^{14}C ages. The robustness of this estimation was confirmed by comparing it with the contemporaneous ΔR of -111 $\pm$ 46 years for the Western Isles of Scotland (Ascough *et al.*, 2007, 2017), re-calculated using the 2020 calibration curves in Calib v8.2 (Stuiver *et al.*, 2020). This ΔR is the most closely related in time and age to our site and was recently applied to marine shells in a North Sea core approximately 190 km ENE from the Ythan Estuary (Estrella-Martínez *et al.*, 2019). We followed the original method of Russell *et al.* (2011) and Ascough *et al.* (2017) for the multiple paired samples from Ascough *et al.* (2007) to obtain the ΔR and 1σ error.

To produce an age-depth model for core A7.5 we used the *P_Sequence* function in Ox-Cal, which integrates ^{14}C dates and sedimentary information to refine the chronology and interpolate between dated levels (Bronk Ramsey, 2008). In the model the *likelihood* is the directly dated information, our ^{14}C ages, and the *prior* are different components of the sedimentary sequence. The model defines the size and hence rate of the depositional events (k) as essentially random, although it does allows the user to define as a prior whether the rate of depositional events are likely to be relatively constant or more variable (Bronk Ramsey and Lee, 2013). We set our k value as 100 m^{-1}, that is to say one event every cm, but allowed the model to average over a number of different values between two orders of magnitude

larger and smaller by setting the U value to $\pm$ 2. We used the 11 sequential ^{14}C dates from core A7.5 as our tie points. To help constrain the model further we combined the calendar age 8,130 $\pm$ 50 for the Storegga tsunami with sample yt-11 as a single *Storegga* event using the *Combine* function. After an initial run to identify outliers we used the *Outlier_Model* to adjust the probability and downweight two samples (yt-05 and yt-09) as a further prior (Bronk Ramsey, 2009*b*). Finally we assigned a *boundary* between the intercalated peat and salt-marsh clay allowing the model more flexibility to choose different accumulation rates either side of the boundary.

4.2.2.2   Palaeo sea levels

To determine palaeo sea level position we applied the North Sea foraminifera modern training set of Rush *et al.* (in review) to fossil foraminiferal assemblages from samples taken between the basal peats and the tsunami deposit in two cores, A7.5 and B7.5. We sub-sampled the cores for foraminifera iteratively at appropriate depths with respect to litho-logical and biological changes following standard laboratory procedures (Scott and Medioli, 1980, Gehrels, 2002, Edwards and Wright, 2015). Samples were split using a wet splitter (Scott and Hermelin, 1993) and picked and counted until a target of at least 200 individuals was met in even 1/8 splits. Individuals were identified with reference to the existing taxon-omy of (de Rijk, 1995, Wright *et al.*, 2011, Edwards and Wright, 2015, Müller-Navarra *et al.*, 2017, Hayward *et al.*, 2020). Consequently, a total of 24 samples were counted in each core with individual taxa expressed as their percentage relative abundance of the sample.

To most accurately and precisely reconstruct the indicative meanings of the core samples, i.e. the elevation at which the sediment was originally deposited relative to tide levels, we compared transfer functions trained on different regional sub-sets of the North Sea modern training set following the methodology of Rush *et al.* (in review) in R-3.6.1 using the rioja (Juggins, 2017), vegan (Oksanen *et al.*, 2013) and cluster (Maechler *et al.*, 2012) packages. The final training set comprises samples (n = 125) from five sites on the eastern coast of Scotland and England, including the Ythan Estuary, ranging in elevation from highest astronomical tide (HAT) to just below mean tide level (MTL) (Fig. B.1).

Predicted elevation relative to MTL for each sample was given as a value of standardised water level index *(SWLI)* and was converted into the indicative meaning *(IM)* by reversing the standardisation equation (Horton *et al.*, 1999*a*) shown in Eq. 4.1a. The conversion

requires the relevant tidal datums to be known for the site. It is commonly assumed that tidal range remains unchanged; however, in response to sea-level change, tidal ranges in the north-west European continental shelf sea have varied during the Holocene (van der Molen and de Swart, 2001, Uehara *et al.*, 2006, Ward *et al.*, 2016). The cause of the increase was likely the sea-level rise between 9,000 and 8,000 yr BP that increased water depth, connected the North Sea and English Channel and drove amphidromic changes (Ward *et al.*, 2016, Hill, 2020). However, whether the connection and hence the rise in amplitude occurred before or after the rapid sea-level rise prior to the 8.2 ka climate event is hitherto unresolved. To account for this we applied the estimated mean high water spring tide (MHSWT), taken as the $M^2 + S^2$ components produced by modelling of palaeotides (Hill, 2020), in Eq. 4.1a. The model uses the Fluidity model (Piggott *et al.*, 2008) on an unstructured mesh with resolution varying from 20 km to 1.5 km around the coastlines, with palaeobathymetry derived from the 2011 glacial-isostatic adjustment (GIA) modelling of Bradley *et al.* (2011) We compared the effect of using different MHWST values in Eq. 4.1a on each fossil sample obtained from the following three methods assuming a constant MTL of 0.3 m: *i*) nearest neighbour interpolation using the modelled palaeotide at 9,000 yr BP , *ii*) linear interpolation of predictions between the modelled 9,000 and 8,000 yr BP time slices, and *iii*) the present day value. The age for each interpolated sample in method *ii* was taken as the median sample age from our age-depth model.

The final step to calculating the palaeo sea level for each index point is to remove any effects of post-depositional compaction (Brain *et al.*, 2012). The sediments immediately below the Storegga deposit provides a useful marker as we can calculate and compare the palaeo surface elevation of our reconstructed samples in core A7.5 with core B2.4, where the deposit lies directly on top of the basal peat. We therefore took the difference between the indicative meaning and the difference in measured elevation of the two samples as the maximum post depositional compaction. We interpolated between 0 cm at the base of the core and this difference, as described in Section 4.3.3, and raised the elevations within core A7.5 by the relevant amount with an uncertainty captured in Eq. 4.1c.

The palaeo sea level (SL) for each index point ($_t$) is given by Eq. 4.1b, whereby the indicative meaning *(I)*, calculated in Eq. 4.1a with the paleao tidal datums ($MHWST_p$, MTL_p), is subtracted from the sample elevation (E) and the total post-depositional compaction (C) added. The total 2σ vertical uncertainty (U) was calculated using 4.1c with the following

components: u_1) transfer function sample specific error [$\bar{\mathrm{X}}$ = 0.36 m]; u_2) palaeotide [0.15 m]; u_3) compaction correction [0–0.15 m]; u_4) non-vertical coring [$\bar{\mathrm{X}}$ = 0.09 m]; and $u_{5\text{-}8}$) sample thickness, sampling, core shortening/stretching and DGPS surveying [all 0.01 m]. $u_{3,4,7}$ are only applied to the positive (i.e. upward) uncertainty.

$$I_t = \frac{(SWLI - 100)(MHWST_p - MTL_p)}{100} + MTL_p \tag{4.1a}$$

$$SL_t = E_t - I_t + C_t \tag{4.1b}$$

$$U_t = \sqrt{u_1^2 + u_2^2 + u_3^2 + u_4^2 + u_5^2 + u_6^2 + u_7^2 + u_8^2} \tag{4.1c}$$

4.2.2.3 Statistical Analysis

We used a probabilistic approach to reconstruct sea level and rates of change (cf Grant *et al.*, 2012, 2014, Rohling *et al.*, 2014) using the following approach:

1) Using Monte Carlo sampling we generated point clouds (n = 50,000) for each index point with an x and y component. The x is the age taken by randomly sampling the PDF produced in the OxCal age-depth model and therefore fully accounts for uncertainty as opposed to assuming a normal distribution as is common (Cahill *et al.*, 2016). The y is the palaeo sea level taken by randomly sampling a split normal distribution, implemented in the 'fanplot' package in R (Julio, 2006) following Abel (2015), around the mean allowing for different positive and negative uncertainties produced as above in Eq. 4.1c. We organised each point cloud into groups determined by the difference in the median age of each index point and its next youngest, effectively producing stratified random sampling such that age reversals are restricted in the sequence. The ordered realisations of the index points were then tied together to produce 50,000 realisations. A curve was fitted through each realisation with kernel smoothing using local polynomial regression of approximately 50 years allowing determination of sea level at 10 year age intervals. Fitting a curve to the data can be considered somewhat subjective, however we verified the accuracy of our choice of smoothing parameter by linearly interpolating between points and calculating a 50 year rolling mean which produced similar results. To determine the rate of sea-level change we differentiated between each pair of successive 10 year sea-level predictions for every realisation (i.e. Δsea level/Δtime). From this ensemble we calculated the probability maximum (P-max) and the 68% and 95% probability interval for sea level and the rate of change (effectively 1σ and 2σ

and referred to as such hereon, but not necessarily symmetrical). The simulated sea levels and rates of change provide the basis to identify the timing and magnitude of a SLE.

2) In order to identify the timing of a SLE we used linear regression Bayesian change-point analysis to detect abrupt changes in the rate of sea-level change using the 'bcp' package in R (Erdman and Emerson, 2007, 2008, Wang and Emerson, 2015). Bayesian change-point analysis calculates the posterior probability of an abrupt change at each time interval by fitting a piecewise linear function through blocks. We identify an abrupt change when the probability is > 0.5 and quantify the age range by incorporating neighbouring time intervals until a combined probability of $> 95\%$ is reached. We used these probabilities to generate a PDF for the timing of the start and end of the SLE.

3) To calculate the magnitude of the SLE we first generated a point cloud (n = 50,000) for the start and end point of the reconstruction and of each SLE by sampling the PDFs of sea level from our original simulation at each age interval and tying them to the corresponding age. We adopted a randomly stratified approach to the sampling such that the sea level components were grouped by the probability intervals (i.e. $< 16^{\text{th}}$, 16th–84th, $>$ 84th percentiles) on the premise that any vertical errors will have propagated through the reconstruction. Where multiple ages for the timing were observed, the number of realisations of each age within the point cloud was proportional and dictated by the PDF for the timing as generated above. Calculating the background rate is necessary in order to correct for the longer term local glacial-isostatic adjustment, steric (change in density) and manometric (change in mass) relative sea-level components. The background rates were calculated by differentiating between the point clouds of the start and finish of periods pre, post and between SLEs and combining them to generate an ensemble of background realisations (Eq. 4.2a). Although our method for establishing the background rate relies on the data itself, we prefer this method over using a GIA prediction which is averaged over the full millennium and hence will include any SLE within it. We are also able to include an uncertainty for the rate, which is generally overlooked for GIA predictions despite potentially being $> \pm$ 20% (Simon and Riva, 2020). Finally, we differentiate between the start and finish of the SLE and subtract the tied background rate for each of the realisations from the point clouds using Eq. 4.2b. From this ensemble we calculated the probability intervals for the magnitude as above. Barystatic–GRD fingerprint modelling indicates that the east coast of Scotland would have experienced about 70% of the global mean (Kendall *et al.*, 2008). We therefore

up-scaled the local magnitude by the same factor to give the barystatic sea-level rise.

$$B = \left(\frac{\Delta SL_{pre}}{\Delta T_{pre}} + \frac{\Delta SL_{int}}{\Delta T_{int}} + \frac{\Delta SL_{post}}{\Delta T_{post}} \right) 1000 \qquad (4.2a)$$

$$M = \Delta SL_{sle} - (B \Delta T_{sle}) \qquad (4.2b)$$

where B is the background rate in mm/yr; ΔSL is the change in sea level in metres and ΔT is the change in time of: before ($_{pre}$), after ($_{post}$) or between ($_{int}$) the abrupt departures from the background RSL change, or for the calculation of the magnitude (M) of the sea-level event ($_{sle}$).

4.2.3   Reanalysis of RSL data for the Cree Estuary, southwest Scotland

The stratigraphic sequence and RSL reconstruction of (Lawrence *et al.*, 2016) from the Cree Estuary is similar to the Ythan Estuary and enables comparisons and wider interpretations to be made regarding meltwater pulses prior the 8.2 ka climate event. The original results showed three SLEs prior to the 8.2 ka climate event. Although based on a similar probabilistic assessment, there are a number of important differences in the methodologies: the Cree Estuary SLIPs were calibrated using IntCal13 calibration curve (Reimer *et al.*, 2013) which has since been updated (IntCal20 (Reimer *et al.*, 2020)); the probabilistic reconstruction was developed using normal distributions for both age and sea level of the SLIPs and then linearly interpolated; they defined the background rate as the modelled GIA rate; and finally used a less cautious approach in assuming that the shape of the reconstruction is correct at the $\pm 1\sigma$ and 2σ intervals to calculate both the timing and the magnitude of SLEs. In order to standardise the reconstructions using a more cautious approach, and by using Intcal20 allow for a more direct comparison we reanalysed the original Cree data. We used the original age-depth model but calibrated using the IntCal20 curve (Reimer *et al.*, 2020), then reconstructed RSL and calculated the timing and magnitudes of SLEs following the methodology as described in Section 4.2.2.3.

4.3 Results and palaeoenvironmental interpretation

4.3.1 Lithostratigraphy and biostratigraphy

The locations of the boreholes are shown in Fig. 4.1. The stratigraphy that is documented from the new cores is in good agreement with the transects from Smith *et al.* (1999) (Fig. 4.2). Glacial deposits comprising coarse sands and gravels are overlain by a widespread layer of basal peat around 5 cm thick between -3.18 and 0.42 m OD. Foraminifera are absent from this peat unit. However, diatom analysis of the same peat unit by Smith *et al.* (1999) shows saline tolerant species suggesting a marine influence. At the lower elevations the basal peat is overlain by a silty organic horizon containing macroscopic salt-marsh plant fragments which grades seaward into a thin intercalated peat. Smith *et al.* (1999) found mesohalobous to euhalobous diatom species indicating a fluctuating marine influence. Above this peat a second silty organic horizon is observed that in places contains much macroscopic salt-marsh plant material. Foraminifera are generally found in relatively low numbers in this horizon and are dominated by salt-marsh taxa *Miliammina fusca* and *Entzia macrescens*. This horizon transitions into a grey silty clay with occasional organic lamination and, again, salt-marsh plant fragments, but including calcareous foramanifera taxa such as *Elphidium williamsoni, Buliminella elegantissima* and *Haynesina germanica* indicating a tidal-flat environment that is in close proximity to a salt marsh. A widespread sand deposit around 5–7 cm thick is found across the site at elevations between -0.2 and 0.45 m OD that was identified as a Storegga tsunami deposit by Smith *et al.* (1999). Above the sand layer the silts grade into peaty silts and finally into an upper horizon of present-day salt-marsh peat.
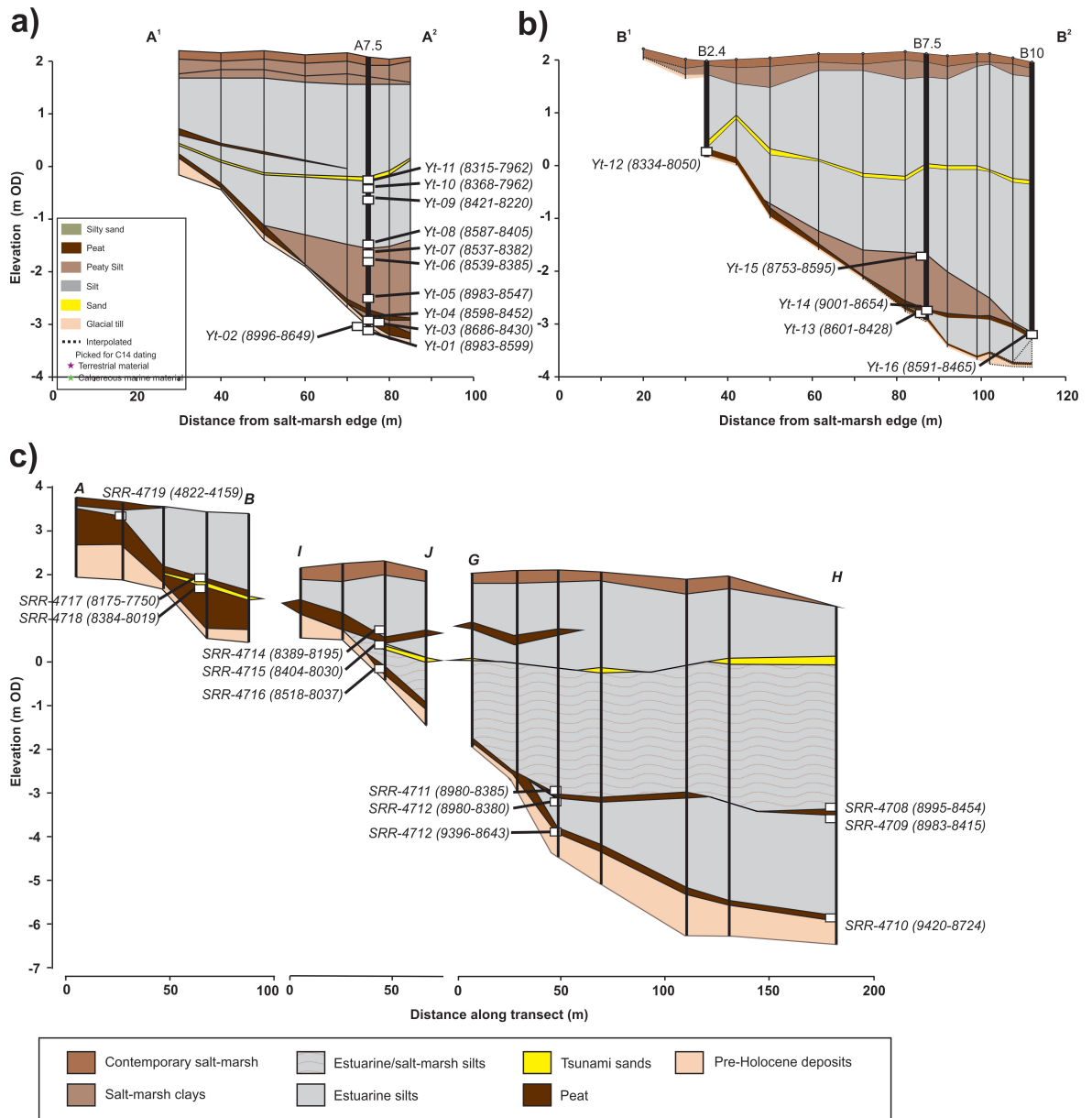
Figure 4.2: Lithostratigraphy of the Ythan Estuary along the transects cross-referenced in Fig. 4.1. Transects A and B shown in A) and B) respectively are from this study. The highlighted cores are those sampled used for radiocarbon or microfossil analysis and referred to in the text. C) shows the transects of Smith *et al.* (1999) redrawn from the original descriptions. The calibrated unmodelled radiocarbon ages are shown for the samples from this study, as presented in Table 4.1, along with the recalibrated ages of the samples in Smith *et al.* (1999) and given as calibrated ages BP.

4.3.2   Chronology

Sixteen AMS ^{14}C ages were collected across the site (see Fig. 4.2 & Table 4.1). The calibrated ^{14}C ages show 2σ ranges of between 86 and 234 years (Fig. 4.2 & Table 4.1). A number of ^{14}C plateaus in the calibration curve results in relatively wide calibrated ages, particularly for the older samples. The basal peat, sampled at similar elevations in three cores, show the peat formed between c. 9,000–8,500 cal yr BP. Above this peat, in the critical section, we collected nine further ^{14}C ages from core A7.5. The unmodelled calibrated ages are sequential in both time and depth covering ca. 400 years, through to a youngest age of 8,315–7,962 cal yr BP. On the other hand the three calibrated ages from the overlying sediment in core B7.5 showed an age reversal at 2.73 m OD. The cause of the reversal is unclear, but alongside a lack of suitable organic material and thus chronological control, we did not use this core any further for our RSL reconstruction and focused on A7.5.

The age-depth model for core A7.5 (Fig. 4.3) is modelled to a satisfactory overall level of agreement (78%), with 10 of the 11 tie-points having an agreement index > 60% between the prior and posterior ages (Table 4.1). The estimated accumulation rate increases from 1 mm/yr during peat formation, to around 15 mm/yr for the salt-marsh deposition before reducing to around 7 mm/yr during the tidal-flat clay accumulation. The use of boundaries in the model introduces an element of subjectivity but is based on stratigraphical knowledge and has the effect of improving the quality of the model. Despite the use of the P-sequence model and greater precision of the local reservoir correction, some dates still have a relatively wide range that is mainly an artefact of the plateaus in the calibration curve. The Bayesian age-depth model for the sequence improves the precision of dated samples and generates age PDFs at other depths that we include in the sea-level reconstruction.

Table 4.1: Radiocarbon (^{14}C) dates from the Ythan Estuary and calibrated to 2σ yr BP in OxCal 4.4 (Bronk Ramsey, 2009) using $_a$ = IntCal20 (Reimer $et~al.$, 2020) or $_b$ = Marine20 (Heaton $et~al.$, 2020). Modelled ages are produced using the P_sequence deposition model with yt-11 (*) combined with the Storegga calendar age from (Bondevik $et~al.$, 2012) of 8130 $\pm$ 50 BP. The agreement index is a measure of the performance of the overall model and individual calibration solution where a threshold value of 60% is appropriate (Bronk Ramsey, 1995). Overall agreement index = 77.7%.

| Lab code	Sample code	Core	Depth (m)	Elevation (m OD)	Material dated	^{14}C yr BP ($\pm~2\sigma$)	Calibrated age (2σ cal. yr BP)	Modelled age (2σ cal. yr BP)	Agreement Index (%)
SUERC-87636	yt-01	A7.5	5.17	-3.10	Plant macrofossil	$7,917 \pm 40_a$	8,983–8,599	8,993–8,643	106
SUERC-87637	yt-02	A7.5	5.14	-3.07	Plant macrofossil	$7,980 \pm 39_a$	8,996–8,649	8,814–8,605	74
SUERC-87638	yt-03	A7.5	5.02	-2.95	Plant macrofossil	$7,774 \pm 40_a$	8,634–8,430	8,686–8,542	84
SUERC-87639	yt-04	A7.5	4.97	-2.90	Plant macrofossil	$7,768 \pm 40_a$	8,598–8,452	8,631–8,485	117
SUERC-87644	yt-05	A7.5	4.59	-2.52	Plant macrofossil	$7,880 \pm 56_a$	8,983–8,547	8,574–8,444	69
SUERC-87645	yt-06	A7.5	3.71	-1.64	Plant macrofossil	$7,658 \pm 38_a$	8,539–8,385	8,483–8,395	132
SUERC-87646	yt-07	A7.5	3.62	-1.55	Plant macrofossil	$7,651 \pm 37_a$	8,537–8,382	8,470–8,388	135
SUERC-87647	yt-08	A7.5	3.57	-1.50	Plant macrofossil	$7,696 \pm 39_a$	8,587–8,405	8,465–8,384	89
SUERC-87648	yt-09	A7.5	2.59	-0.52	Plant macrofossil	$7,559 \pm 37_a$	8,421–8,220	8,395–8,188	33
SUERC-87634	yt-10	A7.5	2.40	-0.33	Marine gastropods	$7,780 \pm 37_b$	8,288–8,087	8,288–8,087	118
SUERC-87635	yt-11*	A7.5	2.36	-0.29	Marine gastropods	$7,712 \pm 37_b$	8,315–7,962	8,282–8,087	124
SUERC-87649	yt-12	B2.4	1.67	0.32	Plant macrofossil	$7,409 \pm 37_a$	8,334–8,050	NA	NA
SUERC-87654	yt-13	B7.5	5.00	-2.86	Plant macrofossil	$7,767 \pm 39_a$	8,601–8,428	NA	NA
SUERC-87655	yt-14	B7.5	4.87	-2.73	Plant macrofossil	$8,015 \pm 42_a$	9,001–8,654	NA	NA
SUERC-87656	yt-15	B7.5	3.39	-1.25	Plant macrofossil	$7,876 \pm 39_a$	8,753–8,595	NA	NA
SUERC-87657	yt-16	B10	5.16	-3.19	Plant macrofossil	$7,760 \pm 42_a$	8,591–8,465	NA	NA
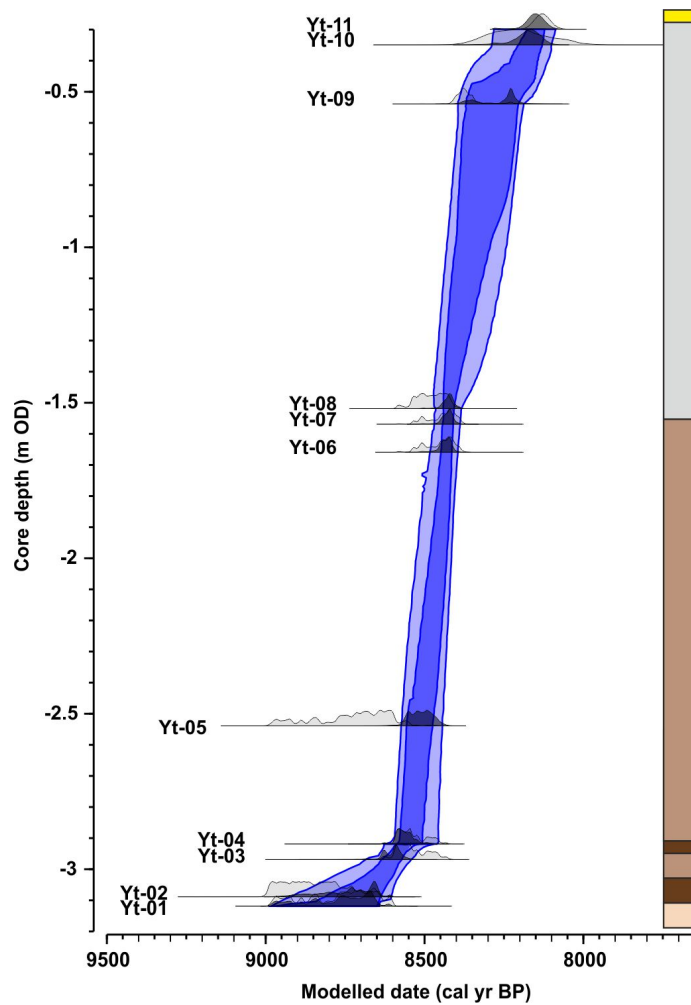
Figure 4.3: Age-depth model based on the 11 tie points from core A7.5. The unmodelled calibrated ^{14}C ages for each sample (light grey) and modelled ages (dark grey) are shown, along with the 1σ and 2σ age-depth model. The core stratigraphy is shown with the lithology corresponding to the colours in Fig. 4.2.

4.3.3   Palaeo sea level

In order to calculate the indicative meaning of the core samples we applied the foraminifera training set and transfer function of Rush *et al.* (in review) to the fossil foraminifera (Fig. 4.4). Detrended correspondence analysis (DCA) and cluster analysis using partitioning around medoids with euclidean distances (Kaufmann and Rousseeuw, 1990, Rousseeuw, 1987) demonstrates that the fossil samples group well around the modern samples (Figs. B.3 & B.1). In common with other studies the agglutinated taxa appear particularly well suited for predictions, although may lack more definitive zonation observed by others (e.g. Horton *et al.*, 1999*b*, Gehrels, 2000, Gehrels *et al.*, 2005, Horton and Edwards, 2006, Kemp *et al.*, 2013, Barnett *et al.*, 2016). Modern tidal-flat samples are predominantly made up of calcareous taxa which can be problematic and are sometimes excluded (e.g. Horton and Edwards, 2006, Kemp *et al.*, 2009, Leorri *et al.*, 2011, Mills *et al.*, 2013) due to uncertainty in their response to elevation and identifying their lowest occurrence (Hamilton and Shennan, 2005, Edwards and Wright, 2015). We retain them in the transfer model because: *i*) the dominant taxa show an apparent linear response to elevation in the training set, and *ii*) the indicative meanings are supported by the lithological interpretation, the continued presence of salt-marsh foraminifera taxa and plant macrofossils suggesting a tidal flat in close proximity to the salt marsh.

The species response to elevation is unimodal with an environmental gradient > 2 standard deviations (gradient length $= 4.25$) and we therefore applied a weighted averaging with partial least square regression (WAPLS) transfer function cross-validated by bootstrapping (n $= 1,000$) and leave-one-site-out (LOSO) to confirm the quality of the transfer functions and the independence of samples (Telford and Birks, 2005, Payne *et al.*, 2012) (Figs. B.4 & B.5). We selected WAPLS with two components over the one component model because of a significant transfer function performance improvement of $> 5\%$ based on the R^2 and RMSEP values (Barlow *et al.*, 2013) and confirmed that as a result of adding the 2nd component the coefficient updates of taxa that also occur in the fossil samples are fundamentally unaltered (Fig. B.6) (Wright *et al.*, 2011). The exclusion of samples from Cowpen and eastern North Sea sites does not reduce the apparent accuracy of the reconstruction, whereby the reconstructed sea level is well inside the range when all samples were included (Fig. B.7). Additionally, applying the modern analogue technique (MAT) as outlined by Watcham *et al.* (2011) shows that the fossil samples contain zero 'poor' analogues in the trimmed modern

training set, and excluding the Cowpen samples results in no reduction in the number of 'good' or 'close' analogues (Fig. B.7). Finally, the transfer function passes the test proposed by Telford and Birks (2011) and produces a sea-level reconstruction that outperforms transfer functions run on random data, with 53% of the species variance explained by the reconstructed elevation relative to the tidal frame.

We corrected the indicative meanings to account for changes in Holocene tides using palaeotidal modelling (Hill, 2020). The model predictions show that a sharp rise in tidal range in the region occurred between 9,000–8,000 yr BP and lasted until around 7,000 yr BP from when tides remained similar to modern day consistent with other studies (Uehara *et al.*, 2006, Ward *et al.*, 2016) (Fig. B.9a). The resultant indicative meanings and hence relative sea level after applying the MHWST from our three methods described in Section 4.2.2.2 are shown in (Fig. B.9b). The difference between the indicative meanings using the two interpolation methods of palaeotides (*i* and *ii*) was small (7–12 cm), as opposed to a much larger discrepancy of 12–66 cm between either and when using the modern value (*iii*). It is therefore clear that modelling and including palaeotides has a profound effect and is thus essential, although the choice of which palaeotide interpolation method used has a minimal effect. We consider the likelihood of the shift in tidal amplitude to have occurred towards the end of the our reconstructions as a result of the sea-level rise (Hijma and Cohen, 2019, Lawrence *et al.*, 2016) and therefore we used the simulated MHWST at 9,000 yr BP (1.69 m) as it most closely represented conditions throughout the period of the reconstruction.

The resultant predicted indicative meanings are presented in Fig. 4.4 and range between the upper salt marsh and upper tidal flats. Foraminifera were absent in the peat samples, but the diatoms suggest an indicative meaning close to HAT. There are two notable reductions in indicative meaning in core A7.5. The first shows a reduction of around 35 cm from around HAT to mid-marsh which persisted for ca. 100 years until a second reduction of around 30 cm elevation to a tidal-flat environment.

To correct for any post-depositional compaction we compared the indicative meaning of the sample from directly below the Storrega deposit with that of core B2.4 where the deposit sits directly on top of basal peat. Based on our analysis core A7.5 had a surface elevation around 70 cm lower than B2.4 as opposed to the measured present day elevation difference at these points of 60 cm. Assuming that compaction of the thin basal peat was not significantly greater in core B2.4 (which is unlikely given the similar lithology and far thinner overburden

thickness of B2.4) then compaction of the intercalated peat and salt-marsh sediment in A7.5 cannot have been greater than 10 cm. Given the apparent small amount of compaction and the low organic content of the inter-tidal deposits (LOI < 10%), we consider the majority of compaction to have occurred in the basal and intercalated peat horizons. We therefore raised the elevations within core A7.5 by interpolating between 0 cm at the base and 10 cm at the top of the peat with an uncertainty captured in Eq. 4.1c.
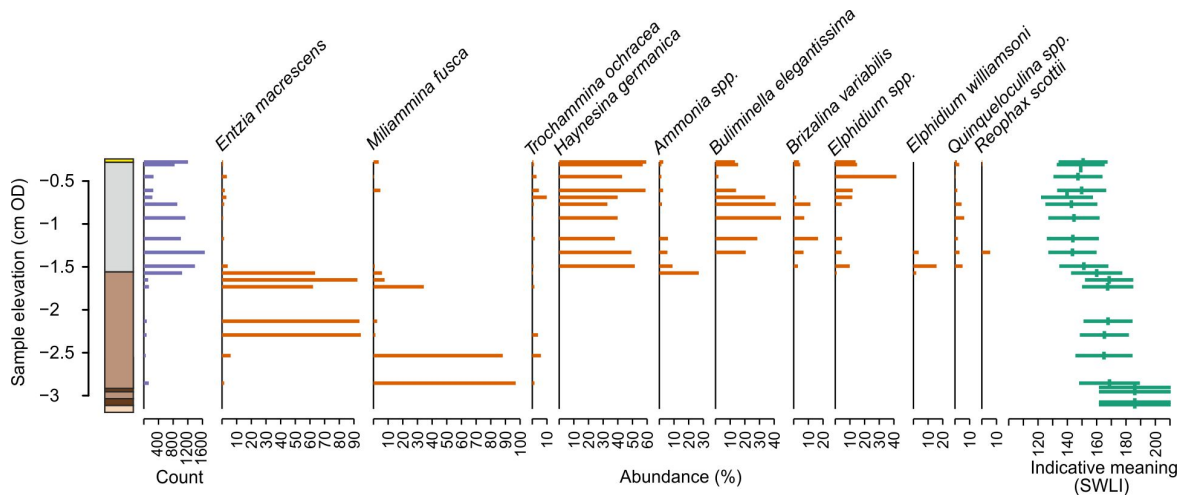
Figure 4.4: Litho- and biostratigraphy of core A7.5. Foraminifera taxa that exceed a maximum of 5% abundance in any sample are displayed in orange as % of the sample total ('Count' in purple). The indicative meaning is displayed in green and is given as the 1σ range predicted palaeo surface elevation relative to a mean tide level of 0.3 m as calculated by the transfer function prediction and accounts for the palaeo tide.

4.3.4   Sea-level reconstruction

The probabilistic sea-level reconstruction is based on the age PDFs and normally distributed sea level predictions after accounting for tidal amplitude and compaction for each of the SLIPs in core A7.5. Fig. 4.5 shows that a RSL rise, with fluctuating rates, of approximately 4 m occurred between $8{,}770 \pm 97$ and $8{,}130 \pm 50$ cal yr BP before the Storegga tsunami struck. The change-point analysis shows that a SLE, with a rapid increase in rates from the longer term background sea-level rise occurred at $8{,}610 \pm 5$ cal yr BP and returned at $8{,}340 \pm 5$ cal yr BP (Fig. 4.5c). Within this prolonged period, two distinct stages are identified by a significant change point that is contemporaneous with the litho- and biostratigraphy shifts described above and shown in Fig. 3.5b. The first stage (Y-SLE[1a]), beginning at $8{,}610 \pm 5$ cal yr BP, saw rates rise to around 10 mm/yr in around 50 years
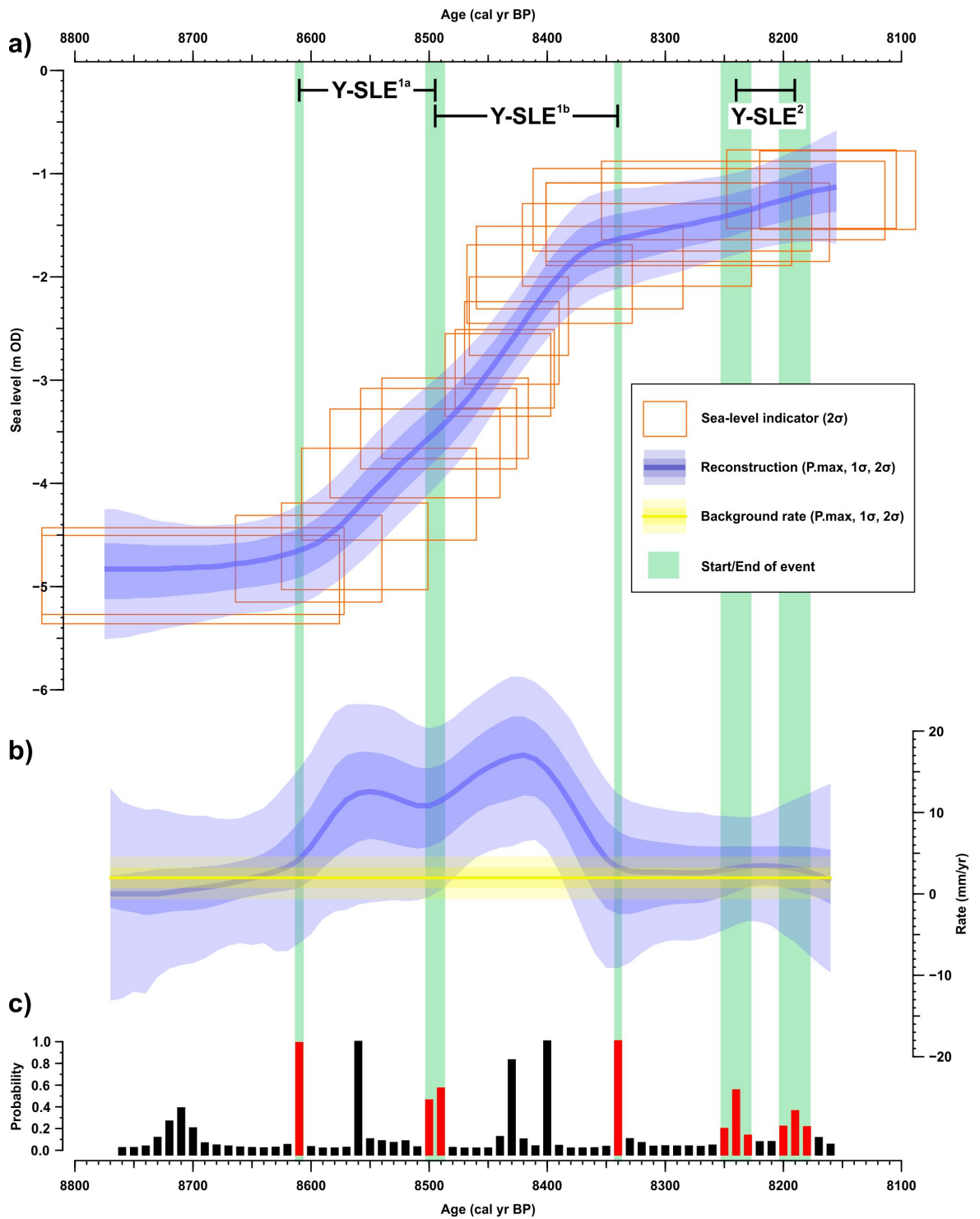
Figure 4.5: Relative sea-level reconstruction for the Ythan Estuary, W Scotland. a) Relative sea-level reconstruction. b) Rates of relative sea-level change produced using the probabilistic statistical method. c) The probabilities of a change point occurring with red bars indicating the start and end of sea-level events.

before appearing to gradually decline until $8{,}495 \pm 10$ cal yr BP. This was immediately followed by the second stage (Y-SLE^{1b}) when rates rose again and peaked at around 17 mm/yr at $8{,}430 \pm 5$ cal yr BP, before returning to the background rates at $8{,}340 \pm 5$ cal yr BP. A third period of higher rates and possible SLE (Y-SLE^2) is identified between $8{,}240 \pm 15$ and $8{,}190 \pm 15$ cal yr BP, although the combined probability of a change point at the start (74%) and end (84%) are below 95%. The rate of RSL change is similar both before (P.max $= 1.2$ mm/yr), between (P.max $= 2.6$ mm/yr) and after (P.max $= 2.3$ mm/yr) the prolonged period of higher rates (Fig. 4.5b), providing confidence that these periods are representative of a longer term RSL rise. The resultant magnitudes of the SLEs quantified probabilistically based on the change-point age distributions and the sea level reconstructions are shown in Table 4.2. It is 'very likely' (95% probability) that Y-SLE^{1a} and Y-SLE^{1b} had a global magnitude of at least 0.91 m and 1.64 m respectively, with a P.max of 1.42 m and 2.22 m. Y-SLE^2 had a global magnitude P.max of 0.11 m and potentially as large as 0.48 m at the 95% probability boundary.

Table 4.2: The timing and local and global (scaled to the barystatic-GRD fingerprint) magnitudes of the Ythan Estuary sea-level events. The 1σ and 2σ ranges are taken as the 68% and 95% probability and are given along with the corresponding IPCC terminology in brackets.

	Timing (cal yr BP)		Local magnitude (m)			Global magnitude (m)		
	Start	End	P.max	1σ ('likely')	2σ ('very likely')	P.max	1σ ('likely')	2σ ('very likely')
Y-SLE^{1a}	$8{,}610 \pm 5$	$8{,}495 \pm 10$	0.99	0.82–1.17	0.64–1.35	1.42	1.16–1.66	0.91–1.92
Y-SLE^{1b}	$8{,}495 \pm 10$	$8{,}340 \pm 5$	1.55	1.37–1.74	1.15–1.96	2.22	1.95–2.48	1.64–2.81
Y-SLE^2	$8{,}240 \pm 15$	$8{,}190 \pm 15$	0.08	-0.05–0.20	-0.18–0.34	0.11	-0.20–0.29	-0.25–0.48

4.4 Discussion

4.4.1 Ythan RSL reconstruction

Our method for reconstructing RSL attempts to fully quantify the error terms of both age and sea-level. Along with the stratified random sampling we produced a reconstruction with realistic, yet relatively large 1σ and 2σ confidence intervals (Fig. 4.5). The subsequent change-point analysis identifies a number of points where a significant shift occurs in the pattern of the rate of sea-level change from which we identify two SLEs, with the first showing two distinct stages that we discuss in isolation. The initial departure from the background rates at 8,610 cal yr BP is clearly identified (Fig. 4.5c) and corresponds with the evidence of a shift in the litho- and biostratigraphy (Figs. 4.3 & 4.4). Although there

is not the litho- or biostratigraphic evidence supporting the return to background rates at 8,340 $\pm$ 5 cal yr BP, the timing is well constrained in the probabilistic reconstruction (Fig. 4.5c). Using these dates as boundaries for calculating the background rates produces predictions that are consistent with predicted rates from GIA modelling (Bradley *et al.*, 2011) of 2.87 mm/yr between 10,000 and 9,000 yr BP and 4.25 mm/yr between 9,000 and 8,000 yr BP suggesting our background rates are appropriate. Therefore, the assertion that the period of higher rates, from 8,610 $\pm$ 5 to 8,340 $\pm$ 5 cal yr BP, is a definitive departure from the background trend is strengthened. Furthermore, we note that if we did adopt the less conservative method of Lawrence *et al.* (2016) and assume the shape of the sea-level reconstruction at the $\pm$ 1σ and 2σ intervals to be correct and take the point at which the differentials of each of these all exceed the rate of GIA, then we generate start and end points of the prolonged SLE that fall within 10 years of our predictions (see Lawrence *et al.* (2016) for full methods). Although we do not use this method owing to its less conservative nature in the assumptions it makes and the reliance on modelled GIA rates for the background, it does provide support for our predicted timings of the event.

Within the prolonged period of high rates two distinct stages are identified in our analysis (Fig. 4.5c). Similarly, the litho- and biostratigraphy across the site indicates a transgressive sequence with a marked shift in palaeo-marsh elevation synchronous with the boundary between Y-SLE[1a] and Y-SLE[1b] at 8,495 $\pm$ 10 cal yr BP (Figs. 4.3 & 4.4).

The second stage (Y-SLE[1b)] appears to have lasted for 40–60 years longer than the first (Y-SLE[1a]) and is very likely to have had a larger magnitude. Although by our definition this is defined as a single SLE with two separate stages, it may be that two distinct SLEs occurred but they are unable to be separated by the reconstruction. A second SLE (Y-SLE[2]) is less well defined and is as likely as not to have occurred. However, it cannot be ruled out and we therefore quantified its magnitude in the same manner as Y-SLE[1a] and Y-SLE[1b]. The timing of Y-SLE[2], immediately preceding the 8.2 ka climate event and contemporaneous with other palaeo records (Li *et al.*, 2012, Hijma and Cohen, 2010, 2019, Lawrence *et al.*, 2016) discussed in detail in Sections 4.4.3, provides an indication that this is more than an artefact of the statistical methods and is indeed a genuine SLE. The magnitude of Y-SLE[2], although smaller than Y-SLE[1a] and Y-SLE[1b], could be as large as 0.48 m and hence a meltwater pulse that should not be overlooked.

Thus far we have discussed the SLEs with reference to meltwater pulses but it is necessary

to examine other processes that act at different scales and could have caused the observed RSL rise. A change in morphology could have induced a fall in surface elevation locally to core A7.5 by way of tidal creek migration or erosion of a tidally cut cliff at the salt-marsh edge and hence apparent relative sea-level rise. The wider lithostratigraphy of the site and biostratigraphy of core B7.5 mean that such a local effect appears highly unlikely (Fig. 4.2). A local tectonic subsidence event is unlikely given that it would have resulted in a much more instantaneous rise than observed (e.g. Atwater, 1987) which allied to the tectonic stability of the region enables us to rule this out as this similarly local cause. Regionally, the UK sea-level database demonstrates that the site is in a region of isostatic uplift and therefore GIA related subsidence must not have been the cause (Shennan *et al.*, 2018). On the other hand, evidence from around the Earth (see Section 4.4.3) show contemporaneous periods of rapid sea-level rise distinct from background rates supporting an interpretation of a barystatic rise acting on a global scale being the driver for the observed SLEs in the Ythan Estuary. We have argued that our RSL reconstruction contains at least two, and quite possibly three, distinct SLEs. However, as it is unclear whether Y-SLE^1 separates into two distinct events (i.e. Y-SLE^{1a} and Y-SLE^{1b}), and the magnitude of Y-SLE^2 means it may not be an additional event, based on the Ythan reconstruction alone, we cannot with certainty disprove hypothesis *i*- that there was only one meltwater pulse. The global magnitude of the SLEs, shown in Fig. 4.7, allows us to investigate the likely source of the barystatic sea-level rise. Y-SLE^{1a} and Y-SLE^{1b} are both 'very likely' to be greater than the potential rise resulting from drainage of LAO at its maximum volume. Godbout *et al.* (2019) recently demonstrated that this was less than the original estimate by Leverington *et al.* (2002) of 1.63×10^14 and therefore LAO drainage would have resulted in less than 0.45 m of barystatic sea-level rise. We can therefore reject hypothesis *ii* - that the two initial meltwater pulses, Y-SLE^{1a} and Y-SLE^{1b}, were as a result of LAO drainage. On the other hand Y-SLE^2 is smaller in magnitude and on the basis of its size and coincidence with evidence of LAO drainage (Jennings *et al.*, 2015) suggests that Y-SLE^2 was driven by lake drainage. Our findings from the Ythan Estuary indicate that a contribution from the HBIS is necessary to explain both stages of the first SLE, while the possible second SLE can be explained by the drainage of LAO. In order to derive a hypothesis of the sequence of deglacial processes that caused the SLEs we turn to other global evidence for comparison in Section 4.4.3.

4.4.2   Cree RSL reanalysis

The original analysis from the Cree Estuary showed three 'sea-level jumps' at $\sim$ 8,760–8,640, 8,595–8,465 and 8,323–8,218 cal yr BP with mean global magnitudes of 0.57, 0.95 and 0.52 m respectively (Lawrence *et al.*, 2016). We reanalysed the data in order to make the results from the Cree and Ythan directly comparable. The RSL reconstruction shows a similar pattern to the original reconstruction (see Fig. 4.6), but we only identify one clear SLE (C-SLE[1]), which occurred between $8,600 \pm 5$ and $8,430 \pm 5$ cal yr BP and a second, less clear, between $8,260 \pm 5$ and $8,060 \pm 10$ (C-SLE[2]) (Fig. 4.6c). The magnitudes are shown in Table 4.3 and demonstrate that C-SLE[1] was 'likely' to have been larger than C-SLE[2]. The relatively large uncertainty is due to the large original RSL uncertainties of the SLIPs and our method of including the full uncertainty in the background rates as opposed to simply taking a single GIA modelled rate. Both SLEs coincide with the calibrated ^{14}C ages of marsh drowning in the stratigraphic record (Fig. 5 of Lawrence et al. 2016) suggesting that the SLEs identified are genuine and not simply artefacts of the statistical model.

The initial sea-level rise in the Cree record is in close agreement with the Ythan, whereby the start of C-SLE[1] occurs around 30 years earlier than Y-SLE[1a] (Fig. 4.7). The end of the SLEs are less well aligned however, with the Cree event lasting around 90 years longer and with a larger global P.max magnitude. C-SLE[1] does appear to have a small double step within it (Fig. 4.6b), similar to the first Ythan SLE (Fig. 4.5b), that is identified with around 50% probability by the change-point analysis (Fig. 4.6c). Along with the longer duration and possible larger magnitude the pattern suggests that C-SLE[1] may be the equivalent Y-SLE[1a] and Y-SLE[1b] combined. The start of C-SLE[2] is similarly offset from a SLE in the Ythan records, beginning around 30 years before Y-SLE[2] (Fig. 4.7). Again, C-SLE[2] lasts longer than Y-SLE[2] and has a larger P.max. The end point of both of the these SLEs are not entirely clear and it cannot be discounted that the duration of C-SLE[2] was shorter than our analysis suggests.

Table 4.3: The timing and local and global (scaled to the barystatic-GRD fingerprint) magnitudes of the Cree sea-level events. The 1σ and 2σ ranges are taken as the 68% and 95% probability and are given along with the corresponding IPCC terminology in brackets.

	Timing (cal yr BP)		Local magnitude (m)			Global magnitude (m)		
	Start	End	P.max	1σ ('likely')	2σ ('very likely')	P.max	1σ ('likely')	2σ ('very likely')
C-SLE[1]	$8,600 \pm 5$	$8,430 \pm 5$	1.76	1.31–2.14	0.87–2.50	2.52	1.88–3.05	1.25–3.57
C-SLE[2]	$8,260 \pm 5$	$8,060 \pm 15$	0.63	0.31–0.96	0.00–1.26	0.90	0.44–1.37	0.01–1.81
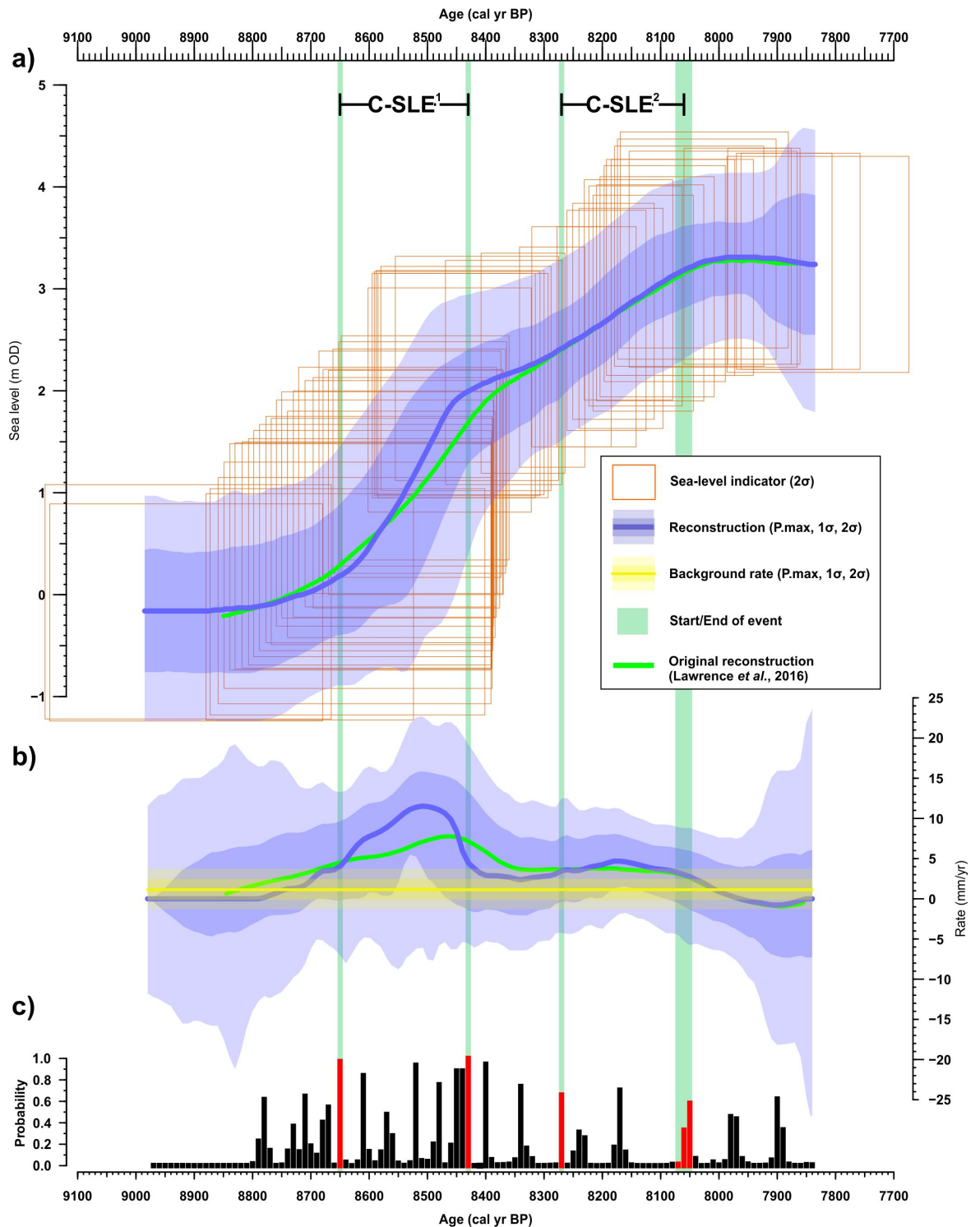
Figure 4.6: Relative sea-level reconstruction for the Cree Estuary, W Scotland following reanalysis of the data from Lawrence *et al.* (2016) a) Relative sea-level reconstruction. b) Rates of relative sea-level change produced using the probabilistic statistical method. c) The probabilities of a change point occurring with red bars indicating the start and end of sea-level events. The original calculation for sea level and the rates are shown by the green lines.

4.4.3   The global evidence of meltwater events

Results from geomorphological analysis, oceanic reconstructions, ice-sheet and climate modelling, along with other sea-level reconstructions provide evidence of the deglacial process prior to the 8.2 ka climate event and are summarised in Fig. 4.7. The data appear to group around two phases which we now discuss in turn. Based on this, we then hypothesise about the sequence of deglacial events that ultimately forced the 8.2 ka climate event.

4.4.3.1   Phase 1

The first set of data that appear to group together chronologically, including the first two Ythan SLEs, suggest two distinct meltwater pulses occurred between 8,650 and 8,350 cal yr BP in phase 1. Submarine sediment records from the Labrador shelf show an ocean freshening event at c. 8,580 cal yr BP and a second, more pronounced event, at 8,500 cal yr BP (Fig. 4.7c) (Lochte *et al.*, 2019). The events are similarly recorded in previous studies of marine cores (Hillaire-Marcel *et al.*, 2007, Hoffman *et al.*, 2012, Jennings *et al.*, 2015) (Fig. 4.7b) from the region, including the 'red bed' at around 8,500 cal yr BP (Barber *et al.*, 1999). A signal of change in deepwater circulation is also observed further afield in the North Atlantic (Fig. 4.7d) and has been tied to weakening of the AMOC (Ellison *et al.*, 2006, Kleiven *et al.*, 2008). The latter record was recalibrated by Lawrence *et al.* (2016) and suggests that the first of these events was broadly concurrent with this first phase of freshwater events although the chronologies remain problematic. The chronologies of all of these marine records rely on accurately quantifying the local reservoir effect, which is especially challenging in a time and region of substantial land-ocean freshwater interaction as demonstrated by Lochte *et al.* (2019). With the exception of the reconstruction by Lochte *et al.* (2019), the ΔR was largely calculated by assuming synchronicity with known climate events such as the 8.2 ka climate event and tying the freshwater events to them and so the accuracy of the absolute timing of the events is somewhat equivocal from the marine records. Within this uncertainty, it appears that two meltwater pulses are recorded in marine records around the Labrador shelf which are recorded as a single deepwater signal indicating AMOC weakening within phase 1.

The two freshwater events resulted in rapid sea-level rises that are observed in the Ythan RSL reconstruction (Fig. 4.7) and possibly within C-SLE[1] (see Section 4.4.2). The larger second stage also coincides with the timing of the first SLE observed in the Rhine-Meuse RSL
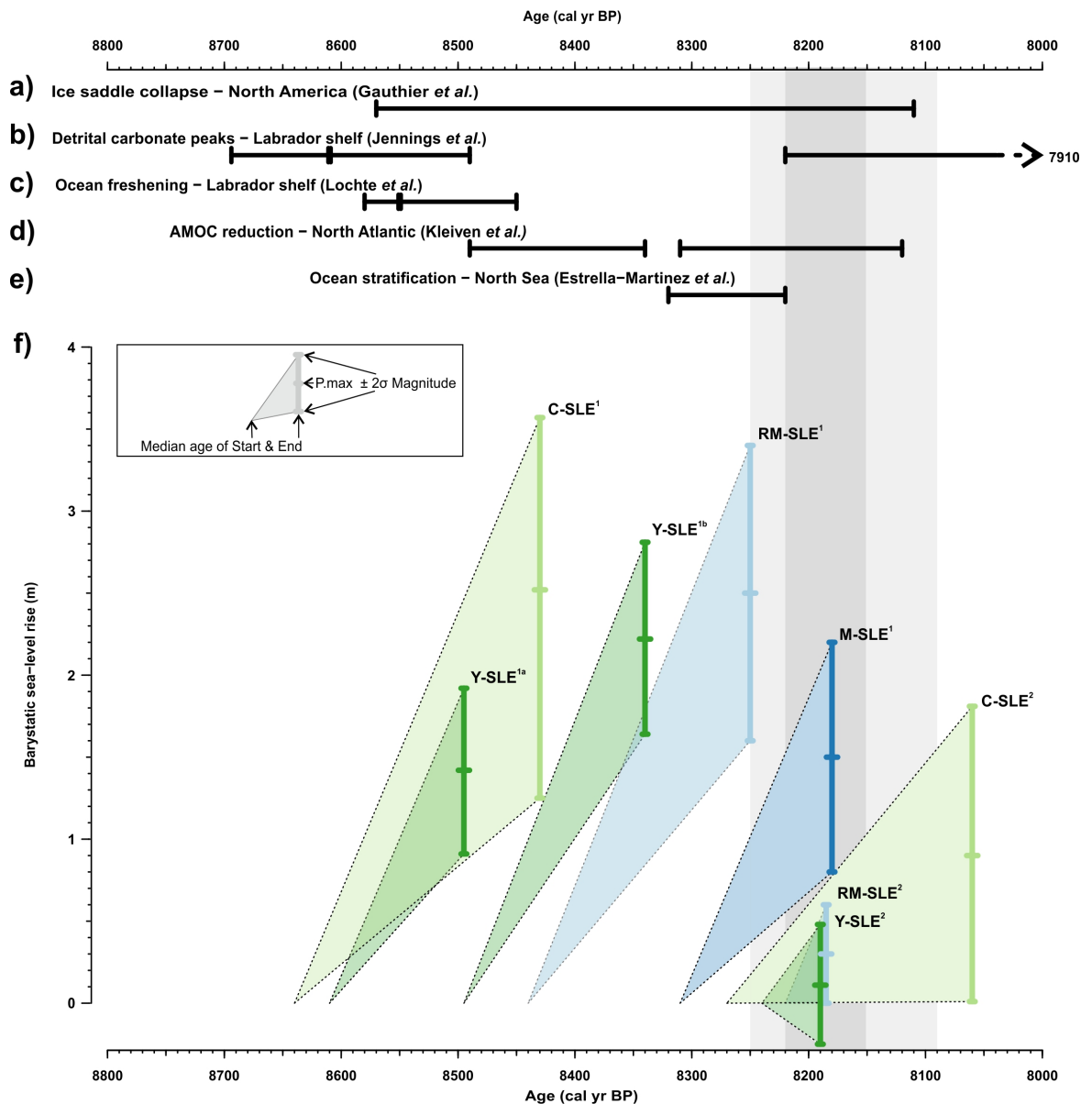
Figure 4.7: Records of climate, oceanographic and sea-level change prior to and including the 8.2 ka climate event. The black bars in a–e show the timing of events from proxy records that are referred to in the text. f) Shows the timing and magnitude of sea-level events from the well resolved relative sea-level records referred to in the text. The inset box shows how each sea-level event is graphically represented, whereby the start is marked by the left edge and the end by the right edge where the vertical bar that shows the maximum probability and 2σ magnitude of the barystatic, or global, sea-level event. C-SLE = Cree Estuary Sea (reanalysed in this study from Lawrence et al. 2016) (Lawrence *et al.*, 2016), Y-SLE = Ythan Estuary Sea (This study), RM-SLE = Rhine-Meuse Delta (Hijma and Cohen, 2019), MSLE = Mississippi Delta (Li *et al.*, 2012). The timing of the 8.2 ka climate event is shown by the grey bar, with the central event indicated by the darker grey bar. (Note: the ranges of the start and end points for the events are not shown in a–f).

reconstruction (Hijma and Cohen, 2010, 2019), (RM-SLE[1] in Fig. 4.7f), providing further evidence of a SLE with a global magnitude of around 2 m, compared to the first SLE of around 1 m. The first stage of the SLE is not observed in the Rhine-Meuse record which may be due to the lower rate of rise, such that accretion rates meant that peat formation was able to keep pace with sea level. Indeed Törnqvist *et al.* (2020) show that only when rates are between 3–6 mm does marsh drowning occur. It may be therefore that rates were not high enough to produce the signature of a 'sea-level jump' in these environments and only the second SLE was captured with its higher rates. Less well-resolved evidence of SLEs are also observed contemporaneously in reconstructions from the the Po Delta, Italy, at c. 8,500 cal yr BP (Amorosi *et al.*, 2017), Maputo Bay, Mozambique, at c. 8,600 cal yr BP (De Lecea *et al.*, 2017) and a number of far-field sites in southeast Asia. The southeast Asian sites in the Pearl Delta (Zong *et al.*, 2012), Yangtze Delta (Wang *et al.*, 2013), Hangzou Bay (Xiong *et al.*, 2020) and Mekong Delta (Tamura *et al.*, 2009, Nguyen *et al.*, 2010, Tjallingi *et al.*, 2014) all show similar drowning events with rates appearing to increase to around 30 mm/yr between c. 8,600 and 8,300 cal yr BP, set against background rates of around 10 mm/yr. As far-field sites the local magnitude of around 3.8 ± 1 m is equivalent to the global magnitude and similar to the combined magnitudes of Y-SLE[1a] and Y-SLE[1b] (3.62 ± 1.1 m).

The timing of the events in phase 1 fits within the period of $8{,}570 \pm 280$ cal yr BP to $8{,}110 \pm 190$ cal yr BP for the HBIS collapse described by a geomorphology based regional LIS deglacial reconstruction (Gauthier *et al.*, 2020) (Fig. 4.7a), that the authors suggest was preceded by drainage of LAO. Godbout *et al.* (2020) recently added to the geological evidence of a two-step drainage of LAO (Roy *et al.*, 2011, Godbout *et al.*, 2019) and demonstrated that lake levels were lower than previously estimated (Leverington *et al.*, 2002) and hence a barystatic sea-level rise would have been < 0.45 m. In contrast, although hard to quantify, the HBIS is estimated to have stored the equivalent of around 1.25 m barystatic sea-level rise (Ullman *et al.*, 2016, Lochte *et al.*, 2019). The potential contributions of each show that LAO alone was not large enough to have caused the two observed SLEs and that the ice-saddle collapse was likely the major component. It is difficult to single out a lake drainage from the melting HBIS in the sea-level reconstructions, or indeed other records, but LAO appears to form part the first SLE. If the magnitude of the SLE is at its lower range then the lake drainage could have contributed nearly half of the meltwater of the first SLE. In addition

to the HBIS collapse, ice-sheet modelling shows a demise of the Labrador and Keewatin ice domes and hence a larger contribution to sea-level rise of between 2.12–3.42 m from the LIS on top of the background rate (Matero *et al.*, 2020). This may account for the larger apparent magnitude of the combined SLEs that is observed in the sea-level records than from the HBIS alone.

Phase 2

The second group of data are clustered around the period either immediately preceding or within the 8.2 ka climate event itself and appear to express a much smaller magnitude meltwater pulse than the previous two. A SLE is consistently observed in the sea-level records from the Ythan Estuary, Mississippi Delta, Rhine-Meuse Delta and Cree Estuary. Although there are possible variations in the timing and magnitude from the records, the large overlap suggests that they are all an expression of the same meltwater event, which is also observed in the Labrador Sea in the Cartwright Saddle record (Jennings *et al.*, 2015) at a corresponding time (Fig. 4.7b). A second ocean circulation slowdown is also observed (Ellison *et al.*, 2006, Kleiven *et al.*, 2008) (Fig. 4.7d) that given the chronological uncertainties may well be tied to this third event. Finally, a hydrographical reconstruction shows evidence of stratification occurring in the North Sea at c 8,270 cal yr BP (Estrella-Martínez *et al.*, 2019) (Fig. 4.7e) that appears to have been a result of this final meltwater pulse. The chronology in this record does not extend back past 8,290 cal yr BP and so it is not possible to understand if the previous meltwater events caused a similar effect. The smaller apparent magnitude of the SLE (< 1 m) suggest that this final event could have been caused by the terminal drainage of LAO which fits the timing proposed by Gauthier *et al.* (2020) of 8,110 ± 190 cal yr BP.

Sequence of deglacial processes

Our findings are consistent with the hypothesis of Lochte *et al.* (2019) and Gauthier *et al.* (2020) that an initial thinning of the HBIS resulted in the hydraulic pressure of LAO causing fractures and uplifting of the ice, such that LAO drained through sub-glacial channels identified by Gauthier *et al.* (2020). This is expressed by the first freshwater event in the Labarador Sea (Fig. 4.7b–c) and the first, smaller, SLE in the Ythan and Cree records (Fig. 4.7f). Marine transgression then occurred, causing an acceleration in ice melt until

the conduits closed and the lake reformed at its lower level. This was followed by the HBIS collapse. Gregoire *et al.* (2012) demonstrated how HBIS surface lowering produced a positive feedback and Lochte *et al.* (2019) propose that subsurface warming also forced a positive feedback mechanism. We suggest that LAO itself may have acted as an additional forcing acting on the south western margin and driving further retreat in much the same manner, as demonstrated by Sutherland *et al.* (2020) in a glacier-lake setting. The large magnitude meltwater pulse is observed in the SLE of the Ythan Estuary and Rhine-Meuse Delta (Fig. 4.7f) and the Labrador Sea freshwater event (Fig. 4.7b–c) and caused the shift in oceanic currents observed in the North Atlantic (Fig. 4.7d), thereby setting up the conditions for the 8.2 ka climate event. Our sea-level reconstruction, along with existing evidence, supports this hypothesis on the basis of the timing of the events and apparent magnitude being too large for lake drainage alone. It is difficult to single out a lake drainage from the melting HBIS in Phase 1 of our sea-level reconstruction, but we suggest the initial drainage is contained within the first period of rise and that the second, higher magnitude reflects further increased melting of the LIS. The final demise of the HBIS resulted in the terminal drainage of LAO, observed in sea-level records (Fig. 4.7f), and forced shifts in the AMOC, observed in the oceanic records (Kleiven *et al.*, 2008, Estrella-Martínez *et al.*, 2019) (Fig. 4.7d–e), that ultimately forced the 8.2 ka climate event.

Until this point we have assumed that the LIS contributed all of the meltwater, however it is necessary to examine the other major extant ice sheets at the time, namely the Greenland (GrIS) and Antarctic (AIS) ice sheets. Geophysical modelling (Lecavalier *et al.*, 2014, Briner *et al.*, 2020) and geological evidence (Seidenkrantz *et al.*, 2013) of long term meltwater discharge and small rapid meltwater inputs (Young *et al.*, 2020) suggest that as a result of retreating glaciers the GrIS did discharge freshwater in to the North Atlantic during the centuries prior to the 8.2 ka climate event. However, the relatively small magnitude of meltwater compared to the LIS and its geographical location relative to the North Atlantic sites mean that the GrIS was unlikely to have contributed a meaningful portion of the reconstructed relative sea-level rise in Scotland. On the other hand, it is quite possible that the AIS could have contributed more significantly, but there is still much debate over the amount of retreat or thinning of the AIS and its contribution to early Holocene sea level remains poorly constrained (Noble *et al.*, 2020). Geophysical models are ambiguous about the timing and magnitude of deglaciation and whether ice loss was gradual or more periodic,

but overall do suggest that at least part of the background barystatic sea-level rise was as a consequence of AIS deglaciation (e.g. Whitehouse *et al.*, 2012, Ivins *et al.*, 2013, Argus *et al.*, 2014, Briggs *et al.*, 2014, Lambeck *et al.*, 2014). Growing geological evidence does suggest that abrupt periods of glacial retreat and/or thinning may well have occurred (e.g. Bentley *et al.*, 2014, Small *et al.*, 2019, Kingslake *et al.*, 2018, Johnson *et al.*, 2019, 2020, Kawamata *et al.*, 2020), although spatial and temporal heterogeneity is manifest in the records and we found no direct evidence around 8,500–8,000 cal yr BP. It may be that the changes in ocean circulation and associated oceanic temperature regimes impacted the AIS themselves, such as by driving warm circumpolar deep water incursions and hence increased glacial retreat (Hillenbrand *et al.*, 2013, DeConto and Pollard, 2016). It is worth noting that if the AIS did contribute significant amounts to the SLEs then it would increase the relative contribution of the GrIS in comparison to the LIS to freshwater inputs into the North Atlantic, which may be important in forcing changes to the AMOC. Indeed, even if it didn't contribute significantly to the SLEs, GrIS meltwater may have been a factor in causing the oceanic changes that occurred and hence should not be overlooked when considering the driving mechanisms of the 8.2 ka climate event. Whilst it is not possible to rule out an AIS contribution to the SLEs or that the GrIS was a minor contributing factor, on account of the current evidence it still appears most likely that the vast majority of meltwater originated from the retreating LIS.

We upscaled the local magnitudes to global for the SLEs using the barystatic-GRD fingerprint model of LAO (Kendall *et al.*, 2008). It is clear that there are other components that need to be considered, such as the collapse of the HBIS and possible contributions from the AIS and GrIS. Although likely to be similar given its geographic location, it is uncertain whether the barystatic–GRD fingerprint of a collapse of the HBIS would differ from LAO and this therefore warrants investigation. Furthermore, in order to better identify the source location(s), well-resolved sea-level reconstructions from far-field locations in conjunction with updated barystatic–GRD fingerprinting and considering different meltwater inputs offers the opportunity to identify the source(s). This would further improve understanding of the drivers of the 8.2 ka climate event and consequently the possible impacts of present and future North Atlantic melting.

4.5   Conclusions

This study presents a continuous RSL record for the centuries leading up to the 8.2 ka climate event based on an exceptionally well resolved ^{14}C chronology and litho- and biostratigraphical analysis. We have built on probabilistic methods for modelling sea-level change by including the full uncertainty for the age component that also limits age reversals without over restricting the age shifts between SLIPs. The results from the Ythan Estuary suggest a sea-level event occurred with two distinct stages, one between 8,610 ± 5 and 8,495 ± 10 cal yr BP and the second between 8,495 ± 10 and 8,340 ± 5 cal yr BP with rates of around 10 mm/yr and 15 mm/yr respectively. Once corrected for the ongoing background rate the two stages of the sea-level event have barystatic magnitudes of 0.91–1.92 m and 1.64–2.81 m. A second, less definitive sea-level event is observed between 8,240 ± 15 and 8,190 ± 15 cal yr BP with rates of around 4 mm/yr and a barystatic magnitude of -0.25–0.48 m. Our reconstructions add to the evidence that there was more than one meltwater pulse leading up to the 8.2 ka climate event. Based on the magnitude of the sea-level events, we reject the hypothesis that Lake Agassiz-Ojibway (LAO) was the major contributor of the meltwater pulses.

Integrating our record with marine, terrestrial and other coastal reconstructions enabled us to derive a sequence of meltwater events leading up to and forcing the 8.2 ka climate event. We propose a three-stage drainage hypothesis, where each stage is set up by the preceding one:

1. Driven by a warming climate, the Hudson Bay Ice Saddle began to thin and lose elevation around 8,650 cal yr BP, creating a positive feedback through increasing surface temperature.

2. Because of hydraulic pressure, LAO drained sub-glacially and caused a marine transgression around 8,500 cal yr BP that, along with possible interactions at the renewed LAO-LIS margin, caused a further acceleration in ice melt.

3. Terminal LAO drainage occurred after the final demise of the Hudson Bay Ice Saddle around 8,300 cal yr BP.

Our work is a step forward in understanding the driver(s) of the 8.2 ka climate event. We have shown that LAO was not the main contributor of the meltwater pulses prior to 8,200

cal yr BP and as such, although convenient, should no longer be referred to as such. Further work is still required in order that the magnitude and source of the meltwater can be fully derived, enabling climate models to be tested with confidence and increase understanding of climate-AMOC interactions.

Acknowledgements

CRediT roles.

Graham Rush: Methodology, Formal analysis, investigation, Data curation, Writing - Original Draft, Visualization, Project administration, Funding acquisition. Ed Garrett: Supervision, Writing - Review & Editing, Visualization. Mark Bateman: Supervision, Writing - Review & Editing. Grant Bigg: Supervision, Writing - Review & Editing. Fiona Hibbert: Formal analysis, Writing - Review & Editing. David Smith: Writing - Review & Editing. Roland Gehrels: Conceptualization, Methodology, Supervision, Writing - Review & Editing, Project administration, Funding acquisition

References

Abel, G. J. (2015), 'fanplot: An R Package for Visualising Sequential Distributions', *The R Journal* **7**(2), 15–23.

Alley, R. B., Mayewski, P. A., Sowers, T., Stuiver, M., Taylor, K. C. and Clark, P. U. (1997), 'Holocene climatic instability: A prominent, widespread event 8200 yr ago', *Geology* **25**(6), 483–486.

Amorosi, A., Bruno, L., Campo, B., Morelli, A., Rossi, V., Scarponi, D., Hong, W., Bohacs, K. M. and Drexler, T. M. (2017), 'Global sea-level control on local parasequence architecture from the Holocene record of the Po Plain, Italy', *Marine and Petroleum Geology* **87**, 99–111.

Argus, D. F., Peltier, W. R., Drummond, R. and Moore, A. W. (2014), 'The Antarctica component of postglacial rebound model ICE-6G_C (VM5a) based on GPS positioning, exposure age dating of ice thicknesses, and relative sea level histories', *Geophysical Journal International* **198**(1), 537–563.

Ascough, P. L., Church, M. J. and Cook, G. T. (2017), 'Marine radiocarbon reservoir effects for the mesolithic and medieval periods in the western isles of Scotland', *Radiocarbon* **59**(1), 17–31.

Ascough, P. L., Cook, G. T., Dugmore, A. J. and Scott, E. M. (2007), 'The North Atlantic marine reservoir effect in the Early Holocene: Implications for defining and understanding MRE values', *Nuclear Instruments and Methods in Physics Research, Section B: Beam Interactions with Materials and Atoms* **259**(1), 438–447.

Atwater, B. F. (1987), 'Evidence for great holocene earthquakes along the outer coast of Washington state', *Science* **236**(4804), 942–944.

Barber, D. C., Dyke, A., Hillaire-Marcel, C., Jennings, A. E., Andrews, J. T., Kerwin, M. W., Bilodeau, G., McNeely, R., Southon, J., Morehead, M. D. and Gagnon, J. M. (1999), 'Forcing of the cold event of 8,200 years ago by catastrophic drainage of Laurentide lakes', *Nature* **400**(6742), 344–348.

Barlow, N. L., Shennan, I., Long, A. J., Gehrels, W. R., Saher, M. H., Woodroffe, S. A.

and Hillier, C. (2013), 'Salt marshes as late Holocene tide gauges', *Global and Planetary Change* **106**, 90–110.

Barnett, R. L., Garneau, M. and Bernatchez, P. (2016), 'Salt-marsh sea-level indicators and transfer function development for the Magdalen Islands in the Gulf of St. Lawrence, Canada', *Marine Micropaleontology* **122**, 13–26.

Bentley, M. J., Ocofaigh, C., Anderson, J. B., Conway, H., Davies, B., Graham, A. G. C., Hillenbrand, C. D., Hodgson, D. A., Jamieson, S. S. R., Larter, R. D., Mackintosh, A., Smith, J. A., Verleyen, E., Ackert, R. P., Bart, P. J., Berg, S., Brunstein, D., Canals, M., Colhoun, E. A., Crosta, X., Dickens, W. A., Domack, E., Dowdeswell, J. A., Dunbar, R., Ehrmann, W., Evans, J., Favier, V., Fink, D., Fogwill, C. J., Glasser, N. F., Gohl, K., Golledge, N. R., Goodwin, I., Gore, D. B., Greenwood, S. L., Hall, B. L., Hall, K., Hedding, D. W., Hein, A. S., Hocking, E. P., Jakobsson, M., Johnson, J. S., Jomelli, V., Jones, R. S., Klages, J. P., Kristoffersen, Y., Kuhn, G., Leventer, A., Licht, K., Lilly, K., Lindow, J., Livingstone, S. J., Massé, G., McGlone, M. S., McKay, R. M., Melles, M., Miura, H., Mulvaney, R., Nel, W., Nitsche, F. O., O'Brien, P. E., Post, A. L., Roberts, S. J., Saunders, K. M., Selkirk, P. M., Simms, A. R., Spiegel, C., Stolldorf, T. D., Sugden, D. E., van der Putten, N., van Ommen, T., Verfaillie, D., Vyverman, W., Wagner, B., White, D. A., Witus, A. E. and Zwartz, D. (2014), 'A community-based geological reconstruction of Antarctic Ice Sheet deglaciation since the Last Glacial Maximum', *Quaternary Science Reviews* **100**, 1–9.

Bondevik, S., Stormo, S. K. and Skjerdal, G. (2012), 'Green mosses date the Storegga tsunami to the chilliest decades of the 8.2 ka cold event', *Quaternary Science Reviews* **45**, 1–6.

Bradley, S. L., Milne, G. A., Shennan, I. and Edwards, R. (2011), 'An improved glacial isostatic adjustment model for the British Isles', *Journal of Quaternary Science* **26**(5), 541–552.

Brain, M. J., Long, A. J., Woodroffe, S. A., Petley, D. N., Milledge, D. G. and Parnell, A. C. (2012), 'Modelling the effects of sediment compaction on salt marsh reconstructions of recent sea-level rise', *Earth and Planetary Science Letters* **345-348**, 180–193.

Briggs, R. D., Pollard, D. and Tarasov, L. (2014), 'A data-constrained large ensemble analysis of Antarctic evolution since the Eemian', *Quaternary Science Reviews* **103**, 91–115.

Briner, J. P., Cuzzone, J. K., Badgeley, J. A., Young, N. E., Steig, E. J., Morlighem, M., Schlegel, N. J., Hakim, G. J., Schaefer, J. M., Johnson, J. V., Lesnek, A. J., Thomas, E. K., Allan, E., Bennike, O., Cluett, A. A., Csatho, B., de Vernal, A., Downs, J., Larour, E. and Nowicki, S. (2020), 'Rate of mass loss from the Greenland Ice Sheet will exceed Holocene values this century', *Nature* **586**(7827), 70–74.

Bronk Ramsey, C. (1995), 'Radiocarbon Calibration and Analysis of Stratigraphy: The OxCal Program', *Radiocarbon* **37**(2), 425–430.

Bronk Ramsey, C. (2008), 'Deposition models for chronological records', *Quaternary Science Reviews* **27**(1-2), 42–60.

Bronk Ramsey, C. (2009*a*), 'Bayesian Analysis of Radiocarbon Dates', *Radiocarbon* **51**(1), 337–360.

Bronk Ramsey, C. (2009*b*), 'Dealing with Outliers and Offsets in Radiocarbon Dating', *Radiocarbon* **51**(3), 1023–1045.

Bronk Ramsey, C. and Lee, S. (2013), 'Recent and Planned Developments of the Program OxCal', *Radiocarbon* **55**(2), 720–730.

Cahill, N., Kemp, A. C., Horton, B. P. and Parnell, A. C. (2016), 'A Bayesian hierarchical model for reconstructing relative sea level: From raw data to rates of change', *Climate of the Past* **12**(2), 525–542.

Crump, S. E., Young, N. E., Miller, G. H., Pendleton, S. L., Tulenko, J. P., Anderson, R. S. and Briner, J. P. (2020), 'Glacier expansion on Baffin Island during early Holocene cold reversals', *Quaternary Science Reviews* **241**, 106419.

Daley, T. J., Thomas, E. R., Holmes, J. A., Street-Perrott, F. A., Chapman, M. R., Tindall, J. C., Valdes, P. J., Loader, N. J., Marshall, J. D., Wolff, E. W., Hopley, P. J., Atkinson, T., Barber, K. E., Fisher, E. H., Robertson, I., Hughes, P. D. and Roberts, C. N. (2011), 'The 8200yr BP cold event in stable isotope records from the North Atlantic region', *Global and Planetary Change* **79**(3-4), 288–302.

Dawson, A., Bondevik, S. and Teller, J. T. (2011), 'Relative timing of the Storegga submarine slide, methane release, and climate change during the 8.2 ka cold event', *Holocene* **21**(7), 1167–1171.

De Lecea, A. M., Green, A. N., Strachan, K. L., Cooper, J. A. G. and Wiles, E. A. (2017), 'Stepped Holocene sea-level rise and its influence on sedimentation in a large marine embayment: Maputo Bay, Mozambique', *Estuarine Coastal and Shelf Science* **193**, 25–36.

de Rijk, S. (1995), 'Salinity control on the distribution of salt marsh foraminifera (Great Marshes, Massachusetts)', *The Journal of Foraminiferal Research* **25**(2), 156–166.

DeConto, R. M. and Pollard, D. (2016), 'Contribution of Antarctica to past and future sea-level rise', *Nature* **531**(7596), 591–597.

Dyke, A. S. (2004), An outline of North American deglaciation with emphasis on central and northern Canada, *in* J. Ehlers and P. L. Gibbard, eds, 'Quaternary Glaciations-extent and Chronology, Part II', Elsevier Science and Technology Books, Amsterdam.

Edwards, R. J. and Wright, A. (2015), Foraminifera, *in* B. P. Shennan, I., Long, A. J., Horton, ed., 'Handbook of Sea-level Research', 1 edn, John Wiley & Sons, Ltd, chapter 13, pp. 191–217.

Egbert, G. and Erofeeva, L. (2010), 'The OSU TOPEX/Poseidon Global Inverse Solution TPXO 8 Atlas v. 1 Africa'.

Ellison, C. R. W., Chapman, M. R. and Hall, I. R. (2006), 'Surface and deep ocean interactions during the cold climate event 8200 years ago', *Science* **312**(5782), 1929–1932.

Erdman, C. and Emerson, J. W. (2007), 'bcp: An R Package for Performing a Bayesian Analysis of Change Point Problems', *Journal of Statistical Software* **23**(3), 1–13.

Erdman, C. and Emerson, J. W. (2008), 'A Fast Bayesian Change Point Analysis for the Segmentation of Microarray Data', *Bioinformatics* **24**(19), 2143–2148.

Estrella-Martínez, J., Ascough, P. L., Schöne, B. R., Scourse, J. D. and Butler, P. G. (2019), '8.2 ka event North Sea hydrography determined by bivalve shell stable isotope geochemistry', *Scientific Reports* **9**(1), 1–9.

Fisher, T. G. (2020), 'Megaflooding associated with glacial Lake Agassiz', *Earth-Science Reviews* **201**, 102974.

Gauthier, M. S., Kelley, S. E. and Hodder, T. J. (2020), 'Lake Agassiz drainage bracketed Holocene Hudson Bay Ice Saddle collapse', *Earth and Planetary Science Letters* **544**, 116372.

Gehrels, W. R. (2000), 'Using foraminiferal transfer functions to produce high-resolution sea-level records from salt-marsh deposits, Maine, USA', *Holocene* **10**(3), 367–376.

Gehrels, W. R. (2002), Intertidal foraminifera as palaeoenvironmental indicators, *in* 'Quaternary environmental micropalaeontology', Arnold Publishers, pp. 91–114.

Gehrels, W. R., Kirby, J. R., Prokoph, A., Newnham, R. M., Achterberg, E. P., Evans, H., Black, S. and Scott, D. B. (2005), 'Onset of recent rapid sea-level rise in the western Atlantic Ocean', *Quaternary Science Reviews* **24**(18-19), 2083–2100.

Godbout, P. M., Roy, M. and Veillette, J. J. (2019), 'High-resolution varve sequences record one major late-glacial ice readvance and two drainage events in the eastern Lake Agassiz-Ojibway basin', *Quaternary Science Reviews* **223**, 105942.

Godbout, P. M., Roy, M. and Veillette, J. J. (2020), 'A detailed lake-level reconstruction shows evidence for two abrupt lake drawdowns in the late-stage history of the eastern Lake Agassiz-Ojibway basin', *Quaternary Science Reviews* **238**, 106327.

Grant, K. M., Rohling, E. J., Bar-Matthews, M., Ayalon, A., Medina-Elizalde, M., Ramsey, C. B., Satow, C. and Roberts, A. P. (2012), 'Rapid coupling between ice volume and polar temperature over the past 50,000 years', *Nature* **491**(7426), 744–747.

Grant, K. M., Rohling, E. J., Bronk Ramsey, C., Cheng, H., Edwards, R. L., Florindo, F., Heslop, D., Marra, F., Roberts, A. P., Tamisiea, M. E. and Williams, F. (2014), 'Sea-level variability over five glacial cycles', *Nature Communications* **5**(1), 1–9.

Gregoire, L. J., Payne, A. J. and Valdes, P. J. (2012), 'Deglacial rapid sea level rises caused by ice-sheet saddle collapses', *Nature* **487**(7406), 219–222.

Gregory, J. M., Griffies, S. M., Hughes, C. W., Lowe, J. A., Church, J. A., Fukimori, I., Gomez, N., Kopp, R. E., Landerer, F., Cozannet, G. L., Ponte, R. M., Stammer,

D., Tamisiea, M. E. and van de Wal, R. S. (2019), 'Concepts and Terminology for Sea Level: Mean, Variability and Change, Both Local and Global', *Surveys in Geophysics* **40**(6), 1251–1289.

Hamilton, S. and Shennan, I. (2005), 'Late Holocene relative sea-level changes and the earthquake deformation cycle around upper Cook Inlet, Alaska', *Quaternary Science Reviews* **24**(12-13), 1479–1498.

Hayward, B. W., Le Coze, F., Varchard, D., Gross, O. and Gross, O. (2020), 'World modern foraminifera database'.

Heaton, T. J., Köhler, P., Butzin, M., Bard, E., Reimer, R. W., Austin, W. E. N., Ramsey, C. B., Grootes, P. M., Hughen, K. A., Kromer, B., Reimer, P. J., Adkins, J., Burke, A., Cook, M. S., Olsen, J. and Skinner, L. C. (2020), 'Marine20 – The Marine Radiocarbon Age Calibration Curve (0 – 55,000 Cal BP)', *Radiocarbon* **00**(62), 779–820.

Hijma, M., Engelhart, S., Tornqvist, T., Horton, B., Hu, P. and Hill, D. (2015), A protocol for a geological sea-level database, *in* I. Shennan, A. Long and B. Horton, eds, 'Handbook of Sea-Level Research', John Wiley & sons, Chichester, chapter 34, pp. 295–311.

Hijma, M. P. and Cohen, K. M. (2010), 'Timing and magnitude of the sea-level jump preluding the 8200 yr event', *Geology* **38**(3), 275–278.

Hijma, M. P. and Cohen, K. M. (2019), 'Holocene sea-level database for the Rhine-Meuse Delta, The Netherlands: Implications for the pre-8.2 ka sea-level jump', *Quaternary Science Reviews* **214**, 68–86.

Hill, J. (2020), 'Palaeotidal atlas of the UK for the last 10,000 years', *Open Quaternary* .

Hillenbrand, C. D., Kuhn, G., Smith, J. A., Gohl, K., Graham, A. G. C., Larter, R. D., Klages, J. P., Downey, R., Moreton, S. G., Forwick, M. and Vaughan, D. G. (2013), 'Grounding-line retreat of the West Antarctic Ice Sheet from inner Pine Island Bay', *Geology* **41**(1), 35–38.

Hoffman, J. S., Carlson, A. E., Winsor, K., Klinkhammer, G. P., LeGrande, A. N., Andrews, J. T. and Strasser, J. C. (2012), 'Linking the 8.2 ka event and its freshwater forcing in the Labrador Sea', *Geophysical Research Letters* **39**(17), 2005–2009.

Horton, B. P. and Edwards, R. J. (2006), 'Quantifying holocene sea-level change using inter-tidal foraminifera: lessons from the British Isles', *Cushman Foundation Special Publication* **40**, 1–97.

Horton, B. P., Edwards, R. J. and Lloyd, J. M. (1999*a*), 'Reconstruction of former sea levels using a foraminiferal-based transfer function', *Journal of Foraminiferal Research* **29**(2), 117–129.

Horton, B. P., Edwards, R. J. and Lloyd, J. M. (1999*b*), 'UK intertidal foraminiferal distributions: implications for sea-level studies', *Marine Micropaleontology* **36**(4), 205–223.

Ivins, E. R., James, T. S., Wahr, J., O. Schrama, E. J., Landerer, F. W. and Simon, K. M. (2013), 'Antarctic contribution to sea level rise observed by GRACE with improved GIA correction', *Journal of Geophysical Research: Solid Earth* **118**(6), 3126–3141.

Jamieson, T. F. (1865), 'On the history of the last geological changes in Scotland', *Quarterly Journal of the Geological Society of London* **21**(1-2), 161–204.

Jennings, A., Andrews, J., Pearce, C., Wilson, L. and Olfasdotttir, S. (2015), 'Detrital carbonate peaks on the Labrador shelf, a 13-7 ka template for freshwater forcing from the Hudson Strait outlet of the Laurentide Ice Sheet into the subpolar gyre', *Quaternary Science Reviews* **107**, 62–80.

Johnson, J. S., Nichols, K. A., Goehring, B. M., Balco, G. and Schaefer, J. M. (2019), 'Abrupt mid-Holocene ice loss in the western Weddell Sea Embayment of Antarctica', *Earth and Planetary Science Letters* **518**, 127–135.

Johnson, J. S., Roberts, S. J., Rood, D. H., Pollard, D., Schaefer, J. M., Whitehouse, P. L., Ireland, L. C., Lamp, J. L., Goehring, B. M., Rand, C. and Smith, J. A. (2020), 'Deglaciation of Pope Glacier implies widespread early Holocene ice sheet thinning in the Amundsen Sea sector of Antarctica', *Earth and Planetary Science Letters* **548**, 116501.

Juggins, S. (2017), 'rioja: Analysis of Quaternary Science Data'.

Julio, J. M. (2006), The Fan Chart: The Technical Details of the New Implementationn, Technical report, Banco de la Republica and Department of Statistics, Universidad Nacional de Colombia. Bogota D. C., Colombia.

Kaufmann, L. and Rousseeuw, P. J. (1990), *Finding groups in data: an introduction to cluster analysis*, John Wiley, New York.

Kawamata, M., Suganuma, Y., Doi, K., Misawa, K., Hirabayashi, M., Hattori, A. and Sawagaki, T. (2020), 'Abrupt Holocene ice-sheet thinning along the southern Soya Coast, Lützow-Holm Bay, East Antarctica, revealed by glacial geomorphology and surface exposure dating', *Quaternary Science Reviews* **247**, 106540.

Kemp, A. C., Horton, B. P. and Culver, S. J. (2009), 'Distribution of modern salt-marsh foraminifera in the Albemarle-Pamlico estuarine system of North Carolina, USA: Implications for sea-level research', *Marine Micropaleontology* **72**(3-4), 222–238.

Kemp, A. C., Telford, R. J., Horton, B. P., Anisfeld, S. C. and Sommerfield, C. K. (2013), 'Reconstructing Holocene sea level using salt-marsh foraminifera and transfer functions: Lessons from New Jersey, USA', *Journal of Quaternary Science* **28**(6), 617–629.

Kendall, R. A., Mitrovica, J. X., Milne, G. A., Tornqvist, T. E. and Li, Y. X. (2008), 'The sea-level fingerprint of the 8.2 ka climate event', *Geology* **36**(5), 423–426.

Kingslake, J., Scherer, R. P., Albrecht, T., Coenen, J., Powell, R. D., Reese, R., Stansell, N. D., Tulaczyk, S., Wearing, M. G. and Whitehouse, P. L. (2018), 'Extensive retreat and re-advance of the West Antarctic Ice Sheet during the Holocene', *Nature* **558**(7710), 430–434.

Kleiven, H. F., Kissel, C., Laj, C., Ninnemann, U. S., Richter, T. O. and Cortijo, E. (2008), 'Reduced North Atlantic Deep Water coeval with the glacial Lake Agassiz freshwater outburst', *Science* **319**(5859), 60–64.

Lambeck, K., Rouby, H., Purcell, A., Sun, Y. Y. and Sambridge, M. (2014), 'Sea level and global ice volumes from the Last Glacial Maximum to the Holocene', *Proceedings of the National Academy of Sciences of the United States of America* **111**(43), 15296–15303.

Lawrence, T., Long, A. J., Gehrels, W. R., Jackson, L. P. and Smith, D. E. (2016), 'Relative sea-level data from southwest Scotland constrain meltwater-driven sea-level jumps prior to the 8.2 kyr BP event', *Quaternary Science Reviews* **151**, 292–308.

Lecavalier, B. S., Milne, G. A., Simpson, M. J., Wake, L., Huybrechts, P., Tarasov, L., Kjeldsen, K. K., Funder, S., Long, A. J., Woodroffe, S., Dyke, A. S. and Larsen, N. K.

(2014), 'A model of Greenland ice sheet deglaciation constrained by observations of relative sea level and ice extent', *Quaternary Science Reviews* **102**, 54–84.

Leorri, E., Fatela, F., Cearreta, A., Moreno, J., Antunes, C. and Drago, T. (2011), 'Assessing the performance of a foraminifera-based transfer function to estimate sea-level changes in northern Portugal', *Quaternary Research* **75**(1), 278–287.

Leverington, D. W., Mann, J. D. and Teller, J. T. (2002), 'Changes in the bathymetry and volume of glacial Lake Agassiz between 9200 and 7700 C-14 yr BP', *Quaternary Research* **57**(2), 244–252.

Li, Y. X., Törnqvist, T. E., Nevitt, J. M. and Kohl, B. (2012), 'Synchronizing a sea-level jump, final Lake Agassiz drainage, and abrupt cooling 8200 years ago', *Earth and Planetary Science Letters* **315**, 41–50.

Lloyd, M. J., Shennan, I., Kirby, J. R. and Rutherford, M. M. (1999), 'Holocene relative sea-level changes in the inner Solway Firth', *Quaternary International* **60**(1), 83–105.

Lochte, A. A., Repschlaeger, J., Kienast, M., Garbe-Schoenberg, D., Andersen, N., Hamann, C. and Schneider, R. (2019), 'Labrador Sea freshening at 8.5 ka BP caused by Hudson Bay Ice Saddle collapse', *Nature Communications* **10**(1), 1–9.

Maechler, M., Rousseeuw, P., Struyf, A., Hubert, M. and Hornik, K. (2012), 'Cluster: cluster analysis basics and extensions', *R package version* **1**(2), 56.

Matero, I. S. O., Gregoire, L. J. and Ivanovic, R. F. (2020), 'Simulating the Early Holocene demise of the Laurentide Ice Sheet with BISICLES', *Geoscientific Model Development* **13**(9), 4555–4577.

Matero, I. S. O., Gregoire, L. J., Ivanovic, R. F., Tindall, J. C. and Haywood, A. M. (2017), 'The 8.2 ka cooling event caused by Laurentide ice saddle collapse', *Earth and Planetary Science Letters* **473**, 205–214.

Mills, H., Kirby, J., Holgate, S. and Plater, A. (2013), 'The distribution of contemporary saltmarsh foraminifera in A macrotidal estuary: An assessment of their viability for sea-level studies', *Journal of Ecosystem & Ecography* **3**, 1–16.

Mitrovica, J. X., Tamisiea, M. E., Davis, J. L. and Milne, G. A. (2001), 'Recent mass balance of polar ice sheets inferred from patterns of global sea-level change', *Nature* **409**(6823), 1026–1029.

Morrill, C., Anderson, D. M., Bauer, B. A., Buckner, R., Gille, E. P., Gross, W. S., Hartman, M. and Shah, A. (2013), 'Proxy benchmarks for intercomparison of 8.2 ka simulations', *Climate of the Past* **9**(1), 423–432.

Müller-Navarra, K., Milker, Y. and Schmiedl, G. (2017), 'Applicability of transfer functions for relative sea-level reconstructions in the southern North Sea coastal region based on salt-marsh foraminifera', *Marine Micropaleontology* **135**, 15–31.

Nguyen, V. L., Ta, T. K. O. and Saito, Y. (2010), 'Early Holocene initiation of the Mekong River delta, Vietnam, and the response to Holocene sea-level changes detected from DT1 core analyses', *Sedimentary Geology* **230**(3-4), 146–155.

Noble, T. L., Rohling, E. J., Aitken, A. R. A., Bostock, H. C., Chase, Z., Gomez, N., Jong, L. M., King, M. A., Mackintosh, A. N., McCormack, F. S., McKay, R. M., Menviel, L., Phipps, S. J., Weber, M. E., Fogwill, C. J., Gayen, B., Golledge, N. R., Gwyther, D. E., Hogg, A. M. C., Martos, Y. M., Pena-Molino, B., Roberts, J., Flierdt, T. and Williams, T. (2020), 'The sensitivity of the Antarctic Ice Sheet to a changing climate: Past, present and future', *Reviews of Geophysics* .

Oksanen, J., Blanchet, F. G., Kindt, R., Legendre, P., Minchin, P. R., O'hara, R. B., Simpson, G. L., Solymos, P., Stevens, M. H. H. and Wagner, H. (2013), 'Package 'vegan'', *Community ecology package, version* **2**(9), 1–295.

Payne, R. J., Telford, R. J., Blackford, J. J., Blundell, A., Booth, R. K., Charman, D. J., Lamentowicz, Ł., Lamentowicz, M., Mitchell, E. A. D., Potts, G., Swindles, G. T., Warner, B. G. and Woodland, W. (2012), 'Testing peatland testate amoeba transfer functions: Appropriate methods for clustered training-sets', *Holocene* **22**(7), 819–825.

Piggott, M. D., Gorman, G. J., Pain, C. C., Allison, P. A., Candy, A. S., Martin, B. T. and Wells, M. R. (2008), 'A new computational framework for multi-scale ocean modelling based on adapting unstructured meshes', *International Journal for Numerical Methods in Fluids* **56**(8), 1003–1015.

Reimer, P. J., Austin, W. E., Bard, E., Bayliss, A., Blackwell, P. G., Ramsey, C. B., Butzin, M., Cheng, H., Edwards, R. L., Friedrich, M., , Grootes, P. M., Guilderson, T. P., Hajdas, I., Heaton, T. J., Hogg, A. G., Hughen, K. A., Kromer, B., Manning, S. W., Muscheler, R., Palmer, J. G., Pearson, C., van der Plicht, J., Reimer, R. W., Richards, D. A., Scott, E. M., Southon, J. R., Turney, C. S. M., Wacker, L., Adolphi, F., Büntgen, U., Capano, M., Fahrni, S. M., Fogtmann-Schulz, A., Friedrich, R., Köhler, P., Kudsk, S., Miyake, F., Olsen, J., Reinig, F., Sakamoto, M., Sookdeo, A. and Talamo, S. (2020), 'The intcal20 northern hemisphere radiocarbon age calibration curve (0–55 cal kbp)', *Radiocarbon* **62**(4), 725–757.

Reimer, P. J., Bard, E., Bayliss, A., Beck, J. W., Blackwell, P. G., Ramsey, C. B., Buck, C. E., Cheng, H., Edwards, R. L., Friedrich, M., Grootes, P. M., Guilderson, T. P., Haflidason, H., Hajdas, I., Hatté, C., Heaton, T. J., Hoffmann, D. L., Hogg, A. G., Hughen, K. A., Kaiser, K. F., Kromer, B., Manning, S. W., Niu, M., Reimer, R. W., Richards, D. A., Scott, E. M., Southon, J. R., Staff, R. A., Turney, C. S. M. and van der Plicht, J. (2013), 'IntCal13 and Marine13 Radiocarbon Age Calibration Curves 0–50,000 Years cal BP', *Radiocarbon* **55**(4), 1869–1887.

Reimer, R. W. and Reimer, P. J. (2017), 'An Online Application for Δr Calculation', *Radiocarbon* **59**(5), 1623–1627.

Rohling, E. J., Foster, G. L., Grant, K. M., Marino, G., Roberts, A. P., Tamisiea, M. E. and Williams, F. (2014), 'Sea-level and deep-sea-temperature variability over the past 5.3 million years', *Nature* **508**(7497), 477–482.

Rousseeuw, P. J. (1987), 'Silhouettes: a graphical aid to the interpretation and validation of cluster analysis', *Journal of Computational and Applied Mathematics* **20**, 53–65.

Roy, M., Dell'Oste, F., Veillette, J. J., de Vernal, A., Hélie, J. F., Parent, M., Dell'Oste, F., Veillette, J. J., de Vernal, A., Helie, J. F. and Parent, M. (2011), 'Insights on the events surrounding the final drainage of Lake Ojibway based on James Bay stratigraphic sequences', *Quaternary Science Reviews* **30**(5-6), 682–692.

Rush, G., MacDarby, P., Edwards, R., Milker, Y., Garrett, E. and Gehrels, R. (in review), 'Development of an intertidal foraminifera training set for the North Sea and an assessment of its application for Holocene sea-level reconstructions', *Marine Micropaleontology* .

Russell, N., Cook, G. T., Ascough, P. L., Scott, E. M. and Dugmore, A. J. (2011), 'Examining the inherent variability in ΔR: New methods of presenting ΔR values and implications for MRE studies', *Radiocarbon* **53**(2), 277–288.

Schmidt, G. A. and LeGrande, A. N. (2005), 'The Goldilocks abrupt climate change event', *Quaternary Science Reviews* **24**(10-11), 1109–1110.

Scott, D. B. and Hermelin, J. O. R. (1993), 'A device for precision splitting of micropaleontological samples in liquid suspension', *Journal of Paleontology* **67**(1), 151–154.

Scott, D. B. and Medioli, F. S. (1980), 'Quantitative studies of marsh foraminiferal distributions in Nova Scotia: Their implications for the study of sea-level changes', *Cushman Foundation for Foraminiferal Research, Special Publication* **17**, 58.

Scott, D. S. and Medioli, F. S. (1978), 'Vertical zonations of marsh foraminifera as accurate indicators of former sea-levels', *Nature* **272**(5653), 528–531.

Seidenkrantz, M. S., Ebbesen, H., Aagaard-Sørensen, S., Moros, M., Lloyd, J. M., Olsen, J., Knudsen, M. F. and Kuijpers, A. (2013), 'Early Holocene large-scale meltwater discharge from Greenland documented by foraminifera and sediment parameters', *Palaeogeography, Palaeoclimatology, Palaeoecology* **391**, 71–81.

Selby, K. A. and Smith, D. E. (2016), 'Holocene Relative Sea-Level Change on the Isle of Skye, Inner Hebrides, Scotland', *Scottish Geographical Journal* **132**(1), 42–65.

Shennan, I., Bradley, S. L. and Edwards, R. (2018), 'Relative sea-level changes and crustal movements in Britain and Ireland since the Last Glacial Maximum', *Quaternary Science Reviews* **188**, 143–159.

Simon, K. M. and Riva, R. E. M. (2020), 'Uncertainty Estimation in Regional Models of Long-Term GIA Uplift and Sea-level Change: An Overview', *Journal of Geophysical Research: Solid Earth* **125**(8).

Small, D., Bentley, M. J., Jones, R. S., Pittard, M. L. and Whitehouse, P. L. (2019), 'Antarctic ice sheet palaeo-thinning rates from vertical transects of cosmogenic exposure ages', *Quaternary Science Reviews* **206**, 65–80.

Smith, D. E., Cullingford, R. A. and Brooks, C. L. (1983), 'Flandrian relative sea-level changes in the Ythan Valley, northeast Scotland', *Earth Surface Processes and Landforms* **8**(5), 423–438.

Smith, D. E., Firth, C. R., Brooks, C. L., Robinson, M. and Collins, P. E. F. (1999), 'Relative sea-level rise during the Main Postglacial Transgression in NE Scotland, UK', *Transactions of the Royal Society of Edinburgh-Earth Sciences* **90**, 1–27.

Smith, D. E., Harrison, S. and Jordan, J. T. (2013), 'Sea level rise and submarine mass failures on open continental margins', *Quaternary Science Reviews* **82**, 93–103.

Smith, D. E., Tipping, R. M., Jordan, J. T. and Blackett, M. (2020), 'Holocene coastal change at Luce Bay, South West Scotland', *Journal of Quaternary Science* **35**(6), 743–759.

Spooner, P. T., Thornalley, D. J. R., Oppo, D. W., Fox, A. D., Radionovskaya, S., Rose, N. L., Mallett, R., Cooper, E. and Roberts, J. M. (2020), 'Exceptional 20th Century Ocean Circulation in the Northeast Atlantic', *Geophysical Research Letters* **47**(10).

Srokosz, M. A. and Bryden, H. L. (2015), 'Observing the Atlantic Meridional Overturning Circulation yields a decade of inevitable surprises', *Science* **348**(6241), 1255575.

Stuiver, M. and Polach, H. A. (1977), ' Discussion Reporting of 14 C Data ', *Radiocarbon* **19**(3), 355–363.

Stuiver, M., Reimer, P. and Reimer, R. (2020), 'CALIB 8.2 [WWW program]'.

Sutherland, J. L., Carrivick, J. L., Gandy, N., Shulmeister, J., Quincey, D. J. and Cornford, S. L. (2020), 'Proglacial lakes control glacier geometry and behavior during recession', *Geophysical Research Letters* **47**(19).

Tamura, T., Saito, Y., Sieng, S., Ben, B., Kong, M., Sim, I., Choup, S. and Akiba, F. (2009), 'Initiation of the Mekong River delta at 8 ka: evidence from the sedimentary succession in the Cambodian lowland', *Quaternary Science Reviews* **28**(3–4), 327–344.

Telford, R. J. and Birks, H. J. (2005), 'The secret assumption of transfer functions: Problems with spatial autocorrelation in evaluating model performance', *Quaternary Science Reviews* **24**(20-21), 2173–2179.

Telford, R. J. and Birks, H. J. (2011), 'A novel method for assessing the statistical significance of quantitative reconstructions inferred from biotic assemblages', *Quaternary Science Reviews* **30**(9-10), 1272–1278.

Teller, J. T., Leverington, D. W. and Mann, J. D. (2002), 'Freshwater outbursts to the oceans from glacial Lake Agassiz and their role in climate change during the last deglaciation', *Quaternary Science Reviews* **21**(8-9), 879–887.

Thomas, E. R., Wolff, E. W., Mulvaney, R., Steffensen, J. P., Johnsen, S. J., Arrowsmith, C., White, J. W. C., Vaughn, B. and Popp, T. (2007), 'The 8.2 ka event from Greenland ice cores', *Quaternary Science Reviews* **26**(1-2), 70–81.

Thornalley, D. J., Elderfield, H. and McCave, I. N. (2009), 'Holocene oscillations in temperature and salinity of the surface subpolar North Atlantic', *Nature* **457**(7230), 711–714.

Thornalley, D. J., Oppo, D. W., Ortega, P., Robson, J. I., Brierley, C. M., Davis, R., Hall, I. R., Moffa-Sanchez, P., Rose, N. L., Spooner, P. T., Yashayaev, I. and Keigwin, L. D. (2018), 'Anomalously weak Labrador Sea convection and Atlantic overturning during the past 150 years', *Nature* **556**(7700), 227–230.

Tjallingi, R., Stattegger, K., Stocchi, P., Saito, Y. and Wetzel, A. (2014), 'Rapid flooding of the southern Vietnam shelf during the early to mid-Holocene', *Journal of Quaternary Science* **29**(6), 581–588.

Tooley, M. J. (1974), 'Sea-level changes during the last 9000 years in northwest England', *Geographical Journal* pp. 18–42.

Törnqvist, T. E., Bick, S. J., Gonzalez, J. L., van der Borg, K. and de Jong, A. F. M. (2004), 'Tracking the sea-level signature of the 8.2 ka cooling event: New constraints from the Mississippi Delta', *Geophysical Research Letters* **31**(23).

Törnqvist, T. E., Hijma, M. P., Trnqvist, T. E. and Hijma, M. P. (2012), 'Links between early Holocene ice-sheet decay, sea-level rise and abrupt climate change', *Nature Geoscience* **5**(9), 601–606.

Törnqvist, T. E., Jankowski, K. L., Li, Y. X. and González, J. L. (2020), 'Tipping points of Mississippi Delta marshes due to accelerated sea-level rise', *Science advances* **6**(21), eaaz5512.

Troels-Smith, J. (1955), 'Karakterisering af lose jordarter. Characterization of unconsolidated sediments', *Geologiske Undersagelse, Raekke* .

Uehara, K., Scourse, J. D., Horsburgh, K. J., Lambeck, K. and Purcell, A. P. (2006), 'Tidal evolution of the northwest European shelf seas from the Last Glacial Maximum to the present', *Journal of Geophysical Research* **111**(C9).

Ullman, D. J., Carlson, A. E., Hostetler, S. W., Clark, P. U., Cuzzone, J., Milne, G. A., Winsor, K. and Caffee, M. (2016), 'Final Laurentide ice-sheet deglaciation and Holocene climate-sea level change', *Quaternary Science Reviews* **152**, 49–59.

van der Molen, J. and de Swart, H. E. (2001), 'Holocene tidal conditions and tide-induced sand transport in the southern North Sea', *Journal of Geophysical Research: Oceans* **106**(C5), 9339–9362.

Wang, X. and Emerson, J. W. (2015), 'Bayesian Change Point Analysis of Linear Models on General Graphs', *Working Paper* .

Wang, Z. H., Zhan, Q., Long, H. Y., Saito, Y., Gao, X. Q., Wu, X. X., Li, L. and Zhao, Y. A. (2013), 'Early to mid-Holocene rapid sea-level rise and coastal response on the southern Yangtze delta plain, China', *Journal of Quaternary Science* **28**(7), 659–672.

Ward, S. L., Neill, S. P., Scourse, J. D., Bradley, S. L. and Uehara, K. (2016), 'Sensitivity of palaeotidal models of the northwest European shelf seas to glacial isostatic adjustment since the Last Glacial Maximum', *Quaternary Science Reviews* **151**, 198–211.

Watcham, E. P., Bentley, M. J., Hodgson, D. A., Roberts, S. J., Fretwell, P. T., Lloyd, J. M., Larter, R. D., Whitehouse, P. L., Leng, M. J., Monien, P. and Moreton, S. G. (2011), 'A new Holocene relative sea level curve for the South Shetland Islands, Antarctica', *Quaternary Science Reviews* **30**(21-22), 3152–3170.

Weaver, A. J., Sedláček, J., Eby, M., Alexander, K., Crespin, E., Fichefet, T., Philippon-Berthier, G., Joos, F., Kawamiy, M., Matsumoto, K., Steinacher, M., Tachiiri, K., Tokos, K., Yoshimori, M. and Zickfeld, K. (2012), 'Stability of the Atlantic meridional overturning circulation: A model intercomparison', *Geophysical Research Letters* **39**(20).

Whitehouse, P. L., Bentley, M. J. and Le Brocq, A. M. (2012), 'A deglacial model for

Antarctica: Geological constraints and glaciological modelling as a basis for a new model of Antarctic glacial isostatic adjustment', *Quaternary Science Reviews* **32**, 1–24.

Wright, A. J., Edwards, R. J. and van de Plassche, O. (2011), 'Reassessing transfer-function performance in sea-level reconstruction based on benthic salt-marsh foraminifera from the Atlantic coast of NE North America', *Marine Micropaleontology* **81**(1-2), 43–62.

Xiong, H., Zong, Y., Li, T., Long, T., Huang, G. and Fu, S. (2020), 'Coastal GIA processes revealed by the early to middle Holocene sea- level history of east China', *Quaternary Science Reviews* **233**, 106249.

Young, N. E., Briner, J. P., Miller, G. H., Lesnek, A. J., Crump, S. E., Thomas, E. K., Pendleton, S. L., Cuzzone, J., Lamp, J., Zimmerman, S., Caffee, M. and Schaefer, J. M. (2020), 'Deglaciation of the Greenland and Laurentide ice sheets interrupted by glacier advance during abrupt coolings', *Quaternary Science Reviews* **229**, 106091.

Zong, Y. Q., Huang, K. Y., Yu, F. L., Zheng, Z., Switzer, A., Huang, G. Q., Wang, N. and Tang, M. (2012), 'The role of sea-level rise, monsoonal discharge and the palaeo-landscape in the early Holocene evolution of the Pearl River delta, southern China', *Quaternary Science Reviews* **54**, 77–88.

Zong, Y. Q. and Tooley, M. J. (1996), 'Holocene sea-level changes and crustal movements in Morecambe Bay, northwest England', *Journal of Quaternary Science* **11**(1), 43–58.

Summary

In this chapter I have reconstructed RSL for the Ythan Estuary and demonstrated the occurrence of SLEs leading up to the 8.2 ka climate event. The methods I applied and rigorous statistical analysis that incorporates the full uncertainties I believe the results are a significant step forward from previous calculations for the magnitudes of the meltwater pulses. I have used the results to test hypothesis 1 (Chapter 1) but am unable to reject it although suggest that at least two meltwater pulses occurred prior to the 8.2 ka climate event. By comparing the results with other RSL reconstructions and environmental evidence I have demonstrated that LAO was very unlikely to have been the main source of the first two meltwater pulses and that the HBIS contributed a large amount of meltwater, therefore disproving hypothesis 2. Because the site is in the same region as other well-resolved RSL reconstructions I am unable to test hypothesis 3. RSL reconstructions from far-field locations are required to do so and for that reason the study of Swan Inlet in the Falkland Islands was conceived (Chapter 5).

Chapter 5

Relative sea-level reconstruction for the Falkland Islands (Islas Malvinas)

Graham Rush[1], Tom Newton[2], Ed Garrett[1], Mark Bateman[3], Sarah Bradley[3], Matthew Brain[4], Mike Bentley[4], Anthony Long[4], Emma Brooks[5], Tom Hill[6], Tim Daley[2], Roland Gehrels[1]

[1] *Department of Environment and Geography, University of York,York, UK*

[2] *University of Plymouth, School of Geography, UK*

[3] *Geography Department, University of Sheffield, Winter Street, Sheffield, UK*

[4] *Department of Geography, Durham University, South Road, Durham, UK*

[5] *Falkland Islands College, Sapper Hill, Stanley, Falkland Islands*

[6] *Department of Earth Sciences, Natural History Museum, Cromwell Road, London, UK*

Abstract

Holocene relative sea-level (RSL) data from the Falkland Islands provide important constraints on meltwater contributions from polar ice sheets, both on millennial and centennial timescales, and the processes of glacial-isostatic adjustment (GIA). In this paper, we present 20 sea-level index points (SLIPs) for the Falkland Islands based on analyses of fossil salt-marsh sediments and associated microfossils (diatoms, foraminifera and testate amoebae). The SLIPs are combined with SLIPs for the last century to produce the first Holocene sea-level reconstruction for the Falkland Islands (8500 cal yr BP to present). The reconstruction shows an early Holocene sea-level rise that is punctuated by a series of drowning events that are tentatively linked to meltwater pulses. We find evidence for a RSL highstand around 4500 cal yr BP that was close to present day RSL. The highstand is lower than sites on the South American Atlantic coastline. We suggest that this is a result of continental levering; as such this is the first documention of its effect from offshore of the South American Atlantic coast. Our results have implications for models of GIA as they provide constraints to study the history of global ice melt and understand the processes of isostatic adjustment on continental shelves.

5.1 Introduction

During the Holocene, long-term relative sea-level (RSL) changes have varied because of tectonic, isostatic and Earth gravity and rotation processes in combination with climate-driven ocean volume changes (Khan *et al.*, 2015). In the early Holocene, climate-driven ice-sheet retreat between 11,600–7,000 cal yr BP caused an increase in ocean volume, resulting in a global mean sea-level rise in the order of 60 m (Fairbanks, 1989, Bard *et al.*, 1996). Changes in Earth gravity, Earth rotation and viscoelastic solid-Earth deformation (GRD) produced a distinctive and highly varied spatial pattern of RSL change (Mitrovica *et al.*, 2001, Gregory *et al.*, 2019) with a rise in the far field and fall in the near field. Following the termination of ice-sheet decay, forebulge collapse resulted in ocean syphoning (water moving poleward to fill the space) and as such a sea-level fall in mid to high latitudes (Mitrovica and Milne, 2002). A resultant mid-Holocene highstand is recorded in many locations in the Southern Hemisphere (Mitrovica and Milne, 2002). Quantifying RSL change and the altitude of the highstand at Southern Hemisphere sites can therefore be used to constrain the history of the melting of the large ice sheets using glacial-isostatic adjustment (GIA) models (Yokoyama *et al.*, 2012).

The Falkland Islands, an archipelago ca. 500 km east of Argentina on the widest part of the Patagonian continental shelf, are unaffected by tectonics, local ice-loading effects or large tidal range changes, unlike mainland South America (Rostami *et al.*, 2000, Bentley and McCulloch, 2005, Milne *et al.*, 2005). Furthermore, GIA-modelled sea-level reconstructions for the Falkland Islands are relatively insensitive to Earth model parameters (Milne and Mitrovica, 2008). Middle and late Holocene RSL in the Falkland Islands are therefore predicted to be predominantly controlled by barystatic sea-level change (Milne and Mitrovica, 2008) and hence provide the opportunity to study the net ice-ocean mass flux from the major ice sheets.

To date, there are is a lack of high-quality Holocene sea-level data for the Falkland Islands. Several raised beach deposits have been reported 1–8 m above mean sea level (Adie, 1953, Roberts, 1984, Clapperton and Roberts, 1987, Aldiss and Edwards, 1999). A single age, taken from peat overlying one of the raised beach deposits, of 4,090–3,840 cal yr BP suggests RSL may have been several metres higher than present during the mid Holocene. A RSL reconstruction for the last century from the Falkland Islands has recently been produced (Frederikse *et al.*, 2021) but the RSL history for the rest of the Holocene remains poorly

studied.

RSL reconstructions from the central and southern Patagonian mainland coast show a possible Holocene highstand of 1.5–7 m (Codignotto *et al.*, 1992, Zanchetta *et al.*, 2014, Bini *et al.*, 2018), although the quality of the data is somewhat variable (Milne *et al.*, 2005, Pappalardo *et al.*, 2019) and the reconstructions are complicated by tectonic activity (Bentley and McCulloch, 2005, Bini *et al.*, 2018). The closest locations of GIA model simulations, for the Strait of Magellan and Beagle Channel, estimate a highstand at 5,000 cal yr BP of up to 1 m above mean sea level (Milne *et al.*, 2005). In this study we aim to reconstruct Holocene RSL from the Falkland Islands and test the hypothesis that a mid-Holocene sea-level highstand occurred on this part of the Patagonian continental shelf.

5.2 Materials and Methods

5.2.1 Site description and fieldwork

Swan Inlet (S 51.83°, W 58.59°) is the largest salt marsh on East Falkland, part of the Falkland Islands archipelago, also known as Las Islas Malvinas (Fig. 5.1). The site is microtidal and the area of salt marsh occurs between peatland in the river valleys to the north and west and the open estuary to the south, which is around 9 km from the open ocean. The Falkland Islands' climate is maritime and the coastline is exposed to storms with typical wave height of $\sim$ 10 m (Upton and Shaw, 2002), although it is unclear how these affect the site.

Stratigraphic descriptions were taken from a total of 60 gouge cores (5, 8 and 47 in 2005, 2012 and 2018 respectively) and two exposed bank sections following Troels-Smith (1955). We subsequently collected samples for dating across the main stratigraphic contacts that were identified with a Russian peat corer. We also collected four cores using a vibrocorer to obtain samples from a prominent inorganic sand unit for optically stimulated luminescence (OSL) dating following the design of Lanesky *et al.* (1979). All core locations and elevations were measured using a Trimble R4 differential global positioning system (DGPS) and tied to a local benchmark. In turn, we tied the local benchmark to Stanley chart Datum (SD) by running a real time DGPS kinematic survey both there and at a known benchmark (PWD, Stanley) and processed the data with the permanent GNSS station FALK.
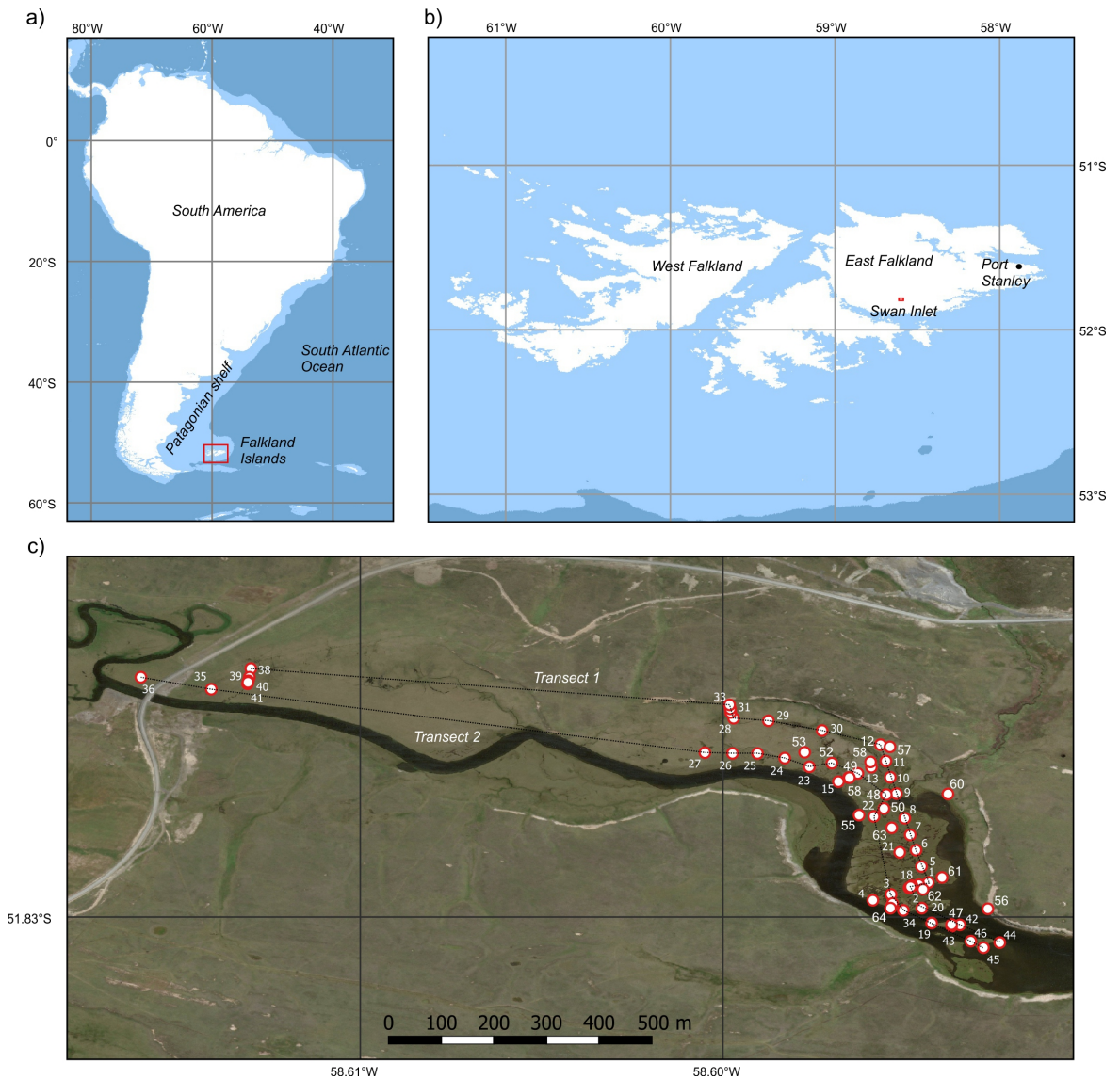
Figure 5.1: Location maps of Swan Inlet. a) An overview of South America with the continental shelf shown by the light blue, showing the location of b) the Falkland Islands, with the location of Swan Inlet shown. c) Location of all cores. The two transects shown in Fig. 5.2 are also highlighted.

5.2.2   Laboratory analyses

In the laboratory we performed litho-, bio- and chronostratigraphic analysis on 33 sediment samples to determine sea-level index points (SLIPs). The age attributes of our SLIPs were obtained by radiocarbon (^{14}C) for 28 samples and OSL dating for five samples. We collected horizontally bedded plant fragments or, in their absence, bulk sediment, from the highly humified organic sediments for accelerator mass spectrometry (AMS) (^{14}C) dating. Sample preparation and dating was carried out at the Scottish Universities Environmen-

tal Research Centre (SUERC), NERC Radiocarbon Facility, East Kilbride, UK following standard procedure (Stuiver and Polach, 1977) unless samples were exceptionally small. In such cases the dating was carried out at the Keck Carbon Cycle AMS Facility, University of California, Irvine, USA. All ^{14}C ages were calibrated in Oxcal v4.4 (Bronk Ramsey, 2009) using the SHCal20 calibration curve (Hogg *et al.*, 2020) and are reported as 2σ ranges in calibrated years before present (cal yr BP), where present is 1950.

To obtain ages through the sand unit we first used a SUERC portable OSL reader to calculate the equivalent dose determination to understand the depositional history of the unit and to be able to better target our OSL dating (Sanderson and Murphy, 2010). We subsequently took 5 cm samples from cores SI-31, SI-34 and SI-36 as far from the base and top of the sand unit as possible whilst avoiding the cut ends of the core segments. Dose rates were estimated based on elemental concentrations determined by inductively coupled plasma mass spectrometry undertaken at SGS laboratories, Canada and moisture content of samples from the sand unit itself and the underlying and overlying units in each core. Prior to OSL measurement samples were pre-treated to remove the carbonates and separate out the 90–180 µm quartz grains (Bateman and Catt, 1996). To measure the equivalent dose we took 24 replicate measurements of each sample following the single aliquot regeneration protocol (Murray, 2003). We applied an experimentally derived preheat for 10 seconds to remove unstable traps and an infrared signal to avoid feldspar contamination to single aliquot regeneration measurement with three regeneration points. All OSL sample preparation and dating was performed at Sheffield Luminescence Dating Laboratory.

To determine the indicative meaning (*IM*) of samples we used diatoms, foraminifera and testate amoebae as sea-level indicators. Sea-level transfer functions based on these microfossil groups were developed for Swan Inlet by Newton *et al.* (2021). Application of the Modern Analogue Technique (Watcham *et al.*, 2013) however, showed that the modern training set provides very poor analogues for many of the assemblages that were found in the fossil sediments. We therefore inferred the indicative meanings from a qualitative assessment of the litho- and biostratigraphy (e.g. Gehrels *et al.*, 2006, Xiong *et al.*, 2020).

To correct the elevation of samples for possible post-depositional lowering in the sediment (Allen, 2000), we applied the geotechnical approach of Brain (2011, 2012, 2015) to core SI-34. Based on the results we estimated possible compaction in other cores that we sampled.

We subtracted the indicative meaning (*I*) from the sample elevation (*E*), corrected for

post-depositional lowering (C) to give the palaeo sea level for each SLIP ($_s$) in m SD shown in Eq. 5.1a. The total 2σ vertical uncertainty (U) was calculated using Eq. 5.1b with the following components described further in section 5.3.4: u_a) indicative range [$\bar{\text{X}}$ = 0.27 m]; u_b) palaeotide [0.20 m]; u_c) compaction correction [$\bar{\text{X}}$ = 0.02 m]; u_d) non-vertical coring [$\bar{\text{X}}$ = 0.03 m]; and u_{e-h}) sample thickness, sampling, core shortening/stretching and DGPS surveying [all 0.01 m]. $u_{c,d,g}$ are only applied to the positive (i.e. upward) uncertainty.

$$SL_s = E_s - I_s + C_s \tag{5.1a}$$

$$U_s = \sqrt{u_a^2 + u_b^2 + u_c^2 + u_d^2 + u_e^2 + u_f^2 + u_g^2 + u_h^2} \tag{5.1b}$$

Based on the litho-, chrono- and biostratigraphical analyses of each core we made an interpretation of the development of the inter-tidal zone of Swan Inlet and its palaeogeography. We interpolated between the cores based on the elevation of the main stratigraphic contacts and constrained the timing using the final set of accepted calibrated ages.

5.3 Results

5.3.1 Stratigraphy

The lithology of Swan Inlet is summarised in Fig. 5.2 and is characterised by six units overlying bedrock of Permian black shale (Aldiss and Edwards, 1999): blue-grey consolidated clay (unit 1), grey-brown peaty clay (unit 2), grey coarse sands (unit 3), grey-brown fibrous clayey peat (unit 4), brown fibrous peat (unit 5) and a dark brown fibrous peat (unit 6). We interpreted the sedimentary facies based on the microfossils and lithology of each unit and the modern analogues (Table 5.1).
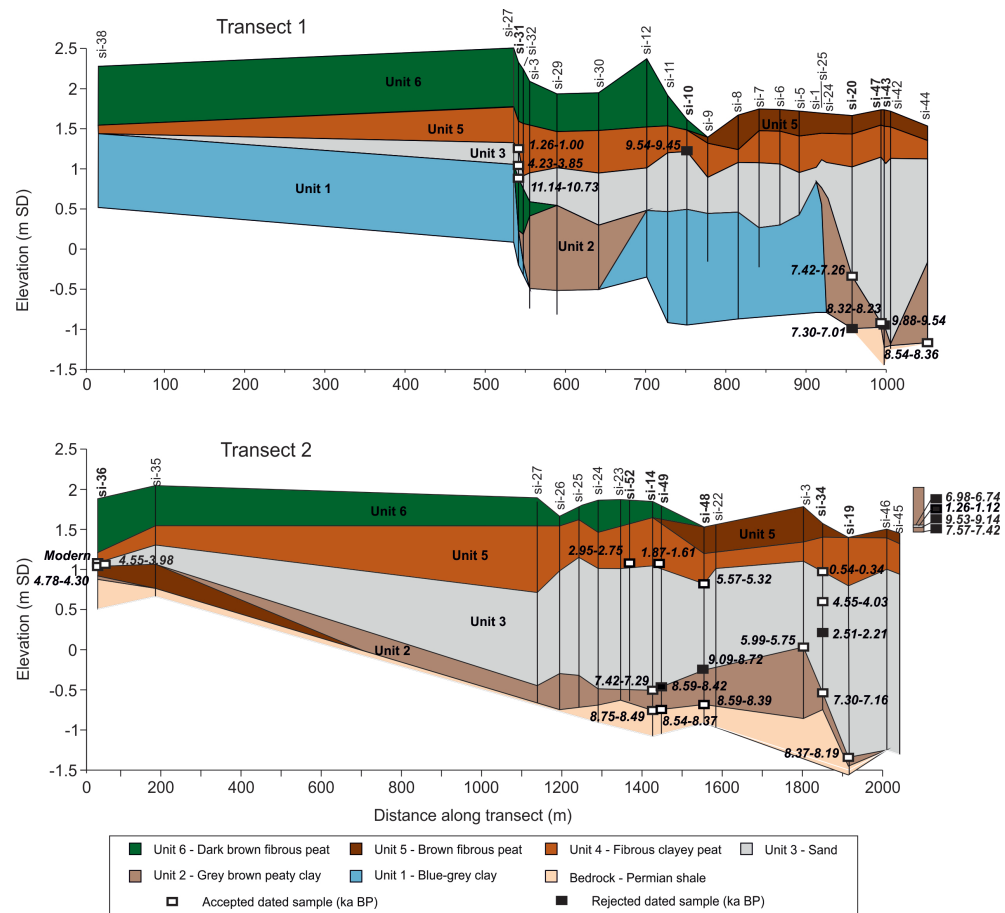
Figure 5.2: Stratigraphy of the two transects indicated in Fig. 5.1, showing the main lithological groups and the calibrated ages of ^{14}C and OSL ages in ka BP.

Unit 1: A blue-grey clay which is found at the base of the sequence in steeply banked sections on the western side of the site and on the most northern extremities. The clay is highly compacted and entirely inorganic. It appears widely across East Falkland and is likely to be a Pleistocene alluvial or lacustrine deposit (Aldiss and Edwards, 1999).

Unit 2: A grey-brown peaty clay low in organic material with an LOI of around 5% that is found widely across the site. Testate amoebae concentrations are generally low but are characterised by species that occupy the lowest elevations of testate occurrence in the modern marsh. Foraminifera are generally absent that may be because of preservation issues, but where identified comprise salt-marsh taxa, such as *Trochamminita salsa* and *Miliammina fusca*. Diatom assemblages are relatively diverse and include taxa with a range of salinity preferences including *Pinnularia viridis* and *Pinnularia microstauron* and other freshwater-brackish taxa, alongside brackish-marine taxa such as *Ctenophora pulchella* and *Paralia sulcata*. The microfossils and the lithology indicate that unit 2 is of a salt-marsh origin. We

take the upper and lower margin of *Pinnularia viridis* and *Pinnularia microstauron* (1.47 – 2.02 m SD) as the indicative range, which is also coincidental with the modern salt-marsh elevation range. Although the higher abundances of *Pinnularia viridis* and/or *Pinnularia microstauron* suggest a high marsh, the constant presence of lower marsh taxa prevent us from confidently assigning a more precise indicative meaning. In places the unit shows signs of reworking such as sandy stratification and broken diatoms.

Unit 3: A sand unit, ubiquitous across the site and contains gravelly sand and angular clasts up to > 20 mm length. It forms an abrupt contact on top of underlying sediments between -1.45 to 1.38 m SD and at the deepest elevations directly on top of bedrock. Nearshore/marine diatom taxa are found in the unit, with *Paralia sulcata* dominating the diatom assemblage. *Miliammina fusca* is the dominant foraminifera taxa which is similarly dominant in the modern tidal-flat samples, while the unit is also marked by the absence of testate amoebae. We interpret this unit to be of tidal-flat origin based on the lithology being very similar to the modern tidal flat, and the microfossils that are present being characteristic of a tidal flat. We therefore assigned an indicative range of 0.87 – 1.47 m SD to ensure we capture the full tidal-flat environment.

Unit 4: A grey-brown clayey peat, that contains much fibrous organic material overlies unit 3 across the site. The contact is generally gradual that is indicative of a regressive sequence with a reducing marine influence. The microfossil assemblages are very similar to those in unit 2, along with *Planothidium delicatulum* indicating a salt-marsh origin and we therefore assigned the same indicative range (1.47 – 2.02 m SD).

Unit 5: A brown fibrous peat containing clay forming on the modern day salt marsh. Unit 4 very gradually grades into this unit. The diatom assemblages down core are very similar to unit 4 and we interpret the unit to be of the same origin but less humified.

Unit 6: A dark-brown fibrous peat that is found in the upper reaches of tidal influence in the modern environment. The unit contains high abundances of brackish-freshwater diatoms such as *Pinnularia microstauron* and *Pinnularia viridis* and testate amoebae species, such as *Euglyphid spp.*. A similar unit is occasionally found underlying the sand in the most landward locations and contains many fragments of herbaceous and ligneous material. We interpret this unit to have an origin of upper salt marsh to freshwater marsh and assign a indicative meaning of > 1.97 m SD.

Our interpretations of the stratigraphic sequence indicates that a transgressive sequence

Table 5.1: Stratigraphical units of Swan Inlet. The lithology and biostratigraphy are summarised which form the interpretations and the indicative ranges. Microfossil taxa are: # = diatom taxa, * = foraminifera, + = testate amoebae.

Unit	Sediment description	Indicative microfossil taxa	Palaeoenvironment	Indicative modern range (m SD)
1	Blue-grey clay	NA	NA	NA
2	Grey brown peaty clay Occasional sand laminations	*Pinnularia viridis*# *Pinnularia microstauron*# *Ctenophora pulchella*# *Trochamminita salsa** *Miliammina fusca**	Salt marsh	1.47–2.02
3	Sand Inorganic gravelly sand Clasts > 2 cm	*Achnanthes kuelbsii*# *Paralia sulcata*# *Miliammina fusca** Testate amoebae - absent	Tidal flat	0.82–1.47
4	Grey-brown clayey peat Much rooting	*Planothidium delicatulum*# *Trochamminita salsa** *Pinnularia spp.*# *Centropyxiella sp.*+	Salt marsh	1.47–2.02
5	Brown fibrous peat	*Planothidium delicatulum*# *Trochamminita salsa** *Centropyxiella sp.*+	Salt marsh	1.47–2.02
6	Dark brown fibrous peat	*Navicula elegans*# *Pinnularia spp.*# *Hyalosphenia subflava*+ Foraminifera - absent	Upper marsh–freshwater peat	> 1.97

is evident through to the unit 3. Following the deposition of unit 3 a regressive sequence is found.

5.3.2 Chronology

We collected 30 ^{14}C samples from the base of the sequence and the transgressive and regressive contacts (unit 2/3 and unit 3/4 respectively). The samples were a mixture of plant macrofossils and bulk sediment because the sediments were highly humified and we were unable to find suitable organic fragments in many samples. The calibrated ages of the samples vary from 12,060–11,760 cal yr BP to 540–340 cal yr BP (Table 5.2). Ages within single cores do not always occur in chrono-stratigraphic order, suggesting that there was significant reworking of sediment or movement of material. A number of the dates fall out of sequence and so we reject ten samples that show either age reversals or signs of reworking. Four samples taken from the exposed bank in 2005 lack accurate survey data and so we also do not use these as SLIPs.

Unit 3 is devoid of organic material and thus we applied OSL dating techniques to calculate its age and understand its depositional history. Portable OSL sampling of core SI-34 at 2 cm intervals across the unit shows a gradual decline in the luminescence signal

Table 5.2: Radiocarbon (^{14}C) dating results. All dates were calibrated using the SHCal20 calibration curve and are given as calibrated years BP (BP = 1950).

Lab code	Core ID	Material	Stratigraphic position	Core depth (m)	Elevation (m SD)	^{14}C age	Calibrated age (yr BP)	Calibrated age range (1σ)	Calibrated age range (2σ)	Assessment	SLIP index no.
UCIAMS-219326	SI-3	Plant fragment	Unit 2 - top	1.72	0.06	$6{,}485 \pm 35$	7,362	7,422–7,327	7,428–7,278	Accepted	7
SUERC-87675	SI-10	Plant fragment	Unit 4 - base	0.62	0.87	$8{,}539 \pm 40$	9,504	9,534–9,485	9,544–9,447	Reworked	–
SUERC-87667	SI-14	Bulk sediment	Unit 2 - base	2.37	-0.76	7849 ± 39	8,586	8,640–8,541	8,752–8,448	Accepted	1
UCIAMS-219327	SI-14	Plant fragment	Unit 2 - top	1.96	-0.35	$5{,}180 \pm 20$	5,910	5,984–5,768	5,992–5,754	Accepted	10
SUERC-87673	SI-19	Bulk sediment	Unit 2 - top	2.23	-1.35	$7{,}516 \pm 38$	8,288	8,365–8,208	8,375–8,190	Accepted	5
SUERC-87659	SI-20	Plant fragment	Unit 2 - top	2.02	-0.49	$6{,}458 \pm 38$	7,348	7,422–7,310	7,425–7,264	Accepted	8
SUERC-87663	SI-20	Plant fragment	Unit 2 - base	2.59	-1.06	$6{,}308 \pm 39$	7,202	7,260–7,160	7,305–7,014	Age reversal	–
SUERC-87665	SI-31	Plant fragment	Unit 6 - top	1.46	0.66	$9{,}619 \pm 42$	10,932	11,079–10,775	11,145–10,735	Freshwater	–
SUERC-87664	SI-31	Plant fragment	Unit 4 - base	1.30	0.82	$1{,}259 \pm 35$	1,126	1,167–1,072	1,264–1,000	Accepted	18
UCIAMS-219328	SI-34	Plant fragment	Unit 2 - top	1.98	-0.41	$6{,}330 \pm 20$	7,212	7,258–7,167	7,305–7,159	Accepted	9
SUERC-87666	SI-34	Plant fragment	Unit 4 - base	0.89	0.68	484 ± 37	500	526–472	540–337	Accepted	20
SUERC-87658	SI-36	Plant fragment	Unit 2 - top	0.98	0.89	$4{,}040 \pm 35$	4,477	4,520–4,420	4,780–4,299	Accepted	12
SUERC-87668	SI-43	Bulk sediment	Unit 2 - top	2.69	-1.08	$8{,}713 \pm 39$	9,625	9,667–9,549	9,880–9,538	Reworked	–
SUERC-87669	SI-44	Bulk sediment	Unit 4 - base	2.37	-0.96	$7{,}662 \pm 38$	8,415	8,449–8,378	8,537–8,365	Accepted	4
SUERC-87674	SI-47	Bulk sediment	Unit 2 - base	2.70	-1.09	$7{,}394 \pm 38$	8,147	8,281–8,038	8,320–8,027	Accepted	6
SUERC-50086	SI-48	Bulk sediment	Unit 2 - top	1.99	-0.64	$8{,}087 \pm 38$	8,913	9,023–8,780	9,090–8,723	Age reversal	–
SUERC-48880	SI-48	Bulk sediment	Unit 2 - base	2.28	-0.93	7724 ± 45	8,476	8,520–8,417	8,588–8,389	Accepted	2
SUERC-47991	SI-48	Bulk sediment	Unit 4 - base	0.82	0.54	$4{,}730 \pm 37$	5,406	5,473–5,324	5,575–5,318	Accepted	11
SUERC-47992	SI-49	Bulk sediment	Unit 2 - top	2.33	-0.45	$7{,}759 \pm 38$	8,496	8,544–8,430	8,590–8,418	Age reversal	–
SUERC-48884	SI-49	Bulk sediment	Unit 2 - base	2.95	-1.08	$7{,}672 \pm 45$	8,428	8,514–8,379	8,542–8,366	Accepted	3
SUERC-50458	SI-49	Bulk sediment	Unit 4 - base	0.88	0.99	$1{,}860 \pm 37$	1,748	1,815–1,704	1,866–1,614	Accepted	17
SUERC-50089	SI-52	Bulk sediment	Unit 2 - top	1.88	0.02	$10{,}256 \pm 41$	11,894	11,952–11,840	12,056–11,759	Reworked	–
SUERC-47993	SI-52	Bulk sediment	Unit 2 - base	2.70	-0.80	$9{,}229 \pm 40$	10,351	10,402–10,254	10,495–10,243	Reworked	–
SUERC-50459	SI-52	Bulk sediment	Unit 4 - base	0.82	1.07	$2{,}639 \pm 37$	2,737	2,769–2,710	2,844–2,499	Accepted	16
SUERC-47994	SI-55	Bulk sediment	Unit 4 - base	0.70	0.96	948 ± 35	819	903–744	912–737	Accepted	19
SUERC-9986	SI-56	Bulk sediment	Unit 2 - top	0.41	1.36	$8{,}411 \pm 55$	9,389	9,476–9,306	9,530–9,144	Not surveyed	–
SUERC-9988	SI-56	Bulk sediment	Unit 2 - base	0.45	1.32	$6{,}617 \pm 44$	7,482	7,553–7,429	7,573–7,422	Not surveyed	–
SUERC-9984	SI-56	Bulk sediment	Unit 4 - base	0.37	1.40	$6{,}054 \pm 41$	6,859	6,936–6,793	6,986–6,740	Not surveyed	–

up core suggesting that the sand was deposited over a longer time period, as opposed to a single deposition event (Fig. 5.3). We OSL dated the quartz grains of five samples from four cores. Three of the samples, all from different cores, have a consistent age of around 4,200 ± 250 cal yr BP, while the others are younger (Table 5.3). In core SI-34 an age reversal and a degree of mixing is evident in the portable OSL results represented by reversals in the luminescence signal (Fig. 5.3). It is apparent from the dates that large areas of the site were a tidal flat c. 4,200 cal yr BP.
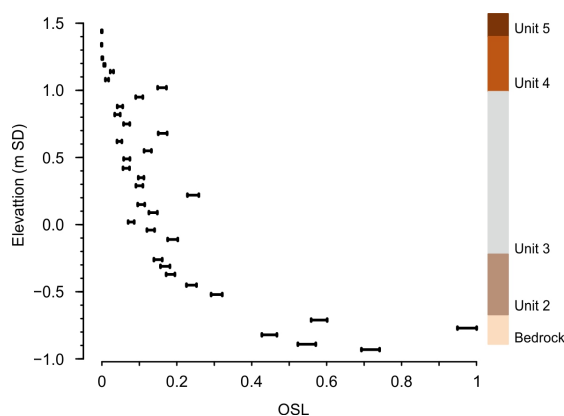

Figure 5.3: Results of relative OSL dating of sediment from core SI-34. The OSL signal is corrected for infra-red OSL signal. Values are normalised and a larger value represents an older post-depositional age of the sediment. The core stratigraphy is shown in the bar to the right and corresponds to Fig. 5.1.

Table 5.3: OSL dating results. Dose rate and moisture were measured on core sediments in the laboratory. Ages are given as years BP (BP = 1950).

Lab code	Core ID	Core depth (m)	Elevation (m SD)	Equivalent dose (Gy)	Dose Rate (uGy yr^{-1})	Moisture (%)	Age (yr BP)	Age range (1σ)	Age range (2σ)	Assessment	SLIP index no.
shfd19017	SI-36	0.83	1.04	8.91 ± 0.4	2,089 ± 103	22.99	4,260	4,403–4,117	4,540–3,980	Accepted	14
shfd19018	SI-34	1.25	0.32	11.4 ± 0.38	2,656 ± 135	42.55	4,290	4,423–4,157	4,550–4,030	Accepted	13
shfd19019	SI-34	1.40	0.17	6.26 ± 0.22	2,652 ± 135	42.55	2,360	2,437–2,283	2,510–2,210	Reworked	–
shfd19020	SI-31	1.36	0.76	9.69 ± 0.18	2,400 ± 105	41.74	4,040	4,137–3,943	4,230–3,850	Accepted	15
shfd19021	SI-56	0.39	1.38	4.28 ± 0.12	3,607 ± 174	22.69	1,190	1,226–1,154	1,260–1,120	Too high	–

5.3.3 Palaeogeography

We interpret the development of the inter-tidal zone of Swan Inlet and its palaeogeography based on litho-, chrono- and bio-stratigraphical analyses. We refer to the dated samples used as SLIPs, derived in section 5.3.4, by their SLIP index number (Table 5.4).

The first inundation of the site occurred around 8,500 cal yr BP as indicated by the seaward cores where salt marsh formed directly on the bedrock at similar elevations, including SLIPs 1–4 (Fig. 5.4b). Much of this marsh appears to flood at a similar time as indicated by the sharp contact between the marsh deposits and the overlying sand occurring at an elevation of -1.35 – -1 m SD and dated to c. 8,200 cal yr BP in SLIPs 5–6 (Fig. 5.4c). An increasingly higher transgressive contact indicates that the marsh continued to accrete vertically and accommodation space allowed the marsh to grow horizontally as areas at lower elevations became part of the inter-tidal zone. A second period where much of the marsh is apparently drowned is indicated by several cores where the peat-tidal flat contact occurs at similar elevations (around -0.5 m SD), three of which were dated between 7,400 and 7,200 cal yr BP (SLIPs 7–9). The drowning resulted in retreat of the marsh front (Fig. 5.4d). The site then appears
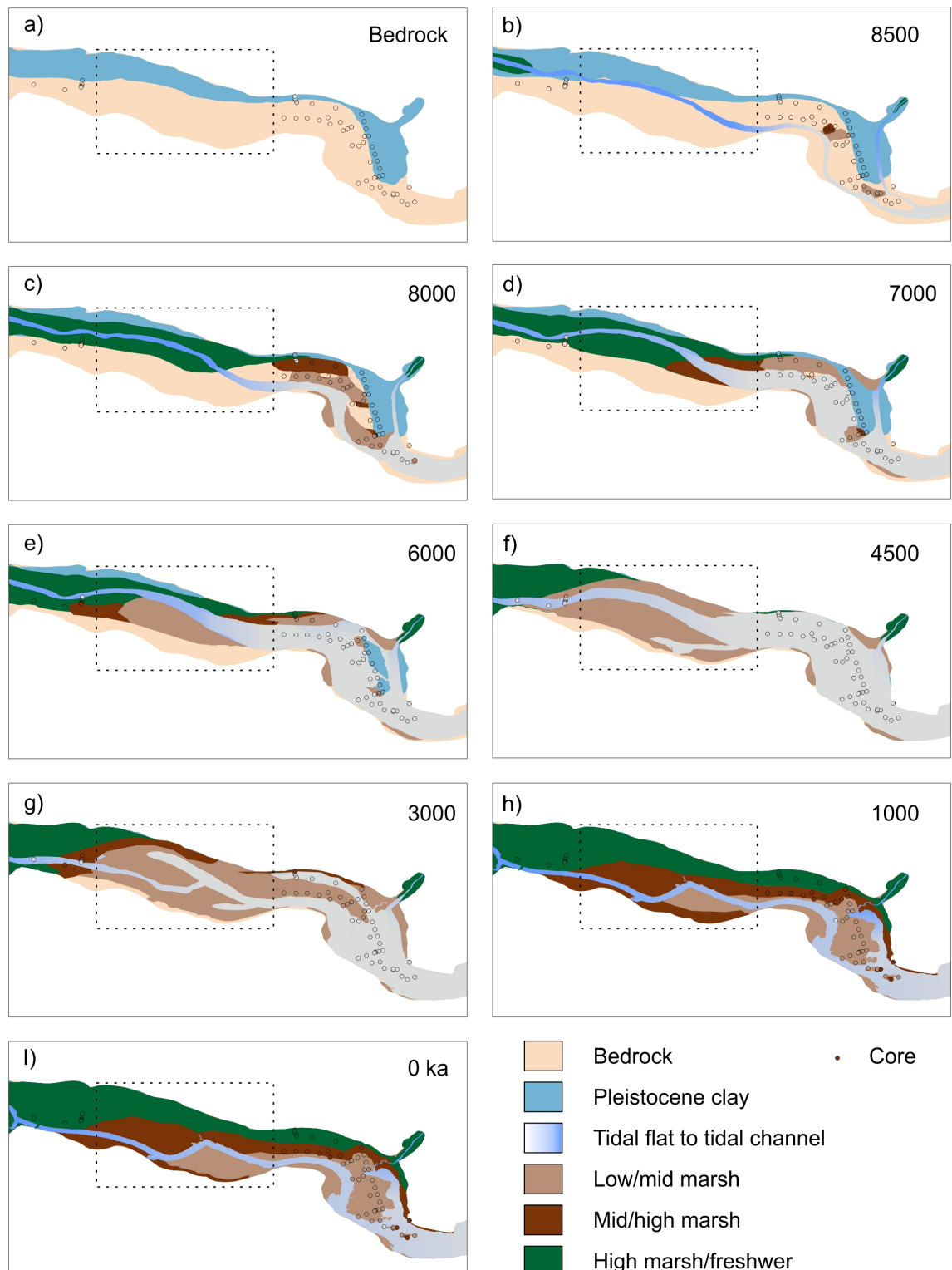
Figure 5.4: Palaeogeographical reconstructions for Swan Inlet. Ages are given in cal yr BP The area in the dashed box indicates the area with a lack of cores and we tentatively interpolate through this central zone. Channel positions are inferred and only shown schematically.

to undergo a gradual period of continued transgression (Fig. 5.4e), with the marsh front further retreating as indicated by the gradual increase in elevation of the marsh-tidal flat contact along with decreasing ages (SLIPs 10–12). We found the maximum elevation of the marsh-tidal flat contact at around 1 m SD where it was dated to c. 4,500 cal yr BP (SLIP 12), which along with the age of unit 3 itself at c. 4,200 cal yr BP (SLIPs 23-25) suggests that by this time much of the marsh had become tidal flat. The variable elevation of the contact at the eastern edge of the site and its absence in core SI-38, however, suggest a combination of a shifting river/tidal channel and storm overwash in landward locations and not of a site-wide tidal flat (Fig. 5.4f). Evidence of a shifting channel is also evident in core SI-20 (schematically shown in Fig. 5.4). After the deposition of the tidal flat unit, a regressive contact is observed across the site with ages varying between 2,700 cal yr BP and 500 cal yr BP (SLIPs 16–20), suggesting the salt marsh regressed gradually seaward (Fig. 5.4g–h). Frederikse *et al.* (2021) document a 20th century RSL rise at Swan Inlet during which the marsh likely shrunk somewhat (Fig. 4h-i).

5.3.4   Relative sea level

Based on the elevation, stratigraphical and chronological information obtained from samples taken at the contacts between the sedimentary facies described above we produced a dataset of 20 SLIPs and 1 terrestrial limiting point (Table 5.4). In order to reconstruct RSL we applied the indicative ranges (section 5.3.1 and Table 5.1) based on the modern sampled elevation preferences of indicative taxa. The wide elevation preferences of taxa found within the fossil assemblages mean we are unable to confidently refine the indicative range any further than the range of the modern salt marsh or tidal flat. We did not correct for changes in palaeotides because the regional tidal range is believed to have been stable since the continental shelf was flooded by c. 14,000 cal yr BP (Wilmes and Green, 2014) and local effects, such as frictional drag due to infilling and changing water depths, are likely small and would require extensive surveying and modelling (e.g. Gehrels *et al.*, 1995). We did add an addition uncertainty of $\pm$ 0.2 m to account for possible palaeotidal changes. Finally, our analysis of PDL in core SI-34 suggests that the sediments were lowered by a maximum of 0.06 m in unit 3 (Fig. 5.5). We therefore corrected SLIPs at the top of unit 2 or within unit 3 by interpolating from this value depending on the depth to bedrock.

Table 5.4: Swan Inlet sea-level index points (SLIPs). The new SLIPs developed in this work are shown (1–20) along with the SLIPs from (Frederikse *et al.*, 2021) (21–35). The indicative meaning is given where: salt marsh = 1.47 – 2.02 m SD; tidal flat = 0.87 – 1.47 m SD; Diatom TF = transfer functions predictions from the original publication.

| Index no.	Core	Age (2σ range) (cal yr BP)	Elevation (m SD)	Indicative meaning	RSL (2σ range) (m SD)
1	SI-14	8,586 (8,752 − 8,448)	-0.76	Salt marsh	-1.42 (-1.69 − -1.14)
2	SI-47	8,476 (8,588 − 8,389)	-0.93	Salt marsh	-1.59 (-1.86 − -1.31)
3	SI-49	8,428 (8,542 − 8,366)	-1.08	Salt marsh	-1.74 (-1.83 − -1.63)
4	SI-36	8,415 (8,537 − 8,365)	-0.96	Salt marsh	-1.57 (-1.84 − -1.29)
5	SI-19	8,288 (8,375 − 8,190)	-1.35	Salt marsh	-1.96 (-2.23 − -1.68)
6	SI-44	8,147 (8,320 − 8,027)	-1.09	Salt marsh	-1.75 (-2.02 − -1.47)
7	SI-14	7,364 (7,428 − 7,278)	-0.35	Salt marsh	-0.96 (-1.23 − -0.68)
8	SI-20	7,348 (7,425 − 7,264)	-0.49	Salt marsh	-1.1 (-1.37 − -0.82)
9	SI-31	7,212 (7,305 − 7,159)	-0.41	Salt marsh	-1.02 (-1.29 − -0.74)
10	SI-3	5,910 (5,992 − 5,754)	0.06	Salt marsh	-0.55 (-0.82 − -0.27)
11	SI-48	5,406 (5,575 − 5,318)	0.54	Salt marsh	-0.07 (-0.34 − 0.21)
12	SI-34	4,477 (4,780 − 4,299)	0.89	Salt marsh	0.28 (0.00 − 0.56)
13	SI-34	4,290 (4,550 − 4,030)	0.32	Tidal flat	0.22 (-0.30 − 0.51)
14	SI-36	4,260 (4,540 − 3,980)	1.04	Tidal flat	0.94 (0.43 − 1.22)
15	SI-31	4,040 (4,230 − 3,850)	0.76	Tidal flat	0.66 (0.14 − 0.94)
16	SI-52	2,737 (2,844 − 2,499)	1.07	Salt marsh	0.46 (0.19 − 0.74)
17	SI-49	1,748 (1,866 − 1,614)	0.99	Salt marsh	0.38 (0.11 − 0.66)
18	SI-31	1,126 (1,264 − 1,000)	0.82	Salt marsh	0.16 (-0.12 − 0.44)
19	SI-55	819 (912 − 737)	0.96	Salt marsh	0.35 (0.07 − 0.63)
20	SI-34	500 (540 − 337)	0.68	Salt marsh	0.02 (-0.25 − 0.3)
21	SI-49	42 (74 − 19)	1.86	Diatom TF	0.89 (0.95 − 0.82)
22	SI-49	33 (61 − 12)	1.85	Diatom TF	0.97 (1.03 − 0.91)
23	SI-49	24 (49 − 6)	1.84	Diatom TF	0.96 (1.02 − 0.91)
24	SI-49	14 (37 − 0)	1.83	Diatom TF	0.97 (1.03 − 0.92)
25	SI-49	5 (22 − -4)	1.82	Diatom TF	0.99 (1.04 − 0.93)
26	SI-49	-4 (-1 − -6)	1.81	Diatom TF	0.99 (1.05 − 0.94)
27	SI-49	-7 (-3 − -12)	1.80	Diatom TF	1.01 (1.07 − 0.95)
28	SI-49	-11 (-6 − -15)	1.79	Diatom TF	0.94 (1.00 − 0.87)
29	SI-49	-14 (-11 − -17)	1.78	Diatom TF	0.96 (1.02 − 0.89)
30	SI-49	-22 (-14 − -35)	1.77	Diatom TF	1.1 (1.17 − 1.03)
31	SI-49	-28 (-17 − -42)	1.76	Diatom TF	1.14 (1.20 − 1.09)
32	SI-49	-35 (-22 − -50)	1.75	Diatom TF	1.01 (1.08 − 0.93)
33	SI-49	-42 (-28 − -55)	1.74	Diatom TF	1.08 (1.15 − 1.02)
34	SI-49	-49 (-35 − -60)	1.73	Diatom TF	1.12 (1.18 − 1.05)
35	SI-49	-56 (-44 − -62)	1.72	Diatom TF	1.1 (1.15 − 1.04)
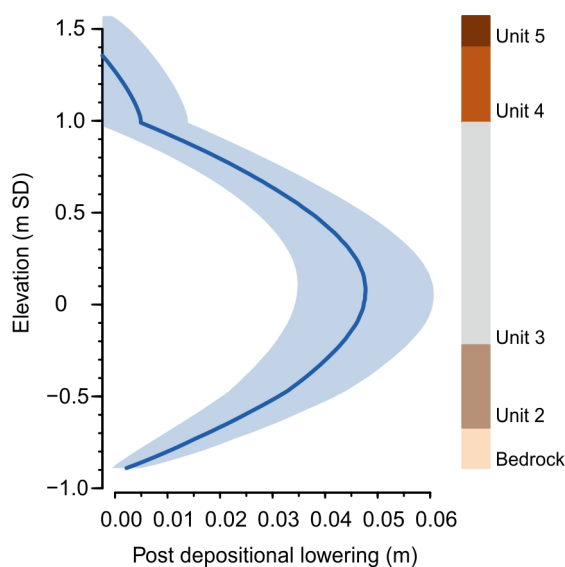
Figure 5.5: Modelled post-depositional lowering of core SI-34. The mean and 1σ uncertainty is shown along with the core lithology. The core stratigraphy is shown and corresponds to Fig. 5.1.

The SLIPs are plotted in Fig. 5.6, which provides a Holocene RSL reconstruction for Swan Inlet from c. 8,450 cal yr BP until present. For the last 100 years we use the SLIPs presented by Frederikse *et al.* (2021) and tide-gauge data (Woodworth *et al.*, 2010, PSMSL, 2020). The reconstruction shows a general pattern of RSL rise from c. 8,450 cal yr BP until c. 4,500 cal yr BP. of around 2 m, equivalent to an average rate of 0.5 mm/yr. At around this point a sea-level highstand is apparent, although we cannot quantify the precise timing of it, only to say that by at least 2,740 cal yr BP RSL had started to fall. RSL continued to fall until an apparent shift in the trend occurs prior to the observed rise in the last 100 years. Within this general pattern, the evidence suggests there are periods of distinct variability that we discuss further in section 5.4.1.

We compare the SLIPs with relative sea-level curves predicted by a GIA model (Bradley *et al.*, 2011). We placed zero of the model output at the pre-industrial RSL at the start of the Frederikse *et al.* (2021) data (SLIP 20). We present the model outputs that used the same lithosphere thickness (96 km) and upper and lower mantle viscosity (5 x 10^{20} Pas and 1 x 10^{22} Pas respectively) to be able to focus on the different simulations of regional ice-sheet history. ICE-5G (Peltier, 2004) and ICE-6G (Peltier *et al.*, 2015), containing different ice-sheet simulations for Antarctica (Argus *et al.*, 2014), appear to fit the data around 8,500 cal yr BP but diverge from it in the mid Holocene, with both showing a higher and earlier start of the highstand than the data. Different Northern Hemisphere ice-sheet histories are represented by HUY3 (Lecavalier *et al.*, 2014) and ICE-5G. Both simulations match the data at different times in the early Holocene. Notably, although predicting higher RSL, the shape of the HUY3 curve is similar to our SLIPs from 7,500 cal yr BP onwards and the highstand occurs at the same time as our data. From the mid Holocene onwards, the data - model misfit is around 1 m.
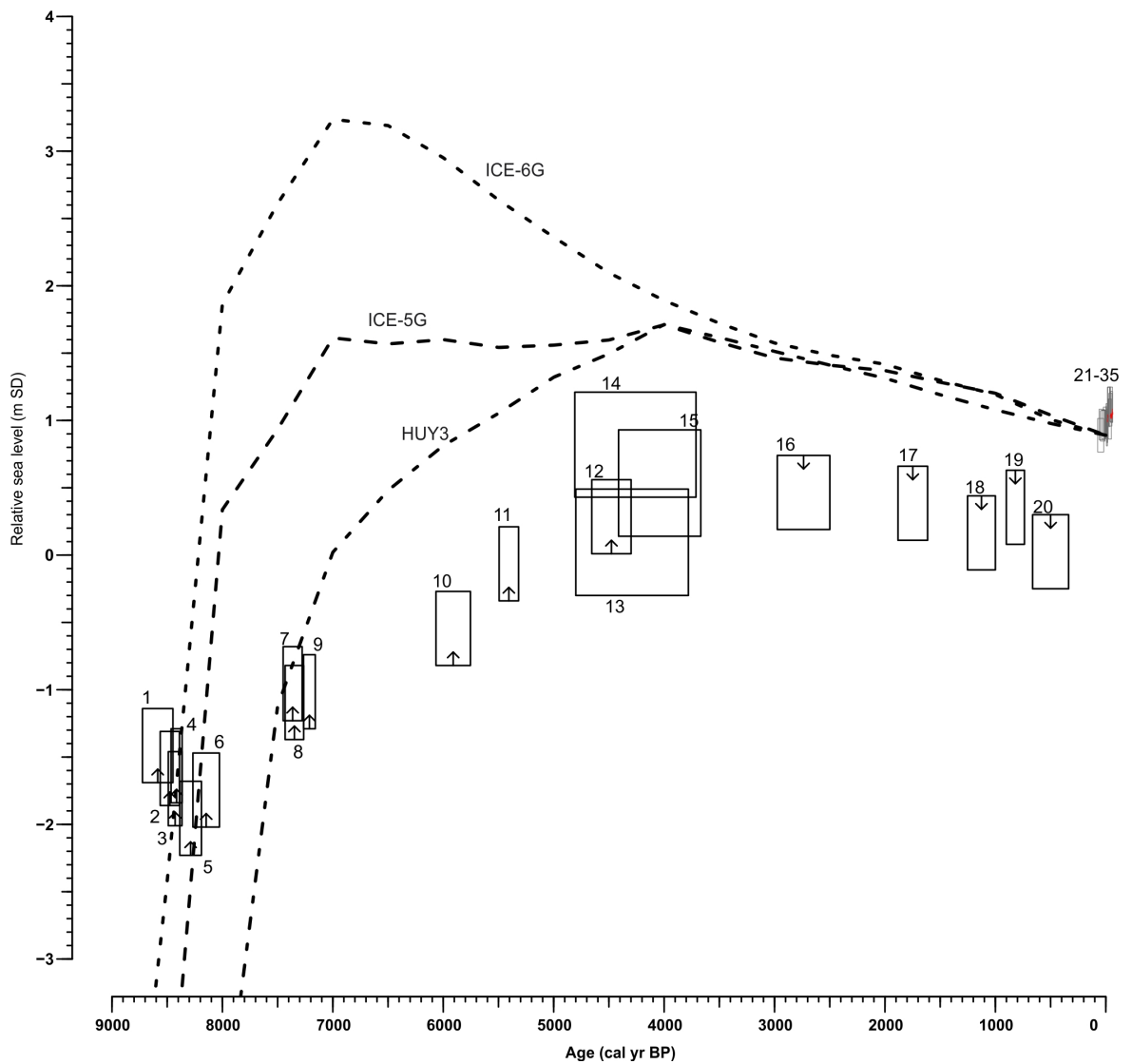
Figure 5.6: Sea-level index points (SLIP) and GIA predictions for Swan Inlet. Arrows indicate the tendency of the SLIP. The grey SLIPs are taken from (Frederikse et al., in Review). Present day mean sea level is 1.08 m SD.

5.4 Discussion

5.4.1 Relative sea level and palaeogeography

Our analyses indicate that there have been periods of abrupt change that may be linked to RSL change. Here, we discuss the periods of change and their causes within a sea-level context.

8,500 − 4,500 cal yr BP

The first inundation of the site occurred around 8,500 cal yr BP, as indicated by SLIPs 1–4 and the most seaward cores (Fig. 5.4b). As marsh tends to form first towards the top of the tidal frame upon a rise in water level (Törnqvist *et al.*, 2004), sea level would have likely been towards the lower range of these SLIPs ($\sim$ -2 m SD). Before this we suggest a rapid RSL rise occurred such that rates were too fast for coastal marsh to develop. This is based on the observation that below the elevation of dated basal peat, the sand (unit 3) lies directly on top of the bedrock. To test the hypothesis that peat formation began simultaneously, we combined the four ^{14}C ages of the SLIPs to test for agreement in OxCal, whereby a value of A > 60 % is considered reliable (Bronk Ramsey, 1995). The four SLIPs fail the test (A = 31 %), but when SLIP 1, taken at a higher elevation from a more inland core that shows possible signs of reworking is removed, the test is passed (A = 118 %) with an age of 8,520-8,380 cal yr BP. The results do not rule out the ages of all four SLIPs overlapping, but the reason for the poor agreement may be that SLIP 1 is reworked or that the SLIPs may be representative of a more prolonged period of marsh development indicating a more gradual rise.

The apparent RSL rise could have been caused by a number of processes. We rule out tectonic movement and a rapid change in tidal range because, as described in section 5.1, the region is not exposed to such processes (Milne *et al.*, 2005, Rostami *et al.*, 2000, Wilmes and Green, 2014). Therefore a barystatic sea-level rise appears most likely. The weighted mean age of 8,430 cal yr BP (with SLIP 1 removed) is broadly coincidental with the end of a sea-level event recorded in Scotland, UK that has been linked to a meltwater pulse prior to the 8.2 ka climate event (Lawrence *et al.*, 2016, Rush *et al.*, in review). Although the timing does appear to be earlier than is recorded in the Netherlands (Hijma and Cohen, 2010, 2019), the end of the event is less well constrained than in Scotland. It is also coincidental with the end of an apparent period of rapid sea-level rise from far-field sites in southeast Asia (Tamura *et al.*, 2009, Nguyen *et al.*, 2010, Zong *et al.*, 2012, Wang *et al.*, 2013, Tjallingi *et al.*, 2014, Xiong *et al.*, 2020), and Mozambique where the only current clear evidence of a contemporaneous sea-level event from the Southern Hemisphere has been observed (De Lecea *et al.*, 2017). Although we suggest a rapid RSL rise is evident that appears broadly coincidental with those recorded in the North Atlantic and possibly further afield, we can neither confirm that a sea-level event linked to the 8.2 ka climate event occurred nor

quantify its magnitude. Barystatic-GRD fingerprint modelling of the meltwater pulse from the retreating Laurentide Ice Sheet (LIS) shows that the Falkland Islands would record the full magnitude of the meltwater (Kendall *et al.*, 2008) and thus this warrants further study. It may be possible to test whether a sea-level event occurred around 8,500 cal yr BP in the Falkland Islands by going further offshore in an attempt to sample submarine peat deposits.

The drowning of the existing marsh is indicated by the sharp unit 2–3 contact (Fig. 5.4c) and is dated in SLIPs 5–6 (Fig. 5.4c). The ages show good agreement when combined in OxCal (A = 64 %) and suggest the small areas of marsh that had formed drowned at c 8,260 cal yr BP. Our estimation of the timing of this apparent rapid drowning corresponds to the later sea-level event recorded in the North Atlantic immediately prior to the 8.2 ka climate event that is believed to be evidence of the final drainage of the coalesced proglacial lakes Agassiz-Ojibway (LAO) (Li *et al.*, 2012, Lawrence *et al.*, 2016, Hijma and Cohen, 2019, Rush *et al.*, in review). It is difficult to draw any firm conclusions from the two SLIPs alone, but given the site stratigraphy and the contemporaneous rise in the North Atlantic, we hypothesise the drowning could have been a result of the final drainage of LAO that ultimately forced the 8.2 ka climate event. The data from the North Atlantic sites suggests the global magnitude was very likely < 0.5 m assuming a LIS source of the meltwater (Rush *et al.*, in review). The relatively small magnitude would make the signal difficult to detect and thus testing the hypothesis appears challenging based on our investigations and may require many more ^{14}C ages in combination with off-shore sampling as proposed above.

The third apparent drowning indicated by the unit 2–3 contact occurring at similar elevations is dated to between c. 7,400 and 7,200 cal yr BP (SLIPs 7–9). Unlike the previous drownings there is no clear consensus on a major sea-level event at this time other than a rapid RSL rise with a local magnitude of 2–3 m identified in Sweden at c. 7,600 cal yr BP by Yu *et al.* (2007), that they ascribed to the final collapse of the LIS. No large sea-level rise is evident in our RSL reconstruction, but an Antarctic meltwater pulse could produce a large RSL rise in Sweden and small RSL rise in the Falkland Islands. Geological evidence suggests that abrupt periods of glacial retreat and/or thinning may well have occurred in Antarctica (e.g. Bentley *et al.*, 2014, Small *et al.*, 2019, Kingslake *et al.*, 2018, Johnson *et al.*, 2019, 2020, Kawamata *et al.*, 2020); however nothing of the scale required to produce such a large barystatic sea-level rise is identified. We are therefore unable to ascertain whether the apparent drowning was a sea-level event or a local storm or even a tsunami. We note that

Nicholson *et al.* (2020) suggested that submarine slides were a potential source for tsunamis that struck the Falkland Islands some time in the Quaternary.

After 7,000 cal yr BP the site appears to undergo a gradual period of RSL rise indicated by SLIPs 10-12. Although we interpret the transgression to have been gradual over time, the abrupt contact in each core indicates a rapid transition from salt marsh to tidal flat that we suggest was caused by erosion from wave action at the marsh edge (Allen, 2000).

4,500 cal yr BP – present

The RSL reconstruction and stratigraphy provide evidence of a probable sea-level highstand. The tidal flat (unit 3) is widespread and has a regressive upper contact. The age of the highstand is constrained by SLIP 4 underlying unit 3 at its highest elevation and dated to c. 4,480 cal yr BP; and the SLIPs from within unit 3 itself that were dated by OSL to c. 4,200 cal yr BP. The end of the highstand is constrained by the earliest date for the regressive contact at c. 2,730 cal yr BP (SLIP 16) although it may have occurred earlier and we have not captured it. The precise elevation of the highstand is difficult to assess but is likely to be at least as high as SLIP 4 and within the range of SLIPs 13–15, therefore between 0 and 1.22 m SD. We compare this to observations of the highstand in South America in section 5.4.2. Following the highstand, RSL appears to have slowly fallen indicated by SLIPs 16–20 between 2,700 cal yr BP and 500 cal yr BP (Fig. 5.4g–h). The SLIPs were taken immediately above the sand unit and thus are likely to be from the lower marsh, putting the RSL towards the upper estimate of the SLIPs. The Frederikse *et al.* (2021) SLIPs (21–35) show a 20th century RSL rise, although the difference between SLIPs 20 and 21 suggests that RSL rise began earlier. The rate of RSL rise calculated by Frederikse *et al.* (2021) (1.7 mm/yr) would need to be extended back 500 years to close the gap, which seems unlikely given late Holocene reconstructions (Kopp *et al.*, 2016). It therefore seems more likely that SLIP 20 may be under predicting RSL. Newton (2016) shows that a number of dated samples in the core SI-49 are younger than overlying ages through unit 4 most likely because of roots from above, suggesting that SLIP 20 may be inaccurate. The evidence suggests that following the sea-level highstand, a very gradual RSL fall occurred with relatively high sedimentation such that marsh emergence occurred and continued to accrete with steadily increasing rates of sea-level rise from some point in the last millennium through to the present day.

5.4.2   Regional sea-level comparison

RSL change has been studied at a number of sites along the Argentinian Atlantic coast using various methods although the quality of the data have been described as relatively poor, mainly due to problems constraining indicative meanings (Milne *et al.*, 2005, Prieto *et al.*, 2017). Despite these issues, all of the reconstructions from Argentina show a mid-Holocene highstand (Fig. 5.7). Regional and sub-regional differences in the timing and magnitude of the highstand are evident: up to 4 m above mean sea level in the Rio de la Plata at 6,200 – 4,900 cal yr BP (Cavallotto *et al.*, 2004, Prieto *et al.*, 2017); around 3.4 ± 0.6 m above mean sea level between 7,000 – 5,300 cal yr BP in Golfo San Jorge (Bini *et al.*, 2018); and between 1.5 – 6 m above mean sea level at around 6,000 cal yr BP in the most southerly part of the continent (Porter *et al.*, 1984, Borromei and Quattrocchio, 2007, Gordillo *et al.*, 1992). Neotectonics are shown to have affected the most southerly sites (Bentley and McCulloch, 2005), while the other sites may be affected by Andean uplift and the loading effects of the Patagonian and Antarctic ice sheets (Milne *et al.*, 2005). Notwithstanding the problems in the data from the mainland coastline, it appears that the highstand is larger and earlier than in the Falkland Islands, where it appears to occur just above or around 0 m above mean sea level at c 4,500 cal yr BP. The cause of the difference is likely to be the spatially varying signal from Antarctic ice-sheet melting and continental levering due to hydro-isostatic adjustment. The effects of continental levering on the continental mainland have been described for the region by Rostami *et al.* (2000) and Milne *et al.* (2005). Our reconstruction is the first to document the effect from offshore of the South American Atlantic coast. Having shown that a sea-level highstand likely occurred on the edge of the Patagonian continental shelf, its lower magnitude compared to the mainland offers an opportunity to tune GIA models which may be over or under-estimating its effect and help understand and model the effect of hyrdo-isostatic adjustment.
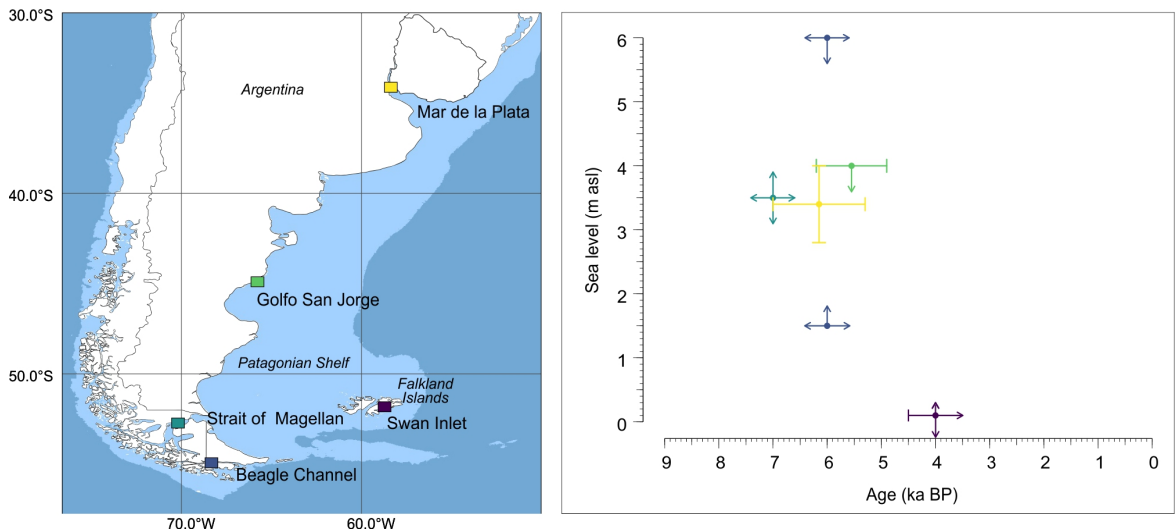
Figure 5.7: Compilation of reconstructions of the sea-level highstand from the southern Patagonian Shelf. The heights are given relative to mean local sea level. The bars show the uncertainty and where it is unknown it is represented by arrows that may be uni- or bi-directional.

5.4.3 GIA modelling

We compared the SLIPs with GIA model outputs using different ice-sheet histories to compare our data to simulated RSL (Fig. 5.6). None of the models produce a very good fit to our data, although with the ICE-5G and HUY3 ice-sheet histories provide simulations that broadly fit the pattern of RSL change. A number of different factors may explain the data - model misfit. Simply lowering the presented GIA simulations or raising our SLIPs would improve the fit; alternatively the GIA models may be providing inaccurate predictions because the wrong Earth models have been used, or there are processes at play not included in the models. Our SLIPs could be too low because we have not adjusted enough for post-decompositional lowering; however the modelled post-depositional lowering would need to be increased by an order of magnitude, which seems unlikely. We did not model palaeotides and although these may have varied, the large decrease in range that would be required to increase the elevation of RSL seems similarly unlikely. We only compared the effect of using different ice-sheet histories and only used a single Earth model, but the Falkland Islands may be more sensitive to mantle parameters than previously believed (Milne and Mitrovica, 2008). Furthermore, the GIA models may not be capturing all of the requisite processes, for example the influence of the Patagoninan Ice Sheet or continental levering. We suggest that no single process to raise or lower the SLIPs or model output respectively can explain

the data - model misfit, but a combination of these factors could close the gap. To resolve the discrepancies between modelled and observed Holocene sea-level changes in the Falkland Islands requires further work.

5.5   Conclusion

Following litho-, chrono- and biostratigraphical analyses we have developed the first dataset of Holocene sea-level index points for the Falkland Islands. The dataset provides a Holocene relative sea-level (RSL) reconstruction from 8,500 cal yr BP to present. We show that sea-level rise during the early Holocene was possibly punctuated by shorter periods of rapid rise and culminated in a sea-level highstand at c. 4,200 cal yr BP with a height close to present day mean sea level. In subsequent millennia RSL fell until a reversal to RSL rise some time in the last millennium. The highstand in the Falkland Islands is lower and later than the continental mainland demonstrating the probable effects of regional continental levering and ocean syphoning.

We suggest that the periods of rapid relative sea-level rise between 8,500–8,000 cal yr BP could be related to meltwater draining from the LIS prior to the 8.2 ka climate event. We cannot exclude that storms/tsunamis have also impacted the estuary.

GIA model predictions using the Antarctic and Laurentide ice-sheet histories in ICE-5G and HUY3 produce the most aligned predictions, although all produce a data - model mismatch. The mismatch between the RSL data and GIA model predictions indicate the importance of including appropriate solid Earth processes and parameters.

As a result of this study we suggest the following avenues of future research:

- Testing our hypothesis that the Falkland Islands were impacted by meltwater discharge originating from the LIS by locating and coring peats at an elevation of approximately 3–8 m below present sea level.

- More stratigraphic coastal studies to test whether the Falkland Islands may have been impacted by tsunami events during the Holocene.

- Further GIA modelling of the Falkland Islands and the continental mainland to understand and quantify the effects of continental levering on the Patagonian shelf.

Acknowledgements

CRediT roles.

Graham Rush: Methodology, Formal analysis, Investigation, Data curation, Writing - Original Draft, Visualization, Project administration, Funding acquisition. Tom Newton: Investigation. Ed Garrett: Supervision, Writing - Review & Editing. Mark Bateman: Supervision, Formal anlaysis, Writing - Review & Editing. Sarah Bradley: Formal analysis. Matthew Brain: Formal analysis. Mike Bentley: Investigation, Funding acquisition. Anthony Long: Investigation, Funding acquisition. Emma Brooks: Investigation. Tim Hill: Investigation. Tim Daley: Investigation, Funding acquisition. Roland Gehrels: Conceptualization, Methodology, Investigation, Supervision, Writing - Review & Editing, Project administration, Funding acquisition.

References

Adie, R. J. (1953), New Evidence of Sea-level Changes in the Falkland Islands: Falkland Islands Dependencies Survey Scientific Reports, V. No. 9, Technical report.

Aldiss, D. T. and Edwards, E. J. (1999), 'The geology of the Falkland Islands. British Geological Survey Technical Report WC/99/10'.

Allen, J. R. (2000), 'Morphodynamics of Holocene salt marshes: A review sketch from the Atlantic and Southern North Sea coasts of Europe', *Quaternary Science Reviews* **19**(12), 1155–1231.

Argus, D. F., Peltier, W. R., Drummond, R. and Moore, A. W. (2014), 'The Antarctica component of postglacial rebound model ICE-6G_C (VM5a) based on GPS positioning, exposure age dating of ice thicknesses, and relative sea level histories', *Geophysical Journal International* **198**(1), 537–563.

Bard, E., Hamelin, B., Arnold, M., Montaggioni, L., Cabioch, G., Faure, G. and Rougerie, F. (1996), 'Deglacial sea-level record from Tahiti corals and the timing of global meltwater discharge', *Nature* **382**(6588), 241–244.

Bateman, M. D. and Catt, J. A. (1996), 'An absolute chronology for the raised beach and associated deposits at Sewerby, East Yorkshire, England', *Journal of Quaternary Science* **11**(5), 389–395.

Bentley, M. J. and McCulloch, R. D. (2005), 'Impact of neotectonics on the record of glacier and sea level fluctuations, Strait of Magellan, southern Chile', *Geografiska Annaler: Series A, Physical Geography* **87**(2), 393–402.

Bentley, M. J., Ocofaigh, C., Anderson, J. B., Conway, H., Davies, B., Graham, A. G. C., Hillenbrand, C. D., Hodgson, D. A., Jamieson, S. S. R., Larter, R. D., Mackintosh, A., Smith, J. A., Verleyen, E., Ackert, R. P., Bart, P. J., Berg, S., Brunstein, D., Canals, M., Colhoun, E. A., Crosta, X., Dickens, W. A., Domack, E., Dowdeswell, J. A., Dunbar, R., Ehrmann, W., Evans, J., Favier, V., Fink, D., Fogwill, C. J., Glasser, N. F., Gohl, K., Golledge, N. R., Goodwin, I., Gore, D. B., Greenwood, S. L., Hall, B. L., Hall, K., Hedding, D. W., Hein, A. S., Hocking, E. P., Jakobsson, M., Johnson, J. S., Jomelli, V., Jones, R. S., Klages, J. P., Kristoffersen, Y., Kuhn, G., Leventer, A., Licht, K., Lilly,

K., Lindow, J., Livingstone, S. J., Massé, G., McGlone, M. S., McKay, R. M., Melles, M., Miura, H., Mulvaney, R., Nel, W., Nitsche, F. O., O'Brien, P. E., Post, A. L., Roberts, S. J., Saunders, K. M., Selkirk, P. M., Simms, A. R., Spiegel, C., Stolldorf, T. D., Sugden, D. E., van der Putten, N., van Ommen, T., Verfaillie, D., Vyverman, W., Wagner, B., White, D. A., Witus, A. E. and Zwartz, D. (2014), 'A community-based geological reconstruction of Antarctic Ice Sheet deglaciation since the Last Glacial Maximum', *Quaternary Science Reviews* **100**, 1–9.

Bini, M., Isola, I., Zanchetta, G., Pappalardo, M., Ribolini, A., Ragaini, L., Baroni, C., Boretto, G., Fuck, E., Morigi, C., Cristina Salvatore, M., Bassi, D., Marzaioli, F. and Terrasi, F. (2018), 'Mid-Holocene relative sea-level changes along Atlantic Patagonia: New data from Camarones, Chubut, Argentina', *The Holocene* **28**(1), 56–64.

Borromei, A. M. and Quattrocchio, M. (2007), 'Holocene sea-level change inferred from palynological data in the Beagle Channel, southern Tierra del Fuego, Argentina', *Ameghiniana* **44**(1), 161–171.

Bradley, S. L., Milne, G. A., Shennan, I. and Edwards, R. (2011), 'An improved glacial isostatic adjustment model for the British Isles', *Journal of Quaternary Science* **26**(5), 541–552.

Brain, M. J. (2015), Compaction, *in* I. Shennan, A. J. Long and B. P. Horton, eds, 'Handbook of Sea-level Research', 1 edn, John Wiley & Sons, Ltd, chapter 30, pp. 452–469.

Brain, M. J., Long, A. J., Petley, D. N., Horton, B. P. and Allison, R. J. (2011), 'Compression behaviour of minerogenic low energy intertidal sediments', *Sedimentary Geology* **233**(1-4), 28–41.

Brain, M. J., Long, A. J., Woodroffe, S. A., Petley, D. N., Milledge, D. G. and Parnell, A. C. (2012), 'Modelling the effects of sediment compaction on salt marsh reconstructions of recent sea-level rise', *Earth and Planetary Science Letters* **345-348**, 180–193.

Bronk Ramsey, C. (1995), 'Radiocarbon Calibration and Analysis of Stratigraphy: The OxCal Program', *Radiocarbon* **37**(2), 425–430.

Bronk Ramsey, C. (2009), 'Bayesian Analysis of Radiocarbon Dates', *Radiocarbon* **51**(1), 337–360.

Cavallotto, J. L., Violante, R. A. and Parker, G. (2004), 'Sea-level fluctuations during the last 8600 years in the de la Plata river (Argentina)', *Quaternary International* **114**(1), 155–165.

Clapperton, C. M. and Roberts, D. E. (1987), Quaternary sea level changes in the Falkland Islands , *in* J. Rabassa, ed., 'Quaternary of South America and Antarctic Peninsula', 1 edn, CRC Press, London, chapter 6.

Codignotto, J. O., Kokot, R. R. and Marcomini, S. C. (1992), 'Neotectonism and Sea-Level Changes in the Coastal Zone of Argentina', *Source: Journal of Coastal Research* **8**(1), 125–133.

De Lecea, A. M., Green, A. N., Strachan, K. L., Cooper, J. A. G. and Wiles, E. A. (2017), 'Stepped Holocene sea-level rise and its influence on sedimentation in a large marine embayment: Maputo Bay, Mozambique', *Estuarine Coastal and Shelf Science* **193**, 25–36.

Fairbanks, R. G. (1989), 'A 17,000-Year Glacio-Eustatic Sea-Level Record - Influence of Glacial Melting Rates on the Younger Dryas Event and Deep-Ocean Circulation', *Nature* **342**(6250), 637–642.

Frederikse, T., Adhikari, S., Daley, T., Dangendorf, S., Gehrels, R., Landerer, F., Marcos, M., Newton, T., Rush, G. and Slangen, A. (2021), 'Constraining 20th-century sea-level rise in the South Atlantic Ocean', *Journal of Geophysical Research: Oceans* **126**(3).

Gehrels, W. R., Belknap, D. F., Pearce, B. R. and Gong, B. (1995), 'Modeling the contribution of M2 tidal amplification to the Holocene rise of mean high water in the Gulf of Maine and the Bay of Fundy', *Marine Geology* **124**(1-4), 71–85.

Gehrels, W. R., Szkornik, K., Bartholdy, J., Kirby, J. R., Bradley, S. L., Marshall, W. A., Heinemeier, J. and Pedersen, J. B. (2006), 'Late Holocene sea-level changes and isostasy in western Denmark', *Quaternary Research* **66**(2), 288–302.

Gordillo, S., Bujalesky, G. G., Pirazzoli, P. A., Rabassa, J. O. and Saliège, J. F. (1992), 'Holocene raised beaches along the northern coast of the Beagle Channel, Tierra del Fuego, Argentina', *Palaeogeography, Palaeoclimatology, Palaeoecology* **99**(1-2), 41–54.

Gregory, J. M., Griffies, S. M., Hughes, C. W., Lowe, J. A., Church, J. A., Fukimori, I., Gomez, N., Kopp, R. E., Landerer, F., Cozannet, G. L., Ponte, R. M., Stammer,

D., Tamisiea, M. E. and van de Wal, R. S. (2019), 'Concepts and Terminology for Sea Level: Mean, Variability and Change, Both Local and Global', *Surveys in Geophysics* **40**(6), 1251–1289.

Hijma, M. P. and Cohen, K. M. (2010), 'Timing and magnitude of the sea-level jump preluding the 8200 yr event', *Geology* **38**(3), 275–278.

Hijma, M. P. and Cohen, K. M. (2019), 'Holocene sea-level database for the Rhine-Meuse Delta, The Netherlands: Implications for the pre-8.2 ka sea-level jump', *Quaternary Science Reviews* **214**, 68–86.

Hogg, A. G., Heaton, T. J., Hua, Q., Palmer, J. G., Turney, C. S., Southon, J., Bayliss, A., Blackwell, P. G., Boswijk, G., Bronk Ramsey, C., Pearson, C., Petchey, F., Reimer, P., Reimer, R. and Wacker, L. (2020), 'SHCal20 Southern Hemisphere Calibration, 0-55,000 Years cal BP', *Radiocarbon* **62**(4), 759–778.

Johnson, J. S., Nichols, K. A., Goehring, B. M., Balco, G. and Schaefer, J. M. (2019), 'Abrupt mid-Holocene ice loss in the western Weddell Sea Embayment of Antarctica', *Earth and Planetary Science Letters* **518**, 127–135.

Johnson, J. S., Roberts, S. J., Rood, D. H., Pollard, D., Schaefer, J. M., Whitehouse, P. L., Ireland, L. C., Lamp, J. L., Goehring, B. M., Rand, C. and Smith, J. A. (2020), 'Deglaciation of Pope Glacier implies widespread early Holocene ice sheet thinning in the Amundsen Sea sector of Antarctica', *Earth and Planetary Science Letters* **548**, 116501.

Kawamata, M., Suganuma, Y., Doi, K., Misawa, K., Hirabayashi, M., Hattori, A. and Sawagaki, T. (2020), 'Abrupt Holocene ice-sheet thinning along the southern Soya Coast, Lützow-Holm Bay, East Antarctica, revealed by glacial geomorphology and surface exposure dating', *Quaternary Science Reviews* **247**, 106540.

Kendall, R. A., Mitrovica, J. X., Milne, G. A., Tornqvist, T. E. and Li, Y. X. (2008), 'The sea-level fingerprint of the 8.2 ka climate event', *Geology* **36**(5), 423–426.

Khan, N. S., Ashe, E., Shaw, T. A., Vacchi, M., Walker, J., Peltier, W. R., Kopp, R. E. and Horton, B. P. (2015), 'Holocene Relative Sea-Level Changes from Near-, Intermediate-, and Far-Field Locations', *Current Climate Change Reports* **1**(4), 247–262.

Kingslake, J., Scherer, R. P., Albrecht, T., Coenen, J., Powell, R. D., Reese, R., Stansell, N. D., Tulaczyk, S., Wearing, M. G. and Whitehouse, P. L. (2018), 'Extensive retreat and re-advance of the West Antarctic Ice Sheet during the Holocene', *Nature* **558**(7710), 430–434.

Kopp, R. E., Kemp, A. C., Bittermann, K., Horton, B. P., Donnelly, J. P., Gehrels, W. R., Hay, C. C., Mitrovica, J. X., Morrow, E. D. and Rahmstorf, S. (2016), 'Temperature-driven global sea-level variability in the Common Era', *Proceedings of the National Academy of Sciences of the United States of America* **113**(11), E1434–E1441.

Lanesky, D. E., Logan, B. W., Brown, R. G. and Hine, A. C. (1979), 'A new approach to portable vibracoring underwater and on land', *Journal of Sedimentary Research* **49**(2), 654–657.

Lawrence, T., Long, A. J., Gehrels, W. R., Jackson, L. P. and Smith, D. E. (2016), 'Relative sea-level data from southwest Scotland constrain meltwater-driven sea-level jumps prior to the 8.2 kyr BP event', *Quaternary Science Reviews* **151**, 292–308.

Lecavalier, B. S., Milne, G. A., Simpson, M. J., Wake, L., Huybrechts, P., Tarasov, L., Kjeldsen, K. K., Funder, S., Long, A. J., Woodroffe, S., Dyke, A. S. and Larsen, N. K. (2014), 'A model of Greenland ice sheet deglaciation constrained by observations of relative sea level and ice extent', *Quaternary Science Reviews* **102**, 54–84.

Li, Y. X., Törnqvist, T. E., Nevitt, J. M. and Kohl, B. (2012), 'Synchronizing a sea-level jump, final Lake Agassiz drainage, and abrupt cooling 8200 years ago', *Earth and Planetary Science Letters* **315**, 41–50.

Milne, G. A., Long, A. J. and Bassett, S. E. (2005), 'Modelling Holocene relative sea-level observations from the Caribbean and South America', *Quaternary Science Reviews* **24**(10-11), 1183–1202.

Milne, G. A. and Mitrovica, J. X. (2008), 'Searching for eustasy in deglacial sea-level histories', *Quaternary Science Reviews* **27**(25-26), 2292–2302.

Mitrovica, J. X. and Milne, G. A. (2002), 'On the origin of late Holocene sea-level highstands within equatorial ocean basins', *Quaternary Science Reviews* **21**(20-22), 2179–2190.

Mitrovica, J. X., Tamisiea, M. E., Davis, J. L. and Milne, G. A. (2001), 'Recent mass balance of polar ice sheets inferred from patterns of global sea-level change', *Nature* **409**(6823), 1026–1029.

Murray, J. W. (2003), 'Patterns in the cumulative increase in species from foraminiferal time-series', *Marine Micropaleontology* **48**(1-2), 1–21.

Newton, T. (2016), Holocene and Common Era sea-level changes in the Falkland Islands, PhD thesis, Plymouth University.

Newton, T. L., Gehrels, W. R., Fyfe, R. M. and Daley, T. J. (2021), 'Reconstructing sea-level change in the Falkland Islands (Islas Malvinas) using salt-marsh foraminifera , diatoms and testate amoebae', *Marine Micropaleontology* **162**, 101923.

Nguyen, V. L., Ta, T. K. O. and Saito, Y. (2010), 'Early Holocene initiation of the Mekong River delta, Vietnam, and the response to Holocene sea-level changes detected from DT1 core analyses', *Sedimentary Geology* **230**(3-4), 146–155.

Nicholson, U., Libby, S., Tappin, D. R. and McCarthy, D. (2020), 'The Subantarctic Front as a sedimentary conveyor belt for tsunamigenic submarine landslides', *Marine Geology* **424**(July 2019), 106161.

Pappalardo, M., Baroni, C., Bini, M., Isola, I., Ribolini, A., Salvatore, M. C. and Zanchetta, G. (2019), 'Challenges in relative sea-level change assessment highlighted through a case study: The central coast of atlantic patagonia', *Global and Planetary Change* **182**, 103008.

Peltier, W. R. (2004), 'Global glacial isostasy and the surface of the ice-age earth: The ice-5G (VM2) model and grace', *Annual Review of Earth and Planetary Sciences* **32**, 111–149.

Peltier, W. R., Argus, D. F. and Drummond, R. (2015), 'Space geodesy constrains ice age terminal deglaciation: The global ICE-6G_C (VM5a) model', *Journal of Geophysical Research-Solid Earth* **120**(1), 450–487.

Porter, S. C., Stuiver, M. and Heusser, C. J. (1984), 'Holocene sea-level changes along the Strait of Magellan and Beagle Channel, southernmost South America', *Quaternary Research* **22**(1), 59–67.

Prieto, A. R., Mourelle, D., Peltier, W. R., Drummond, R., Vilanova, I. and Ricci, L. (2017), 'Relative sea-level changes during the Holocene in the Río de la Plata, Argentina and Uruguay: A review', *Quaternary International* **442**, 35–49.

PSMSL (2020), 'Pearmanent Service for Mean Sea Level: Tide Gauge Data'.

Roberts, D. E. (1984), Quaternary history of the Falklands, PhD thesis, University of Aberdeen.

Rostami, K., Peltier, W. R. and Mangini, A. (2000), 'Quaternary marine terraces, sea-level changes and uplift history of Patagonia, Argentina: Comparisons with predictions of the ICE-4G (VM2) model of the global process of glacial isostatic adjustment', *Quaternary Science Reviews* **19**(14-15), 1495–1525.

Rush, G., Garrett, E., Bateman, M., Bigg, G., Hibbert, F., Smith, D. and Gehrels, W. R. (in review), 'Relative sea-level reconstruction for the Ythan Estuary, eastern Scotland, and implications for the cause of the 8.2 ka climate event', *Quaternary Science Reviews* .

Sanderson, D. C. and Murphy, S. (2010), 'Using simple portable OSL measurements and laboratory characterisation to help understand complex and heterogeneous sediment sequences for luminescence dating', *Quaternary Geochronology* **5**(2-3), 299–305.

Small, D., Bentley, M. J., Jones, R. S., Pittard, M. L. and Whitehouse, P. L. (2019), 'Antarctic ice sheet palaeo-thinning rates from vertical transects of cosmogenic exposure ages', *Quaternary Science Reviews* **206**, 65–80.

Stuiver, M. and Polach, H. A. (1977), ' Discussion Reporting of 14 C Data ', *Radiocarbon* **19**(3), 355–363.

Tamura, T., Saito, Y., Sieng, S., Ben, B., Kong, M., Sim, I., Choup, S. and Akiba, F. (2009), 'Initiation of the Mekong River delta at 8 ka: evidence from the sedimentary succession in the Cambodian lowland', *Quaternary Science Reviews* **28**(3–4), 327–344.

Tjallingi, R., Stattegger, K., Stocchi, P., Saito, Y. and Wetzel, A. (2014), 'Rapid flooding of the southern Vietnam shelf during the early to mid-Holocene', *Journal of Quaternary Science* **29**(6), 581–588.

Törnqvist, T. E., Bick, S. J., Gonzalez, J. L., van der Borg, K. and de Jong, A. F. M. (2004), 'Tracking the sea-level signature of the 8.2 ka cooling event: New constraints from the Mississippi Delta', *Geophysical Research Letters* **31**(23).

Troels-Smith, J. (1955), 'Karakterisering af lose jordarter. Characterization of unconsolidated sediments', *Geologiske Undersagelse, Raekke* .

Upton, J. and Shaw, C. (2002), 'An overview of the oceanography and meteorology of the Falkland Islands', *Aquatic Conservation: Marine and Freshwater Ecosystems* **12**(1), 15–25.

Wang, Z. H., Zhan, Q., Long, H. Y., Saito, Y., Gao, X. Q., Wu, X. X., Li, L. and Zhao, Y. A. (2013), 'Early to mid-Holocene rapid sea-level rise and coastal response on the southern Yangtze delta plain, China', *Journal of Quaternary Science* **28**(7), 659–672.

Watcham, E. P., Shennan, I. and Barlow, N. L. M. (2013), 'Scale considerations in using diatoms as indicators of sea-level change: lessons from Alaska', *Journal of Quaternary Science* **28**(2), 165–179.

Wilmes, S. and Green, J. A. M. (2014), 'The evolution of tides and tidal dissipation over the past 21,000 years', *Journal of Geophysical Research: Oceans* **119**(7), 4083–4100.

Woodworth, P. L., Pugh, D. T. and Bingley, R. M. (2010), 'Long-term and recent changes in sea level in the Falkland Islands', *Journal of Geophysical Research-Oceans* **1115**.

Xiong, H., Zong, Y., Li, T., Long, T., Huang, G. and Fu, S. (2020), 'Coastal GIA processes revealed by the early to middle Holocene sea- level history of east China', *Quaternary Science Reviews* **233**, 106249.

Yokoyama, Y., Okuno, J., Miyairi, Y., Obrochta, S., Demboya, N., Makino, Y. and Kawahata, H. (2012), 'Holocene sea-level change and Antarctic melting history derived from geological observations and geophysical modeling along the Shimokita Peninsula, northern Japan', *Geophysical research letters* **39**(13).

Yu, S. Y., Berglund, B. E., Sandgren, P. and Lambeck, K. (2007), 'Evidence for a rapid sea-level rise 7600 yr ago', *Geology* **35**(10), 891–894.

Zanchetta, G., Bini, M., Isola, I., Pappalardo, M., Ribolini, A., Consoloni, I., Boretto, G., Fucks, E., Ragaini, L. and Terrasi, F. (2014), 'Middle- to late-Holocene relative sea-level changes at Puerto Deseado (Patagonia, Argentina)', *The Holocene* **24**(3), 307–317.

Zong, Y. Q., Huang, K. Y., Yu, F. L., Zheng, Z., Switzer, A., Huang, G. Q., Wang, N. and
    Tang, M. (2012), 'The role of sea-level rise, monsoonal discharge and the palaeo-landscape
    in the early Holocene evolution of the Pearl River delta, southern China', *Quaternary
    Science Reviews* **54**, 77–88.

Summary

In this chapter I have presented a Holocene RSL reconstruction for Swan Inlet. The results are important as they provide the opportunity to study the Holocene ice-sheet histories and GIA models. The original conception of my study was to build on the work of Newton (2016) and quantify the magnitude of the rapid sea-level rise and hence the meltwater pulse prior to the 8.2 ka climate event. However, the original hypothesis - that the sand unit was deposited during a short period around 8,400 cal yr BP, proved to be incorrect and thus I was unable to do as originally planned. The results suggest that a rapid sea-level rise occurred prior to the start of the RSL reconstruction and that a sea-level event resulted in drowning of the marsh at c. 8,200 cal yr BP. I link these events to the 8.2 ka climate event and explore the implications further in Chapter 6 alongside the results presented in Chapter 4.

Chapter 6

Conclusions

6.1 Introduction

This study set out to test three hypotheses related to the meltwater pulses that are believed to have forced the 8.2 ka climate event, namely:

1. That there was only one meltwater pulse in the centuries leading up to the 8.2 ka climate event.

2. That Lake Agassiz-Ojibway (LAO) was the source of the meltwater pulse(s) without contributions from the Hudson Bay Ice Saddle (HBIS).

3. That the origin of the meltwater pulse(s) was the Laurentide Ice Sheet (LIS).

The thesis focused on two sites: the Ythan Estuary on the east coast of Scotland (Chapters 3 and 4), and Swan Inlet in the Falkland Islands (Chapter 5). The sites were chosen because previous research indicated that a rapid sea-level rise was recorded that produced widespread drowning c. 8,500 cal yr BP at each site (Chapter 2). In this chapter, the main findings from Chapters 3, 4 and 5 are reviewed and linked to the three hypotheses.

6.2 North Sea foraminifera transfer function

Chapter 3 presented a modern foraminifera training set for the Ythan Estuary. The surface assemblages of foraminifera from the inter-tidal zone show a relationship with elevation relative to sea level that make them suitable sea-level indicators. The results demonstrate that the Ythan Estuary training set alone is not suitable for predicting early-Holocene sea

level at the site because the modern assemblages do not provide appropriate analogues for the fossil assemblages. To overcome this problem a regional training set was developed by incorporating existing data from around the coast of the North Sea basin. Different methods were applied in order to make a robust decision on which transfer function to apply to accurately predict indicative meanings of fossil assemblages, including which data to include in the training set and which numerical model to use. This is an important step, as although continuous RSL reconstructions have been widely applied to reconstruct late-Holocene RSL with high-precision, prioritising accuracy whilst retaining reasonable precision is imperative for early-Holocene reconstructions when it is unlikely that conditions were similar to present day. The final transfer function provides accurate indicative meanings for the fossil assemblages that enables RSL to be reconstructed for the Ythan Estuary with a precision of around 40 cm.

6.3 Ythan Estuary relative sea-level reconstruction

Based on a high-resolution chronological model, the foraminifera transfer function and subsequent analysis a well-resolved continuous RSL reconstruction between c. 8,800–8,100 cal yr BP was produced for the Ythan Estuary in Chapter 4. The probabilistic analysis incorporated the full uncertainties of the data to identify and constrain the timing and magnitude of two sea-level events (SLEs). The SLEs are interpreted as having occurred as a result of three meltwater pulses at $8,610 \pm 5$ to $8,495 \pm 10$ cal yr BP (YSLE^{1a}), $8,495 \pm 10$ to $8,340 \pm 5$ cal yr BP (YSLE^{1b}) and $8,240 \pm 15$ to $8,190 \pm 15$ cal yr BP (YSLE^{2}). After correction for the barystatic-GRD fingerprint, the 2σ global magnitude of the meltwater pulses were calculated to be 0.91–1.92 m (YSLE^{1a}), 1.64–2.81 m (YSLE^{1b}) and 0.00–0.48 m (YSLE^{b}).

The evidence for multiple SLEs at the Ythan Estuary are in agreement with RSL reconstructions from sites in the Netherlands (Hijma and Cohen, 2019) and the west coast of Scotland that was re-modelled in Chapter 4, which all register more than one SLE. Although the relatively small magnitude of the final meltwater pulse c. 8,200 cal yr BP makes it hard to detect (< 0.4 m of global mean sea-level rise), a contemporaneous SLE has now been identified at multiple different sites demonstrating that a meltwater-driven barystatic sea-level rise is most likely the cause, as opposed to processes local to the given sites. A larger

SLEs is registered at the Ythan Estuary between 8,600 and 8,300 cal yr BP, and again in the Netherlands (Hijma and Cohen, 2019) and western Scotland (Lawrence *et al.*, 2016) that is interpreted to contain two stages suggesting meltwater pulses also occurred during this time period. Indeed these earlier stages also coincide with numerous apparent drowning events and periods of rapid sea-level rise elsewhere around the Earth (see Fig. 6.1), possibly including Swan Inlet (Chapter 5). The results from the Ythan Estuary add to the evidence that there was more than one meltwater pulse; however, they do not permit hypothesis 1 to be definitively rejected. The close timing may make identifying possible distinct events within the first SLE elusive at other sites, but because they will contain a larger local magnitude, at suitable far-field sites it may be possible to identify any small second SLE.

Having added evidence to the hypothesis that that there were multiple meltwater pulses, I now consider the second hypothesis and whether LAO was the sole contributor through multiple drainage and re-filling episodes as has been proposed (e.g. Ellison *et al.*, 2006, Li *et al.*, 2012). The maximum volume of LAO has been shown to be equivalent to < 0.4 m of global barystatic sea-level rise (Teller *et al.*, 2002, Godbout *et al.*, 2020). The results from the Ythan Estuary, together with the reanalysis of the Cree Estuary data, show that the magnitude of the two stages of the SLE within the first phase are too large to have originated from LAO drainage alone (see Fig. 4.7). Based on the large magnitude of the SLEs it is suggested in Chapter 5 that the collapse of the HBIS contributed the majority of the freshwater. This interpretation is supported by evidence from various sources, including ice-sheet modelling (Gregoire *et al.*, 2012, Matero *et al.*, 2020), submarine sediments (Lochte *et al.*, 2019) and terrestrial sediments (Gauthier *et al.*, 2020). Hypothesis 2, that LAO was the source of the meltwater pulse(s) without contributions from the HBIS, is therefore rejected.

Contrary to previous experiments using LAO drainage as the input (e.g. Morrill *et al.*, 2014), Matero *et al.* (2020) demonstrated in a global climate model freshwater hosing experiment (whereby a freshwater pulse equivalent to the HBIS collapse is added to the Atlantic Ocean through Hudson Bay), that models can produce a climate signal similar to the 8.2 ka climate event. Research should continue to focus on the role of the HBIS collapse, along with LAO contributions, on cyrosphere-hydrosphere-atmosphere interactions.

6.4   Swan Inlet relative sea-level reconstruction

The study of Swan Inlet presented in Chapter 5 was originally designed to constrain the timing and magnitude of an apparent SLE that was observed by Newton (2016) but this proved elusive. ^{14}C and OSL dating showed the drowning identified by Newton (2016) was indicative of a longer series of events and the lack of modern analogues for the microfossil assemblages prevented precise indicative meanings from being obtained that would have allowed rapid changes in water depth to be quantified. The stratigraphic and chronological analyses did suggest however, that two periods of rapid RSL rise are registered that are contemporaneous with those at the Ythan Estuary, the first ending at $\sim$ 8,430 cal yr BP and the second beginning at $\sim$ 8,260 cal yr BP. Although it was not possible to constrain the timing further or quantify the magnitude of sea-level change and hence define them as SLEs, the two periods are proposed to be linked to the 8.2 ka climate event and provide a degree of evidence for the occurrence of meltwater pulses, as discussed below.

Although the original objective of the study was not met, the results generated some important additional outcomes that allowed for different analysis and conclusions to be drawn. The research produced 20 sea-level index points (SLIPs) from c. 8,500 to present day and therefore provided the first Holocene RSL reconstruction for the Falkland Islands. Interpretations of the results showed a RSL rise from c. 8,500 cal yr BP until the occurrence of a sea-level highstand c. 4,200 cal yr BP, and a subsequent small RSL fall until RSL rise began again some time in the late Holocene. The results were compared to regional RSL reconstructions and glacial-isostatic adjustment (GIA) model predictions and demonstrate the probable effects of continental levering.

The primary reason for studying RSL change at a Southern Hemisphere site was to be able to compare records of SLEs from regions of the Earth that should register differing magnitudes depending on the geographical source of meltwater and test hypothesis 3. The lack of firm constraints for the age and magnitude of SLEs at Swan Inlet limit the ability to test hypothesis 3 because the other sites of registered SLEs are all within a region of similar predicted magnitude. In order to attempt to do so, I turn to other far-field locations where evidence of rapid sea-level rise around 8,500 cal yr BP has come to light, in particular southeast Asia where multiple sites show evidence of drowning and rapid sea-level rise.

The RSL reconstructions from southeast Asia, identified in Chapter 2, for the Mekong Delta (Tamura *et al.*, 2009, Nguyen *et al.*, 2010, Tjallingi *et al.*, 2014), Pearl Delta (Zong
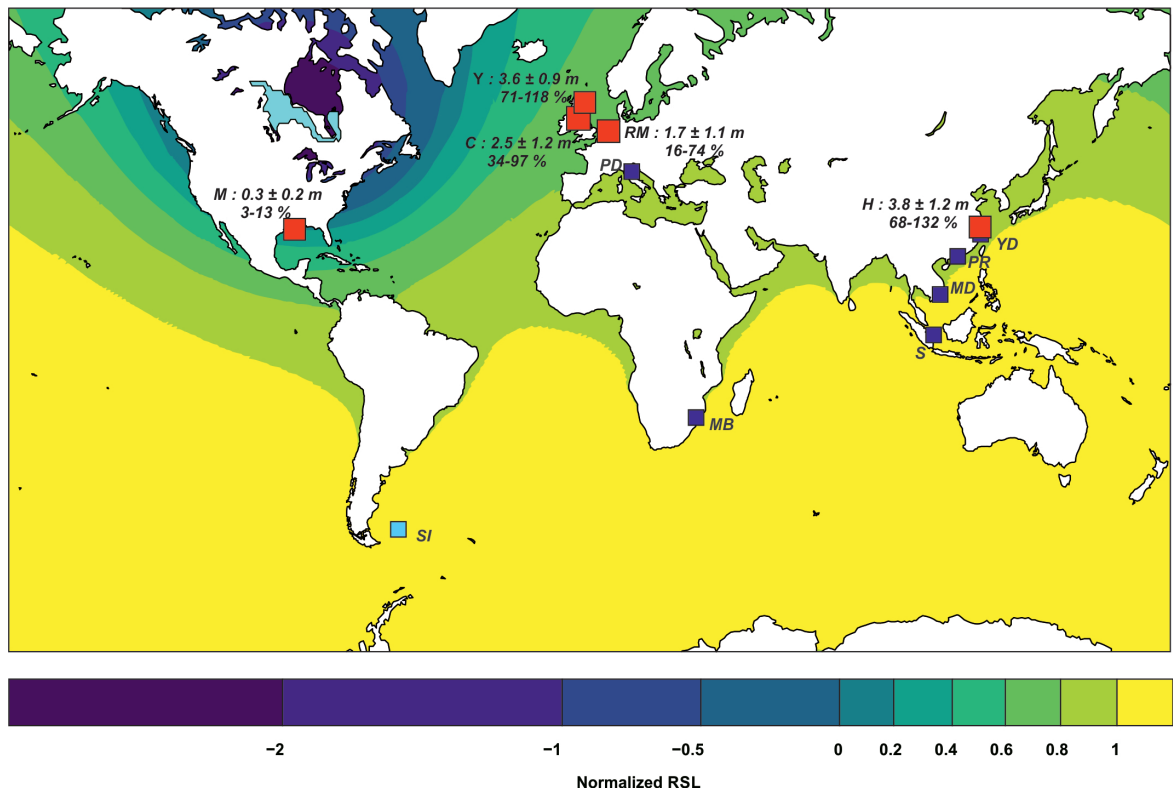
Figure 6.1: Numerically predicted Barystatic-GRD fingerprint following the drainage of LAO (light blue) at c. 8,400 cal yr BP, normalized by the global mean sea-level rise by Kendall et al. (2008). Sites with quantified magnitudes are shown in red: M = Mississippi Delta, C = Cree Estuary, Y = Ythan Estuary, RM = Rhine-Meuse Delta and H = Hangzou Bay. The local magnitude is given along with the percentage of the global mean (assuming a 100 % magnitude of 3.8 m). Sites where a large drowning event is registered but not quntified c. 8500 cal yr BP are shown by the blue boxes (PD = Po Delta, MB = Maputo Bay, S = Singapore, MD = Mekong Delta, PR = Pearl River Delta, YD = Yangtze Delta. Swan Inlet (SI) is also shown.

et al., 2012), Yangtze Delta (Wang *et al.*, 2013) and Hangzou Bay (Xiong *et al.*, 2020) all display periods of rapid RSL rise between 8,600 and 8,300 cal yr BP, where rates of ~ 30 mm yr^{-1} set against longer term background rates of ~ 10 mm yr^{-1} appear evident. GIA modelling shows that rates of RSL rise across the region were very similar, although the predicted rates between 9000 and 8000 cal yr BP are lower than the data (~ 7 mm yr^{-1}) (Bradley *et al.*, 2016). The most well-resolved RSL reconstruction for the period, from Hangzou Bay, shows a RSL rise of approximately 6.74 m from c. 8,539–8,476 to 8,341–8,176 cal yr BP, equivalent to ~ 32 mm yr^{-1} (Xiong *et al.*, 2020). Taking the mean start and end dates and correcting for a background rate of ~ 14 mm yr^{-1} (calculated from the difference between subsequent SLIPs), produces a calculation for the magnitude of the apparent SLE of 3.8 m $\pm$ 1.2 m

(taking the difference between the oldest to youngest dates and vice versa to calculate the rates for the uncertainty). The estimations are somewhat approximate but provide a first estimate for the magnitude of a large SLE beginning around 8,500 cal yr BP that appears to be registered widely in southeast Asia. The estimation for Hangzou Bay, approximately equivalent to the global mean, is added to the existing sites and plotted against the predicted barystatic-GRD fingerprint of LAO drainage in Fig. 6.1 to attempt to test hypothesis 3.

Given the relative local magnitudes of the sites the estimations are consistent with an LIS origin, but a number of caveats mean it is not possible to rule out contributions from other ice sheets and hypothesis 3 cannot therefore be rejected, namely:

1) The numerical predictions of the fingerprint are based on LAO drainage and do not consider the mass balance change of the LIS. For example, Kendall *et al.* (2008) note that the Mississippi Delta would record 40 % of the global magnitude when HBIS loss is included, as opposed to 25 % from LAO drainage alone.

2) The estimate from Hangzou Bay is speculative and as yet the magnitude remains poorly quantified from far-field regions.

3) Although no direct evidence of large Antarctic derived meltwater is available, it is uncertain what the effect of adding contributions would do to the spatial pattern of sea-level and needs testing.

6.5   Future work

This research aimed to test three hypotheses. The research suggests that more than one meltwater pulse preceded the 8.2 ka climate event although this is not definitively confirmed by the analysis, but it has been shown that LAO was not the sole source. Although it cannot be ruled out that the other large ice sheets did not contribute large volumes of freshwater, it appears likely that the HBIS collapse contributed the majority of the freshwater. Although hypothesis 3 could not be tested, the method of plotting data against numerically predicted spatial patterns of sea-level rise provides the potential to fingerprint the origin of meltwater pulses, but relies on both accurate models and RSL data. Based on the investigations I suggest that numerical predictions of the barystatic-GRD fingerprint resulting from HBIS collapse and high-resolution reconstructions from far-field sites are required in order to fingerprint the source.

Additional outcomes from the study lead to further recommendations for future work. Chapter 3 applied a series of quantitative and qualitative techniques and a similar approach is recommended in future studies, prioritising accuracy over precision, when applying transfer functions to reconstruct early-Holocene sea level. Following the Swan Inlet RSL reconstruction, it is evident that further work is required to close the discrepancy between data and GIA model predictions to explore the spatially variable high-stand signal and the underlying causes. GIA modelling developing on the work of Milne *et al.* (2005) is recommended looking at a broader range of earth model parameters alongside updated ice-sheet contributions to global mean sea-level rise. The quality of the SLIPs for the continental mainland also needs addressing. Salt marshes are plentiful on the southern South Atlantic coastline and thus appear worth investigating as they may well provide the opportunity to improve the quality of SLIPs for the region.

References

Bradley, S. L., Milne, G. A., Horton, B. P. and Zong, Y. Q. (2016), 'Modelling sea level data from China and Malay-Thailand to estimate Holocene ice-volume equivalent sea level change', *Quaternary Science Reviews* **137**, 54–68.

Gauthier, M. S., Kelley, S. E. and Hodder, T. J. (2020), 'Lake Agassiz drainage bracketed Holocene Hudson Bay Ice Saddle collapse', *Earth and Planetary Science Letters* **544**, 116372.

Godbout, P. M., Roy, M. and Veillette, J. J. (2020), 'A detailed lake-level reconstruction shows evidence for two abrupt lake drawdowns in the late-stage history of the eastern Lake Agassiz-Ojibway basin', *Quaternary Science Reviews* **238**, 106327.

Gregoire, L. J., Payne, A. J. and Valdes, P. J. (2012), 'Deglacial rapid sea level rises caused by ice-sheet saddle collapses', *Nature* **487**(7406), 219–222.

Hijma, M. P. and Cohen, K. M. (2019), 'Holocene sea-level database for the Rhine-Meuse Delta, The Netherlands: Implications for the pre-8.2 ka sea-level jump', *Quaternary Science Reviews* **214**, 68–86.

Kendall, R. A., Mitrovica, J. X., Milne, G. A., Tornqvist, T. E. and Li, Y. X. (2008), 'The sea-level fingerprint of the 8.2 ka climate event', *Geology* **36**(5), 423–426.

Lawrence, T., Long, A. J., Gehrels, W. R., Jackson, L. P. and Smith, D. E. (2016), 'Relative sea-level data from southwest Scotland constrain meltwater-driven sea-level jumps prior to the 8.2 kyr BP event', *Quaternary Science Reviews* **151**, 292–308.

Lochte, A. A., Repschlaeger, J., Kienast, M., Garbe-Schoenberg, D., Andersen, N., Hamann, C. and Schneider, R. (2019), 'Labrador Sea freshening at 8.5 ka BP caused by Hudson Bay Ice Saddle collapse', *Nature Communications* **10**(1), 1–9.

Matero, I. S. O., Gregoire, L. J. and Ivanovic, R. F. (2020), 'Simulating the Early Holocene demise of the Laurentide Ice Sheet with BISICLES', *Geoscientific Model Development* **13**(9), 4555–4577.

Milne, G. A., Long, A. J. and Bassett, S. E. (2005), 'Modelling Holocene relative sea-level

observations from the Caribbean and South America', *Quaternary Science Reviews* **24**(10-11), 1183–1202.

Newton, T. (2016), Holocene and Common Era sea-level changes in the Falkland Islands, PhD thesis, Plymouth University.

Nguyen, V. L., Ta, T. K. O. and Saito, Y. (2010), 'Early Holocene initiation of the Mekong River delta, Vietnam, and the response to Holocene sea-level changes detected from DT1 core analyses', *Sedimentary Geology* **230**(3-4), 146–155.

Tamura, T., Saito, Y., Sieng, S., Ben, B., Kong, M., Sim, I., Choup, S. and Akiba, F. (2009), 'Initiation of the Mekong River delta at 8 ka: evidence from the sedimentary succession in the Cambodian lowland', *Quaternary Science Reviews* **28**(3–4), 327–344.

Teller, J. T., Leverington, D. W. and Mann, J. D. (2002), 'Freshwater outbursts to the oceans from glacial Lake Agassiz and their role in climate change during the last deglaciation', *Quaternary Science Reviews* **21**(8-9), 879–887.

Tjallingi, R., Stattegger, K., Stocchi, P., Saito, Y. and Wetzel, A. (2014), 'Rapid flooding of the southern Vietnam shelf during the early to mid-Holocene', *Journal of Quaternary Science* **29**(6), 581–588.

Wang, Z. H., Zhan, Q., Long, H. Y., Saito, Y., Gao, X. Q., Wu, X. X., Li, L. and Zhao, Y. A. (2013), 'Early to mid-Holocene rapid sea-level rise and coastal response on the southern Yangtze delta plain, China', *Journal of Quaternary Science* **28**(7), 659–672.

Xiong, H., Zong, Y., Li, T., Long, T., Huang, G. and Fu, S. (2020), 'Coastal GIA processes revealed by the early to middle Holocene sea- level history of east China', *Quaternary Science Reviews* **233**, 106249.

Zong, Y. Q., Huang, K. Y., Yu, F. L., Zheng, Z., Switzer, A., Huang, G. Q., Wang, N. and Tang, M. (2012), 'The role of sea-level rise, monsoonal discharge and the palaeo-landscape in the early Holocene evolution of the Pearl River delta, southern China', *Quaternary Science Reviews* **54**, 77–88.

Appendix A
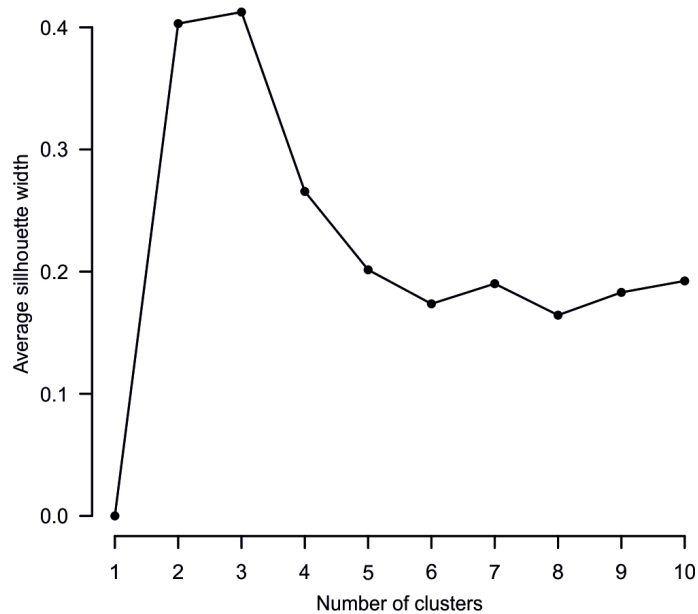
Supplementary information: Chapter 3

Figure A.1: The effect of the number of clusters on the average silhouette width for the *North Sea* training set.

Table A.1: Taxonomic information of all species used in the North Sea training set.

| Foraminifera taxa	Reference
Ammobaculites spp.	Cushman, 1910
Ammodiscus spp.	Reuss, 1862
Ammonia spp.	Brünnich, 1771
Balticammina pseudomacrescens	Brönnimann, Lutze & Whitakker, 1989
Brizalina inflata	Heron-Allen & Earland, 1913
Brizalina pseudopunctata	Höglund, 1947
Brizalina variabilis	Williamson, 1858
Bulimina marginata	d'Orbigny, 1826
Buliminella elegantissima	d'Orbigny, 1839
Cassidulina obtusa	Williamson, 1858
Cibicides lobatulus	Jauhari, 1978
Cornuspira involvens	Reuss, 1850
Cyclogyra involvens	Reuss, 1850
Elphidium earlandi	Cushman, 1936
Elphidium excavatum	Terquem, 1875
Elphidium gerthi	van Voorthuysen, 1957
Elphidium incertum	Williamson, 1858
Elphidium magellanicum	Heron-Allen & Earland, 1932
Elphidium margaritaceum	Cushman, 1950
Elphidium spp.	Montfort, 1808
Elphidium williamsoni	Haynes, 1973
Fissurina lucida	Williamson, 1858
Fissurina marginata	Sequenza, 1862
Gavelinopsis praegeri	Heron-Allen & Earland, 1913
Glabratella millettii	Wright, 1911
Globigerina quinqueloba	Natland, 1938
Haplophragmoides spp.	Cushman, 1910
Haynesina germanica	Ehrenberg, 1840
Entzia macrescens	Brady, 1870
Lagena elongata	Dunikowski, 1879
Lagena semistriata	Williamson, 1848
Lagena sulcata	Walker & Jacob, 1798
Lamarckina haliotidea	Heron-Allen & Earland, 1911
Melonis barleeanus	Williamson, 1858
Miliammina fusca	Brady, 1870
Miliolinella subrotunda	Montagu, 1803
Nonion spp.	Montfort, 1808
Nonionoides turgidus	Williamson, 1858
Paratrochammina haynesi	Atkinson , 1969
Paratrochammina spp.	Brönnimann, 1979
Patellina corrugata	Williamson, 1858
Pateoris hauerinoides	Rhumbler, 1936
Planorbulina mediterranensis	d'Orbigny, 1826
Quinqueloculina spp.	d'Orbigny, 1826
Reophax scottii	Chaster, 1892
Rosalina spp.	d'Orbigny, 1826
Rosalina williamsoni	Chapman & Parr, 1932
Spirillina vivipara	Ehrenberg, 1841
Spiroloculina excavata	d'Orbigny, 1846
Spiroloculina rotunda	d'Orbigny, 1826
Stainforthia fusiformis	Williamson, 1858
Tiphotrocha comprimata	Cushman and Bröennimann, 1948
Trochammina inflata	Montagu, 1808
Trochammina ochracea	Williamson, 1858
Trochammina squamata	Jones & Parker, 1860
Trochamminita spp.	Cushman and Bröennimann, 1948
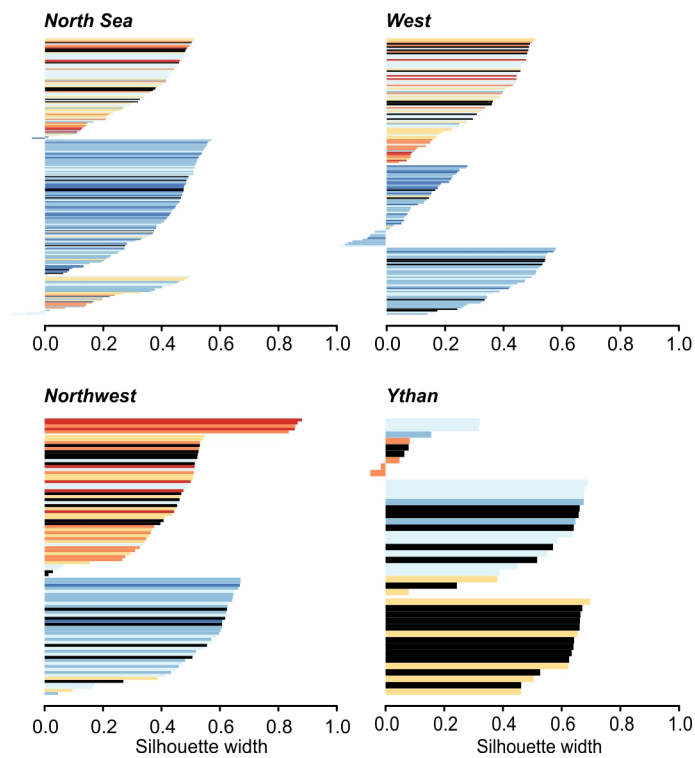
Figure A.2: Cluster analysis of training sets and fossil data showing the clustering of modern samples and A7.5 fossil samples for each region identified using PAM. The bars for the modern samples are coloured from light orange to dark blue according to SWLI (¡100: red, 100-125: orange, 125-150: yellow, 150-175: pale blue, 175-200: blue, ¿200: dark blue) and the fossil samples are coloured black. Average sillhouette widths: North Sea = 0.36, West = 0.36, Northwest = 0.48, Ythan = 0.47.

Table A.2: The five closest modern analogues (1–5) for each of the fossil samples in core A7.5 using the modern analogue technique (MAT) with squared chord dissimilarity coefficient. The site and SWLI of the modern analogue is shown for each of the fossil samples from 1 (closest) to 5.

Sample depth (m)	Analogue 1		Analogue 2		Analogue 3		Analogue 4		Analogue 5	
-0.29	Ythan	139	Welwick	163	Ythan	137	Welwick	169	Welwick	162
-0.39	Ythan	139	Ythan	137	Welwick	163	Welwick	170	Welwick	169
-0.53	Alnmouth	137	Cowpen	172	Welwick	170	Cowpen	170	Thornham	171
-0.69	Ythan	139	Welwick	163	Welwick	162	Welwick	169	Welwick	163
-0.77	Ythan	139	Ythan	137	Ythan	140	Ythan	133	Ythan	130
-0.85	Ythan	139	Ythan	137	Ythan	133	Ythan	130	Ythan	140
-1.01	Ythan	139	Ythan	133	Ythan	137	Ythan	130	Ythan	140
-1.25	Ythan	139	Ythan	137	Ythan	133	Ythan	130	Ythan	140
-1.41	Ythan	139	Cowpen	135	Welwick	169	Ythan	133	Ythan	137
-1.57	Brancaster	175	Brancaster	162	Welwick	169	Cowpen	135	Thornham	171
-1.65	Brancaster	181	Brancaster	184	Brancaster	180	Brancaster	184	Kjelst	162
-1.73	Ythan	179	Alnmouth	188	Ythan	150	Kjelst	159	Cowpen	209
-1.81	Ythan	148	Ythan	150	Cowpen	180	Kjelst	159	Ythan	173
-2.21	Ythan	153	Alnmouth	188	Ythan	150	Ythan	154	Ythan	179
-2.37	Alnmouth	188	Ythan	179	Ythan	153	Kjelst	189	Thornham	196
-2.61	Ythan	148	Brancaster	185	Ythan	173	Cowpen	178	Cowpen	182
-2.93	Brancaster	185	Ythan	148	Ythan	173	Cowpen	178	Cowpen	179

Appendix B

Supplementary information: Chapter 4

Table B.1: Details of the sea-level index points from core A7.5 including the sources of uncertainty.

| Sample	Core depth (m)	Elevation (m OD)	Indicative meaning (m OD)		Compaction correction (m)	Corrected RSL (m OD)	Vertical uncertainty (m)							Corrected positive RSL	Corrected negative RSL	Age (cal yr BP)	
			Modern tide	Palaeotide-corrected Indicative meaning			Indicative meaning	Sample thickness	Sampling	Core shortening /stretching	Non-vertical drilling	Palaeotide	Compaction correction			Mean	Uncertainty
1	2.28	-0.28	1.38	1.01	0.10	-1.16	0.33	0.01	0.01	0.01	0.05	0.15	0.04	0.37	0.37	8154	65
2	2.38	-0.31	1.32	0.98	0.10	-1.15	0.33	0.01	0.01	0.01	0.05	0.15	0.04	0.37	0.37	8168	78
3	2.52	-0.45	1.28	0.95	0.10	-1.26	0.33	0.01	0.01	0.01	0.05	0.15	0.04	0.37	0.37	8234	118
4	2.68	-0.61	1.35	0.99	0.10	-1.47	0.33	0.01	0.01	0.01	0.05	0.15	0.05	0.37	0.37	8281	118
5	2.76	-0.69	1.05	0.80	0.10	-1.35	0.35	0.01	0.01	0.01	0.06	0.15	0.05	0.39	0.38	8294	116
6	2.84	-0.77	1.14	0.85	0.10	-1.49	0.35	0.01	0.01	0.01	0.06	0.15	0.05	0.39	0.38	8307	112
7	3.00	-0.93	1.19	0.89	0.10	-1.69	0.35	0.01	0.01	0.01	0.06	0.15	0.05	0.39	0.38	8333	104
8	3.24	-1.17	1.17	0.88	0.10	-1.91	0.35	0.01	0.01	0.01	0.06	0.15	0.06	0.39	0.38	8372	86
9	3.40	-1.33	1.16	0.87	0.10	-2.07	0.33	0.01	0.01	0.01	0.07	0.15	0.06	0.38	0.37	8398	69
10	3.56	-1.49	1.39	1.02	0.10	-2.38	0.33	0.01	0.01	0.01	0.07	0.15	0.06	0.38	0.37	8424	41
11	3.64	-1.57	1.66	1.20	0.10	-2.64	0.35	0.01	0.01	0.01	0.07	0.15	0.06	0.40	0.38	8430	39
12	3.72	-1.65	1.92	1.37	0.10	-2.89	0.33	0.01	0.01	0.01	0.07	0.15	0.07	0.38	0.37	8436	41
13	3.80	-1.73	1.89	1.35	0.10	-2.95	0.35	0.01	0.01	0.01	0.08	0.15	0.07	0.40	0.38	8443	45
14	4.20	-2.13	1.90	1.36	0.10	-3.36	0.33	0.01	0.01	0.01	0.08	0.15	0.08	0.38	0.37	8478	61
15	4.36	-2.29	1.82	1.30	0.10	-3.46	0.33	0.01	0.01	0.01	0.09	0.15	0.08	0.38	0.38	8492	65
16	4.60	-2.53	1.81	1.30	0.10	-3.70	0.39	0.01	0.01	0.01	0.09	0.15	0.08	0.44	0.42	8512	71
17	4.92	-2.85	1.93	1.37	0.10	-4.09	0.41	0.01	0.01	0.01	0.10	0.15	0.09	0.46	0.44	8534	73
18	4.97	-2.90	2.45	1.72	0.10	-4.49	0.49	0.01	0.01	0.01	0.10	0.15	0.09	0.53	0.53	8563	61
19	5.02	-2.95	2.45	1.72	0.06	-4.61	0.49	0.01	0.01	0.01	0.10	0.15	0.07	0.53	0.29	8602	61
20	5.14	-3.07	2.45	1.72	0.06	-4.73	0.49	0.01	0.01	0.01	0.10	0.15	0.07	0.53	0.29	8742	167
21	5.17	-3.10	2.45	1.72	0.00	-4.82	0.49	0.01	0.01	0.01	0.10	0.15	0.01	0.52	0.29	8774	194
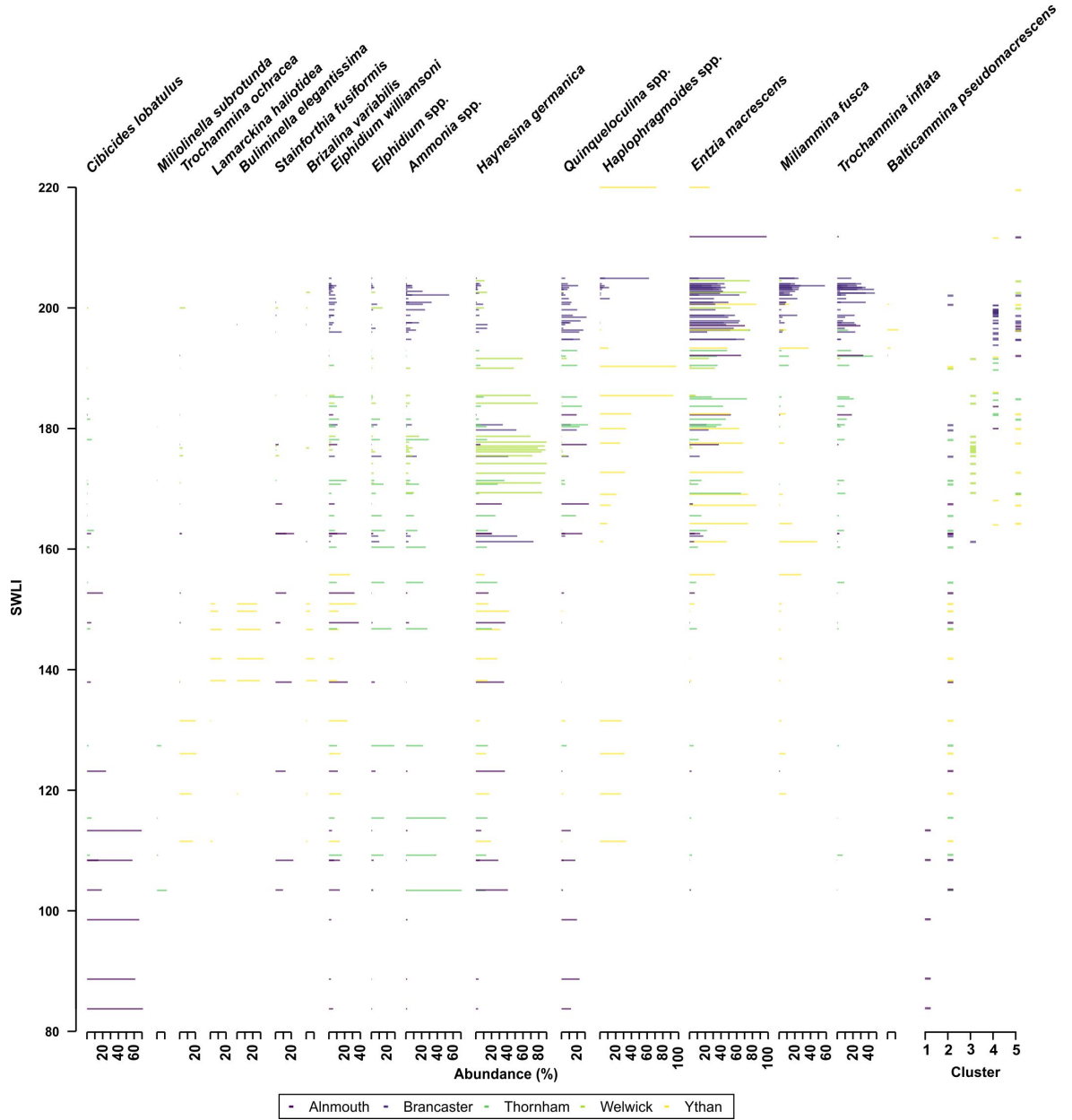
Figure B.1: The combined North Sea foraminifera data of the 125 samples from the five sites included in our final transfer function plotted against SWLI value. Taxa are included that have a maximum abundances > 10 % and occur in more than 10 % of the samples. The bar colour denotes the site corresponding to the legend. The final column shows the groups according to PAM clustering.
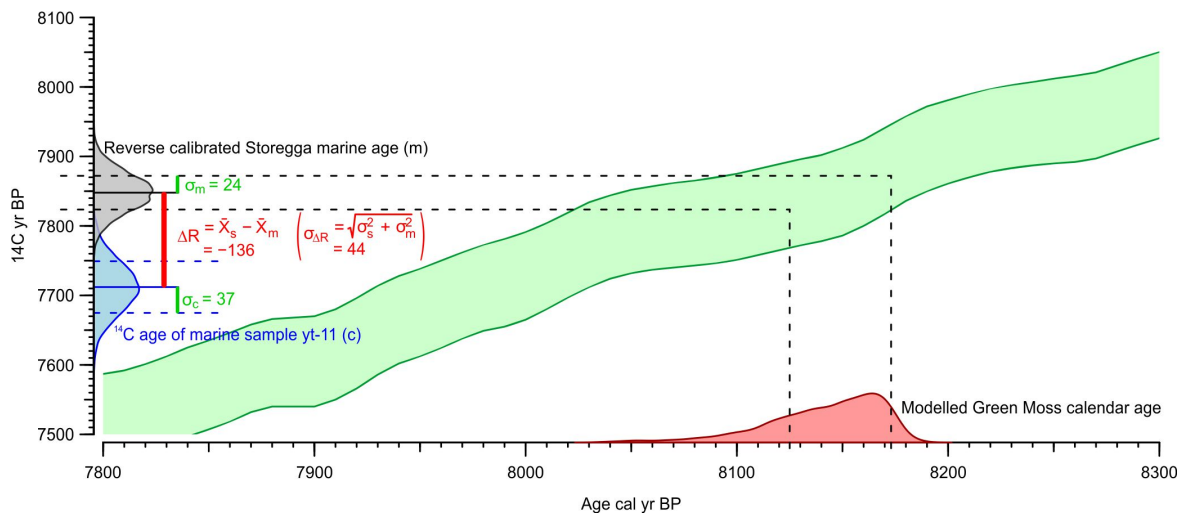
Figure B.2: Diagram to demonstrate the calculation for the ΔR value that we applied to calibrate the marine ^{14}C samples. The green band is the Marine20 calibration curve from Heaton *et al.* (2020). The ^{14}C age probability distribution function of yt-11 is shown in blue. The calendar age of the Storegga tsunami (obtained by re-calibrating the Green Moss sequence (Bondevik *et al.*, 2012)) is shown in red and its reverse calibrated ^{14}C in grey. The means are shown by the solid lines and the 1σ ranges by the dashed lines. The method for calculating the ΔR and its uncertainty are shown and result in a value of -36 $\pm$ 44.
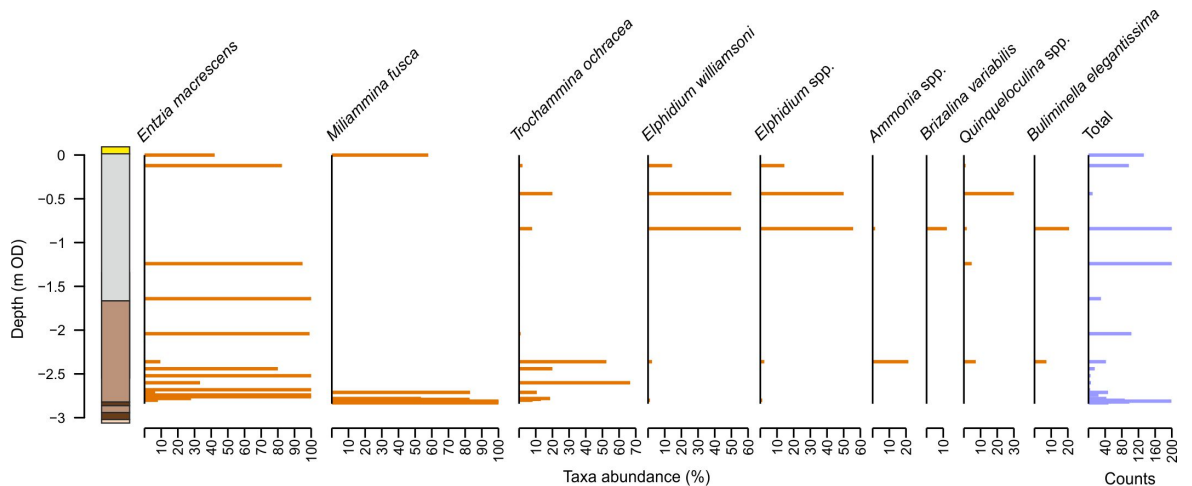
Figure B.3: Litho and bio-stratigraphy of core B7.5. Foraminifera taxa that exceed a maximum of 5% abundance in any sample are displayed in orange as % of the sample total ('Count' in purple).
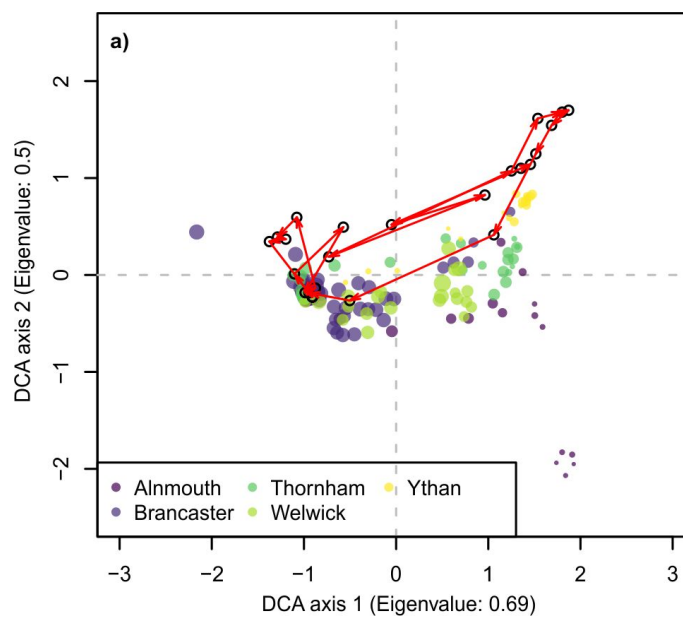
Figure B.4: Detrended Correspondence Analysis (DCA) of the modern training set and fossil data from core A7.5. The modern samples are coloured by site and the size is scaled by SWLI. The core samples are shown by the black circles and reflect the stratigraphic succession shown by the red lines with arrows indicating the stratigraphic order.
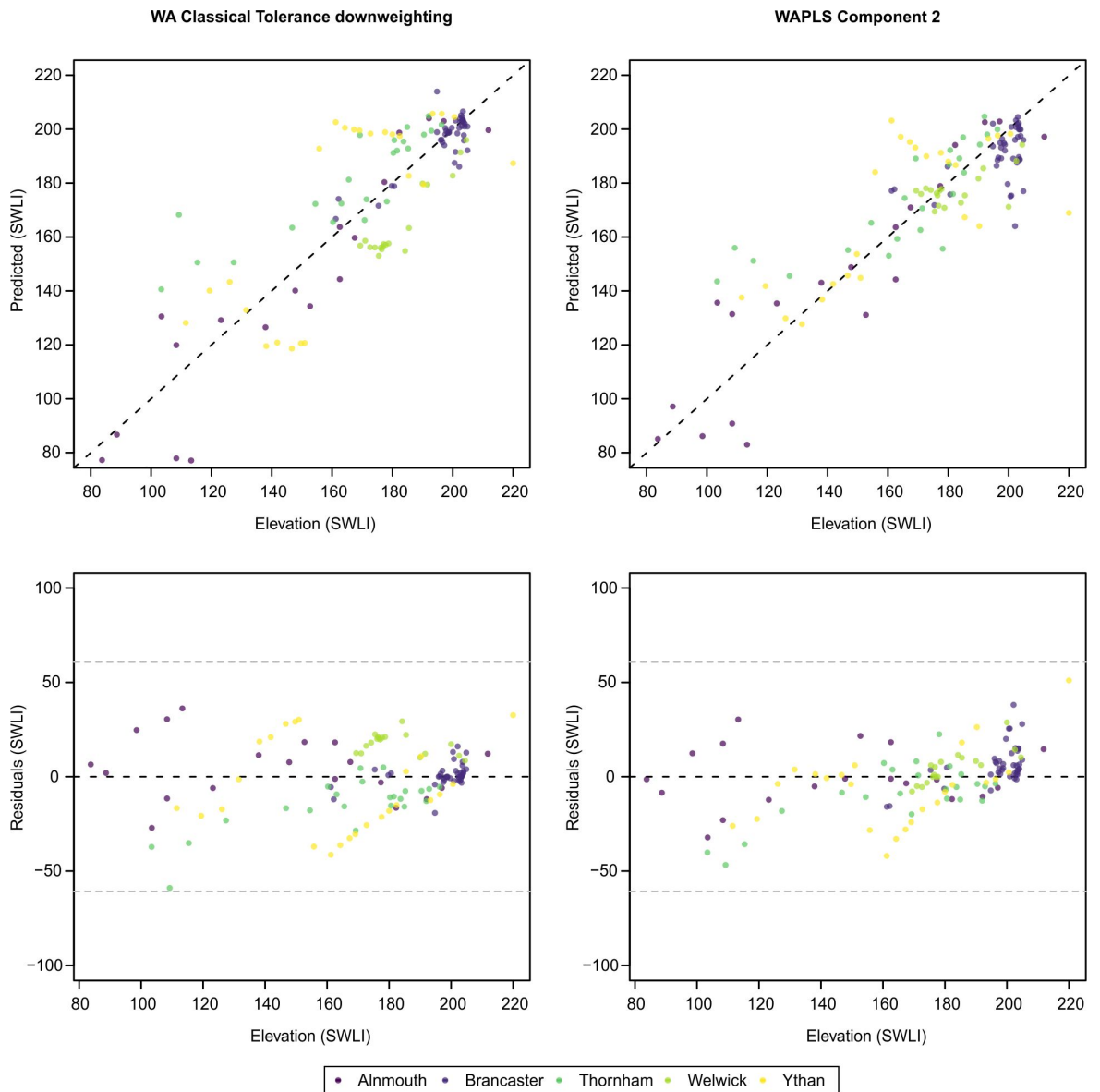
Figure B.5: Scatterplots of the observed SWLI against the predicted SWLI and the residuals for WA classical deshrinking and WA-PLS component 2. The samples are coloured according to site as shown in the legend.
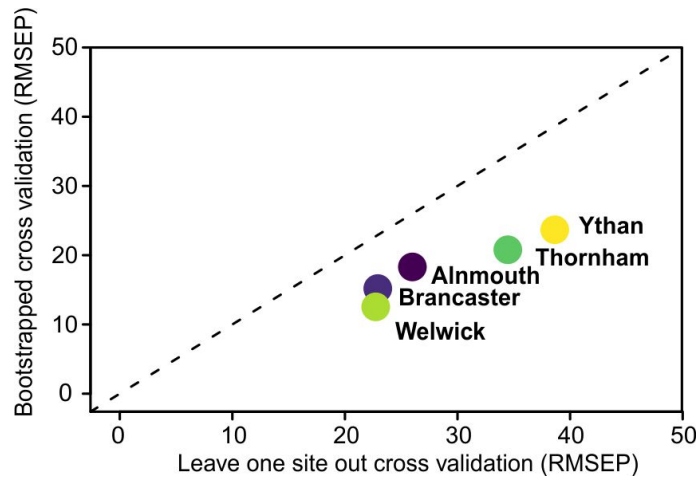
Figure B.6: Comparison of root-mean-square error prediction (RMSEP) under bootstrapping (boot) and leave-one-site-out (LOSO) cross-validation using a WA-PLS component 2 model. The points represent the value when an individual site is excluded.
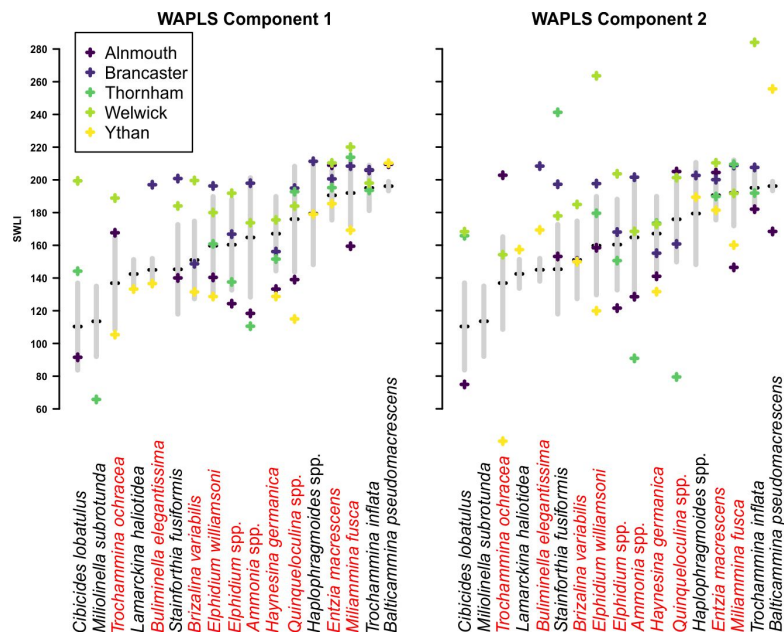

Figure B.7: Comparison of the progressive taxa optima updates for the North Sea training set from WAPLS component 1 (equivalent to WA with inverse deshrinking) to WA-PLS component 2 transfer functions. Overall taxa optima and tolerances are shown for WAPLS 1 by the black cross and grey bar. Taxa optima for individual sites are shown and colour coded. Taxa are included that have a maximum abundance > 10 % and occur in more than 10 % of the samples. Taxa labels coloured red are taxa that are also found in the Ythan core (A7.5).
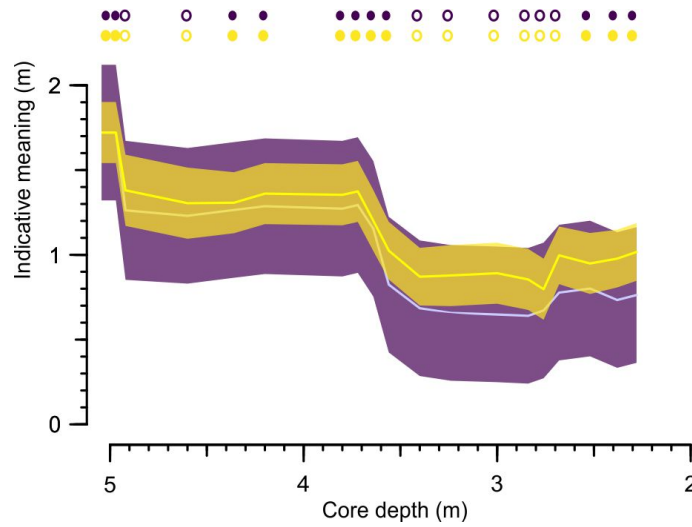
Figure B.8: Comparison of the predicted indicative meanings and 1σ ranges of the fossil samples from the transfer functions based on the full North Sea training set (purple) and the reduced training set that we used (yellow). Good (closed circles) and close (open circles) analogues are shown for each training set.
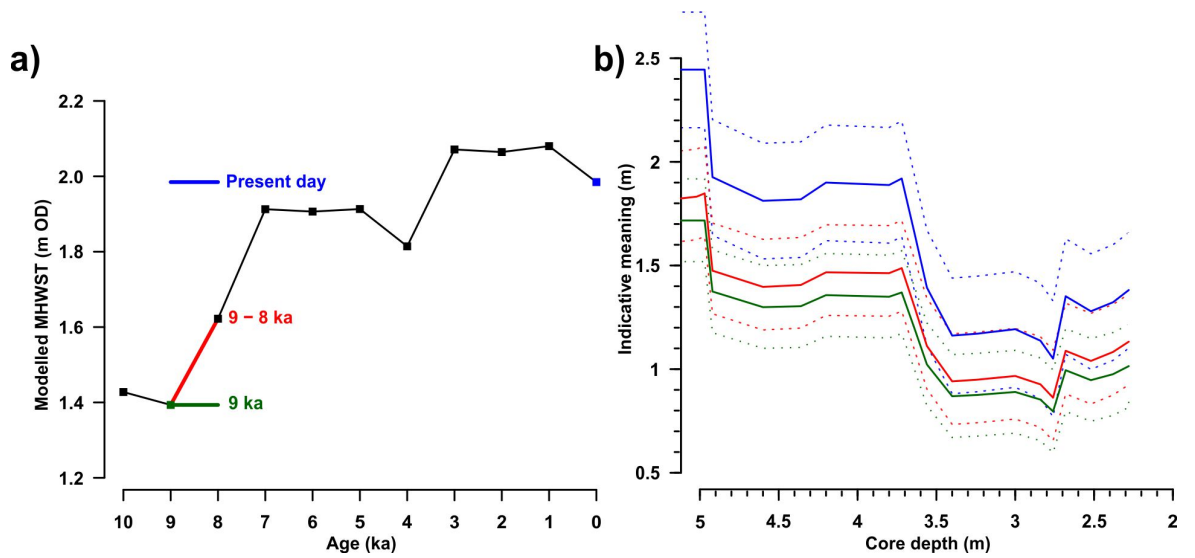

Figure B.9: Simulated mean high water spring tide (MHWST) at the Ythan Estuary from palaeotidal modelling (Hill, 2020) (a). b) shows the effect of the choice of interpolation on the predicted indicative meanings of the sea-level index points, with the dashed lines showing the 1σ uncertainty. The three colour coded choices (described in section 4.2.2.2) are as follows: green) nearest neighbour interpolation using the modelled palaeotide at 9,000 yr BP, red) linear interpolation of predictions between the modelled 9,000 and 8,000 yr BP time slices, and blue) the present day value.